Modeling and high performance numerical simulation of complex fluid flows

Etienne Ahusborde

Habilitation à Diriger des Recherches

UPPA - Université de Pau et des Pays de l'Adour

Spécialité Mécanique

Etienne AHUSBORDE

Chargé de Recherche CNRS

CNRS et Laboratoire de Mathématiques et de leurs Applications UMR CNRS 5142

Modeling and high performance numerical simulation of complex fluid flows

Directeur de recherche : Brahim Amaziane

Soutenue le 3 décembre 2019

Jury

Jocelyne ERHEL	Directrice de Recherche, INRIA Rennes, France	Rapporteur
Bernd FLEMISCH	Professeur, Université de Stuttgart, Allemagne	Rapporteur
Chuanju XU	Professeur, Université de Xiamen, Chine	Rapporteur
Mohamed AMARA	Professeur, UPPA, France	Examinateur
Brahim AMAZIANE	Maître de Conférences HDR, UPPA, France	Examinateur
Mejdi AZAIEZ	Professeur, I2M Bordeaux, France	Examinateur
Guillaume GALLIERO	Professeur, UPPA, France	Examinateur
Michel QUINTARD	Directeur de Recherche CNRS, IMFT, France	Examinateur

Abstract

This dissertation aims at gathering some contributions of my research activity devoted to the development and implementation of mathematical and High Performance Computing (HPC) methods for modeling complex flows. Chapter 1 contains a detailed Curriculum Vitae and administrative data while Chapter 2 presents a general introduction.

Over the last decade, I have focused on two areas of research forming the two parts of this manuscript.

Part I concerns CFD simulations of incompressible flows for which a wide range of issues have been raised. One of the major difficulty when solving computationally the incompressible Navier-Stokes equations consists in ensuring the solenoidal constraint on the velocity. It can be done by the computation of a pressure field which will guarantee a solenoidal velocity field. From all the methods dealing with this point, we can sort them in two categories: exact (as Uzawa method) and approximative methods. Chapter 3 discusses several exact strategies to compute the 2D Stokes eigenvalue problem using spectral element methods. Among the approximative methods, pressure-correction schemes decouple the pressure from the velocity: pressure is treated explicitly in a first sub-step, and is corrected in a second one by projecting the predicted velocity onto an ad-hoc space during a pressure correction step. Chapter 4 proposes a new original method to compute the Hodge Helmoltz decomposition, drawing a parallel between this decomposition and the pressure correction step. In addition to the pressure correction scheme, the velocity-correction scheme switches the two sub-steps: a pressure prediction problem is solved, followed by a velocity correction step. Most of the studies made on these time-splitting methods consider only Dirichlet boundary conditions while few references deal with outflow boundary conditions. That is why Chapter 5 proposes a new numerical scheme treating outflow boundary conditions, for both pressure and velocity correction schemes. An additional issue on this theme concerns the computational geometry. When flows are calculated for complex geometries, one can either use a block-structured grid or an unstructured one. Chapter 6 describes a domain decomposition method to run the Navier-Stokes equations efficiently on non-matching and overlapping block-structured meshes. Chapter 7 describes how we developed a mesh partitioner to carry out HPC simulations on block-structured meshes.

Part II is dedicated to the modeling and finite volume numerical simulation of multiphase flows in porous media. Chapter 8 proposes a non exhaustive state of the art and the description of the environment DuMu^X in which we have been implementing and integrating all our developments for several years. Chapter 9 describes our main contributions concerning these methods and their implementations in a HPC context. We have been involved in the European project FORGE (Fate of Repository Gases) that aimed at studying gas migration in deep repository for radioactive waste. We participated to several benchmarks and we coupled DuMu^X with an upscaling strategy to treat the strong heterogeneities present in the nuclear waste disposal. Our method allowed to reduce drastically the 3D computational time, while producing results that were very close to those of the other participants. Since 2013, we have been interested in the numerical simulation of multiphase reactive flows. We started with a sequential scheme that consists in solving a two-phase compositional flow followed by a reactive transport problem. Several successive strategies involving significant developments have been considered to improve the resolution of the reactive transport problem. Nonetheless, sequential approaches can introduce splitting errors necessitating reduction for the time steps that can become prohibitive. As a consequence, we decided to complete our study by the development of fully coupled fully implicit strategies. Sequential and implicit strategies were validated through numerical benchmarks with applications to geological storage of CO_2 and nuclear waste. We present here a part of these results and focus on the comparison between sequential and global implicit approaches in terms of accuracy and computational time. Some parallel computations are also discussed.

Lastly, some concluding remarks and perspectives are formulated in Chapter10.

Résumé

Ce manuscrit vise à rassembler des contributions de mes activités de recherche dédiées au développement et l'implémentation de méthodes numériques et de calcul haute performance (HPC) pour la modélisation d'écoulements de fluides complexes. Le Chapitre 1 contient un Curriculum Vitae détaillé ainsi que des données administratives tandis que le Chapitre 2 présente une introduction générale.

Durant les dix dernières années, je me suis focalisé sur deux axes de recherche constituant les deux parties de ce manuscrit.

La Partie I concerne des simulations de Mécanique des Fluides Numérique (MFN) concernant des écoulements incompressibles pour lesquels un grand nombre de problèmes ont été abordés. L'une des difficultés majeures dans la résolution des équations de Navier-Stokes incompressibles consiste à assurer la contrainte solénoïdale sur la vitesse. Cela peut se faire par le calcul d'un champ de pression qui garantira un champ de vitesse solénoïdal. Les méthodes traitant de ce point peuvent être classées en deux catégories : les méthodes exactes (comme la méthode d'Uzawa) et les méthodes approchées. Le Chapitre 3 discute de plusieurs stratégies exactes pour calculer le problème aux valeurs propres de Stokes 2D en utilisant des méthodes d'éléments spectraux. Parmi les méthodes approchées, les méthodes de correction de pression découplent la pression de la vitesse : la pression est traitée explicitement dans un premier sous-problème, puis elle est corrigée en projetant la vitesse prédite sur un espace approprié lors d'une étape dite de correction de pression. Le Chapitre 4 propose une nouvelle méthode originale pour calculer la décomposition de Hodge Helmoltz, établissant un parallèle entre cette décomposition et l'étape de correction de pression. Outre les méthodes de correction de pression, les méthodes de correction de vitesse commute les deux sous-problèmes : un problème de prédiction de pression est résolu, suivi d'une étape de correction de vitesse. La plupart des études réalisées sur ces méthodes de time-splitting ne tiennent compte que de conditions aux limites de Dirichlet, tandis que peu de références portent sur les conditions aux limites de sortie. Ainsi, le Chapitre 5 propose une nouvelle stratégie numérique traitant des conditions aux limites de sortie, à la fois pour les schémas de correction de pression et de vitesse. Une autre question sur ce thème concerne la géométrie de calcul. Lorsque la géométrie de calcul est complexe, on peut utiliser soit une maillage structuré par blocs, soit un maillage non structuré. Le Chapitre 6 décrit une méthode de décomposition de domaine pour résoudre efficacement les équations de Navier-Stokes sur des maillages structurés par blocs non-conformes avec recouvrement. Le chapitre 7 décrit le développement d'un partitionneur de maillage pour effectuer des simulations HPC sur des maillages structurés par blocs.

La partie II est consacrée à la modélisation et à la simulation numérique d'écoulements multiphasiques en milieux poreux par la méthode des volumes finis. Le Chapitre 8 propose un état de l'art non exhaustif et la description de l'environnement DuMu^X dans lequel nous avons mis en œuvre et intégré tous nos développements depuis plusieurs années. Le Chapitre 9 décrit nos principales contributions concernant ces méthodes numériques et leurs implémentations dans un contexte HPC. Nous avons participé au projet européen FORGE (Fate of Repository Gases) qui visait à étudier la migration de gaz dans un stockage profond de déchets radioactifs. Nous avons participé à plusieurs benchmarks et nous avons couplé DuMu^X avec une stratégie d'upscaling pour traiter les fortes hétérogénéités présentes dans le site de stockage. Notre méthode a permis de réduire drastiquement le temps de calcul 3D, tout en produisant des résultats très proches de ceux des autres participants. Depuis 2013, nous nous intéressons à la simulation numérique d'écoulements réactifs multiphasiques. Nous avons commencé par considérer une approche séquentielle qui consiste à résoudre un écoulement multiphasique compositionnel suivi d'un problème de transport réactif. Plusieurs stratégies successives impliquant des développements significatifs ont été envisagées pour améliorer la résolution du problème du transport réactif. Néanmoins, les approches séquentielles peuvent introduire des erreurs de splitting qui nécessitent des réductions de

pas temps pouvant devenir rédhibitoires. En conséquence, nous avons décidé de compléter notre étude par l'élaboration de stratégies totalement couplées et totalement implicites. Les stratégies séquentielles et implicites ont été validées par de nombreux benchmarks numériques avec des applications au stockage géologique du CO_2 et de déchets nucléaires. Nous présentons ici une partie de ces résultats et nous nous concentrons sur la comparaison entre les approches séquentielle et globale implicite en termes de précision et de temps de calcul. Quelques calculs parallèles sont également discutés.

Pour conclure, quelques remarques finales et perspectives sont formulées dans le Chapitre 10.

Contents

List of Figures

List of Tables

Chapter 1

Administrative overview

1.1 Curriculum vitae

AHUSBORDE Etienne

Date and place of birth:	May 12, 1980, Oloron Sainte Marie, France
Address:	LMAP UMR CNRS 5142 Bâtiment IPRA - UPPA Avenue de l'Université - BP 1155 64013 PAU CEDEX
Tel:	0540175055
Email:	etienne.ahusborde@univ-pau.fr
Webpage:	https://lma-umr5142.univ-pau.fr/eahusbor.html

Education

- **PhD in Mechanics**, "High order methods for the -**grad**(div(.)) operator and applications", 2007, University Bordeaux 1.
- **Master degree in Mechanical Engineering**, 2004, University Bordeaux 1.
- **Engineering Degree in Mathematical and Mechanical Modeling**, 2004, Graduate School of Engineering MATMECA, University Bordeaux 1.

Professional experience

- **Current position:** Since 2010, **CNRS researcher**, Laboratory of Mathematics and their Applications of Pau, University of Pau & Pays Adour.
- **Previous positions**
  2009-2010: Post-doctoral fellow, TREFLE Laboratory, University Bordeaux 1.
  Research topic: "Thermal characterization by inverse method of homogeneous and heterogeneous materials".
  2008-2009: Post-doctoral fellow, TREFLE Laboratory, University Bordeaux 1.
  Research topic: "Parallel computing for the resolution of Navier Stokes equations".
  2007-2008: Temporary research and teaching assistant, University Bordeaux 1.
  Research topic: "Domain decomposition method for the resolution of Navier Stokes equations".

1.2 Professional activities

1.2.1 International and national collaborations

Previous collaborations:

- 2004-2007. Partners: Ecole Polytechnique Fédérale de Lausanne (EPFL), Switzerland and Université Libre de Bruxelles, Belgium.
  Research topic: Numerical approximation of the -**grad**(div(.)) operator.

- 2011-2012. Partners: Laboratory of Mathematical Modeling and Computer science, Meknès, Morocco; University Sidi Mohamed Ben Abdellah, Department of Geology, Fès, Morocco and University of Zagreb, Faculty of Sciences, Department of Mathematics, Zagreb, Croatia.
  Research topic: Modeling, analysis and numerical simulation of multiphase flows in porous media. Application to marine intrusion. Project funded by the Francophone University Agency (AUF).

- 2011-2014. Partners: INRIA Rocquencourt & Maison de la Simulation.
  Research topic: Numerical simulation of compressible immiscible two-phase flows with reactive transport in porous media.

Ongoing collaborations:

- Since 2010. Partner: Institute of Mechanics and Engineering of Bordeaux, Department TREFLE.
  Research topic: Modeling and numerical simulation of incompressible flows.

- Since 2010. Partner: University of Zagreb, Faculty of Sciences, Department of Mathematics, Zagreb, Croatia.
  Research topic: Modeling, analysis and numerical simulation of multiphase flows in porous media. Application to energy and environmental issues.

- Since 2014. Partner: Laboratory of Mathematical Modeling and Computer science, Meknès, Morocco.
  Research topic: Numerical simulation of multiphase flows with reactive transport in porous media.

Stay in other laboratories:

- Stay at the Laboratory in Numerical Engineering, Ecole Polytechnique Fédérale de Lausanne.
  Duration: 4 months (September - December 2006).

- Stay at the University of Zagreb, Faculty of sciences, Department of Mathematics.
  Duration: 1 week (December 2011), 1 week (December 2012), 1 week (June 2018).

1.2.2 Organization of scientific events

- May 2017, International Conference on Approximation Methods and Numerical Modeling in Environment and Natural Ressources - MAMERN'17, Oujda, Morocco. Member of the organizing and scientific committees.

- October 2016, 13èmes Journées d'Etudes des Milieux Poreux - JEMP2016, Anglet, France. Member of the organizing and scientific committees.

- June 2015, International Conference on Approximation Methods and Numerical Modeling in Environment and Natural Resources - MAMERN'15, Pau, France. Member of the organizing and scientific committees.
- October 2014, International Conference on Mathematical and Numerical Modeling of Flow and Transport in Porous Media, Dubrovnik, Croatia. Member of the organizing and scientific committees.
- September 2014, Thirteenth International Conference Zaragoza-Pau on Mathematics, Jaca, Spain. Member of the organizing committee.
- April 2013, International Conference on Approximation Methods and Numerical Modeling in Environment and Natural Resources - MAMERN'13, Granada, Spain. Member of the organizing and scientific committees.
- September 2012, Twelfth International Conference Zaragoza-Pau on Mathematics, Jaca, Spain. Member of the organizing committee.

1.3 Students supervision

- 2016-2019: Co-supervision with Brahim Amaziane (UPPA) of the PhD thesis of Mohamed Id Moulay entitled "Modeling and 3D numerical simulation of reactive multiphase flows in porous media". Defense scheduled for December 09, 2019.
- 2016: Co-supervision of the Master 2 internship of Mohamed Id Moulay entitled "Modeling and numerical simulation of single-phase miscible and two-phase flows in porous media". Co-supervised internship with Brahim Amaziane and Hassan El Amri (LMA, ENS, Université Hassan II, Casablanca, Morocco).
- 2015-2016: Co-supervision of the Master 2 internship of Amine Zaoutini entitled "Numerical simulation of non-isothermal immiscible two-phase flows in porous media" in the second year of the UPPA Master MMS (Mathematics, Modeling and Simulation). Co-supervision with Brahim Amaziane.
- 2011-2014: Co-supervision of the PhD thesis of Viacheslav Vostrikov entitled "Numerical simulation of compressible immiscible two-phase flows with reactive transport in porous media" defended on December 15, 2014. PhD thesis directed by Brahim Amaziane and Michel Kern (Inria Rocquencourt & Maison de la Simulation).

1.4 Teaching and administrative activities

1.4.1 Teaching activities

Frame	Formations	Course	Time volume (hours)
University of Bordeaux, Temporary research and teaching assistant (2008-2009)	2nd Year - Bachelor of Mechanics, Energy and Conception	Material Science	32 h.
	3rd Year - Bachelor of Mechanics, Energy and Conception	Fluid Mechanics	18 h.
	1st Year - Graduate School of Engineering MATMECA	Mechanics of continuous media	52 h.
UPPA, Since 2011, each year	1st Year - Master Petroleum Engineering	Algorithms and scientific computing	20 h.
	2nd Year - Master Petroleum Engineering	Numerical Upscaling	15 h.
UPPA, Since 2016, each year	2nd Year - Master Mathematics, Modeling and Simulations	Porous Media	30 h.

Others

- Summer school E2S "Energy and Environment Chalenges", UPPA, Pau, July 2018. "Reservoir simulation and upscaling", 7 h.
- Special course of Ecole Normale Supérieure de Kouba, Alger, March 2012. "Presentation of the platform DuMu^X for the numerical simulation of transport and flow in porous media", 10 h.
- School "Mathematical models for energy and environmental issues", National School of the Mineral Industry of Rabat, January 2012. Presentation of the platform DuMu^X for the numerical simulation of transport and flow in porous media, 3.5h.

1.4.2 Participation in administrative tasks

- Reviewer for referred papers in international journals: International Journal of Numerical Methods in Fluids, Lecture Notes in Computational Science and Engineering, Numerical Methods for Partial Differential Equations, Mathematics and Computers in Simulation, Journal of Mathematical Study, Mathematical Modeling and Analysis.
- Member of the selection committee for an assistant professor position in fluid mechanics at University Bordeaux 1, 2015.
- In charge of the seminar of de Mathematics and their applications of LMAP from 01/09/2011 to 31/12/2015.
- Responsible for the second year internships of the UPPA Master MMS (Mathematics, Modeling and Simulation) from 01/09/2011 to 30/09/2018.

- Member of the steering and improvement committees of the UPPA Master of Mathematics since 01/09/2011.

1.5 Publications

Papers published or accepted in peer-reviewed journals

1. **Ahusborde E.**, Amaziane B., El Ossmani M., Id Moulay M., *Numerical modeling and simulation of fully coupled processes of reactive multiphase flow in porous media*, Accepted for publication in Journal of Mathematical Study, 2019.

2. **Ahusborde E.**, El Ossmani M., Id Moulay M., A fully implicit finite volume scheme for single phase flow with reactive transport in porous media, Mathematics and Computers in Simulation, Vol 164, 3-23, 2019.

3. **Ahusborde E.**, Amaziane B., El Ossmani M., *Improvement of numerical approximation of coupled two-phase multicomponent flow with reactive geochemical transport in porous media*, Oil & Gas Science and Technology - Rev. IFP Energies nouvelles, Vol 73, 73, 2018.

4. **Ahusborde E.**, Azaïez M., Gruber R., *Numerical assessment of a class of high order Stokes spectrum solver*, Journal of Mathematical Study, Vol 51, 1-14, 2018.

5. **Ahusborde E.**, El Ossmani M., *A sequential approach for numerical simulation of two-phase multicomponent flow with reactive transport in porous media*, Mathematics and Computers in Simulation, Vol 137, 71-89, 2017.

6. **Ahusborde E.**, Azaïez M., Ben Belgacem F., Palomo Del Barrio E., *Mercer's spectral decomposition for the characterization of thermal parameters*, Journal of Computational Physics, Vol 294, 1-19, 2015

7. **Ahusborde E.**, Amaziane B., Jurak M., *3D numerical simulation by upscaling of gas migration through engineered and geological barriers for a deep repository for radioactive waste*, Geological Society, London, Special Publications, Vol 415, 123-141, 2015.

8. **Ahusborde E.**, Azaïez M., Ben Belgacem F., Bernardi C., *Automatic simplification of Darcy's equation with pressure dependent permeability*, ESAIM: Mathematical Modelling and Numerical Analysis, Vol 47, 1797-1820, 2013.

9. Poux A., Glockner S., **Ahusborde E.**, Azaïez M., *Open and traction boundary conditions for velocity correction scheme for Navier-Stokes equations*, Computers and Fluids, Vol 70, 29-43, 2012.

10. **Ahusborde E.**, Glockner, S., *A 2D block-structured mesh partitioner for accurate flow simulations on non-rectangular geometries*, Computers and Fluids, Vol 43, 2-13, 2011.

11. Gruber R., **Ahusborde E.**, Azaïez M., Keller V., Latt J., *High performance computing for partial differential equation*, Computers and Fluids, Vol 43, 68-73, 2011.

12. **Ahusborde E.**, Glockner S., *An implicit method for the Navier-Stokes equations on overlapping block-structured grids*, International Journal for Numerical Methods in Fluids, Vol 62, 784-801, 2010.

13. **Ahusborde E.**, *Legendre spectral methods for the* -**grad***(div(.)) operator with free boundary conditions*, Numerical Algorithms, Vol 55, 151-171, 2009.

14. **Ahusborde E.**, Azaïez M., Deville M., Mund, E., *An iterative domain decomposition algorithm for the* -**grad***(div(.)) operator*, Communications in Computationnal Physics, Vol 5, 391-397, 2009.

15. **Ahusborde E.**, Azaïez M., Deville M.O., Gruber R., Mund, E.H., *Constructive spectral approaches for the Helmholtz decomposition of a vector field*, Applied Numerical Mathematics, Vol 58, 955-967, 2008.

16. **Ahusborde E.**, Gruber R., Azaïez M., Sawley M.L., *Physics-conforming constraints-oriented numerical method*, Physical Review E, Vol 75, Issue 5, Article number 056704, 2007.

17. **Ahusborde E.**, Azaïez M., Caltagirone J.P, *A primal formulation for the Helmholtz decomposition*, Journal of Computational Physics, Vol 225, Issue 1, 13-19, 2007.

18. **Ahusborde E.**, Azaïez M., Deville M.O., Mund E.H., *Legendre spectral method for the* -**grad***(div(.)) operator*, Computer Methods in Applied Mechanics and Engineering, Vol 196, Issues 45-48, 4538-4547, 2007.

Papers published in peer-reviewed conference proceedings

19. **Ahusborde E.**, Amaziane B., El Ossmani M., *Finite volume scheme for coupling two-phase flow with reactive transport in porous media*, Springer Proceedings in Mathematics and Statistics, Vol 200, 407-415, 2017.

20. **Ahusborde E.**, Kern M., Vostrikov V., *Numerical simulation of two-phase multi-component flow with reactive transport in porous media: application to geological storage of* CO_2, ESAIM: Proceedings and Surveys, Vol 49, 21-39, 2015.

21. **Ahusborde E.**, Azaïez M., Caltagirone J.P., Gerritsma M., Lemoine A., *Discrete Hodge Helmoltz Decomposition*, Monografías Matemáticas "García de Galdeano", Vol 39, 1-10, 2014.

22. **Ahusborde E.**, Azaïez M., Glockner S., Poux A., *A contribution to the outflow boundary conditions for Navier-Stokes time-splitting methods*, Lecture Notes in Computational Science and Engineering, Vol 95, 75-86, 2014.

23. **Ahusborde E.**, Azaïez M., Gruber R., *Constraint oriented spectral element method*, Lecture Notes in Computational Science and Engineering, Vol 76, 93-100, 2011.

24. Feugeas J.L., Nicolaï P., Schurtz G., Charrier P., **Ahusborde E.**, *High order scheme for the nonlocal transport in ICF plasmas*, Journal De Physique. IV: JP, 133, 205-207, 2006.

Co-edited books

25. Lopez de Silanes M.C., Palacios M., Sanz G., **Ahusborde E.**, Amrouche C., Carbou G., *Fourteenth International Conference Zaragoza-Pau on Mathematics and its Applications*, Monografias del Seminario Matematico "Garcia De Galdeano", Vol 41, Prensas Universitarias de Zaragoza, 2018 [ISBN 978-84-17358-00-6].

26. **Ahusborde E.**, Amrouche C., Lopez de Silanes M.C., Palacios M., Sanz G., *Thirteenth International Conference Zaragoza-Pau on Mathematics*, Monografias del Seminario Matematico "Garcia De Galdeano", Vol 40, Prensas Universitarias de Zaragoza, 2015 [ISBN 978-84-16515-28-8].

27. Amaziane B., **Ahusborde E.**, Barrera D., Ibáñez-Pérez M. J., Romero-Zalir R., Sbibih D., *Proceedings of the 6th International Conference on Approximation Methods and Numerical Modeling in Environment and Natural Resources: MAMERN 15*, Editorial Universidad de Granada, 2015 [ISBN 978-8433857835].

28. Lopez de Silanes M.C., Palacios M., Sanz G., **Ahusborde E.**, Amrouche C., *Twelfth International Conference Zaragoza-Pau on Mathematics*, Monografias del Seminario Matematico "Garcia De Galdeano", Vol 39, Prensas Universitarias de Zaragoza, 2014 [ISBN 978-84-16028-35-1].

Others

29. Wendling J., Yu L., Treille E., Dymitrowska M., Pellegrini D., **Ahusborde E.**, Jurak M., Amaziane N., Caro F., Genty A., Poskas P., Justinavicius D., Sentis M., Norris S., Bond A., Leung H., Calder N.J., *Final report on benchmark studies on repository-scale numerical simulations Part 1: cell scale benchmark*, performed in the framework of the european project FORGE, 2009-2012, (180 pages).

30. Wendling J., Yu L., Treille E., Dymitrowska M., Pellegrini D., **Ahusborde E.**, Jurak M., Amaziane N., Caro F., Genty A., Poskas P., Justinavicius D., Sentis M., Norris S., Bond A., Leung H., Calder N.J., *Final report on benchmark studies on repository-scale numerical simulations Part 2: module scale benchmark*, performed in the framework of the european project FORGE, 2009-2012, (182 pages).

1.6 Communications

International conferences given at the invitation of the organization committee

1. **Ahusborde E.**, Amaziane B., El Ossmani M., *A parallel finite volume method for two-phase multicomponent flow with reactive transport in porous media*, Numerical Methods for Challenging Problems, Mulhouse, July 2018, France.

2. **Ahusborde E.**, Amaziane B., Jurak M., *3D numerical simulation by upscaling of gas migration through engineered and geological barriers for a deep repository for radioactive waste*, Numerical Methods and Applications to Some Challenging Problems, Sevilla, June 2013, Spain.

3. **Ahusborde E.**, Azaïez M., Gruber R., *The Constraints Oriented Library method. Part II: Reduction, Preconditionner and Applications*, High Performance Computing Methods Symposium, Lausanne, June 2008, Switzerland.

Other communications, symposium, workshop

4. **Ahusborde E.**, Amaziane B., Id Moulay M., Simulation numérique des couplages entre écoulements diphasiques et réactions géochimiques en milieux poreux, Congrès SMAI 2019, Guidel, May 2019, France.

5. **Ahusborde E.**, Amaziane B., El Ossmani M., Numerical scheme for coupling two-phase compositional flow and reactive transport in porous media, TAMTAM 2019: Tendances dans les Applications Mathématiques en Tunisie Algérie Maroc, Tlemcen, February 2019, Algeria.

6. **Ahusborde E.**, Amaziane B., Id Moulay M., A fully implicit finite volume scheme for two-phase flow with reactive transport in porous media, 14èmes Journées d'Etude sur les Milieux Poreux JEMP, Nantes, October 2018, France.

7. **Ahusborde E.**, El Ossmani M., Id Moulay M., A finite volume method for fully coupled multiphase flow and chemical processes in porous media - Application to CO_2 storage, Fifteenth International Conference Zaragoza-Pau on Mathematics, Jaca, September 2018, Spain.

8. 6- **Ahusborde E.**, Amaziane B., Id Moulay M., A fully implicit finite volume scheme for flows with reactive transport in porous media, Computational Methods in Water Resources (CMWR XXII), Saint-Malo, May 2018, France.

9. **Ahusborde E.**, Amaziane B., El Ossmani M., Reactive-DuMu^X: a collaborative parallel platform for numerical simulation of multiphase multicomponent flow with reactive transport in porous media, Reactive Transport Modeling Workshop, Paris, January 2018, France.

10. **Ahusborde E.**, Amaziane B., Id Moulay M., A fully implicit finite volume scheme for single phase flow with reactive transport in porous media, Reactive Transport Modeling Workshop, Paris, January 2018, France.

11. **Ahusborde E.**, Amaziane B., El Ossmani M., *Finite volume scheme for coupling two–phase flow with reactive transport in porous media*, Finite Volume for Complex Applications 8, Lille, June 2017, France.

12. **Ahusborde E.**, Amaziane B., El Ossmani M., *A sequential semi-implicit algorithm for computing two-phase multicomponent flow with reactive transport in porous media*, International Conference on Approximation Methods and Numerical Modeling in Environment and Natural Resources MAMERN VII, Oujda, May 2017, Morocco.

13. **Ahusborde E.**, Amaziane B., El Ossmani M., *A numerical study of two–phase multicomponent flow with reactive transport in porous media*, 5th International Congress of the SM2A, Meknes, March 2017, Morocco.

14. **Ahusborde E.**, Amaziane B., El Ossmani M., Poncet P., *Benchmark for coupled two-phase multicomponent flow with reactive geochemical transport in porous media*, Subsurface Environmental Simulation Benchmarking Workshop V, A Coruna, October 2016, Spain.

15. **Ahusborde E.**, Amaziane B., El Ossmani M., Poncet P., *Numerical modeling of coupled two-phase multicomponent flow with reactive geochemical transport in porous media*, 13èmes Journées d'Etudes des Milieux Poreux 2016, Anglet, October 2016, France.

16. **Ahusborde E.**, Amaziane B., El Ossmani M., Poncet P., *Numerical simulation of flows with reactive transport in porous media: towards a validation for two-phase flow*, Reactive Transport Modeling in the Geological Sciences, Paris, November 2015, France.

17. **Ahusborde E.**, Amaziane B., El Ossmani M., Poncet P., *A sequential numerical simulator for two-phase multicomponent flow with reactive transport in porous media*, MoMaS Multiphase Seminar Days - Journées MoMaS Multiphasiques, Nice, October 2015, France.

18. Poncet P., **Ahusborde E.**, Amaziane B., *Particle methods for transport in porous media at the pore scale*, Complex Fluid Flow in Porous Media, Bordeaux, October 2015, France.

19. Kern M., **Ahusborde E.**, Vostrikov V., *Numerical simulation of two-phase multi-component flow with reactive transport in porous media*, SIAM Conference on Mathematical & Computational Issues in the Geosciences, Stanford, June 2015, USA.

20. **Ahusborde E.**, Amaziane B., El Ossmani M., Poncet P., *An integrated two-phase flow with reactive transport model in porous media*, MAMERN'15, Pau, June 2015, France.

21. **Ahusborde E.**, Kern M., Vostrikov V., *Simulation numérique d'écoulements diphasiques multiconstituants avec transport réactif en milieu poreux : application au stockage géologique du CO_2*, 12 èmes Journées d'Etudes des Milieux Poreux 2014, Toulouse, October 2014, France

22. **Ahusborde E.**, Kern M., Vostrikov V., *Simulation numérique d'écoulements diphasiques multiconstituants avec transport réactif en milieu poreux : application au stockage géologique du CO_2*, CANUM 2014, Carry le Rouet, April 2014, France.

23. **Ahusborde E.**, Amaziane B., Kern M., Vostrikov V., *Numerical simulation of two-phase multicomponent flow with reactive transport in porous media: application to geological storage of carbon dioxide*, MoMaS Multiphase Seminar Days - Journées MoMaS Multiphasiques, Bures-sur-Yvette, October 2013, France.

24. **Ahusborde E.**, Amaziane B., Kern M., Vostrikov V., *Modeling and numerical simulation of two-phase multi-component flow with reactive transport in porous media: application to geological storage of carbon dioxide*, Second Sustainable Earth Sciences Conference & Exhibition, Pau, September 2013, France.

25. Vostrikov V., **Ahusborde E.**, Kern M., *Simulation numérique d'écoulements diphasiques immiscibles compressibles avec transport réactif en milieu poreux*, Congrès SMAI 2013, Seignosse, May 2013, France.

26. **Ahusborde E.**, Amaziane B., Jurak M., *3D numerical simulation by upscaling of gas migration through engineered and geological barriers for a deep repository for radioactive waste*, MAMERN'13, Grenade, April 2013, Spain.

27. **Ahusborde E.**, Amaziane B., Jurak M., *3D numerical simulation of gas migration through engineered and geological barriers for a deep repository for radioactive waste: FORGE WP1.2 benchmark*, Gas Generation and Migration International Symposium and Workshop, Luxembourg, February 2013, Luxembourg.

28. **Ahusborde E.**, Amaziane B., Jurak M., *Contribution of CNRS/MoMaS to FORGE WP1.2 benchmark at module scale by mathematical upscaling*, FORGE General Assembly, Gent, December 2012, Belgium.

29. **Ahusborde E.**, Amaziane B., Jurak M., *3D numerical simulation by upscaling of gas migration through engineered and geological barriers for a deep repository for radioactive waste*, MoMaS Multiphase Seminar Days - Journées MoMaS Multiphasiques, Nice, October 2012, France.

30. **Ahusborde E.**, Azaïez M., Lemoine A, Gerritsma M., *Discrete Hodge Helmoltz Decomposition*, Twelfth International Conference Zaragoza-Pau on Mathematics, Jaca, September 2012, Spain.

31. **Ahusborde E.**, Azaïez M., Glockner S., Poux A., *A contribution to the open boundary conditions for Navier-Stokes time-splitting methods*, International Conference On Spectral and High Order Methods, Tunis, June 2012, Tunisia.

32. Godin A., Palomo Del Barrio E., Azaïez M., **Ahusborde E.**, Dauvergne J.L., *Thermal characterization of heterogeneous materials: phases and interfaces recognition*, Third international Conference on Porous Media, Bordeaux, March 2011, France.

33. **Ahusborde E.**, Azaïez M., Gruber R., *COOL@HPC*, International Conference of Numerical Analysis and Applied Mathematics, Rhodes, September 2010, Greece.

34. Glockner S., **Ahusborde E.**, *Multiphase flow simulations in a block-structured framework*, High Accuracy Flow Simulations, Lausanne, February 2010, Switzerland.

35. Azaïez, M., **Ahusborde E.**, *Calcul de spectre sous contraintes : Cas de l'opérateur* -**grad***(div(.))*, Congrès français de mécanique, Marseille, August 2009, France.

36. Azaïez M., **Ahusborde E.**, Gruber R., *Modes of a plasma-filled waveguide determined by a high order method*, International Conference On Spectral and High Order Methods, Trondheim, June 2009, Norway.

37. **Ahusborde E.**, Azaïez M., Gruber R., *A physics conforming constraints oriented numerical method*, International Conference On Spectral and High Order Methods, Beijing, June 2007, China.

38. Feugeas J.L, Nicolaï P., Schurtz G., Charrier P., **Ahusborde E.**, *High order scheme for the non-local transport in ICF plasmas*, Inertial Fusion Sciences and Applications, Biarritz, September 2005, France.

39. **Ahusborde E.**, Azaïez M., *Etude d'un solveur rapide pour le problème de Darcy*, 7èmes Journées d'Etude sur les Milieux Poreux, Bordeaux, April 2005, France.

Chapter 2

General introduction

Mathematical modeling and numerical simulation are essential for studying a large number of physical problems. The modeling step consists in finding a system of partial differential equations (PDE) relevant to represent the problem. A compromise has to be found between the richness of the model that must ensure a realistic modeling and its ability to be solved with moderate computational costs. Then, the elaboration of adequate numerical methods includes, besides the mathematical analysis (existence, stability), the study of numerical schemes, the analysis of their convergence, their complexity and their validation on benchmarks. Finally, the computational implementation must depend on the complexity of the geometries, the size of the problems to be solved and the orders of magnitude of the different characteristic scales.
In this context, this manuscript aims at gathering my contributions since my PhD thesis entitled "High order method for the -**grad**(div(.)) operator and applications" and defended in 2007 in the laboratory TREFLE (Transfer Fluid Energy) at the University of Bordeaux 1 [12]. The purpose of this work was to contribute to the approximation of the -**grad**(div(.)) operator by spectral element methods. Several applications related to Stokes problem, and the steady and unsteady Navier-Stokes incompressible equations were considered. After my PhD defense in 2007, I spent three years in the laboratory TREFLE as temporary research and teaching assistant (09/2007-09/2008) and as post-doctoral fellow (10/2008-09/2010). During the first two years, I focused on the implementation of new features on a Finite-Volume code named Thetis dedicated to the modeling and simulation of incompressible flows. In 2010, I was recruited as a CNRS researcher in the Laboratory of Mathematics and its Applications of Pau at the University of Pau & Pays Adour. I have been working in the teams "Analysis ans Numerical Simulation" and then "Numerical methods and complex fluids" on the numerical simulation of multiphase flows in porous media. Therefore, since my PhD thesis, I mainly work around two research areas: the numerical simulation of incompressible fluids and the numerical simulation of multiphase flow in porous media. The common point between these two activities is the development and implementation of mathematical and high performance computational methods for modeling complex flows. As a consequence, this manuscript is divided into two parts.

Part I deals with contributions for Computational Fluid Dynamics (CFD) of incompressible flows. It is composed of five chapters presenting work that has been published in 7 articles [20, 23, 24, 25, 26, 27, 247], the content of which is briefly detailed thereafter. Computational fluid mechanics is an essential tool to analyze fluid behavior in many environmental and industrial issues. Given the constant progress in computing resources and the need to model increasingly complex problems, sophisticated numerical schemes must be developed to take benefit from these computational facilities. Many issues are related to the numerical simulation of incompressible fluids (such that water or blood). Solving computationally

an accurate solution to the unsteady incompressible Navier-Stokes equations is an intricate task. Beside the treatment of nonlinearities, a solenoidal constraint on the velocity (div $\vec{u} = 0$) must be ensured. In can be done by the computation of a pressure field which will ensure a solenoidal velocity field. From all the methods dealing with this point, we can sort them in two categories: exact and approximative methods. In the first one, there are all the methods based on the idea proposed by Uzawa. In this context, Chapter 3 discusses several exact strategies to compute the 2D Stokes eigenvalue problem in the framework of spectral element methods. We focus on formulations considering only the velocity as variable (the pressure gradient is eliminated in a relevant way): the penalty method and a so-called "divergence-free Galerkin approach" [24, 25]. Another class of non-exact methods consists in decoupling the pressure from the velocity by means of a time-splitting scheme. This scheme significantly reduces the computational cost of an approximate solution satisfying the incompressibility constraint but with a diminished accuracy. The most popular methods are pressure-correction schemes. They require the solution of two sub-steps: the pressure is treated explicitly in the first one, and is corrected in the second one by projecting the predicted velocity onto an ad-hoc space during a pressure correction step. Chapter 4 draws a parallel between this pressure correction step and the Hodge Helmoltz decomposition that consists, among other things, in extracting the solenoidal part of a vector field. Still using spectral element methods, a new original method is proposed in Chapter 4 to perform this decomposition [20]. In addition to the pressure correction scheme, there is a less studied alternative technique known as the velocity-correction scheme. It consists in switching the two sub-steps: a pressure prediction problem is solved, followed by a velocity correction step. The majority of the studies made on these time-splitting methods consider only Dirichlet boundary conditions while few references deal with outflow boundary conditions. That is why Chapter 5 proposes a new numerical scheme for incompressible Navier-Stokes equations with open boundary conditions, for both pressure and velocity correction schemes [23, 247]. An other difficulty in the numerical computation of the incompressible Navier-Stokes equations can come from the computational geometry. When flows are calculated for complex geometries, one can either use a block-structured grid or an unstructured one. Faced with a software constraint requiring us to use structured meshes, we present in Chapter 6 a domain decomposition method to run the Navier-Stokes equations efficiently on non-matching and overlapping block-structured meshes [26]. For the same software, Chapter 7 describes how we developed a mesh partitioner to carry out high performance parallel simulations of incompressible flows on block-structured meshes [27].

Part II is composed of two chapters and is dedicated to the modeling and numerical simulation of multiphase flows in porous media. Seven journal publications have arisen out of the results of this work [13, 14, 15, 16, 29, 30, 31]. This theme has also been the subject of 2 thesis co-supervision [215, 301], 2 master's thesis co-supervision and numerous communications in international conferences. Multiphase multicomponent flow in porous media play a significant role for many applications in geological and reservoir engineering processes. We can mention for instance the hydrocarbon recovery, the sequestration of CO_2 in saline aquifers, the geological storage of nuclear waste or the prevention of groundwater pollution and the contaminant remediation. Numerical models have been increasingly used for this purpose, a trend that will continue because more sophisticated models and codes are being developed and computer costs keep decreasing. Significant efforts and attempts have been made during recent years toward the development of such tools. It is why since several years, we have integrated all our developments in DuMu^X (DUNE for Multi-{Phase, Component, Scale, Physics, ...} flow and transport in porous media) [3, 119], a free and open-source simulator for flow and transport processes in porous media. Thus, Chapter 8 proposes a non exhaustive state of the art dedicated to the numerical simulation of reactive multiphase flow in porous media, followed by a short description of the main features of the simulator DuMu^X. Chapter 9 describes our main contributions related to the development and

the implementation of new numerical schemes in the DuMu^X framework in a high performance computing context. From 2009 to 2013, we have been involved in the European project FORGE (Fate Of Repository Gases: http://www.bgs.ac.uk/forge/) that aimed at studying gas migration in deep repository for radioactive waste. In order to deal with the complexity of the geometries to be considered and the strong heterogeneity of the different materials, we coupled DuMu^X with an upscaling strategy [13]. Section 9.2 shows that our mathematical upscaling method combined to a finite-volume method was capable to reduce drastically the computational time, while producing results in a robust and accurate fashion. From January 2013, in the frame of the PhD thesis of V. Vostrikov [301] that I co-advised with B. Amaziane (University of Pau & Pays Adour) and M. Kern (INRIA Paris), we were interested in the numerical simulation of two-phase reactive flow in porous media, with an application to the geological storage of CO_2. We chose a sequential approach to tackle the problem: a two-phase compositional flow is solved, followed by a reactive transport problem. For this latter, several strategies were considered. In [29, 301], the reactive transport problem was tackled by a sequential iterative approach (SIA) where transport and equilibrium chemical reactions were solved sequentially in a iterative loop. Precisely, we developed and integrated in DuMu^X a multicomponent transport module, coupled iteratively with a locally developed code for chemical equilibrium, called ChemEqLib using the GSL library [5]. In [30], the code ChemEqLib was dropped and the chemistry calculations were directly integrated in DuMu^X. Still considering a SIA, kinetic chemical reactions that were not taken into account until now were added to the transport, and equilibrium chemical calculations. To reduce the possible splitting errors and increase the robustness of our strategy, in [14, 15] the SIA was replaced by a global implicit approach (GIA) to solve the reactive transport subproblem. These developments have been validated by numerous benchmarks with applications concerning geological sequestration of CO_2 [15, 29, 30] and geological storage of nuclear waste in deep repository [14]. Section 9.3 is dedicated to the presentation of simulations using this sequential approach with some comparison between different strategies. Since January 2017, I have been co-supervising the PhD thesis of M. Id Moulay [215] with B. Amaziane. This PhD thesis aims at developing a fully coupled fully implicit strategy to perform numerical simulation of two-phase reactive flow. Indeed, sequential approaches can introduce operator splitting errors requiring restrictions on the time step that can be prohibitive. First, a fully implicit approach has been considered to deal with single phase reactive flows and intensively validated through benchmarks including parallel computations [15]. Then, this methodology has been extended for two-phase reactive flows [16]. Section 9.4 presents some numerical simulations of reactive flows using fully implicit approach. Particular attention is paid to the comparison between sequential and global implicit approaches in terms of accuracy and computational time.

For the sake of consistency of the present manuscript, some of my research activities have been purposely discarded. From October 2009 to September 2010, I was a post-doctoral fellow in the laboratory TREFLE in collaboration with the company ABENGOA. During this position, we investigated a Singular Value Decomposition (SVD) method to process thermography data for the characterization of thermal parameters. The inverse problem to solve is based on the model of transient heat transfer. The most significant advantage is the transformation of the dynamic identification problem into a steady identification equation. Truncated SVD provided and accurate thermal parameters estimation, even for noisy data [17]. In [18], we proposed a strategy to automatically simplify Darcy's equations with pressure dependent permeability. In the framework of spectral element methods, *a posteriori* estimates allowed us to omit this dependence where the pressure does not vary too much. We performed the numerical analysis of a spectral element discretization of the simplified model and we proposed a strategy which leads to an automatic identification of the part of the domain where the simplified model can be used without increasing significantly the error.

Finally, Chapter 10 presents some conclusions and research perspectives for the next years. Two upcoming projects are directly related to our recent work. First we will be involved in the Horizon 2020 European Joint Programme on Radioactive Waste Management (EURAD). For this project, we aim at going towards simulations taken into account coupled thermo-hydro-mechanical-chemical (THMC) processes in porous media that represent a crucial issue for the performance assessment of geological disposal of radioactive waste. Secondly, we will be involved in the CO2ES project (CO_2 Enhanced Storage) whose objective is to provide a better understanding of the various CO_2 trapping and transport processes involved in CO_2 geological storage. The project is mainly experimental but we will perform some numerical simulations to scale-up the phenomena pointed out in the experimental part by using homogenization tools as well as guiding further experimental activities. A third project will be dedicated to the numerical simulation of multicomponent fluid in nano-porous media. For this kind of simulation, classical approaches such as Darcy's or Stokes' formulations that are at the heart of Parts I and II are not always relevant and a new paradigm will be proposed, using among others, molecular dynamics simulations. Finally, we would like to apply and adapt reduced-order models to the applications described above.

Part I

CFD simulations of incompressible flows

Introduction

Computational Fluid Dynamics (CFD) combines numerical analysis and computer science to analyze and solve problems involving fluid flows. CFD has numerous applications, ranging from academic research to industrial issues. We can mention non exhaustively aerodynamic, weather simulation, natural and environmental science or biological engineering. Most of the works described in this Part are devoted to the particular case of incompressible flows governed by the incompressible Navier-Stokes equations. In recent years, one can observe a trend regarding flow simulations: the requirement for higher accuracy in the computational resolution with a need to obtain results faster. To meet the high accuracy requirements, a part of my contributions deal with spectral elements methods [78, 103]. It is the continuity of my PhD thesis [12] where I used spectral element methods for the approximation of the -**grad**(div(.)) operator and several applications related to Stokes eigenvalues problem and Navier-Stokes equations were considered.

In this context of high order methods, Chapter 3 discusses several strategies to compute the 2D Stokes eigenvalue problem. The content of the chapter is based on the articles [24, 25]. We consider the 2D Stokes eigenvalue problem as model example for the approximation of eigenvalues and associated eigenfunctions of a linear operator under an incompressibility constraint. One of the difficulties is to propose methods of approximation which satisfy in a stable and accurate way the eigenvalues equations, the incompressibility constraint and the boundary conditions. Using any non-stable method leads to the presence of non-physical eigenvalues: a multiple zero one called spurious modes and non-zero ones called pollution modes. One way to eliminate these two families is to favor the constraint equations by satisfying it exactly and to verify the equations of the eigenvalues equations in weak ways. To illustrate our contribution in this field, we considered and described several methods producing the correct number of eigenvalues. Numerical results proved how these methods are adequate to correctly solve the 2D Stokes eigenvalue problem.

Chapter 4 describes a work dedicated to the Hodge Helmholtz decomposition that consists in extracting the solenoidal, irrotational and harmonic parts from a given vector field. It is based on the article [20]. Our method consists in projecting the vector to be decomposed on solenoidal and irrotational basis, constructed in a original way. After validation on analytical test cases, the method has been used to deal with an unsteady Navier-Stokes problem, to solve the projection step in a Goda pressure correction scheme.

In Chapter 5, we present a numerical scheme for incompressible Navier-Stokes equations with open boundary conditions, in the framework of the pressure and velocity correction schemes. It is based on the articles [23, 247]. In [248], the authors presented an almost second-order accurate version of the open boundary condition with a pressure-correction scheme in finite volume framework. We extended this method in spectral element method framework for both pressure- and velocity-correction schemes. A new way to enforce this type of boundary condition has been proposed and provided a pressure and velocity convergence rate in space and time higher than with the present state of the art. Some numerical tests illustrated the efficiency of the approach.

The second part of my contribution to numerical simulation of incompressible flows concerns the implementation of new features on the Finite-Volume code named Thetis developed at the TREFLE laboratory. This CFD code was based on a marker and cell [144] orthogonal curvilinear structured grid. To overcome this software constraint and extend the use of the code to more complex geometries, Chapter 6 describes a domain decomposition method to run the Navier-Stokes equations efficiently on non-matching and overlapping block-structured meshes [26]. Precisely, using a pressure correction scheme, we improved a method first introduced in [258] and [259] where the authors reported a problem of mass conservation and a discontinuity of pressure through the interfaces between different meshes. With our new implementation, the pressure is continuous through the interfaces and the incompressibility constraint is ensured

over the whole domain. Several numerical tests were carried out to assess the proposed method.
Computational fluid dynamics simulations aim at solving increasingly complex and large problems, as quickly as possible. To achieve these requirements, they must rely on High-Performance Computing (HPC). In parallel computing, the computational domain is distributed over several processors. The partitioning strategy must best respect load balancing (each processor must have approximately the same workload) while trying to minimize exchanges between processors. Chapter 7 presents a work based on the article [27] where we developed a mesh partitioner to carry out parallel simulations of incompressible flows on block-structured meshes. Because classical partitioner as CHACO [147], METIS [167], SCOTCH [239] were not suitable for structured meshes, we proposed a new partitioning method. The quality of rectangular partitions was checked and compared with other methods, as regards load balance, edge-cut and block numbers. The partitioner was coupled with the massively parallel HYPRE solver library [110] and good strong and weak parallel efficiencies were obtained. Finally, the code was applied to study laminar flows (steady and unsteady) on non-rectangular geometries, using very fine grids to compute reference solutions.

Chapter 3

Computation of the Stokes eigenvalue problem

Contents

This chapter covers the entirety of article [25] and is also based on article [24] which can be found in the Appendix. Both articles are listed below:

- E. Ahusborde, M. Azaïez, R. Gruber, Numerical Assessment of a Class of High Order Stokes Spectrum Solver, Journal of Mathematical Study, Vol 51, 1-14, 2018.

  Abstract*: It is well known that the approximation of eigenvalues and associated eigenfunctions of a linear operator under constraint is a difficult problem. One of the difficulties is to propose methods of approximation which satisfy in a stable and accurate way the eigenvalues equations, the constraint one and the boundary conditions. Using any non-stable method leads to the presence of non-physical eigenvalues: a multiple zero one called spurious modes and non-zero one called pollution modes. One way to eliminate these two families is to favor the constraint equations by satisfying it exactly and to verify the equations of the eigenvalues equations in weak ways. To illustrate our contribution in this field we consider in this paper the case of Stokes operator. We describe several methods that produce the correct number of eigenvalues. We numerically prove how these methods are adequate to correctly solve the 2D Stokes eigenvalue problem.*

- E. Ahusborde, M. Azaïez, R. Gruber, Constraint oriented spectral element method, Lecture Notes in Computational Science and Engineering, Vol 76, 93-100, 2011.

  Abstract*: An original polynomial approximation to solve partial differential equations is presented. This spectral element version takes into account the underlying nature of the corresponding physical problem. For different types of operators, this approach allows to all terms in a variational form to be represented by the same functional dependence and by the same regularity, thus*

eliminating regularity constraints imposed by standard numerical methods. This method satisfies automatically different type of constraints, such as occur for the grad(div) and curl(curl) operators, and this for any geometry. It can be applied to a wide range of physical problems, including fluid flows, electromagnetism, material sciences, ideal linear magnetohydrodynamic stability analysis, and Alfvèn wave heating of fusion plasmas.

3.1 Introduction

This chapter deals with the numerical computation of the 2D Stokes eigenvalue problem on a square domain. This problem is considered as model example with a conservation law of the type $\nabla \cdot \vec{u} = 0$. With this test example it is possible to discuss the various numerical problems that appear when flux conservation has to be satisfied in the incompressible Navier-Stokes equations. If these constraint condition cannot be satisfied precisely, so-called spectral pollution [132] appears and the numerical approach does not stably converge to the physical solution. The reason is that due to regularity constraints imposed by standard numerical approximation methods, the energy cannot reach the minimum required by the physics. In fact, current numerical methods satisfy the boundary conditions strongly, the operator equations and the constraints only weakly. If the constraint $\nabla \cdot \vec{u} = 0$ is satisfied by a $\vec{u} = \nabla \times \psi$ ansatz, the number of degrees of freedom remains the same as in the unconstrained Laplacian problem. As a consequence, besides the Stokes modes, one finds a whole spectrum of additional unphysical modes, corresponding to those of the heat equation. Thus, the initial physical problem has fundamentally been changed. This approach has been applied to compute the full Stokes spectrum [186] by the first time. Due to the choice of a unit square domain, the authors were able to separate the Stokes modes from those belonging to the heat equation.
In Section (3.2), we present the 2D Stokes eigenvalue problem and we focus on two formulations considering only the velocity as variable: the penalty method and the divergence-free Galerkin approach. In Section (3.3), in the framework of spectral element approximation schemes, a stable spectral element is proposed for each method. For the penalty method, a COOL approach [24, 28] is considered and the unphysical modes can be pushed towards $\lambda = 0$. For the divergence-free Galerkin approach, two strategies christened "explicit" and "implicit" are detailed. The explicit strategy consists in using the properties of the kernel of the grad(div) operator to construct a divergence-free basis. Such a basis has the right number of degrees of freedom, thus delivering the exact number of Stokes eigenfunctions with high precision. The implicit strategy is a direct algebraic elimination process of the $\nabla \cdot \vec{u} = 0$ constraint. This leads to a sparse matrix elimination process, described in detail in [28]. It delivers the right number of highly precise Stokes modes.
Finally, in Section (3.4), some numerical experiments are performed to prove the efficiency of the proposed methods and a comparison between the different approaches is given.

3.2 The Stokes eigenvalue problem: continuous version

Let $\Omega \subset I\!R^d$, $d = 2,3$, be a Lipschitz domain, the generic point of Ω is denoted x. The symbol $L^2(\Omega)$ stands for the usual Lebesgue space and $H^1(\Omega)$, the Sobolev space that involves all the functions that are, together with their gradient, in $L^2(\Omega)$.$\mathscr{C}(\Omega)$ denotes the space of continuous functions defined in Ω.

The continuous Stokes eigenvalue problem reads: *Find a vector* $\vec{u}$ *and* $\lambda^2 \in I\!R^+$ *such that*

$$\begin{array}{rcll} -\Delta\vec{u} & = & \lambda^2\vec{u}, & \text{for } x \in \Omega, \\ \nabla\cdot\vec{u} & = & 0, & \text{for } x \in \Omega, \\ \vec{u} & = & \vec{0}, & \text{for } x \in \partial\Omega, \end{array} \tag{3.1}$$

where $I\!R^+$ denotes the set of positive real numbers, including zero. For the sake of simplicity we assume here that Ω is the reference domain $(-1,+1)^2$.

Problem (3.1) is often solved using different strategies but we prefer to focus on methods involving only $\vec{u}$ as unknown. The first one is called *Penalty method*

Penalty method This method consists in taking into account the divergence free constraint by adding a term of penalty to control the level of divergence when solving the eigenvalue problem.

The penalty formulation, called also regularization method (see [127]), reads: *Find* $\vec{u} \in (H_0^1(\Omega))^2$ *and* $\lambda^2 \in I\!R^+$ *such that*

$$-\Delta\vec{u} - \alpha\nabla(\nabla\cdot\vec{u}) \;=\; \lambda^2\vec{u}, \quad \text{for } x \in \Omega. \tag{3.2}$$

Its variational formulation writes: *Find* $\vec{u} \in (H_0^1(\Omega))^2$ *and* $\lambda^2 \in I\!R^+$ *such that*

$$\int_\Omega \nabla\vec{u}\cdot\nabla\vec{v}dx + \alpha\int_\Omega \nabla\cdot\vec{u}\nabla\cdot\vec{v}dx \;=\; \lambda^2\int_\Omega \vec{u}\cdot\vec{v}d\vec{x}, \forall\vec{v} \in (H_0^1(\Omega))^2. \tag{3.3}$$

In practice, the infinite dimensional problem (3.3) is replaced by a finite dimensional one using a stable spectral element taking into account the constraint by an adequate choice of α (see [24]).

Divergence-free Galerkin approach The second method is called "divergence-free Galerkin approach" and starts from the fact that the system (3.3) can reduce to: *Find* $\vec{u} \in \vec{X}$ *and* $\lambda^2 \in I\!R^+$ *such that*

$$\mathscr{S}(\vec{u},\vec{v}) := \textstyle\int_\Omega \nabla\vec{u}\cdot\nabla\vec{v}dx \;=\; \lambda^2 \int_\Omega \vec{u}\cdot\vec{v}dx, \quad \forall\vec{v} \in \vec{X}, \tag{3.4}$$

where $\vec{X}$ is in the space defined by

$$\vec{X} = \left\{\vec{v} \in (H_0^1(\Omega))^2, \quad \text{such that} \quad \nabla\cdot\vec{v} = 0\right\}. \tag{3.5}$$

Again the infinite dimensional problem (3.4) is replaced by a finite dimensional one using a stable spectral element that will be developed later.

3.3 The Stokes eigenvalue problem: discrete version

We firstly introduce some notations and reminders. Let $\Sigma_{GLL} = \{(\xi_i, \rho_i);\, 0 \le i \le p\}$ and $\Sigma_{GL} = \{(\zeta_i, \omega_i);\, 1 \le i \le p\}$ respectively denote the sets of Gauss-Lobatto-Legendre and Gauss-Legendre quadrature nodes and weights associated to polynomials of degree p. These quantities are such that on $\Lambda :=]-1,+1[$

$$\forall\,\Phi \in I\!P_{2p-1}(\Lambda), \qquad \int_{-1}^{+1}\Phi(\xi)\,d\xi \;=\; \sum_{j=0}^{p}\Phi(\xi_j)\,\rho_j, \tag{3.6}$$

$$\forall\,\Phi \in I\!P_{2p-1}(\Lambda), \qquad \int_{-1}^{+1}\Phi(\zeta)\,d\zeta \;=\; \sum_{j=1}^{p}\Phi(\zeta_j)\,\omega_j, \tag{3.7}$$

where $I\!P_p(\Lambda)$ denotes the space of polynomials with degree $\leq p$. We recall that the nodes $\xi_i\,(0 \leq i \leq p)$ are solution to $(1-x^2)L'_p(x) = 0$ where L_p denotes the Legendre polynomial of degree p, whereas $\zeta_i\,(1 \leq i \leq p)$ are solution to $L_p(x) = 0$ (see [103]).

The canonical polynomial interpolation basis $h_i(x) \in I\!P_p(\Lambda)$ built on Σ_{GLL} is given by the relationships:

$$h_i(x) = -\frac{1}{p(p+1)}\frac{1}{L_p(\xi_i)}\frac{(1-x^2)\,L'_p(x)}{(x-\xi_i)}, \qquad -1 \leq x \leq +1, \quad 0 \leq i \leq p, \tag{3.8}$$

with the elementary cardinality property

$$h_i(\xi_j) = \delta_{ij}, \qquad 0 \leq i,j \leq p, \tag{3.9}$$

where δ_{ij} is Kronecker's delta symbol.

We also introduce a new family of polynomials functions $g_i(x)$ associated to the canonical basis (3.8) through the relationships:

$$g_i(x) = h_i(x) - \beta_i L_p(x), \qquad 0 \leq i \leq p, \tag{3.10}$$

where the constants β_i are such that all $g_i(x) \in I\!P_{p-1}(]-1,+1[)$ [28, 24]. The functions $g_i(x)$ have the following properties:

1. Their moments up to order $(p-1)$ are equal to those of their corresponding element in the Gauss-Lobatto-Legendre canonical basis, *i.e.*: *For* $0 \leq i \leq p$,

$$\int_{-1}^{+1} (g_i(x) - h_i(x))\,x^j\,dx = 0, \qquad \forall\, j, \quad 0 \leq j \leq (p-1). \tag{3.11}$$

   The difference $(g_i(x) - h_i(x))$ being proportional to $L_p(x)$ is orthogonal to all polynomials of degree less or equal to $(p-1)$.

2. Interpolation of their corresponding element in the canonical basis at the Gauss-Legendre nodes, *i.e.*: *For* $0 \leq i \leq p$,

$$g_i(\zeta_j) = h_i(\zeta_j), \qquad \forall\, j, \quad 1 \leq j \leq p. \tag{3.12}$$

3. The constants β_i can be obtained through a series expansion of (3.8) and one gets:

$$\beta_i = \frac{1}{(p+1)\,L_p(\xi_i)}, \qquad 0 \leq i \leq p. \tag{3.13}$$

In [24] one can read more informations concerning these polynomial functions.

3.3.1 Penalty method

In [24], we present a detailed description of this method. The discrete version of problem (3.3) writes: *Find* $\vec{u}_p \in Y_p$ *and* $\lambda^2 \in I\!R^+$ *such that*

$$\mathscr{A}_p(\vec{u}_p,\vec{v}_p) + \alpha\,\mathscr{B}_p(\vec{u}_p,\vec{v}_p) = \lambda^2(\vec{u}_p,\vec{v}_p)_p, \quad \forall \vec{v}_p \in Y_p, \tag{3.14}$$

where:

$$\mathscr{A}_p(\vec{u}_p,\vec{v}_p) = (\nabla\vec{u}_p,\nabla\vec{v}_p)_p, \tag{3.15}$$

$$\mathscr{B}_p(\vec{u}_p,\vec{v}_p) = (\nabla\cdot\vec{u}_p,\nabla\cdot\vec{v}_p)_p. \tag{3.16}$$

Here $(\cdot,\cdot)_p$ is discrete scalar product based on Gauss Lobatto quadrature formula. Y_p is the space of polynomial functions of degree lower or equal to p vanishing on $\partial\Omega$. It is assumed to ensure a stable approximation for grad(div) operator to avoid the phenomenon of spurious pollution [24]. Since $\vec{u}_p$ is equal to zero on the boundary, the solution $\vec{u}_p \in \vec{Y}_p$ is approximated by $u^{(0)}_{rp}(x,y)$, $u^{(1)}_{rp}(x,y)$ or $u^{(2)}_{rp}(x,y)$ according to the functional dependence and the regularity required ($r = x$ or y).

$$\begin{aligned} u^{(0)}_{rp}(x,y) &= \sum_{i=1}^{p-1}\sum_{j=1}^{p-1} u^{rp}(\xi_i,\xi_j)\, g_i(x)\, g_j(y), \\ u^{(1)}_{rp}(x,y) &= \sum_{i=1}^{p}\sum_{j=1}^{p-1} u^{rp}(\xi_i,\xi_j)\, h_i(x)\, g_j(y), \\ u^{(2)}_{rp}(x,y) &= \sum_{i=1}^{p}\sum_{j=1}^{p-1} u^{rp}(\xi_i,\xi_j)\, g_i(x)\, h_j(y). \end{aligned} \tag{3.17}$$

The superscript $^{(1)}$ is used to represent quantities derived in direction x while superscript $^{(2)}$ is used to represent quantities derived in direction y. The coefficients in the previous three expansions are the same thanks to (3.12).
Replacing $\vec{u}_p$ by the previous development in (3.14), the penalty discrete form writes

$$\begin{aligned} (\partial_x u^{(1)}_{xp}, \partial_x v^{(1)}_{xp})_p + (\partial_y u^{(2)}_{yp}, \partial_y v^{(2)}_{yp})_p &+ \alpha\,(\partial_x u^{(1)}_{xp} + \partial_y u^{(2)}_{yp}, \partial_x v^{(1)}_{xp} + \partial_y v^{(2)}_{yp})_p \\ &= \lambda^2 (\vec{u}^{(0)}_p, \vec{v}^{(0)}_p)_p, \quad \forall \vec{v}_p \in Y_p. \end{aligned} \tag{3.18}$$

3.3.2 Divergence-free Galerkin approach

The keystone of the divergence-free Galerkin approach is the construction of a discrete version X_p of the divergence free space $\vec{X}$ defined in equation (3.5).

According to [28], we need the divergence to be a polynomial of degree less or equal to $p-1$. Consequently, we want to build a space:

$$\vec{X}_p = \{\vec{u}_p \in (I\!P_p(\Omega))^2 \mid \nabla\cdot\vec{u}_p \in I\!P_{p-1}(\Omega)\} \cap \vec{X}.$$

Expanding $\vec{u}_p$ according to (3.17) its divergence is a polynomials of degree $p-1$. Consequently, if the divergence is orthogonal to all polynomial of $I\!P_{p-1}(\Omega)$, it is necessarily equal to 0. This point gives a new characterization for $\vec{X}_p$:

$$\vec{X}_p = \{\vec{u}_p \in (I\!P^0_p(\Omega))^2 \mid \int_\Omega (\frac{\partial u^{(1)}_{xp}}{\partial x} + \frac{\partial u^{(2)}_{yp}}{\partial y}) q\, d\vec{x} = 0,\ \forall q \in I\!P_{p-1}(\Omega)\}.$$

We want to build a basis of $\vec{X}_p$. The first step consists in determining the size of this space.

$$\dim \vec{X}_p = \dim\,(I\!P^0_p(\Omega))^2 - p_2,$$

where p_2 is the number of necessary and sufficient equations to ensure $\nabla\cdot\vec{u}_p \equiv 0$.
$\nabla\cdot\vec{u}_p \in I\!P_{p-1}(\Omega)$ therefore $p_2 \le p^2$.
There are 2 dependent equations in $2D$ (see [61] for details) since:

$$\begin{aligned} \int_\Omega \nabla\cdot\vec{u}_p\, L_0(x) L_0(y) d\vec{x} &= 0,\ \forall \vec{u}_p \in (I\!P^0_p(\Omega))^2, \\ \int_\Omega \nabla\cdot\vec{u}_p\, L'_p(x) L'_p(y) d\vec{x} &= 0,\ \forall \vec{u}_p \in (I\!P^0_p(\Omega))^2. \end{aligned}$$

Polynomials $L_0(x)L_0(y)$ and $L'_p(x)L'_p(y)$ are spurious modes and reduce the number of independent equations from p^2 to p^2-2. Consequently, we require $p_2 = p^2-2$ test functions q to ensure $\int_\Omega \nabla\cdot\vec{u}_p\, q\, d\vec{x} = 0$.

$$\dim \vec{X}_p = \dim\,(I\!P_p^0(\Omega))^2 - p_2 = 2(p-1)^2 - (p^2-2) = (p-2)^2.$$

After the computation of the size of $\vec{X}_p$ (denoted $p_1 = (p-2)^2$ in the sequel), we propose two strategies to compute a divergence-free basis.

3.3.2.1 Divergence-free Galerkin explicit approach

We consider the following eigenvalue problem:

$$\begin{array}{rcll} -\nabla(\nabla\cdot\vec{u}) & = & \lambda^2\vec{u}, & \text{for } x \in \Omega, \\ \vec{u} & = & \vec{0}, & \text{for } x \in \partial\Omega. \end{array} \tag{3.19}$$

The kernel of the grad(div) operator includes all the modes $\vec{u}^k_{s,p}$ associated to $\lambda^2 = 0$ and $\nabla\cdot\vec{u}^k_{s,p} = 0$. It constitutes a basis for the subspace $\vec{X}_p$. Its size is $(p-2)^2$ and then $\vec{u}_p \in \vec{X}_p$ can be decomposed according to the following form:

$$\vec{u}_p = \sum_{k=1}^{(p-2)^2} \beta_k\, \vec{u}^k_{s,p}.$$

Replacing $\vec{u}_p$ by the previous development in (3.4), the discrete variational formulation writes: *Find* $\vec{u}_p \in \vec{X}_p$ *and* $\lambda^2 \in I\!R^{+*}$ *such that*

$$\sum_{k=1}^{(p-2)^2} (\nabla\vec{u}^k_{s,p}, \nabla\vec{u}^i_{s,p})_p \beta_k = \lambda^2 \sum_{k=1}^{(p-2)^2} (\vec{u}^k_{s,p}, \vec{u}^i_{s,p})_p\, \beta_k, \forall \vec{u}^i_{s,p} \in \vec{X}_p.$$

This can be written:

$$\underline{\mathscr{S}^e}\,\underline{\beta} = \lambda^2\,\underline{\mathscr{M}^e}\,\underline{\beta}.$$

The stiff matrix $\mathscr{S}^e$ and mass matrix $\mathscr{M}^e$ are symmetric and positive definite and are defined by:

$$\begin{array}{rcl} \underline{\mathscr{S}^e_{ik}} & = & (\nabla\vec{u}^k_{s,p}, \nabla\vec{u}^i_{s,p})_p, \\ \underline{\mathscr{M}^e_{ik}} & = & (\vec{u}^k_{s,p}, \vec{u}^i_{s,p})_p, \end{array}$$

for $(1 \le i,\, k \le (p-2)^2)$.

3.3.2.2 Divergence-free Galerkin implicit approach

As highlighted before, the main difficulty of the problem (3.1) consists in satisfying the incompressibility constraint $\nabla\cdot\vec{u} = 0$. Classical approaches usually satisfy operator equations strongly with as many equations as degrees of freedom for the velocity while incompressibility constraint is only satisfied weakly with fewer equations than degrees of freedom for the divergence. Contrary to the classical approaches, our objective is to favor the incompressibility constraint in comparison with the other equations. Our strategy, introduced in [28], consists in sharing the degrees of freedom of $\vec{u}$ in a relevant way to satisfy:

- The incompressibility constraint in strong sense.

- The other equations in weak sense.

Let $\vec{u}_p$ be in $\vec{X}_p$. The divergence of $\vec{u}_p$ is orthogonal to p^2-2 polynomials of degree $p-1$. It is equivalent to saying that the divergence of $\vec{u}_p \in \vec{X}_p$ nullifies in p^2-2 Gauss points. The algebraic divergence equation writes $D\vec{u}_p = 0$ (see Figure (4.1)).

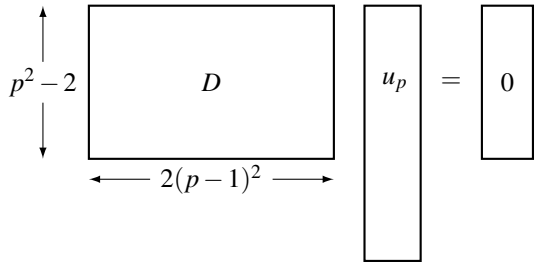

Figure 3.1: Algebraic system.

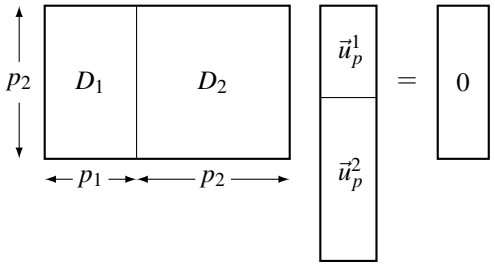

Figure 3.2: Decomposition of D.

D is a rectangular matrix with $p_2 = p^2-2$ rows and $2(p-1)^2$ columns.
Then, one splits D into $D_1 \oplus D_2$ and $\vec{u}_p$ into $\vec{u}_{1\,p} \oplus \vec{u}_{2\,p}$ (see Figure (4.2)).

Since, the p^2-2 lines of D are independent, there is at least one choice of matrix D_2 invertible. Equation $D\vec{u}_p = 0$ becomes:

$$D_1\,\vec{u}_{1\,p} + D_2\,\vec{u}_{2\,p} = 0.$$

For instance, $\vec{u}_1$ contains the p_1 first values of $\vec{u}_p$ and consequently $\vec{u}_{2\,p}$ contains the p_2 remaining values. Figure (4.3) displays the sizes of the matrices D_2 and D_1.

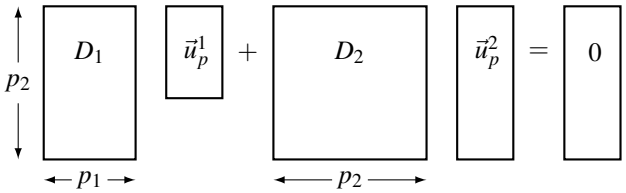

Figure 3.3: Algebraic system $D_1\,\vec{u}_{1\,p} + D_2\,\vec{u}_{2\,p} = 0$.

Since D_2 is invertible, the system leads to a relation between $\vec{u}_{1\,p}$ and $\vec{u}_{2\,p}$:

$$\vec{u}_{2\,p} = -D_2^{-1} D_1 \vec{u}_{1\,p}. \tag{3.20}$$

Eq. (3.20) is crucial since it means that if we have any part $\vec{u}_{1\,p}$ of $\vec{u}_p$, we can build the complementary $\vec{u}_{2\,p}$ such that divergence of $\vec{u}_p$ equals 0. This argument allows us to build a basis of $\vec{X}_p$.

We consider $\vec{v}_p \in (I\!P_p^0(\Omega))^2$. Our strategy consists in combining implicitly:

- A reduction from $\vec{v}_p$ to $\vec{v}_{1\,p}$,
- An extension from $\vec{v}_{1\,p}$ to $\vec{w}_p = (\vec{v}_{1\,p}, \vec{v}_{2\,p})$ such that $\nabla \cdot \vec{w}_p = 0$ ensured by the multiplication of $\vec{v}_{1\,p}$ by the matrix

$$M = \begin{bmatrix} I_{p_1} \\ -D_2^{-1} D_1 \end{bmatrix}.$$

The matrix M is a two blocks matrix. The first block is a matrix of order p_1 equal to identity. The second block contains p_2 rows and p_1 columns. It ensures the passage from $\vec{v}_{1\,p}$ to $\vec{v}_{2\,p}$.

- For each $\vec{v}_p \in (I\!P_p^0(\Omega))^2$, one associates a vector $\vec{w}_p$ of $\vec{X}_p$.

By consequent, our strategy for the construction of a basis of $\vec{X}_p$ consists in:

- Choosing $p_1 = (p-2)^2$ vectors $(v_p^k)_{k=1,\ldots,p_1}$ of the basis of $(I\!P_p^0(\Omega))^2$ (for instance, the $(p-2)^2$ first vectors),
- For each one of these p_1 vectors, we consider its p_1-size reduced part denoted $\vec{v}_{1\,p}^{\,k}$,
- We carry out the divergence-free extension $(\vec{w}_p^k)_{k=1,\ldots,p_1} = (M\,\vec{v}_{1\,p}^{\,k})_{k=1,\ldots,p_1}$.

The $(\vec{w}_p^k)_{k=1,\ldots,p_1}$ family is a basis of $\vec{X}_p$ and every $\vec{u}_p \in \vec{X}_p$ can be decomposed according to the following form:

$$\vec{u}_p = \sum_{k=1}^{p_1} \gamma_k\, \vec{w}_p^k.$$

Replacing $\vec{u}_p$ by the previous development, the discrete variational formulation writes: *Find* $\vec{u}_p \in \vec{X}_p$ *and* $\lambda^2 \in I\!R^{+*}$ *such that*

$$\sum_{k=1}^{p_1} (\nabla \vec{w}_p^k, \nabla \vec{w}_p^{\,\mathrm{i}})_p\, \gamma_k = \lambda^2 \sum_{k=1}^{p_1} (\vec{w}_p^k, \vec{w}_p^{\,\mathrm{i}})_p\, \gamma_k,\ \forall \vec{w}_p^{\,\mathrm{i}} \in \vec{X}_p.$$

This can be written:

$$\underline{\mathscr{S}^i}\,\underline{\gamma} = \lambda^2\,\underline{\mathscr{M}^i}\,\underline{\gamma},$$

with for $(1 \le i,k \le p_1)$,

$$\begin{aligned} \underline{\mathscr{S}^i}_{ik} &= (\nabla \vec{w}_p^k, \nabla \vec{w}_p^{\,\mathrm{i}})_p, \\ \underline{\mathscr{M}^i}_{ik} &= (\vec{w}_p^k, \vec{w}_p^{\,\mathrm{i}})_p. \end{aligned}$$

$\underline{\mathscr{S}^i}$ and $\underline{\mathscr{M}^i}$ refer respectively to the Laplace operator and mass matrices expressed on the basis $\vec{w}_p$.

Finally, this system is equivalent to:

$$M^T A M\, \vec{u}_{p1} = \lambda^2 M^T B M\, \vec{u}_{p1},$$

where A and B refer respectively to the classical Laplacian and mass matrices.

3.4 Numerical results

This section discusses some numerical results. We will apply each of the three approaches to compute the Stokes eigenvalues and associated eigenfunctions.

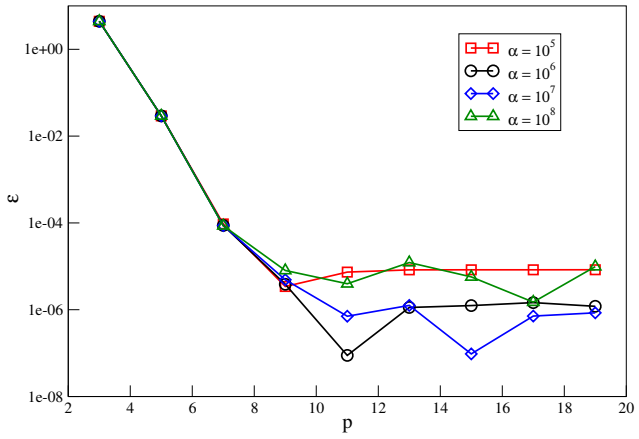

Figure 3.4: Convergence plots obtained using the penalty method for the first Stokes mode ($\lambda^2 = 13.086172791$) as a function of the polynomial order p for several values of α.

p	4	8	12	16	20
min $\|\|\nabla\cdot\vec{u}_p\|\|_{L^2(\Omega)}$	8.1×10^{-7}	8.97×10^{-7}	8.97×10^{-7}	8.97×10^{-7}	8.97×10^{-7}
max $\|\|\nabla\cdot\vec{u}_p\|\|_{L^2(\Omega)}$	8.92×10^{-6}	7.66×10^{-5}	2.54×10^{-5}	5.95×10^{-4}	1.15×10^{-3}

Table 3.1: Maximum and minimum of the $L^2(\Omega)$-norm of the divergence of all the Stokes eigenmodes as a function of p.

Penalty approach Figure (3.4) displays the convergence for the lowest eigenvalue of problem (3.2) for several values of α.

One can see that the choice of α leads to slightly different convergence behaviors. For double precision arithmetic, $\alpha = 10^7$ appears to give the best convergence results. With an increasing polynomial degree to represent the eigenfunction, the eigenvalue converges exponentially as expected for $p \leq 9$. Increasing p further does not improve the accuracy of the eigenvalue, with the precision limited to 10^{-6}. Tab. (3.1) shows the limit in precision for the incompressibility condition for $\alpha = 10^7$ as a function of p.

The eigenvalue problem (3.14) gives $2(p-1)^2$ eigenvalues and associated eigenvectors corresponding to the degrees of freedom in Y_p. Among these eigenvalues, there are the Stokes eigenvalues and the non-zero eigenvalues of the grad(div) operator multiplied by α. The number of Stokes eigenvalues $\mathcal{N}_S$ corresponds to the size of the kernel of the discretized grad(div) operator, *i.e.* to the number of zero eigenvalues. As said in Section (3.3.2.1), it can be proved that this number is equal to $(p-2)^2$. Consequently, the resolution of the problem (3.14) leads to $\mathcal{N}_S = (p-2)^2$ Stokes eigenmodes. The p^2-2 remaining eigenmodes are those of the class of non-zero eigenvalues of the grad(div) operator multiplied by α.

Figure (3.5) illustrates the convergence of the difference ε between the four lowest Stokes eigenvalues as a function of p computed by our method with those produced in [186] for $\alpha = 10^7$ on a semi-logarithmic scale. The error is exponentially decreasing as expected for $p \leq 11$ and then stagnates.

Divergence-free Galerkin explicit approach Figure (3.6) illustrates the convergence of the difference ε between the four lowest Stokes eigenvalues as a function of p computed by the divergence-free

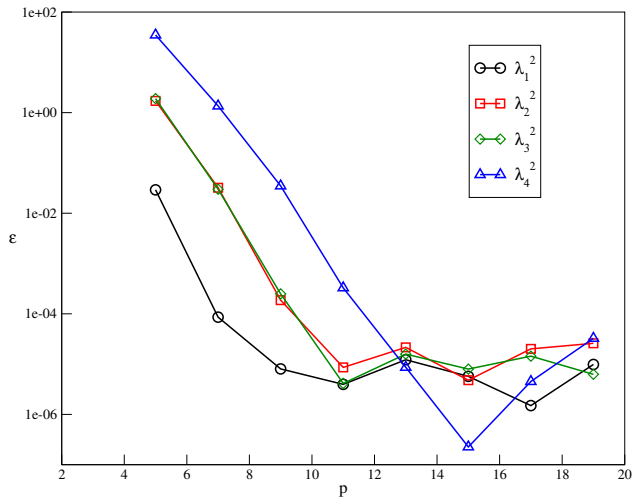

Figure 3.5: Convergence plots obtained using the penalty method for the four lowest divergence-free modes as a function of p. Again, $\alpha = 10^7$.

Galerkin explicit approach with those produced in [186] on a semi-logarithmic scale. The error is exponentially decreasing as expected.

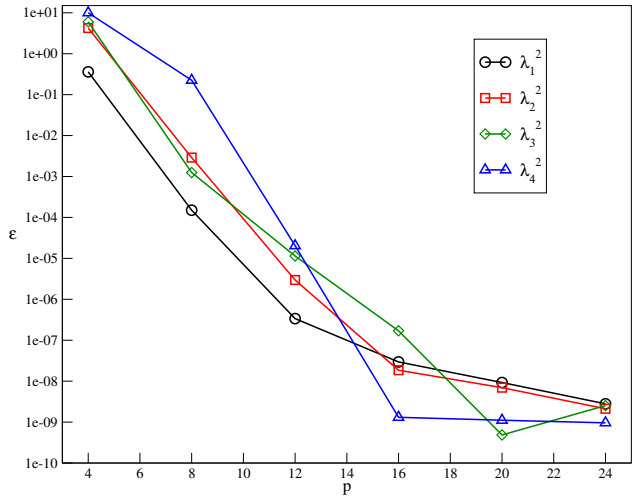

Figure 3.6: Convergence plots obtained using the divergence-free Galerkin explicit approach method for the four lowest divergence-free modes as a function of p.

Divergence-free Galerkin implicit approach To validate our divergence-free Galerkin implicit approach, we have computed the Stokes eigenvalues and compared with those obtained in [186]. Figure (3.7) shows the convergence for the four lowest eigenvalues as a function of p on a semi-logarithmic scale. The calculation of the eigenvalues converges exponentially as expected.

It has been shown theoretically that the eigenmodes have a global structure with an infinite series of

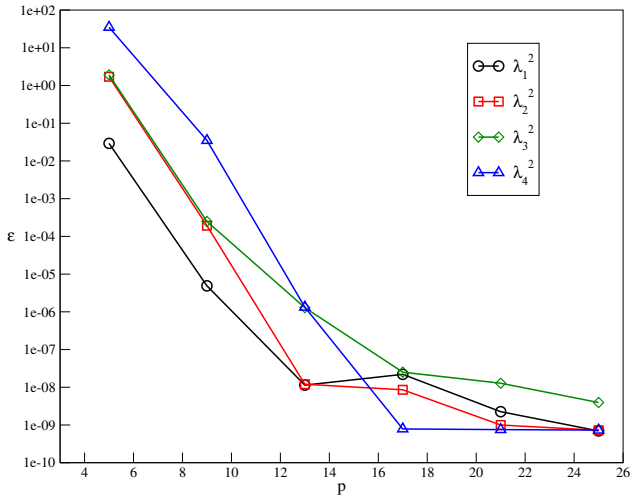

Figure 3.7: Relative error ε for the for the four lowest Stokes eigenvalues as a function of p on a semi-logarithmic scale with the divergence-free Galerkin implicit approach.

Moffat corner vortices [211] of increasingly smaller amplitude. The right part of Figure (3.8) represents the u_{px} component of the thirteenth eigenmode. The amplitude is 0.852. In the center of the figure, we can see the first Moffat vortex in the left upper corner of the geometry with an amplitude of 1×10^{-3}. At last, in the left side of the figure, the second Moffat vortex has an amplitude of 2×10^{-6}. These results are in accordance with the theoretical ones.

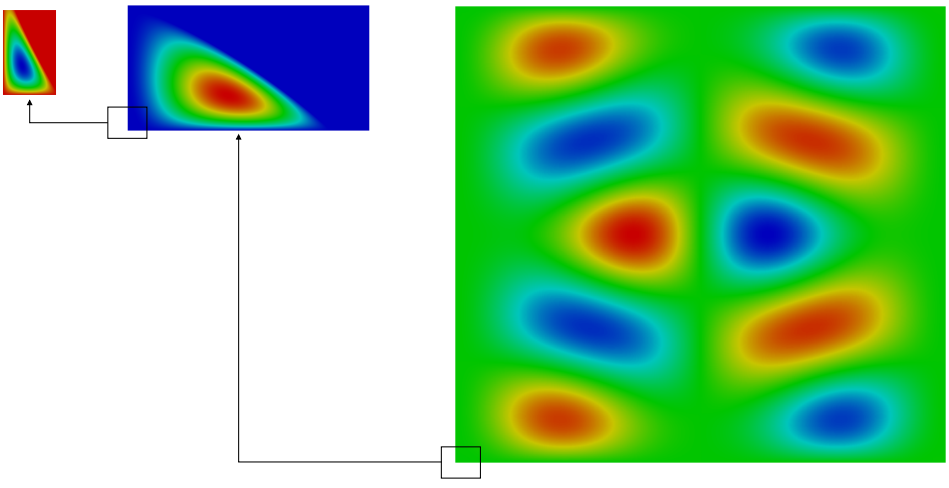

Figure 3.8: u_{px} component of 13^{th} Stokes eigenvector: Moffatt vortices in the corners.

Comparison between the different approaches The three strategies described in this chapter give the expected number of Stokes eigenvalues with a high precision. Nonetheless, Figure (3.5) compared with Figure (3.6) and Figure (3.7) indicates that the penalty approach is less accurate that the two other

ones. Moreover, the divergence of the eigenvectors computed by the penalty approach is not identically null and its level can depend on the tricky choice of the values of α. On the contrary, the divergence-free Galerkin approaches computed eigenvectors that are perfectly divergence-free. As drawback of the explicit version, we can mention that an initial computation of the kernel of the discretized grad(div) operator has to be performed leading to the resolution of two eigenvalue problems. Consequently, due to the reasons mentioned above, in our opinion, among the three strategies studied in this chapter, the best one is the divergence-free Galerkin implicit approach.

Chapter 4

Hodge Helmoltz Decomposition

Contents

The content of this chapter covers the entirety of article [20], completed with an application to unsteady Navier-Stokes equations:

- E. Ahusborde and M. Azaïez and J.P. Caltagirone and M. Gerritsma and A. Lemoine, Discrete Hodge Helmoltz Decomposition, Monografías Matemáticas "García de Galdeano", Vol 39, 1-10, 2014.

  Abstract*: This paper presents a new method using spectral approaches to compute the Discrete Hodge Helmholtz Decomposition (DHHD) of a given vector field. This decomposition consists in extracting the solenoidal (i.e. divergence-free), the non-solenoidal (i.e. rotational-free or, gradient of a scalar field) and the harmonic components (that is divergence-free and rotational-free) of a this vector field. A test case illustrates the proposed method.*

4.1 Introduction

The Hodge Helmholtz decomposition of a general vector field $\vec{u} = \vec{u}_\psi + \vec{u}_\phi + \vec{u}_H$ is a classical problem in applied and computational physics [127]. Application areas include (among others) electromagnetism, linear elasticity, fluid mechanics, image and video processing. A closed form of this decomposition may be obtained for unbounded domains through Biot-Savart type integrals. In finite domains, however such an approach is no longer feasible and computational solutions are the only practical way to perform this decomposition.

In the sequel, we mention a non exhaustive list of applications and references related to the Hodge Helmholtz decomposition. A detailed survey about this topics can be found in [64]. With regard to elasticity, work by Brezzi and Fortin [71], and by Arnold and Falk [44] used the Hodge Helmholtz

decomposition theorem for the study of the Reissner-Mindlin plate model. With regard to incompressible fluid flows, the scalar potential ϕ such that $\vec{u}_\phi = \nabla\phi$ in the Hodge Helmholtz decomposition is usually related to the pressure field p, and the vector potential $\vec{u}_\psi$ corresponds to the solenoidal velocity field $\vec{u}_S$ both quantities being involved in the Navier-Stokes equations. Stokes and Navier-Stokes solvers decouple most of the time the computation of the velocity and pressure fields [103]. The family of correction-pressure time splitting methods [130] generates first a tentative velocity field that is not incompressible but contains the right vorticity. The addition of a pressure gradient to this temporary velocity (equivalent to Hodge Helmholtz decomposition) makes it divergence-free [89, 288]. Another approach resorts to pressure penalization [77, 19] using the **grad**(div(.)) operator. Still considering this operator, we proposed in [22] a constructive spectral approaches for the Helmholtz decomposition of a vector field which consists in projecting the field to be decomposed on the kernel and the ranges of the **grad**(div(.)) operator. Indeed, the kernel of the **grad**(div(.)) operator consists of solenoidal eigenvectors while the eigenvectors related to non-zero eigenvalues are curl-free (see [21]). In video processing, the Hodge Helmholtz decomposition allows to detect the fingerprint reference or hurricanes from satellite pictures [232]. In [243], the authors proposed a meshless approach for the Hodge Helmholtz decomposition while in [145], divergence-free and curl-free wavelets are used. In [184], the authors propose a methodology to perform discrete Hodge Helmoltz decomposition on three-dimensional polyhedral meshes using structure-preserving schemes.

Consider a *given* vector field $\vec{u}$ defined in some domain Ω with boundary $\partial\Omega$. The Helmholtz decomposition writes (see [127])

$$\vec{u} = \vec{u}_\psi + \vec{u}_\phi + \vec{u}_H. \tag{4.1}$$

The solenoidal component $\vec{u}_\psi$ satisfies the equations

$$\begin{cases} \nabla\cdot\vec{u}_\psi = 0 \text{ in } \Omega, \\ \vec{u}_\psi\cdot\vec{n} = 0 \text{ on } \partial\Omega, \end{cases} \tag{4.2}$$

while the irrotational complement $\vec{u}_\phi$ is such that

$$\begin{cases} \nabla\times\vec{u}_\phi = \vec{0} \text{ in } \Omega, \\ \vec{u}_\phi\times\vec{n} = \vec{0} \text{ on } \partial\Omega. \end{cases} \tag{4.3}$$

Finally, the harmonic component is both solenoidal and irrotational:

$$\nabla\cdot\vec{u}_H = 0 \quad \text{and} \quad \nabla\times\vec{u}_H = \vec{0}. \tag{4.4}$$

The main difficulty of the problem (4.1) consists in satisfying the solenoidal (4.2) and irrotational constraints (4.3).

4.2 Divergence-free and curl-free Galerkin approaches

The method we present in this chapter is based on the construction of a basis satisfying the expected constraints. Its originality lies in the way these bases are built. To illustrate this, we will focus our presentation on how we derive a divergence-free basis. The derivation of the rotational-free basis in 2D will be presented in Subsection 4.2.2. We only consider the 2D case and then it is good to distinguish between curl and rot, where

$$\nabla\times\vec{u} = \text{rot}\vec{u} = \frac{\partial u_2}{\partial x_1} - \frac{\partial u_1}{\partial x_2}, \quad \text{curl}\phi = \begin{pmatrix} \partial\phi/\partial x_2 \\ -\partial\phi/\partial x_1 \end{pmatrix}.$$

4.2.1 Computation of the solenoidal component

In order to state the problem in variational form we introduce the relevant spaces of functions:

$$H(\mathrm{div},\Omega) = \left\{\vec{w} \in (L^2(\Omega))^2 \;\middle|\; \nabla\cdot\vec{w} \in L^2(\Omega)\right\},$$
$$L^2_0(\Omega) = \left\{q \in L^2(\Omega) \;\middle|\; \int_\Omega q\,dx = 0\right\}.$$

Let $\vec{v},\vec{w} \in H(\mathrm{div},\Omega)$. We define the inner product

$$(\vec{v},\vec{w})_{H(\mathrm{div},\Omega)} = (\vec{v},\vec{w})_{(L^2(\Omega))^2} + (\nabla\cdot\vec{v},\nabla\cdot\vec{w})_{L^2(\Omega)}, \tag{4.5}$$

and associated norm $||\vec{w}||_{H(\mathrm{div},\Omega)} = \left(||\vec{w}||^2_{(L^2(\Omega))^2} + ||\nabla\cdot\vec{w}||^2_{L^2(\Omega)}\right)^{1/2}$.

Consider also the proper subspace $H_0(\mathrm{div},\Omega) \subset H(\mathrm{div},\Omega)$:

$$H_0(\mathrm{div},\Omega) = \{\vec{w} \in H(\mathrm{div},\Omega) \mid \vec{w}\cdot\vec{n} = 0 \text{ on } \partial\Omega\}.$$

The admissible space for $\vec{u}_\psi$ in Problem (4.1)–(4.4) is a subspace of $H_0(\mathrm{div},\Omega)$:

$$X = \{\vec{u} \in H_0(\mathrm{div},\Omega) \mid \vec{\nabla}\cdot\vec{u} = 0 \text{ in } \Omega\}.$$

4.2.1.1 Variational formulation and its discretization

The variational formulation of problem (4.1) writes: *Find $\vec{u}_\psi \in X$ such that*

$$\int_\Omega \vec{u}_\psi\cdot\vec{v}\,d\vec{x} = \int_\Omega \vec{u}\cdot\vec{v}\,d\vec{x}, \quad \forall\vec{v} \in X. \tag{4.6}$$

Due to the nature of X, $\vec{u}_\phi$ and $\vec{u}_H$ disappear.

We firstly introduce the Raviart-Thomas space [257]

$$R_p = (\mathbb{P}^0_p(\Lambda)\otimes\mathbb{P}_{p-1}(\Lambda)) \times (\mathbb{P}_{p-1}(\Lambda)\otimes\mathbb{P}^0_p(\Lambda)), \tag{4.7}$$

where $\mathbb{P}_N(\Lambda)$ is the space of polynomials with degree $\leq N$ and $\mathbb{P}^0_p(\Lambda)$ denotes the space of polynomials of degree p vanishing on ±1. The dimension of R_p is equal to $2(p-1)p$.

The solution is approximated by $\vec{u}_{\psi,p} = (u^x_{\psi,p}, u^y_{\psi,p})$ in R_p with

$$u^x_{\psi,p}(x,y) = \sum_{i=1}^{p-1}\sum_{j=1}^{p} u^x_{\psi,p}(\xi_i,\zeta_j)\,h_i(x)\,\tilde{h}_j(y),$$
$$u^y_{\psi,p}(x,y) = \sum_{i=1}^{p}\sum_{j=1}^{p-1} u^y_{\psi,p}(\zeta_i,\xi_j)\,\tilde{h}_i(x)\,h_j(y).$$

Let $\Sigma_{GLL} = \{(\xi_i,\rho_i) \mid 0 \leq i \leq N\}$ and $\Sigma_{GL} = \{(\zeta_i,\omega_i) \mid 1 \leq i \leq N\}$ denote respectively the sets of Gauss-Lobatto-Legendre and Gauss-Legendre quadrature nodes and weights (see [103]). Likewise, $h_i(x) \in \mathbb{P}_N(\Lambda)$ and $\tilde{h}_j(x) \in \mathbb{P}_{N-1}(\Lambda)$ are respectively the canonical Lagrange polynomial interpolation basis built on Σ_{GLL} and on Σ_{GL}.

With this choice, the divergence of $\vec{u}_{\psi,p}$ is a polynomial of degree $p-1$. Consequently, if the divergence is orthogonal to all polynomial of $\mathbb{P}_{p-1}(\Omega)$, it is necessarily equal to 0. This point gives a new characterization for $X_p = R_p \cap X$:

$$X_p = \left\{\vec{u}_{\psi,p} \in R_p \;\middle|\; \frac{\partial u^x_{\psi,p}}{\partial x} + \frac{\partial u^y_{\psi,p}}{\partial y} = 0\right\},$$
$$X_p = \left\{\vec{u}_{\psi,p} \in R_p \;\middle|\; \int_\Omega \left(\frac{\partial u^x_{\psi,p}}{\partial x} + \frac{\partial u^y_{\psi,p}}{\partial y}\right) q\,d\vec{x} = 0,\ \forall q \in \mathbb{P}_{p-1}(\Omega)\right\}.$$

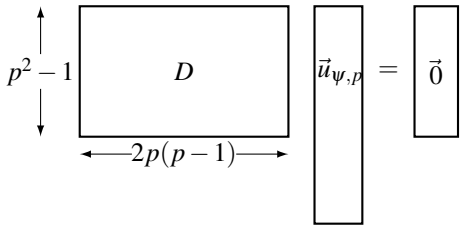

Figure 4.1: Algebraic system.

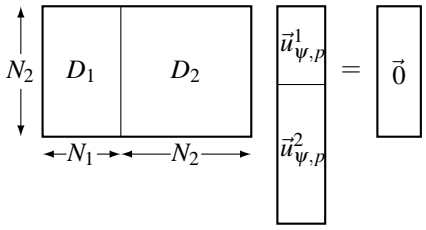

Figure 4.2: Decomposition of D.

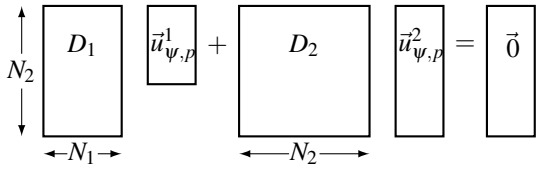

Figure 4.3: Algebraic system.

4.2.1.2 A basis for X_p

The first step consists in determining the dimension of the space X_p, that we denote by N_1:

$$N_1 = \dim R_p - N_2 = 2(p-1)p - N_2,$$

where N_2 is the dimension of the range of the divergence operator which is also the dimension of $P_{p-1}(\Omega) \cap L^2_0(\Omega)$ and then equals to p^2-1. We deduce that $N_1 = (p-1)^2$.

One can also view N_2 as the number of necessary and sufficient equations to ensure $\nabla \cdot \vec{u}_{\psi,p} \equiv 0$:

$$\nabla \cdot \vec{u}_{\psi,p} \in \mathbb{P}_{p-1}(\Omega) \quad \text{so} \quad N_2 \leq p^2.$$

Due to the boundary conditions (here $\vec{u}_{\psi,p} \cdot \vec{n} = 0$ on $\partial\Omega$), there is a dependent equation in the two dimensional case [49], since

$$\int_\Omega \nabla \cdot \vec{u}_{\psi,p} L_0(x) L_0(y) d\vec{x} = 0, \ \forall \vec{u}_{\psi,p} \in R_p.$$

Indeed, the polynomial $L_0(x)L_0(y)$ is a spurious mode and it reduces the number of independent equations from p^2 to p^2-1. Consequently, we require $N_2 = p^2-1$ test functions q to ensure $\int_\Omega \nabla \cdot \vec{u}_{\psi,p}\, q\, d\vec{x} = 0$.

Once the dimension is known, we describe now how to proceed to derive a divergence free basis from any N_1 given vectors of R_p

Algebraic characterization of X_p Let $\vec{u}_{\psi,p}$ be in X_p. The divergence of $\vec{u}_{\psi,p}$ is orthogonal to p^2-1 polynomials of degree $p-1$. It is equivalent to saying that the divergence of $\vec{u}_{\psi,p}$ nullifies into p^2-1 Gauss points. The algebraic divergence equation writes $D\,\vec{u}_{\psi,p} = \vec{0}$, where D is a rectangular matrix with p^2-1 rows and $2p(p-1)$ columns (see Figure 4.1).

One splits D into $D_1 \oplus D_2$ and $\vec{u}_{\psi,p}$ into $\vec{u}^1_{\psi,p} \oplus \vec{u}^2_{\psi,p}$. The vector $\vec{u}^1_{\psi,p}$ contains $N_1 = (p-1)^2$ values of $\vec{u}_{\psi,p}$, whereas $\vec{u}^2_{\psi,p}$ contains the $N_2 = p^2-1$ remaining values (see Figure 4.2). The equation $D\,\vec{u}_{\psi,p} = \vec{0}$ becomes $D_1\,\vec{u}^1_{\psi,p} + D_2\,\vec{u}^2_{\psi,p} = \vec{0}$, as shown in Figure 4.3.

Since, the p^2-1 rows of D are independent, there exists at least one choice of matrix D_2 invertible and the system leads to a relation between $\vec{u}^2_{\psi,p}$ and $\vec{u}^1_{\psi,p}$:

$$\vec{u}^2_{\psi,p} = -D_2^{-1} D_1 \vec{u}^1_{\psi,p}. \tag{4.8}$$

This equation is very important since it means that, if we have any part $\vec{u}^1_{\psi,p}$ of $\vec{u}_{\psi,p}$, we can build the complementary $\vec{u}^2_{\psi,p}$ such that divergence of $\vec{u}_{\psi,p}$ equals 0. This argument allows us to build a basis of X_p.

Basis of X_p The technique we use to project any vector of R_p on X_p is in the spirit of that published in [28] and used to solve the Stokes problem.

We consider $\vec{v}_p \in R_p$. Our strategy consists in combining implicitly:

- A reduction from $\vec{v}_p$ to $\vec{v}^1_p$.
- An extension from $\vec{v}^1_p$ to $\vec{w}_p = (\vec{v}^1_p, \vec{v}^2_p)$ such that $\nabla \cdot \vec{w}_p = 0$ ensured by the multiplication of $\vec{v}^1_p$ by the matrix

$$M = \begin{bmatrix} I_{N_1} \\ -D_2^{-1} D_1 \end{bmatrix}.$$

  The first block of M is the identity matrix of order N_1. The second block contains N_2 rows and N_1 columns. It ensures the passage from $\vec{v}^1_p$ to $\vec{v}^2_p$.
- For each $\vec{v}_p \in R_p$ one associates a vector $\vec{w}_p$ of X_p.

By consequent, our strategy for the construction of a basis of X_p consists in:

- Choosing $N_1 = (p-1)^2$ vectors $(\vec{v}^k_p)_{k=1..N_1}$ of the basis of R_p.
- For each one of these N_1 vectors, we consider its N_1-size reduced part denoted by $\vec{v}^{k,1}_p$.
- We carry out the divergence-free extension $(\vec{w}^k_p)_{k=1..N_1} = (M\,\vec{v}^{k,1}_p)_{k=1..N_1}$.

The $(\vec{w}^k_p)_{k=1..N_1}$ family is a basis of X_p. Consequently, $\vec{u}_{\psi,p} \in X_p$ can be decomposed according to $\vec{u}_{\psi,p} = \sum_{k=1}^{N_1} \alpha_k \vec{w}^k_p$ and the discrete variational formulation similar to (4.6) writes: *Find $\vec{u}_{\psi,p} \in X_p$ such that*

$$\sum_{k=1}^{N_1} (\vec{w}^k_p, \vec{w}^i_p)_p \alpha_k = (\vec{u}_p, \vec{w}^i_p)_p.$$

This can be written as

$$\underline{\mathscr{M}}\,\underline{\alpha} = \underline{\mathscr{F}},$$

with, for $1 \le i,k \le N_1$,

$$\underline{\mathscr{M}}_{ik} = (\vec{w}^k_p, \vec{w}^i_p)_p,$$
$$\underline{\mathscr{F}}_k = (\vec{u}, \vec{w}^k_p)_p.$$

Finally, this system is equivalent to

$$M^T B M\, \vec{u}^1_{\psi,p} = M^T B\, \vec{u}_p,$$

where B refers to the classical mass matrix computed using the $(h_i \times \tilde{h}_j) \otimes (\tilde{h}_i \times h_j)$ basis.

4.2.2 Computation of the irrotational component

A similar strategy to that described previously is used to compute the irrotational component $\vec{u}_\phi$, so we will limit to the description of the outline and we will not give all the details of its implementation.

Firstly, we introduce three spaces of functions:

$$\begin{aligned} H(\mathrm{rot},\Omega) &= \left\{\vec{w} \in (L^2(\Omega))^2 \;\middle|\; \nabla\times\vec{w} \in L^2(\Omega)\right\}, \\ H_0(\mathrm{rot},\Omega) &= \left\{\vec{w} \in H(\mathrm{rot},\Omega) \mid \vec{w}\times\vec{n} = 0 \text{ on } \partial\Omega\right\}, \\ Y &= \left\{\vec{u} \in H_0(\mathrm{rot},\Omega) \mid \nabla\times\vec{u} = 0 \text{ in } \Omega\right\}. \end{aligned}$$

The variational formulation of Problem (4.1) writes: *Find* $\vec{u}_\phi \in Y$ *such that*

$$\int_\Omega \vec{u}_\phi \cdot \vec{v}\, d\vec{x} = \int_\Omega \vec{u}\cdot\vec{v}\, d\vec{x}, \quad \forall \vec{v} \in Y.$$

For the discretization, we introduce the Nédélec space [219]

$$N_p = (\mathbb{P}_{p-1}(\Lambda)\otimes\mathbb{P}^0_p(\Lambda)) \times (\mathbb{P}^0_p(\Lambda)\otimes\mathbb{P}_{p-1}(\Lambda)).$$

The solution is approximated by $\vec{u}_{\phi,p} = (u^x_{\phi,p}, u^y_{\phi,p}) \in Y_p = N_p \cap Y$ with

$$\begin{aligned} u^x_{\phi,p}(x,y) &= \sum_{i=1}^{p}\sum_{j=1}^{p-1} u^x_{\phi,p}(\zeta_i,\xi_j)\,\tilde{h}_i(x)\,h_j(y), \\ u^y_{\phi,p}(x,y) &= \sum_{i=1}^{p-1}\sum_{j=1}^{p} u^y_{\phi,p}(\xi_i,\zeta_j)\,h_i(x)\,\tilde{h}_j(y). \end{aligned}$$

As previously, we build a basis of Y_p. With the same reasoning as for X_p and taking into account the same spurious mode $L_0(x)L_0(y)$, we determine the size of Y_p equal to $N_1 = (p-1)^2$.

Then the constraint $\nabla\times\vec{u}_{\phi,p} = \vec{0}$ is written into $N_1 = (p-1)^2$ Gauss points and gives an algebraic equations $R\vec{u}_{\phi,p} = \vec{0}$. A splitting strategy for the matrix R into $R_1 \oplus R_2$ and the vector $\vec{u}_{\phi,p}$ into $\vec{u}^1_{\phi,p} \oplus \vec{u}^2_{\phi,p}$ gives $R_1\vec{u}^1_{\phi,p} + R_2\vec{u}^2_{\phi,p} = \vec{0}$ and finally $\vec{u}^2_{\phi,p} = -R_2^{-1}R_1\vec{u}^1_{\phi,p}$.

Thanks to the $(N_1+N_2)\times N_1$ matrix

$$N = \begin{bmatrix} I_{N_1} \\ -R_2^{-1}R_1 \end{bmatrix},$$

we can construct a basis of Y_p.

Finally we obtain the system $N^T\tilde{B}N\,\vec{u}^1_{\phi,p} = N^T\tilde{B}\,\vec{u}_p$, where $\tilde{B}$ refers to the classical mass matrix computed using $(\tilde{h}_i\times h_j)\otimes(h_i\times\tilde{h}_j)$ basis.

4.3 Numerical results

4.3.1 Analytical test

To illustrate the efficiency of our approach for the Hodge Helmholtz decomposition, we have made a numerical experiment in the square $\Omega = (-1,+1)^2$ with the case $\vec{u} = \vec{u}_\psi + \vec{u}_\phi + \vec{u}_H$ corresponding to the following components:

$$\begin{aligned} \vec{u}_\psi &= (\sin(\pi x)\cos(\pi y), -\sin(\pi y)\cos(\pi x)), \\ \vec{u}_\phi &= (\sin(\pi y)\cos(\pi x), \sin(\pi x)\cos(\pi y)), \\ \vec{u}_H &= (0.5, -1). \end{aligned}$$

The component $\vec{u}_{\psi,p}$ is approximated as outlined in Subsection 4.2.1, while the irrotational part $\vec{u}_{\phi,p}$ is computed as outlined in Subsection 4.2.2. Finally, $\vec{u}_H$ is calculated by the relation $\vec{u}_H = \vec{u} - \vec{u}_\psi - \vec{u}_\phi$.

Table 4.1 gives $||\nabla \cdot \vec{u}_{\psi,p}||_{L^2(\Omega)}$ and $||\nabla \times \vec{u}_{\phi,p}||_{L^2(\Omega)}$ as a function of the polynomial degree p. As expected, the norms remain close to round-off *independently* of p.

p	4	8	12	16
$\|\|\nabla \cdot \vec{u}_{\psi,p}\|\|_{L^2(\Omega)}$	8.56×10^{-16}	1.71×10^{-15}	1.95×10^{-15}	5.23×10^{-15}
$\|\|\nabla \times \vec{u}_{\phi,p}\|\|_{L^2(\Omega)}$	4.90×10^{-16}	2.18×10^{-15}	3.87×10^{-15}	5.09×10^{-15}

Table 4.1: $L^2(\Omega)$-norm of the divergence and the rotational of solenoidal and irrotational components.

Figure 4.4 exhibits on a semi-logarithmic scale the $(L^2(\Omega))^2$-norm of the error for the three components as a function of the polynomial degree p. We can observe a spectral decrease.

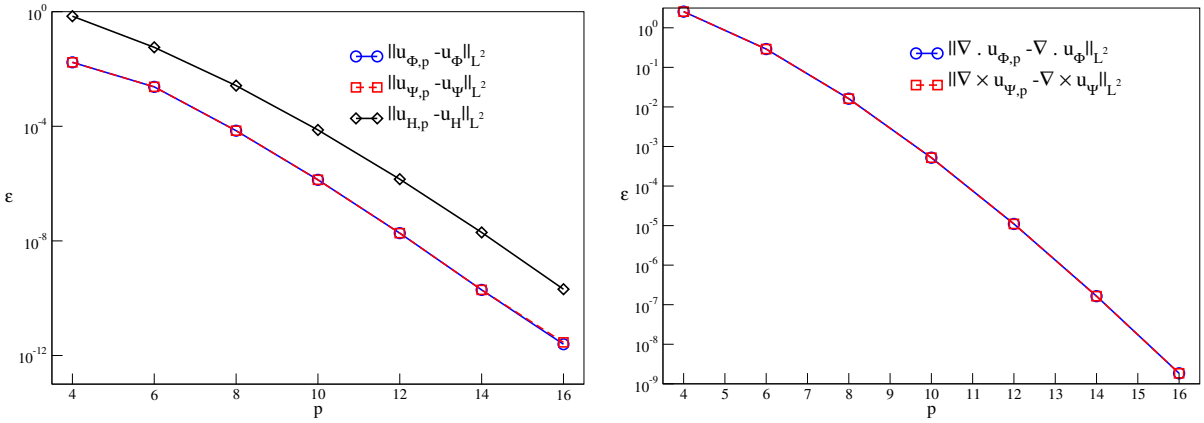

Figure 4.4: $(L^2(\Omega))^2$-norm of the error as a function of the polynomial degree p.

Figure 4.5 displays the Hodge Helmholtz decomposition of the vector $\vec{u}$.

4.3.2 Unsteady Navier-Stokes problems

This second example deals with unsteady Navier-Stokes problems. The use of time splitting schemes involves a projection step which is nothing else than an Hodge Helmholtz decomposition. We want to probe the effects of the new approach introduced previously on the accuracy of the decomposition.

We consider a two-dimensional square cavity filled with an incompressible fluid having density ρ and dynamic viscosity μ. The flow is driven by a prescribed body force $\vec{f}(\vec{x},t)$. Pressure $p(\vec{x},t)$ and velocity $\vec{u}(\vec{x},t)$ satisfy the time dependent Navier-Stokes equations:

$$\rho\left(\frac{\partial \vec{u}}{\partial t} + (\vec{u}\cdot\nabla)\vec{u}\right) - \mu\,\Delta\vec{u} + \nabla p = \vec{f}, \qquad \text{in } \Omega \times [0,t^*], \tag{4.9}$$

$$\nabla \cdot \vec{u} = 0, \qquad \text{in } \Omega \times [0,t^*], \tag{4.10}$$

where Ω denotes the cavity domain $]-1,+1[^2$ and t^* the time span of the transient. We apply Dirichlet boundary conditions on the velocity

$$\vec{u}(\vec{x},t)_{|\partial\Omega} = \vec{g}(\vec{x},t)_{|\partial\Omega}, \qquad \forall t \in [0,t^*], \tag{4.11}$$

with the initial condition $\vec{u}(\vec{x},0) = \vec{u}^0(\vec{x})$.

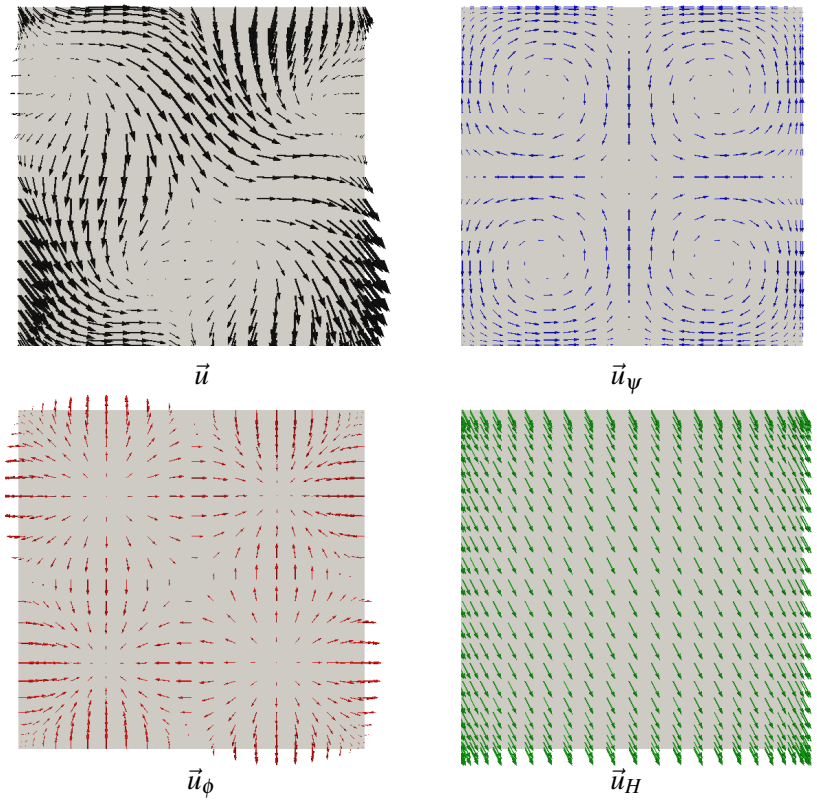

Figure 4.5: Decomposition of the vector and its three components.

We apply the Goda pressure correction time integration scheme which consists in splitting the Stokes system into two stages, a diffusion-prediction and a pressure-correction [130]. The numerical method begins with the treatment of the non-linear term $(\vec{u}.\nabla)\vec{u}$ involved in the material derivative of the velocity, $\frac{d\vec{u}}{dt}(=\frac{\partial\vec{u}}{\partial t}+(\vec{u}.\nabla)\vec{u})$. The scheme adopted here is the classical explicit second-order Adams-Bashforth algorithm. The time interval $[0,t^*]$ is divided into M equidistant time steps of length $\Delta t=\frac{t^*}{M}$. The approximate velocity and pressure fields at time $t^m:=m\Delta t$ $(m=0,\ldots,M)$ are denoted $\vec{u}^m(\vec{x})$ and $p^m(\vec{x})$ respectively. Assuming all quantities are known up to t^m, the solution at t^{m+1} results from the diffusion prediction step: *Find* $\vec{u}_*^{m+1}$ *such that*

$$\rho\,\frac{\frac{3}{2}\vec{u}_*^{m+1}-2\,\vec{u}^m+\frac{1}{2}\vec{u}^{m-1}}{\Delta t}-\mu\,\Delta\vec{u}_*^{m+1}+\nabla p^m = \vec{f}^{m+1}-AB^m \text{ in } \Omega, \tag{4.12}$$

$$\vec{u}_*^{m+1} = \vec{0}, \qquad \text{on } \partial\Omega, \tag{4.13}$$

where $AB^m=2\rho\,\left((\vec{u}.\nabla)\vec{u}\right)^m-\rho\,\left((\vec{u}.\nabla)\vec{u}\right)^{m-1}$,

followed by the pressure correction step: *Find* $\vec{u}^{m+1}$ *and* p^{m+1} *such that*

$$\rho\,\frac{\frac{3}{2}\vec{u}^{m+1}-\frac{3}{2}\vec{u}_*^{m+1}}{\Delta t}+\nabla(p^{m+1}-p^m) = 0, \qquad \text{in } \Omega, \tag{4.14}$$

$$\nabla\cdot\vec{u}^{m+1} = 0, \qquad \text{in } \Omega, \tag{4.15}$$

$$\vec{u}^{m+1}\cdot\vec{n} = 0, \qquad \text{on } \partial\Omega. \tag{4.16}$$

One will notice that the coefficients in the left-hand side of (4.12) and of (4.14) correspond to a second-order backward Euler scheme.

Looking carefully at (4.14)-(4.16) one realizes that these equations correspond exactly to the Hodge Helmholtz decomposition of the auxiliary velocity field $\vec{u}_*^{m+1}$ resulting from the diffusion prediction step, into:

$$\begin{aligned} \vec{u}^{m+1} + \nabla \psi &= \vec{u}_*^{m+1}, \quad \text{in } \Omega, && (4.17)\\ \vec{\nabla} \cdot \vec{u}^{m+1} &= 0, \quad \text{in } \Omega, && (4.18)\\ \vec{u}^{m+1} \cdot \vec{n} &= 0, \quad \text{on } \partial\Omega, && (4.19) \end{aligned}$$

with

$$p^{m+1} = p^m + \frac{3}{2}\frac{\rho}{\Delta t}\psi. \tag{4.20}$$

Consequently, we propose to compute the Hodge Helmholtz decomposition (4.17)-(4.19) thanks to our strategy presented previously.

To assess our new decomposition scheme we have performed the test case of the lid-driven cavity. This problem has long been used as a test for the validation of new codes or new methods. The standard case deals with a fluid contained in a square domain with three wall sides and one moving side (with velocity tangential to the side). We refer to the works of Botella [66] and Ehrenstein and Peyret [106] where the domain $\Omega = [0,1]^2$ and a regularized velocity ($u(x,1) = -16x^2(1-x)^2$) are considered. For this computation two Reynolds numbers ($Re = 100$ and $Re = 400$) are used.
The results are obtained with convergence criteria on stationarity below 10^{-8} and a polynomial degree $p = 24$. In order to compare our results with those obtained in [66] and [106], we have computed the stream function ψ and the vorticity ω where:

$$\omega = \frac{\partial v_p^M}{\partial x} - \frac{\partial u_p^M}{\partial y} \quad \text{with } u_p^M = (u_p^M, v_p^M), \tag{4.21}$$

and

$$\begin{aligned} \Delta\psi &= -\omega \text{ in } \Omega, && (4.22)\\ \psi &= 0 \quad \text{on } \partial\Omega. && (4.23) \end{aligned}$$

Figure (4.6) depicts the streamlines and the stream function for $Re = 100$ and $Re = 400$.

Table (4.2) represents the maximal value of the stream function $|\psi|$ and the position of this maximum for the two values of the Reynolds number. We can see that we are in accordance with the results produced in [66] and [106].

	Re=100			Re=400		
Reference	Maximum	x	y	Maximum	x	y
Present	8.3339×10^{-2}	0.37	0.75	8.5731×10^{-2}	0.43	0.63
Botella [66]	8.3315×10^{-2}	0.37	0.75	8.5716×10^{-2}	0.43	0.63
Ehrenstein and Peyret [106]	8.3315×10^{-2}	0.37	0.75	8.5715×10^{-2}	0.43	0.63

Table 4.2: Intensity and position (x,y) of the maximum of the stream function.

Table (4.3) displays the maximal value of vorticity $|\omega|$ on the upper side $y = 1$. Again, our results present a good accordance with those obtained in [66] and [106].

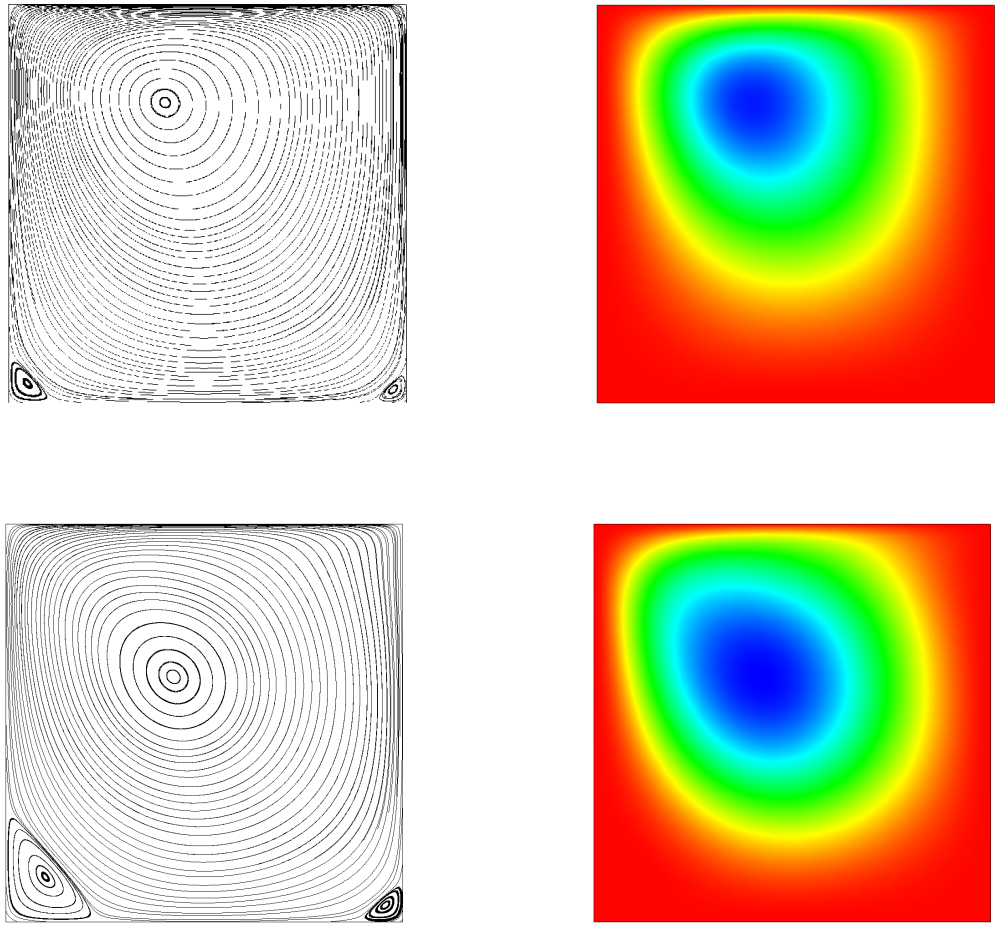

Figure 4.6: Streamlines (left) and stream function (right) computed for the lid driven cavity. Top: $Re = 100$, bottom: $Re = 400$.

	Re=100		Re=400	
Reference	Maximum	x	Maximum	x
Present	13.4323	0.63	24.9222	0.63
Botella [66]	13.4226	0.63	24.9157	0.63
Ehrenstein and Peyret [106]	13.4227	0.63	24.9344	0.63

Table 4.3: Intensity and position x of the maximum of the vorticity on the upper side.

Chapter 5

Outflow boundary conditions for Navier-Stokes time-splitting methods

Contents

This chapter covers the entirety of article [23] and is also based on article [247] which can be found in the Appendix. Both articles are listed below:

- E. Ahusborde, M. Azaïez M., S. Glockner, and A. Poux. A contribution to the outflow boundary conditions for Navier-Stokes time-splitting methods, Lecture Notes in Computational Science and Engineering, 95:75-86, 2014.

  Abstract*: We present in this paper a numerical scheme for incompressible Navier-Stokes equations with open boundary conditions, in the framework of the pressure and velocity correction schemes. In Poux et al. (J Comput Phys 230:4011- 4027, 2011), the authors presented an almost second-order accurate version of the open boundary condition with a pressure-correction scheme in finite volume framework. This paper proposes an extension of this method in spectral element method framework for both pressure- and velocity-correction schemes. A new way to enforce this type of boundary condition is proposed and provides a pressure and velocity convergence rate in space and time higher than with the present state of the art. We illustrate this result by computing some numerical tests.*

- A. Poux, S. Glockner, E. Ahusborde and M. Azaïez. Open and traction boundary conditions for velocity correction scheme for Navier-Stokes equations, Computers and Fluids, 70:29-43, 2012.

  Abstract*: In this paper we propose to study open boundary conditions for incompressible Navier-Stokes equations, in the framework of velocity-correction methods. The standard way to enforce*

this type of boundary condition is described, followed by an adaptation of the one we proposed in [248] that provides higher pressure and velocity convergence rates in space and time for pressure-correction schemes. These two methods are illustrated with a numerical test with both finite volume and spectral Legendre methods. We conclude with three physical simulations: first with the flow over a backward-facing step, secondly, we study, in a geometry where a bifurcation takes place, the influence of Reynolds number on the laminar flow structure, and lastly, we verify the solution obtained for the unsteady flow around a square cylinder.

5.1 Introduction

A difficulty in obtaining the numerical solution of the incompressible Navier-Stokes equations, lies in the Stokes stage and specifically in the determination of the pressure field which will ensure a solenoidal velocity field. Several approaches are possible. We can for instance consider exact methods as the Uzawa [45] and augmented lagrangian [121] ones. In complex geometries or three dimensional methods, theses techniques are inappropriate since their computational time costs are very high. An alternative consists in decoupling the pressure from the velocity by means of a time splitting scheme. A large number of theoretical and numerical studies have been published that discuss the accuracy and the stability properties of such approaches. The most popular methods are pressure-correction schemes. They were first introduced by Chorin-Temam [89, 288], and improved by Goda (the standard incremental scheme) in [130], and later by Timmermans in [292] (the rotational incremental scheme). They require the solution of two sub-steps: the pressure is treated explicitly in the first one, and is corrected in the second one by projecting the predicted velocity onto an ad-hoc space. A less studied alternative technique known as the velocity-correction scheme, developed by Orszag *et al* in [231], Karniadakis *et al* in [166], Leriche *et al* in [185] and more recently by Guermond *et al* in [135], consists in switching the two sub-steps.

In [269] and [136], the authors proved the reliability of such approaches from the stability and the convergence rate points of view. A series of numerical issues related to the analysis and implementation of fractional step methods for incompressible flows are addressed in the review paper [134]. In this reference the authors describe the state of the art for both theoretical and numerical results related to the time splitting approach.

Another difficulty consists in the treatment of outflow boundary conditions. Indeed the majority of the studies made on these methods consider only Dirichlet boundary conditions. We are interested here in outflow boundary conditions. A large variety of boundary conditions of this type exists, such as the non reflecting boundary condition developed by Orlanski [230] or Engquist [107]. Here we present some results on the open and traction boundary condition [133, 193].

With open or traction boundary conditions, while no studies have been reported with a velocity-correction scheme, a few have been done with pressure-correction schemes. In [134] the authors proved that only spatial and time convergence rates between $O(\Delta x+\Delta t)$ and $O(\Delta x^{3/2}+\Delta t^{3/2})$ on the velocity and $O(\Delta x^{1/2}+\Delta t^{1/2})$ on the pressure are to be expected with the standard incremental scheme, and between $O(\Delta x+\Delta t)$ and $O(\Delta x^{3/2}+\Delta t^{3/2})$ on the velocity and pressure for the rotational incremental scheme. In [248], the authors presented a new version of the boundary condition for the pressure-correction scheme in the finite volume framework. They obtained a second-order accuracy for the velocity and rates between $O(\Delta x^{3/2}+\Delta t^{3/2})$ and $O(\Delta x^2+\Delta t^2)$ with the standard incremental scheme while with the rotational version, a second order convergence is reached for both velocity and pressure. We propose here to extend this method in spectral element method framework for both pressure-correction and velocity-correction schemes.

5.2 Pressure-correction scheme for open boundary condition

5.2.1 Governing equations

Let Ω be a regular bounded domain in $\mathbb{R}^d$ with $\vec{n}$ a unit vector on the outward normal along the boundary $\Gamma = \partial\Omega$ oriented outward. We suppose that Γ is partitioned into two portions Γ_D and Γ_N.

Our study consists, for a given finite time interval $]0,t^*]$ in computing velocity $\vec{u} = \vec{u}(\vec{x},t)$ and pressure $p = p(\vec{x},t)$ fields satisfying:

$$\begin{aligned}
\rho\frac{\partial\vec{u}}{\partial t} - \mu\Delta\vec{u} + \nabla p &= \vec{f} \quad \text{in } \Omega\times]0,t^*], && (5.1)\\
\nabla\cdot\vec{u} &= 0 \quad \text{in } \Omega\times]0,t^*], && (5.2)\\
\vec{u} &= \vec{g} \quad \text{on } \Gamma_D\times]0,t^*], && (5.3)\\
(\mu\nabla\vec{u} - p\mathbf{I})\,\vec{n} &= \vec{t} \quad \text{on } \Gamma_N\times]0,t^*], && (5.4)
\end{aligned}$$

where ρ and μ are the density and the dynamic viscosity of the flow respectively and $\mathbf{I}$ the unit tensor. The body force $\vec{f} = \vec{f}(\vec{x},t)$, the constraint $\vec{t} = \vec{t}(\vec{x},t)$ and the boundary condition $\vec{g} = \vec{g}(\vec{x},t)$ are known. For the sake of simplicity, we chose $\vec{g} = \vec{0}$. Finally, the initial state is characterised by a given $\vec{u}(.,0)$.

We shall compute two sequences $(\vec{u}^n)_{0\le n\le N}$ and $(p^n)_{0\le n\le N}$ in a recurrent way that approximate in some sense the quantities $(\vec{u}(.,t^n))_{0\le n\le N}$ and $(p(.,t^n))_{0\le n\le N}$, solutions of unsteady Stokes problem (5.1)-(5.4). Using a second order backward difference formula (BDF) time scheme, its semi-discrete version reads:

$$\begin{aligned}
\rho\frac{\alpha\vec{u}^{n+1} + \beta\vec{u}^n + \gamma\vec{u}^{n-1}}{\Delta t} - \mu\Delta\vec{u}^{n+1} + \nabla p^{n+1} &= \vec{f}^{n+1} \text{ in } \Omega, && (5.5)\\
\nabla\cdot\vec{u}^{n+1} &= 0 \quad \text{in } \Omega, && (5.6)\\
\vec{u}^{n+1} &= \vec{0} \quad \text{on } \Gamma_D, && (5.7)\\
\left(\mu\nabla\vec{u}^{n+1} - p^{n+1}\mathbf{I}\right)\vec{n} &= \vec{t}^{n+1} \text{ on } \Gamma_N. && (5.8)
\end{aligned}$$

Values of parameters α,β,γ depend on the temporal scheme used. Namely:

- $\alpha = 1$, $\beta = -1$, $\gamma = 0$ for the first order Euler time scheme,
- $\alpha = \frac{3}{2}$, $\beta = -2$, $\gamma = \frac{1}{2}$ for the second order Backward Difference Formulae time scheme.

Equations (5.5)-(5.8) are split into two sub-problems. The first one is a prediction diffusion problem that computes a predicted velocity field: *Find* $\vec{u}^{n+1/2}$ *such that*

$$\begin{aligned}
\rho\frac{\alpha\vec{u}^{n+1/2} + \beta\vec{u}^n + \gamma\vec{u}^{n-1}}{\Delta t} - \mu\Delta\vec{u}^{n+1/2} + \nabla p^n &= \vec{f}^{n+1} \text{ in } \Omega, && (5.9)\\
\vec{u}^{n+1/2} &= 0 \quad \text{on } \Gamma_D, && (5.10)\\
\left(\mu\nabla\vec{u}^{n+1/2} - \tilde{p}^{n+1}\mathrm{Id}\right)\vec{n} &= \vec{t}^{n+1} \text{ on } \Gamma_N. && (5.11)
\end{aligned}$$

Expression of $\tilde{p}^{n+1}$ depends on the time scheme:

- for the first order time scheme

$$\tilde{p}^{n+1} = p^n, \qquad (5.12)$$

- for the second order time scheme

$$\tilde{p}^{n+1} = 2p^n - p^{n-1}. \tag{5.13}$$

The second step is a correction pressure-continuity: *Find* $(\vec{u}^{n+1}, \varphi^{n+1})$ *such that*

$$\begin{aligned}
\frac{\rho\alpha}{\Delta t}\left(\vec{u}^{n+1} - \vec{u}^{n+1/2}\right) + \nabla\varphi^{n+1} &= \vec{0} \quad \text{in } \Omega, && (5.14)\\
\nabla\cdot\vec{u}^{n+1} &= 0 \quad \text{in } \Omega, && (5.15)\\
\vec{u}^{n+1}\cdot\vec{n} &= 0 \quad \text{on } \Gamma_D, && (5.16)\\
B.C.\ (\varphi^{n+1}) & \quad \text{on } \Gamma_N. && (5.17)
\end{aligned}$$

The pressure is upgraded via:

$$p^{n+1} = p^n + \varphi^{n+1} - \chi\mu\nabla\cdot\vec{u}^{n+1/2} \quad \text{in } \Omega. \tag{5.18}$$

The parameter χ is used to switch between the standard incremental scheme and the rotational one:

- $\chi = 0$ for the standard incremental scheme,
- $\chi = 0.7$ for the rotational incremental scheme.[1]

In practice, this second step is replaced by a Poisson problem on φ^{n+1}:

$$\begin{aligned}
\frac{\Delta t}{\alpha\rho}\Delta\varphi^{n+1} &= \nabla\cdot\vec{u}^{n+1/2} \quad \text{in } \Omega, && (5.19)\\
\frac{\partial\varphi^{n+1}}{\partial n} &= 0 \quad \text{on } \Gamma_D, && (5.20)\\
B.C.\ (\varphi^{n+1}) & \quad \text{on } \Gamma_N, && (5.21)
\end{aligned}$$

completed by:

$$\begin{aligned}
p^{n+1} &= p^n + \varphi^{n+1} - \chi\mu\nabla\cdot\vec{u}^{n+1/2} \quad \text{in } \Omega, && (5.22)\\
\vec{u}^{n+1} &= \vec{u}^{n+1/2} - \frac{\Delta t}{\alpha\rho}\nabla\varphi^{n+1} \quad \text{in } \Omega. && (5.23)
\end{aligned}$$

The natural choice for B.C. (φ^{n+1}) consists in choosing $\varphi^{n+1} = 0$ on Γ_N. Such a choice involves a numerical locking for $\chi = 0$ since the boundary condition on the pressure increment causes the pressure on the limit to be equal to its initial value. A real improvement is obtained for $\chi = 0.7$ but the expected rates of convergence are not reached.

In the next section we will keep the nature of the boundary condition of φ^{n+1} and will suggest a value of it allowing the reduction of the boundary layer effect mentioned previously.

[1] Ideally, $\chi = 1$ but as Guermond proved [133], for stability issues, χ is necessarily strictly lower than $2\mu/d$.

5.2.2 Improvement of the pressure boundary conditions

For the sake of simplicity we choose a square domain Ω with Γ_N at its right boundary. The starting point of our approach is the derivation on x_1 of the first component of (5.14):

$$-\frac{\Delta t}{\alpha\rho}\frac{\partial^2\varphi^{n+1}}{\partial x_1^2} = \frac{\partial {u_{x_1}}^{n+1}}{\partial x_1} - \frac{\partial {u_{x_1}}^{n+\frac{1}{2}}}{\partial x_1}. \tag{5.24}$$

Then, we project on direction x_1 the equations (5.4) and (5.8):

$$\mu\frac{\partial u_{x_1}^{n+1}}{\partial x_1} - p^{n+1} = t_{x_1}^{n+1}, \tag{5.25}$$

$$\mu\frac{\partial u_{x_1}^{n+\frac{1}{2}}}{\partial x_1} - \tilde{p}^{n+1} = t_{x_1}^{n+1}. \tag{5.26}$$

The combination of those three last equations (5.24)-(5.26) gives:

$$-\frac{\Delta t}{\alpha\rho}\frac{\partial^2\varphi^{n+1}}{\partial x_1^2} = \frac{1}{\mu}(p^{n+1} - \tilde{p}^{n+1}). \tag{5.27}$$

Replacing $\tilde{p}^{n+1}$ by its expressions (5.12) gives for the first order scheme:

$$\left(\frac{\Delta t}{\alpha\rho}\frac{\partial^2}{\partial x_1^2} + \frac{1}{\mu}\right)\varphi^{n+1} = +\chi\nabla\cdot\vec{u}^{n+\frac{1}{2}}. \tag{5.28}$$

Or for a second order scheme using (5.13) :

$$\left(\frac{\Delta t}{\alpha\rho}\frac{\partial^2}{\partial x_1^2} + \frac{1}{\mu}\right)\varphi^{n+1} = \frac{\varphi^n}{\mu} + \chi\nabla\cdot\left(\vec{u}^{n+\frac{1}{2}} - \vec{u}^{n-\frac{1}{2}}\right). \tag{5.29}$$

Moreover taking into account the Poisson problem (5.19):

$$\frac{\partial^2\varphi^{n+1}}{\partial x_1^2} + \frac{\partial^2\varphi^{n+1}}{\partial x_2^2} = \nabla\cdot\vec{u}^{n+1/2}, \tag{5.30}$$

and substracting (5.28) or (5.29) in (5.30) one obtains:

- First-order open boundary condition (OBC1):

$$\left(\frac{\Delta t}{\alpha\rho}\frac{\partial^2}{\partial x_2^2} - \frac{1}{\mu}\right)\varphi^{n+1} = (1-\chi)\nabla\cdot\vec{u}^{n+\frac{1}{2}}, \tag{5.31}$$

- Second-order open boundary condition (OBC2):

$$\left(\frac{\Delta t}{\alpha\rho}\frac{\partial^2}{\partial x_2^2} - \frac{1}{\mu}\right)\varphi^{n+1} = (1-\chi)\nabla\cdot\vec{u}^{n+\frac{1}{2}} - \frac{\varphi^n}{\mu} + \chi\nabla\cdot\vec{u}^{n-\frac{1}{2}}. \tag{5.32}$$

To summarize, we propose a pressure-correction step that writes: *Find* φ^{n+1} *such that*

$$\frac{\Delta t}{\alpha\rho}\Delta\varphi^{n+1} = \nabla\cdot\vec{u}^{n+1/2} \quad \text{in } \Omega, \tag{5.33}$$

$$\frac{\partial\varphi^{n+1}}{\partial n} = 0 \quad \text{on } \Gamma_D, \tag{5.34}$$

$$\varphi^{n+1} = \varphi^* \quad \text{on } \Gamma_N, \tag{5.35}$$

where φ^* is solution of:

$$\left(\frac{\Delta t}{\alpha\rho}\frac{\partial^2}{\partial x_2^2}-\frac{1}{\mu}\right)\varphi^* = (1-\chi)\nabla\cdot\vec{u}^{n+\frac{1}{2}}-2\gamma\left(\frac{\varphi^n}{\mu}-\chi\nabla\cdot\vec{u}^{n-\frac{1}{2}}\right) \text{ on } \Gamma_N, \tag{5.36}$$

$$\frac{\partial\varphi^*}{\partial x_2}(\pm 1) = 0. \tag{5.37}$$

5.2.3 Numerical experiments

5.2.3.1 Spectral Element Method Implementation

The domain Ω is the union of quadrangular elements $\overline{\Omega}=\cup_{k=1}^{K}\overline{\Omega}_k$.
For simplification, we consider only rectilinear elements with edges collinear to the axis x and y, that is:

$$\Omega_k =]c_k,c_k'[\times]d_k,d_k'[.$$

The partition is conforming in the sense that the intersection of two adjacent elements is either a vertex or a whole edge.
The discrete and stable subspaces to approximate the velocity and the pressure, $\vec{X}_p \subset (H_0^1(\Omega))^2$ and $M_p \subset L_0^2(\Omega)$ are chosen to be:

$$\vec{X}_p = \left\{\vec{w}_p \in (H_0^1(\Omega))^2, \qquad \vec{w}_p^k = \vec{w}_{p|\Omega_k} \in (I\!P_p(\Omega))^2\right\}, \tag{5.38}$$

$$M_p = \left\{q_p \in L^2(\Omega), \qquad q_p^k = q_{p|\Omega_k} \in I\!P_{p-2}(\Omega_k), \quad \int_\Omega q_p\, d\vec{x}=0\right\}. \tag{5.39}$$

The spectral Legendre approach consists in using the Legendre-Galerkin methods introduced in [103] applied to the variational formulation of elliptic problems introduced in our algorithms.

5.2.3.2 Numerical results for the Stokes problem

Exact solutions for $\vec{u}^{ex}=\left(u_{x_1}^{ex},u_{x_2}^{ex}\right)$ and p^{ex} correspond to these data:

$$u_{x_1}^{ex}(x_1,x_2,t) = \sin(x_1)\sin(x_2)\cos(2\pi\omega t), \tag{5.40}$$

$$u_{x_2}^{ex}(x_1,x_2,t) = \cos(x_1)\cos(x_2)\cos(2\pi\omega t), \tag{5.41}$$

$$p^{ex}(x_1,x_2,t) = -2\cos(1)\sin(2(x_1-1)-x_2)\cos(2\pi\omega t). \tag{5.42}$$

To study the time splitting error, we consider the unsteady case $\omega=0.7$ and the errors at $t^*=1$ with a second order time discretization for a range of time steps $5\times10^{-4}\leq\Delta t\leq10^{-1}$.

Figure (5.1) depicts results when we use the natural choice for the boundary conditions for φ^{n+1} that is $\varphi^{n+1}=0$ on Γ_N. The left part of the figure displays the error in L^2-norm for both pressure and velocity when using the standard incremental scheme ($\chi=0$). We can see that the results are very bad and no order of convergence can be calculated. The right part exhibits the same quantities when using the rotational scheme with $\chi=0.7$. We can see that only rates close to 1 are obtained while order 2 is expected.

Figure (5.2) displays the same results using our boundary condition (5.32). Again, the left part of the figure depicts the errors with standard incremental scheme whereas the right part depicts the errors with the rotational scheme. Contrary to [248], where the authors obtained an almost second-order for the standard incremental scheme and a full second-order for the rotational scheme, we obtain here, in both cases, convergence rates equal to 2.

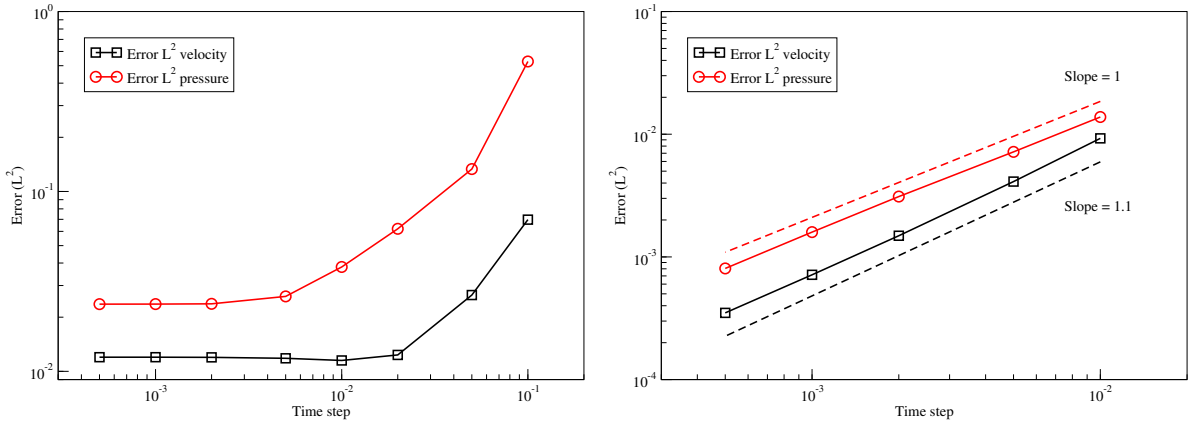

Figure 5.1: Time convergence rates with the standard incremental scheme (left) and the rotational scheme (right) at $t^* = 1$ with $K = 1$ and $p = 18$ with standard open boundary conditions and spectral element method.

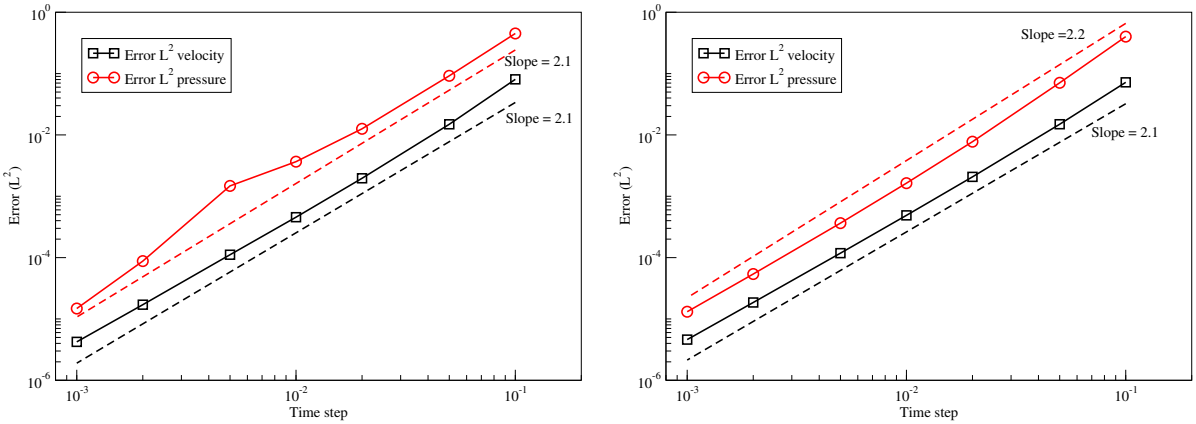

Figure 5.2: Time convergence rates with the standard incremental scheme (left) and the rotational scheme (right) at $t^* = 1$ with $K = 1$ and $p = 18$ with the proposed open boundary conditions and spectral element method.

5.3 Velocity-correction scheme for open boundary condition

5.3.1 Governing equations

We propose now to extend our boundary condition for the velocity-correction scheme. The scheme developed by Guermond and Shen in [135] consists on two sub-steps.
The first one is the prediction problem that computes a pressure increment and a solenoidal velocity: *find* φ^{n+1} *and* $\vec{u}^{n+1}$ *such that:*

$$\rho\frac{\alpha\vec{u}^{n+1}+(\beta-\alpha)\tilde{\vec{u}}^{n}+(\gamma-\beta)\tilde{\vec{u}}^{n-1}-\gamma\tilde{\vec{u}}^{n-2}}{\Delta t}+\nabla\varphi^{n+1}=\vec{f}^{n+1}-\vec{f}^{n} \qquad \text{in } \Omega, \tag{5.43}$$

$$\nabla\cdot\vec{u}^{n+1}=0 \qquad \text{in } \Omega, \tag{5.44}$$

$$\vec{u}^{n+1}\cdot\vec{n}=0 \qquad \text{on } \Gamma_D, \tag{5.45}$$

$$\mu\partial_n(\vec{u}^{n+1}\cdot\vec{n})-p^{n+1}=\vec{t}^{n+1}\cdot\vec{n} \qquad \text{on } \Gamma_N, \tag{5.46}$$

where φ is the pressure increment defined as:

$$\varphi^{n+1} = p^{n+1} - p^n + \chi\mu\nabla\cdot\tilde{\vec{u}}^n. \tag{5.47}$$

In practice, this step is processed by solving the following problem: *find* φ^{n+1} *such that:*

$$\nabla\cdot\left(\frac{\Delta t}{\rho}\nabla\varphi^{n+1}\right) = \nabla\cdot\left(\frac{\Delta t}{\rho}\left(\vec{f}^{n+1}-\vec{f}^{n}\right) - (\beta-\alpha)\tilde{\vec{u}}^n - (\gamma-\beta)\tilde{\vec{u}}^{n-1} + \gamma\tilde{\vec{u}}^{n-2}\right) \quad \text{in } \Omega, \tag{5.48}$$

$$\partial_n\varphi^{n+1} = \left(\vec{f}^{n+1}-\vec{f}^{n}\right)\cdot\vec{n} \quad \text{on } \Gamma_D, \tag{5.49}$$

$$B.C.\ (\varphi^{n+1}) \quad \text{on } \Gamma_N, \tag{5.50}$$

and upgrading the pressure and the solenoidal velocity via (5.47) and (5.43).
The second step is a correction-diffusion problem: *find* $\tilde{\vec{u}}^{n+1}$ *such that:*

$$\rho\frac{\alpha\tilde{\vec{u}}^{n+1}+\beta\tilde{\vec{u}}^{n}+\gamma\tilde{\vec{u}}^{n-1}}{\Delta t} - \mu\Delta\tilde{\vec{u}}^{n+1} = \vec{f}^{n+1} - \nabla p^{n+1} \quad \text{in } \Omega, \tag{5.51}$$

$$\tilde{\vec{u}}^{n+1} = \vec{0} \quad \text{on } \Gamma_D, \tag{5.52}$$

$$\mu\partial_n(\tilde{\vec{u}}\cdot\vec{n})^{n+1} = \vec{t}^{n+1}\cdot\vec{n} + p^{n+1} \quad \text{on } \Gamma_N, \tag{5.53}$$

$$\mu\partial_n(\tilde{\vec{u}}\cdot\vec{\tau})^{n+1} = \vec{t}^{n+1}\cdot\vec{\tau} \quad \text{on } \Gamma_N. \tag{5.54}$$

Again the main difficulty lies on the boundary condition (5.50). The natural choice consisting in choosing $\varphi^* = 0$ leads to the same issues as for the pressure-correction scheme since rates of convergences are lower that the expected ones. In [247], we have carried out the same reasoning as for the pressure-correction scheme and we proposed this formulation for the pressure computation step: *Find* φ^{n+1} *such that*

$$\frac{\Delta t}{\rho}\Delta\varphi^{n+1} = \nabla\cdot\left(\frac{\Delta t}{\rho}\left(\vec{f}^{n+1}-\vec{f}^{n}\right) - (\beta-\alpha)\tilde{\vec{u}}^n - (\gamma-\beta)\tilde{\vec{u}}^{n-1} + \gamma\tilde{\vec{u}}^{n-2}\right) \quad \text{in } \Omega, \tag{5.55}$$

$$\partial_n\varphi^{n+1} = \left(\vec{f}^{n+1}-\vec{f}^{n}\right)\cdot\vec{n} \quad \text{on } \Gamma_D, \tag{5.56}$$

$$\varphi^{n+1} = \varphi^* \quad \text{on } \Gamma_N, \tag{5.57}$$

where φ^* is solution of:

$$\left(\frac{\Delta t}{\rho}\partial_{x_2^2} - \frac{\alpha}{\mu}\right)\varphi^{n+1} = \partial_{x_2}\frac{\Delta t}{\rho}\left(f_{x_2}^{n+1} - f_{x_2}^{n}\right) - \nabla\cdot\left((\beta-\alpha)\tilde{\vec{u}}^n + (\gamma-\beta)\tilde{\vec{u}}^{n-1} - \gamma\tilde{\vec{u}}^{n-2}\right) - H^n, \tag{5.58}$$

with:

$$\begin{aligned} H^n = {} & \chi\nabla\cdot\left(\alpha\tilde{\vec{u}}^n + \beta\tilde{\vec{u}}^{n-1} + \gamma\tilde{\vec{u}}^{n-2}\right) - \frac{1}{\mu}\left(\beta\varphi^n + \gamma\varphi^{n-1}\right) \\ & - \frac{1}{\mu}\left(\alpha\,(t_{x_1}^{n+1} - t_{x_1}^{n}) + \beta(t_{x_1}^{n} - t_{x_1}^{n-1}) + \gamma\,(t_{x_1}^{n-1} - t_{x_1}^{n-2})\right). \end{aligned} \tag{5.59}$$

5.3.2 Numerical experiments

The same numerical experiments as for the pressure-correction scheme are carried out. Again we present firstly in Figure (5.3) the results using the natural choice for φ^* that is $\varphi^* = 0$ on Γ_N. The left part of the figure displays the error in L^2-norm for the pressure and velocity when we use the standard incremental scheme. We can see that the results are very bad and no order of convergence can be calculated.The right part exhibits the same quantities when using the rotational scheme with $\chi = 0.7$. We can see that only rates close to 1 for the pressure and $\frac{3}{2}$ for the velocity are obtained.

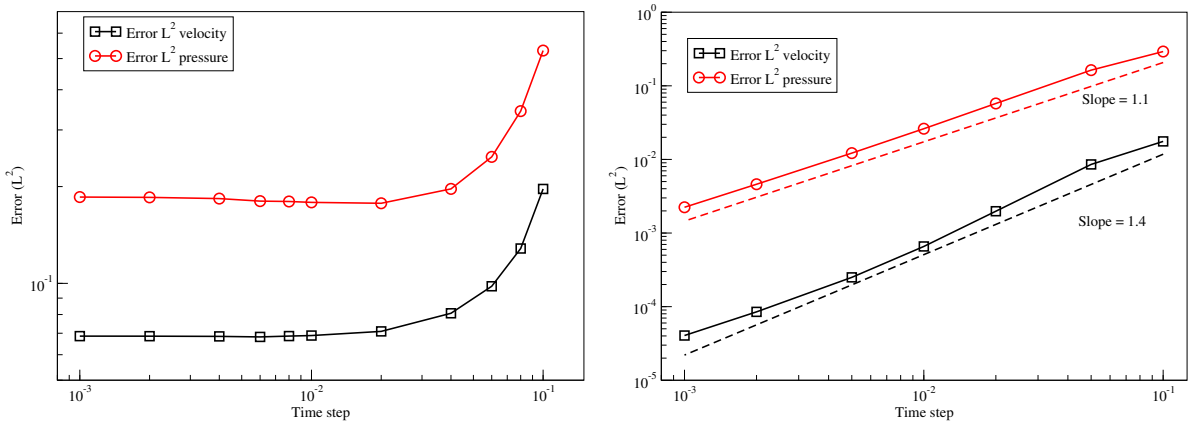

Figure 5.3: Time convergence rates with the standard incremental scheme (left) and the rotational scheme (right) at $t^* = 1$ with $K = 1$ and $p = 18$ with standard open boundary conditions and spectral element method.

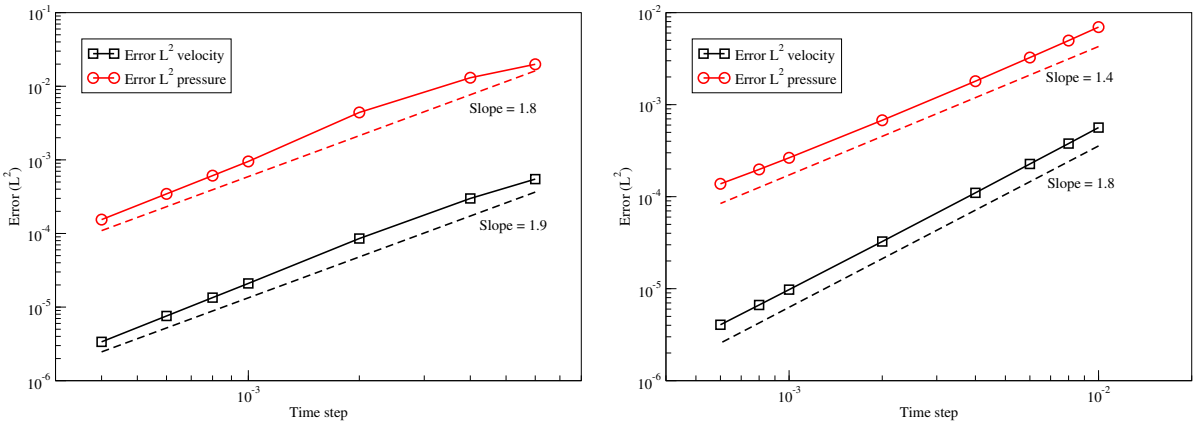

Figure 5.4: Time convergence rates with the standard incremental scheme (left) and the rotational scheme (right) at $t^* = 1$ with $K = 1$ and $p = 18$ with the proposed open boundary conditions and spectral element method.

In Figure (5.4), results corresponding to the proposed boundary condition are exhibited. Again, the left part of the figure depicts the errors with standard incremental scheme whereas the right part depicts the errors with the rotational scheme. We can see that for the standard incremental scheme rates of convergence close to 2 are obtained as expected. For the rotational scheme, we can remark that unlike the pressure-correction scheme for which the standard and rotational schemes give the same results with a slight improvement with the rotational scheme, the results show here a distinct advantage for the

standard version. Indeed, for the pressure, the convergence rate is now 1.4. This conclusion is confirmed by several numerical tests. A similar observation can be found in [135] where the Dirichlet boundary condition is considered for the Stokes problem.

Chapter 6

Domain decomposition method for the resolution of the Navier-Stokes equations

Contents

This chapter summarizes in detail article [26]:

- E. Ahusborde, S. Glockner, An implicit method for the Navier-Stokes equations on overlapping block-structured grids, International Journal for Numerical Methods in Fluids, Vol 62, 784-801, 2010.

  Abstract*: This paper deals with a method first introduced by Romé et al. in two articles. The authors reported that their method was suitable to run the Navier-Stokes equations efficiently on non-matching and overlapping block-structured meshes. However, there was a problem of mass conservation and a discontinuity of pressure through the interfaces in some cases. In the present paper, an improvement of the method based on a pressure correction scheme is proposed. With this improvement, the pressure is continuous through the interfaces and the incompressibility constraint is ensured over the whole domain. Several numerical tests were carried out to assess the proposed method.*

6.1 Introduction

In computational fluid dynamics when flows are calculated on complex geometries, one can use either a block-structured grid or an unstructured one. Unstructured grids allow to mesh very complex geometries

leading to complex discretization schemes and solvers that require table of connectivity between nodes and indirect addressing. If the geometry is not too complicated, it can be divided into a reasonable number of structured blocks. The lexical numbering makes easy the discretization of the equations (specially if the grid remains orthogonal) and the use of many solvers dedicated to the structured grids.
Domain decomposition methods are well suited to these problematics. They can be classified according to several criteria [253]. For instance, the block structured grids can be used with overlapping or non-overlapping. Generally, each block is computed separately and provides the boundary conditions for the neighbouring blocks. Historically, these methods have been introduced by Schwartz. The main drawbacks of this method is that overlapping is required for convergence. An improvement of these method consists in substituting overlapping by another boundary condition. In [192], Lions proposed the use of a Robin boundary condition. Our strategy consists in working with overlapping in order to deal with orthogonal grids. The main difficulty is to find a relevant projection operator on the interfaces between sub-domains. Mortar element methods have been proposed to solve this problem [62, 76]. Chimera methods represent an other approach [283]. These methods are particularly used in aerodynamic simulations.
Non-matching meshes raise the classical question of the interpolation. This difficulty becomes harder when the interpolation must be carried out under constraint. In case of the simulation of an incompressible flow, the constraint $\nabla \cdot \vec{u} = 0$ must be verified. Generally, interpolation is conservative if it is based on finite volume techniques [191, 293]. Fluxes through interfaces are calculated using local balance with a neighbouring block or a projection. Recently, a mass-flux based interpolation algorithm was proposed by Tang *et al* [284, 285]. Some authors who used a non-conservative interpolation have shown that mass conservation is directly linked to the order of the interpolation [148].
In this paper, we propose an implicit method to compute the incompressible Navier-Stokes equations on block-structured meshes based on a non-conservative interpolation. This study proposes an improvement of the method first introduced in [258] and [259]. Indeed, the authors have previously met problems in order to satisfy the incompressibility constraint on the interfaces between blocks leading in some cases to a discontinuity of pressure. They used the augmented Lagrangian method [121] for the pressure-velocity coupling. In the present case, this method has been replaced by a pressure correction scheme [292] in order to circumvent these drawbacks.
We first present the numerical context of this study by describing the models and numerical methods of the CFD code Aquilon (Aq. on figures and tables). Then, we describe the novelties of the method in comparison with the method firstly introduced in [258] and [259]. At last, numerical tests have been carried out in order to validate this method and clearly show the improvements.

6.2 Numerical context

In this chapter, the incompressible Navier-Stokes equations are considered using the pressure correction scheme [292] described in Section 5.2. The spatial discretization is based on the finite volume method on velocity-pressure staggered grid of the Marker and Cells type [144]. Pressure unknowns are associated to the cell vertices whereas velocity components are face centred. A centred scheme of order 2 is used in this work for the inertial and constraint terms.
The multifrontal sparse direct solver MUMPS [35] is used to solve the linear systems stemmed from velocity prediction and pressure correction steps.

6.3 An implicit method for connecting blocks

In order to connect the sub-domain, the missing information are transferred from block to block. Polynomial interpolations are build and integrated as special boundary conditions. The polynomial coefficients of the interpolation are present in the linear system and couple the solution on each block through the interface. The non-conservative interpolation of the variables at the interfaces can be seen as a new implicit boundary condition used for the discretization of the equation at the nodes strictly inside the different blocks.

6.3.1 Pressure correction step

Two blocks (a) and (b) are considered (see Figure 6.1). The pressure increment ϕ defined on block (b) is interpolated, which gives the new boundary conditions on block (a). Interpolation is based on the construction of a polynomial basis of a given order. For instance, the interpolation of ϕ at a point $M_0(x_0,y_0)$ belonging to a block (a) is obtained from the values of ϕ at points $M_i(x_i,y_i)$ on block (b) by the relation:

$$\phi^{(a)}(x_0,y_0) = f_{int}(\phi^{(b)}) = \sum_{i=1}^{N} F_i(x_0,y_0)\phi^{(b)}(x_i,y_i). \tag{6.1}$$

The interpolation must now be constructed locally to each node at the interface. The technique consists in building a canonical basis of Q-type of order d thanks to the neighbouring of $M_0(x_0,y_0)$. The number of nodes required depends on the order of the chosen polynomial. For instance, in case of a $Q^{(1)}$ interpolation Figure 6.1 represents the interpolation of the pressure on the node M_0 belonging to the interface of the block (a) obtained from the values of pressure on the nodes M_1, M_2, M_3 and M_4 belonging to the block (b).

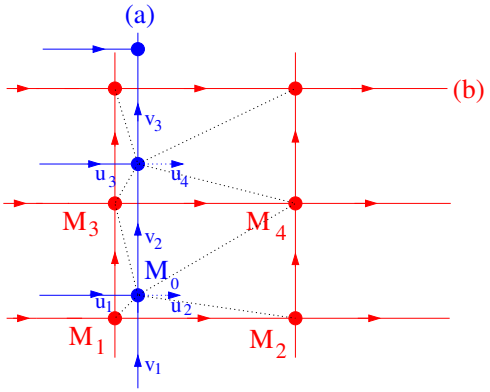

Figure 6.1: Interpolation of the pressure.

In order to reduce the values of the coefficients of the polynomial, M_0 is chosen as the centre of the frame. A polynomial $Q_i^{(d)}$ built using the M_i nodes, $1 \leq i \leq (d+1)^2$ is written:

$$Q_i^{(d)}(x-x_0,y-y_0) = \sum_{m=0}^{d}\sum_{n=0}^{d} a_{mni}\,(x-x_0)^m\,(y-y_0)^n. \tag{6.2}$$

$Q_i^{(d)}$ has the following properties:

$$\forall i,j \quad 1 \leq i,j \leq (d+1)^2, \quad Q_i^{(d)}(x_j - x_0, y_j - y_0) = \delta_{ij}. \tag{6.3}$$

The equation (6.2) associated with the property (6.3) can be seen as a line of the $(d+1)^2 \times (d+1)^2$ linear system $A \times B = Id$ with:

$$A = \begin{bmatrix} a_{001} & \cdots & a_{mn1} & \cdots & a_{dd1} \\ \vdots & & \vdots & & \vdots \\ a_{00i} & \cdots & a_{mni} & \cdots & a_{ddi} \\ \vdots & & \vdots & & \vdots \\ a_{00(d+1)^2} & \cdots & a_{mn(d+1)^2} & \cdots & a_{dd(d+1)^2} \end{bmatrix},$$

and

$$B = \begin{bmatrix} (x_1-x_0)^0(y_1-y_0)^0 & \cdots & (x_i-x_0)^0(y_i-y_0)^0 & \cdots & (x_{(d+1)^2}-x_0)^0(y_{(d+1)^2}-y_0)^0 \\ \vdots & & \vdots & & \vdots \\ (x_1-x_0)^m(y_1-y_0)^n & \cdots & (x_i-x_0)^m(y_i-y_0)^n & \cdots & (x_{(d+1)^2}-x_0)^m(y_{(d+1)^2}-y_0)^n \\ \vdots & & \vdots & & \vdots \\ (x_1-x_0)^d(y_1-y_0)^d & \cdots & (x_i-x_0)^d(y_i-y_0)^d & \cdots & (x_{(d+1)^2}-x_0)^d(y_{(d+1)^2}-y_0)^d \end{bmatrix}.$$

The inversion of this linear system (one for each node of the interface) is performed during the preparation step of a simulation and provides the values of the matrix A. The value of the pressure ϕ at node $M_0(x_0,y_0)$ reads:

$$\phi^{(a)}(x_0,y_0) = \sum_{i=1}^{(d+1)^2} Q_i^{(d)}(x_0,y_0)\,\phi^{(b)}(x_i,y_i). \tag{6.4}$$

The $Q_i^{(d)}$ can be placed in the linear system of the pressure correction step (see Figure 6.2).

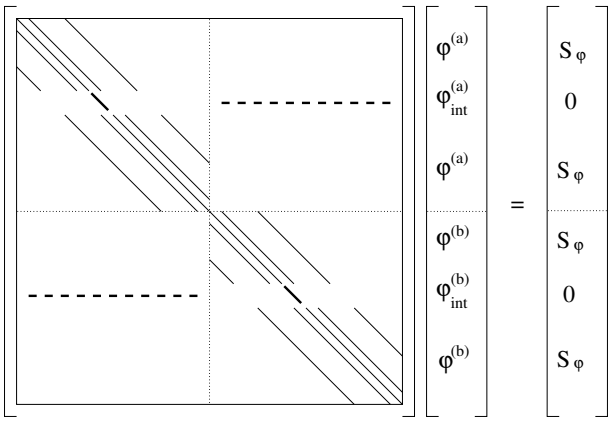

Figure 6.2: Representation of the pressure correction matrix on 2 blocks.

Thus, on a matrix line corresponding to a node at the interface, non-zero elements are the diagonal term and the elements with a column number corresponding to unknowns used to interpolate the pressure.

With this method, the pressure is obviously continuous at the interfaces (up to the order of the polynomial interpolation) but the divergence of the velocity is not null at the interfaces since the velocities u_2, u_4, v_1, v_2, and v_3 (see Figure 6.1) are not corrected by the pressure correction.
In order to circumvent this problem, we propose to increase overlapping between blocks adding a row of ghost nodes (nodes ϕ_1, ϕ_2 and ϕ_3 in figure 6.3).

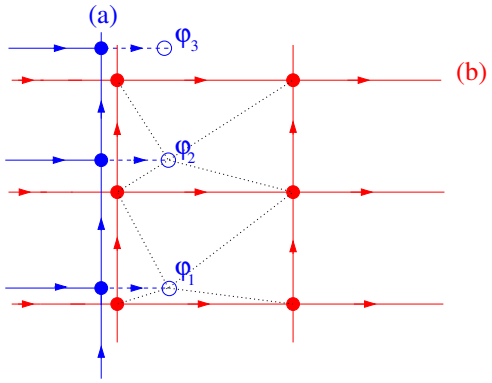

Figure 6.3: New stencil to ensure incompressibility constraint.

The pressure is now connected from one block to each other thanks to these ghost nodes. The pressure gradient can be computed precisely on velocity nodes at the interfaces. This addition allows satisfaction of incompressibility constraint. Nonetheless, the pressure is no longer continuous on the interface. It is probably due to an accumulation on the pressure nodes p^{n+1} at the interface of the interpolation error of ϕ^{n+1} on the ghost nodes. In order to overcome this problem, a new pressure correction scheme is proposed. The velocity prediction step does not change but the pressure correction step is modified and a third interpolation step is added. The new scheme reads as follow.

- Velocity prediction step: *Find* $\vec{u}_*^{n+1}$ *such that*

$$\begin{aligned} \rho\left(\frac{\vec{u}_*^{n+1}-\vec{u}^n}{\Delta t}+\nabla\cdot(\vec{u}_*^{n+1}\otimes\vec{u}^n)-\vec{u}_*^{n+1}\nabla\cdot\vec{u}^n\right) &= -\nabla p^n \\ +\nabla\cdot\mu(\nabla\vec{u}_*^{n+1} &+ \nabla^t\vec{u}_*^{n+1}), \quad \text{in } \Omega, \qquad (6.5)\\ \vec{u}_*^{n+1} &= \mathbf{0}, \quad \text{on } \partial\Omega, \qquad (6.6) \end{aligned}$$

- Pressure correction step: *Find* $\vec{u}^{n+1}$ *and* ϕ^{n+1} *such that*

$$\begin{aligned} \rho\frac{\vec{u}^{n+1}-\vec{u}_*^{n+1}}{\Delta t}+\nabla\phi^{n+1} &= \mathbf{0}, \quad \text{in } \Omega, \qquad (6.7)\\ \nabla\cdot\mathbf{u}^{n+1} &= 0, \quad \text{in } \Omega, \qquad (6.8)\\ \mathbf{u}^{n+1}\cdot\vec{n} &= 0, \quad \text{on } \partial\Omega, \qquad (6.9) \end{aligned}$$

  with:

$$\phi^{n+1}=\tilde{p}^{n+1}-p^n+\mu\nabla\cdot\vec{u}_*^{n+1}, \qquad (6.10)$$

- Interpolation step: *Compute* p^{n+1} *such that*

$$\begin{aligned} p^{n+1} &= \tilde{p}^{n+1}, \quad \text{in } \Omega/\Gamma, \qquad (6.11)\\ p^{n+1} &= f_{int}(\tilde{p}^{n+1}), \quad \text{on } \Gamma, \qquad (6.12) \end{aligned}$$

where Γ is the whole interface between blocks and f_{int} represents the interpolation function on Γ.

This new scheme ensures continuity of the pressure through the interfaces and still verifies the incompressibility constraint.

6.3.2 Velocity prediction step

Interpolation of the velocity is more difficult since it is a vector field. If the blocks have not the same orientation, both velocity components are needed to compute a single component of the velocity field on the interface. For a precise description of the method, particularly the interpolation technique on cartesian blocks with any orientation or on curvilinear blocks, the reader is referred to [259]. Previously, the interpolation of the normal component of the velocity field at the interface was performed on pressure nodes whereas the tangential component was interpolated at the velocity nodes. In the present case, both components are interpolated at the velocity nodes (see Figure 6.4 in case of a $Q^{(1)}$ interpolation).

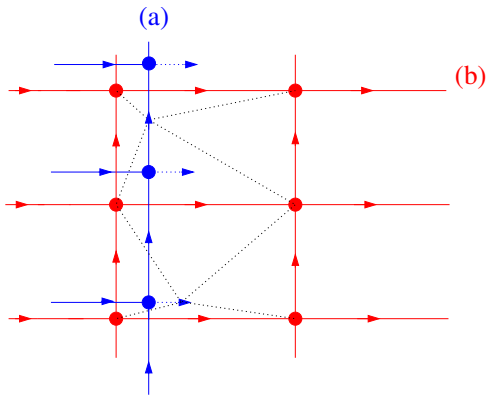

Figure 6.4: New interpolation of the velocity vector on a staggered grid.

In next section, many computations have been carried out to assess the proposal method and to exhibit its improvements in comparison with [259]. $Q^{(2)}$ polynomial interpolation has been systematically used. This leads to a 5-points stencil for the pressure and to a 24-points stencil for the velocity.

6.4 Numerical results

In [26], a series of numerical experiments has been performed to evaluate the accuracy and the efficiency of the method. Here we present only the study of a flow past a triangular cylinder. The Reynolds number is based on the side of the triangular cylinder and the axial velocity inlet. We are interested in two flow ranges according to the value of the Reynolds number in relation to the critical Reynolds Re_c:

- $Re < Re_c$: the flow is stationary. One can observe two steady symmetrical vortices behind the cylinder whose size increases with increase in Re.

- $Re \geq Re_c$: the flow becomes unsteady and periodic. Two vortices form at the rear-end vertices of the cylinder and are shed alternately.

Jackson [156] studied the onset of vortex shedding in flow past variously shaped bodies. For an isosceles triangle with base 1 and height 0.8, he reported a critical Reynolds as 34.318 and a corresponding Strouhal number as 0.13554. Zielinska and Wesfreid [339] computed a flow past an equilateral triangle with a blockage ratio equal to $1/15$ and found a critical Reynolds of 38.3. De and Dalal [99] carried out a similar study and calculated a critical Reynolds of 39.9 for a blockage ratio of $1/20$. This case has been chosen because most of the studies deal with the flow past circular or square cylinder and laminar flow past a triangular cylinder has not been intensively treated so far. Moreover, this configuration is well adapted to validate and illustrate the interest of block-structured meshes.

6.4.1 Parameters of the case test

The configuration is presented in Figure 6.5.

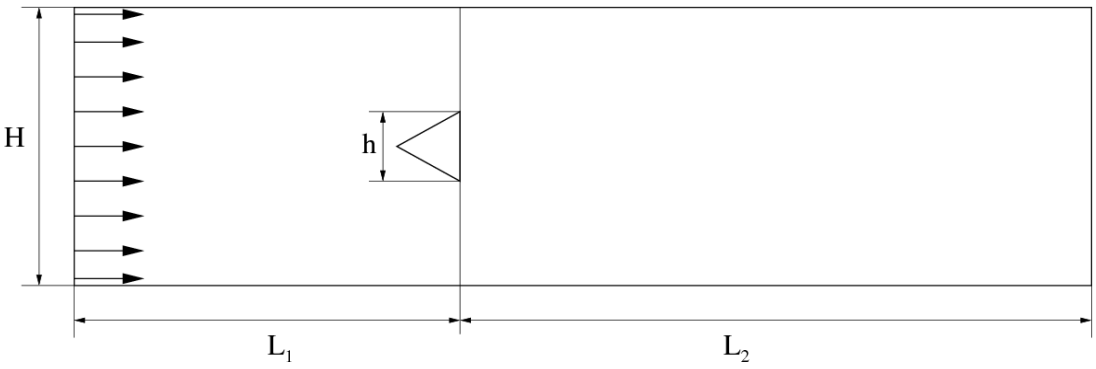

Figure 6.5: Global features of the computational geometry.

Figure 6.6 represents the block-structured mesh used in this case. The grid is fine around the cylinder and space step size increases in front of and behind it. The number of grid nodes distributed over a side of the cylinder is 100. The total number of elements is 137980. At the inlet, a flat profile is imposed for the axial velocity u and zero for the velocity v. At the outlet, a Neumann condition is imposed on both velocity components. We will compare the results with [99].

6.4.2 Steady flow

The streamlines in the vicinity of the cylinder for several Reynolds number are shown in figure 6.7. To assess the method, the recirculation length (L_r) defined by the reattachment of the fluid has been measured and a linear relationship between L_r and Re has been obtained in [99] (see figure 6.8). The results seem to be in good accordance with those presented in [99].

6.4.3 Unsteady and periodic flow

The flow becomes unsteady and periodic for $Re \geq 40$. For $Re = 100$, the time-average drag coefficient (C_D), time-average pressure drag coefficient (C_{D_p}), rms of the lift coefficient ($C_{L_{rms}}$) and the Strouhal number (St) are compared with [99]. We can see in table 6.1 difference below 5% except for the $C_{L_{rms}}$ where the gap is 11%. It can be explained by the difference of the mesh size and the numerical method used by the authors.

Finally, Figure 6.9 shows the streamlines around the triangular cylinder during a period at $Re = 100$.

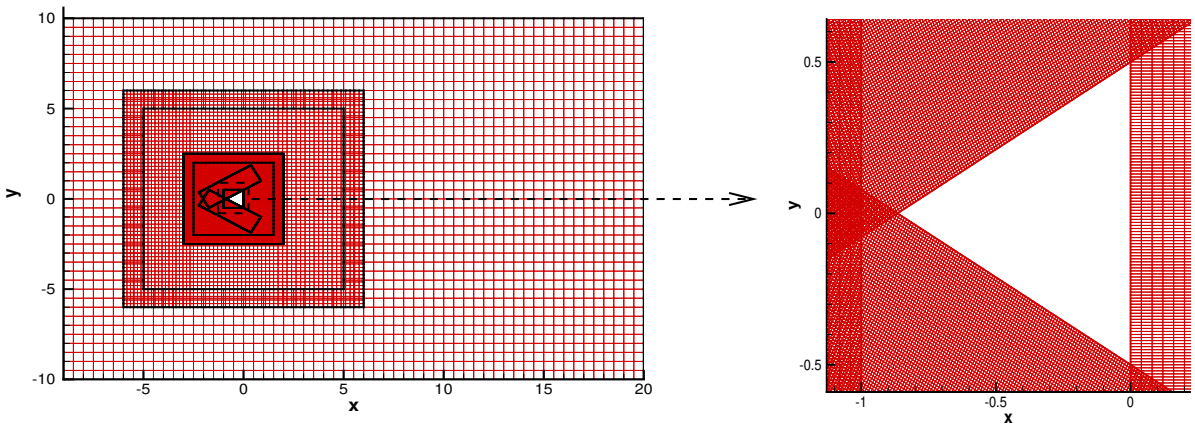

Figure 6.6: Block-structured mesh for the flow past a triangular cylinder.

	C_D	C_{D_p}	$C_{L_{rms}}$	St
Present	1.6698	1.3579	0.2626	0.1960
De and Dalal [99]	1.7549	1.2986	0.2974	0.1962

Table 6.1: Comparison of the results for $Re = 100$.

6.5 Conclusion

In this chapter, we have proposed an improvement of a method firstly introduced by Romé *et al* in [259]. Both methods deal with a domain decomposition technique for non-conforming and overlapping block-structured meshes. They are non-iterative and based on a implicit non-conservative interpolation of the variables at the interfaces. The linear systems are modified in comparison with those obtained on a monoblock mesh since lines are added to take into account the connectivity between blocks.
The main difference of the two methods is the velocity-pressure coupling. In [259], the authors treated this coupling by a augmented Lagrangian method. In some cases, the divergence of the velocity at the interfaces between block was not null leading to a discontinuity for the pressure. In the present work, velocity and pressure have been coupled by a pressure correction scheme. The divergence of the velocity is now null on the whole domain and the discontinuity of pressure has disappeared.
Several numerical test have been carried out in order to validate the proposed method. They have clearly showed its feasibility and its accuracy.

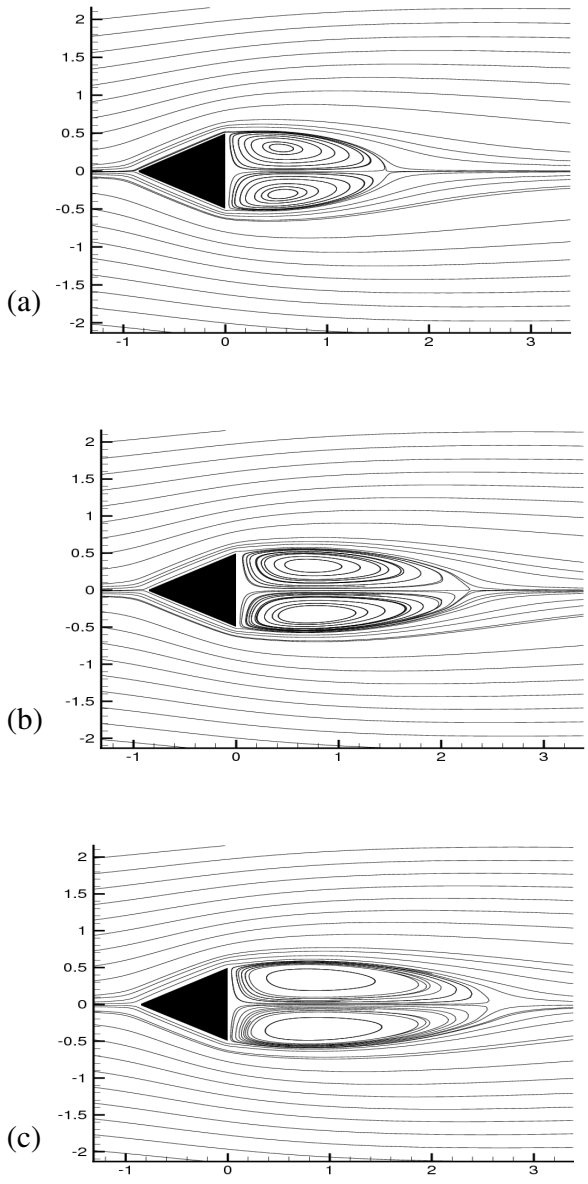

Figure 6.7: Steady state streamlines (a) $Re = 20$, (b) $Re = 30$ and (c) $Re = 35$.

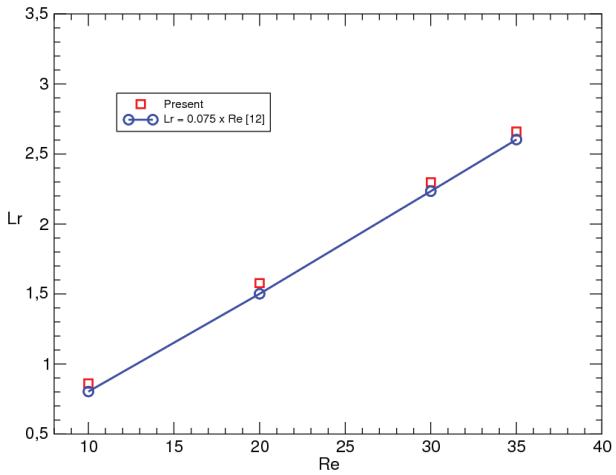

Figure 6.8: $L_r - Re$ relationship.

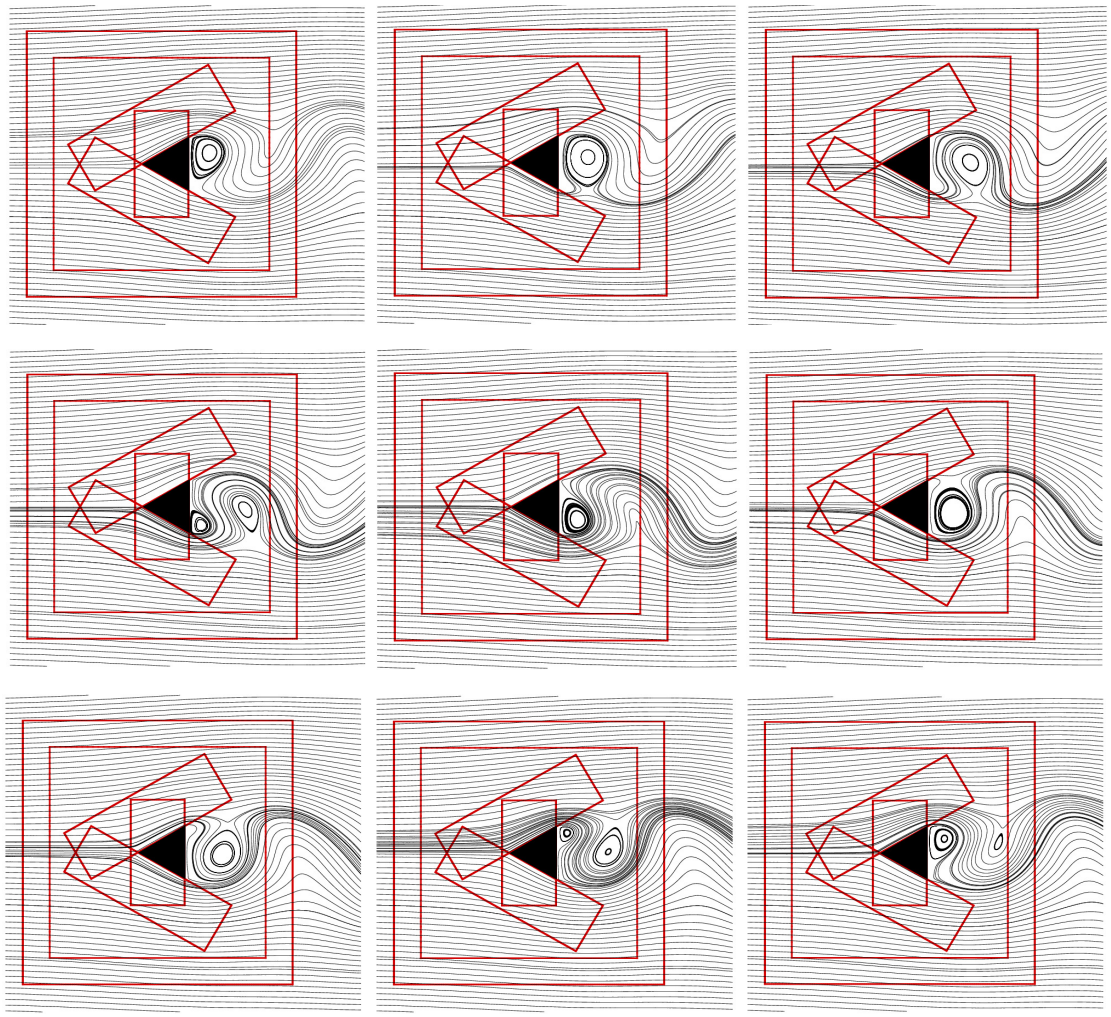

Figure 6.9: Streamlines for the flow past a triangular cylinder during a period at $Re = 100$ (it reads from left to right and vertically).

Chapter 7

Mesh partitioner for numerical simulation of flow on non-rectangular geometries

Contents

This chapter proposes a detailed synthesis of article [27]:

- E. Ahusborde, S. Glockner, A 2D block-structured mesh partitioner for accurate flow simulations on non-rectangular geometries, Computers and Fluids, Vol 43, 2-13, 2011.

Abstract*: The motivation of this work is to carry out parallel simulations of incompressible flows on block-structured meshes. A new partitioning method is proposed. The quality of rectangular partitions is checked and compared with other methods, as regards load balance, edge-cut and block numbers. The partitioner is coupled with the massively parallel HYPRE solver library and efficiency of the coupling is measured. Finally, the code is applied to study laminar flows (steady and unsteady) on three non-rectangular geometries. Very fine grids are used to compute reference solutions of a Z-shaped channel flow and the L-shaped and double lid driven cavities.*

7.1 Introduction

Flow simulations on complex geometries require either block-structured or unstructured grids. The latter allow very complex geometries to be meshed leading to complex discretization schemes and solvers that require a table of connectivity between nodes and indirect addressing. If the geometry is not too complicated, it can be divided into a reasonable number of structured and conforming blocks. The

volume control aspect and lexical numbering facilitate the discretization of the equations (specially if the grid remains orthogonal) and the use of the fastest parallel solvers dedicated to the structured grids.
Solver performances are closely linked to the mesh partitioning or the matrix graph. Partitioning methods can be divided into two classes: geometric and combinatorial [105]. Geometric techniques are based on the coordinates of the mesh nodes whereas combinatorial partitioning uses the graph or the hypergraph of the mesh. Geometric techniques produce lower quality partitions than combinatorial methods but are extremely fast. For unstructured meshes, partitioner libraries such as CHACO [147], METIS [167], SCOTCH [239] are available. Unfortunately, they are not well suited to the block-structured framework since they produce unstructured partitions, as shown in Figure (7.1).

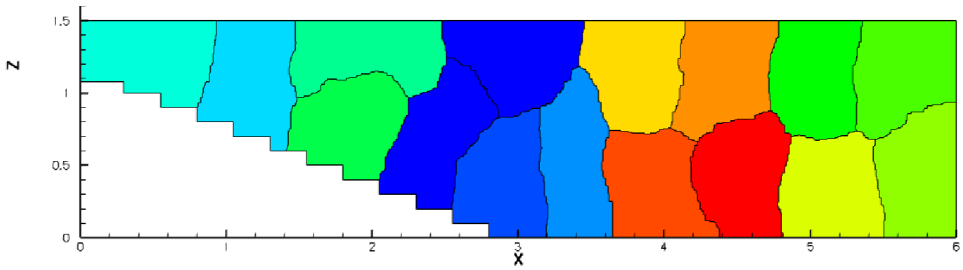

Figure 7.1: Partitioning provided by METIS.

For block-structured meshes, few works have been carried out. The two main strategies used for the partitioning of such meshes are the recursive edge bisection [60] and the so-called greedy algorithm [331]. These geometric techniques are used in elsA software [131] which is devoted to compressible flows around complex geometries. We can also cite the works of Rantakokko [256] who proposes a framework for partitioning composite grids. In our opinion, his more interesting approach consists in a graph strategy applied at the block level instead of the node level (block refinement is also proposed).

Our goal consists in providing a partitioning strategy for block-structured geometries which produces rectangular partitions. It can be classified as a geometric method even if the coordinates of the nodes are not used. The partitioner is coupled with the massively parallel solver and preconditioner HYPRE library [110], more precisely with the semicoarsening geometric multigrid solver [72]-[265]. Firstly, we are going to present the different steps upon which the proposed method relies. Then, on the particular example of a double lid driven cavity studied in [227] and [338], we will compare the quality of the partitions with other approaches and analyze the performance of the coupling with HYPRE solvers. Lastly, we will apply our code to compute incompressible flow on a this particular geometry.

7.2 Partitioning strategy

Firstly, let us recall the two main qualities of a partitioner:

- It must respect load balancing between processors: each processor should have nearly the same amount of work to do to minimize idle processors. In our context, each processor should have around the same number of nodes, close to the ideal load which is equal to the number of nodes divided by the number of processors.
- It must minimize explicit communication between processors, *i.e.* the surface-to-volume ratio or edge-cuts. The goal is to delay as far as possible the moment when communications between

processors increase such that efficiency collapses as the number of processors rises.

The conceptual interface [111] of HYPRE is quite complete and supports four options: structured grid, block-structured grid, finite element interface, and linear algebraic interface. The fastest solvers such as geometric multigrid ones are available for structured grids, and block-structured grids, which is our framework. The interface requires global indexing of the nodes and rectangular boxes that can be non-contiguous. In the next sections, we will present the main steps of the partitioner and finally a complete algorithm that can be used in another solver framework.

7.2.1 An elementary block decomposition

In our opinion, the partitioner should be independent of the initial block construction. For instance, two geometries are defined on the left part of Figure (7.2). On the right part, different ways to decompose them, into 3 or 4 blocks are presented (that can be later meshed). Meshes are not shown but they are continuous through the interfaces between blocks. In the proposed method, the same partition will be produced for any geometry decomposition. This approach avoids having to consider parallelism during the construction phase of the mesh.

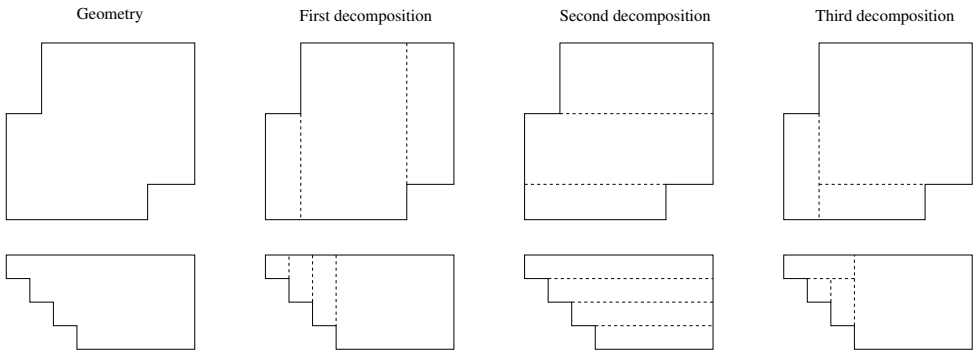

Figure 7.2: Example of geometries.

Consequently, the first step consists of splitting the main blocks into elementary ones. This is done by lengthening each boundary line. Intersections between lines define corners of new elementary blocks. For instance in Figure (7.3), 3 blocks of the geometry are split into 7 elementary ones.

At this point, we can make 3 remarks:

- These elementary blocks are now the starting point of our partitioner.
- There is no reason for these blocks to be balanced.
- These blocks could have been created during the construction phase of the mesh, but it can become really fastidious for a large number of blocks.

7.2.2 Block merging

The second step of the partitioner consists in merging the elementary blocks into macro-blocks. In Figure (7.4), we have merged 10 elementary blocks into 4 macro-blocks. The first macro-block is the largest of all possible macro-blocks. Then with the remaining elementary blocks, we choose the largest remaining macro-block and so on until there is no more elementary blocks. The idea of generating

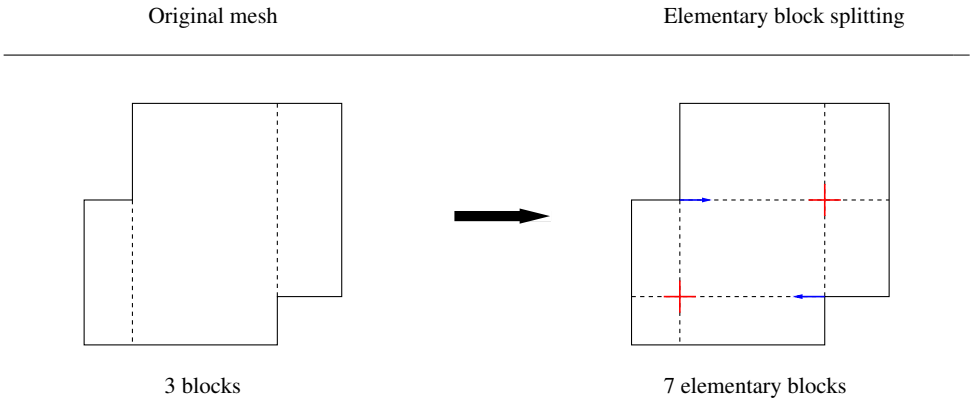

Figure 7.3: Elementary block splitting.

macro-blocks as big as possible is to minimize the number of blocks (and consequently to maximize their size) for which we are able to construct simple and optimal partitioning. Each macro-block is split into 3 zones (see Figure (7.5)). The main zone is zone 1 while zones 2 and 3 are residual zones.

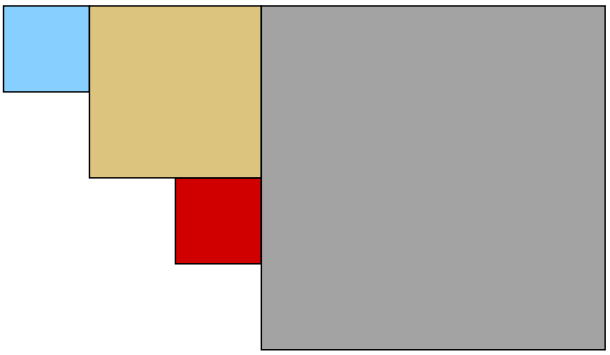

Figure 7.4: Merging of elementary block into rectangular macro-blocks.

7.2.2.1 Main zone

The size of the main zone is chosen such that it is a multiple of the ideal load. Then, straightforward partitioning that minimizes edge-cut and respects load balancing is applied.

The number of cells in each direction of space is taken as an input by the partitioning (N_x = number of cells in the x direction, N_y= number of cells in the y direction). It can produce square or rectangular partitions. We also consider a special case if the number of processor associated to the zone 1 is a prime number (see Figure (7.6)).

7.2.2.2 Residual zones

Residual zones 2 and 3 of two different macro-blocks are associated to one processor so that the sum of their size is equal to the ideal load. Thus, load balancing is ensured (see Figure (7.5)).

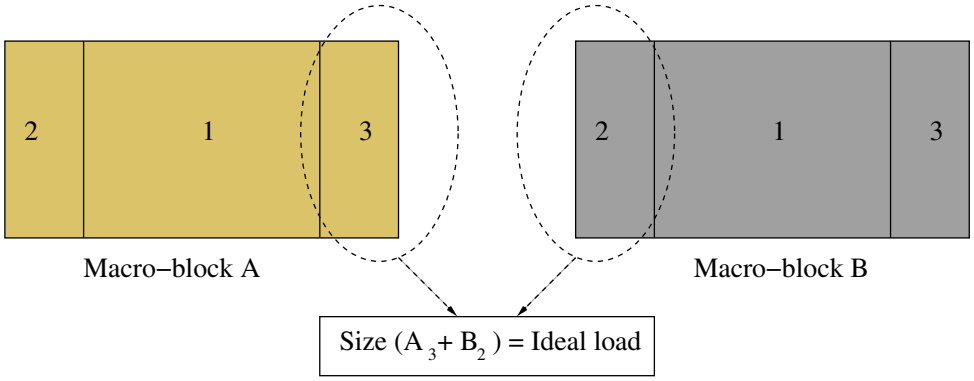

Figure 7.5: Residual zones.

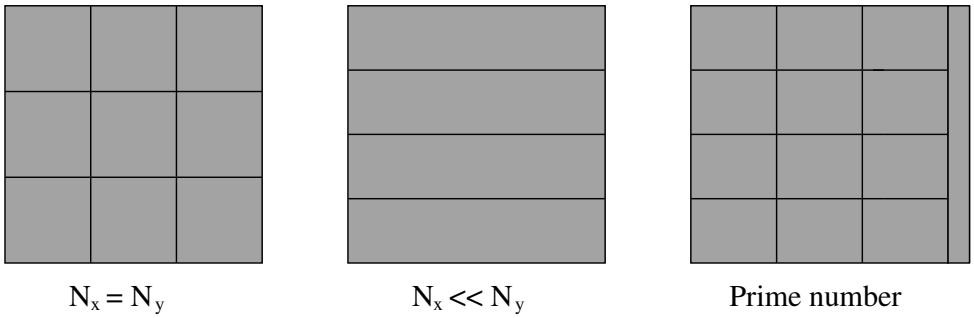

Figure 7.6: Partitioning for the main zone.

We can note in Figure (7.4) that very small macro-blocks (the darker one) can be composed just of one zone 2 or the sum of zone 2 and 3. These zones can create some non-contiguous regions on the same processor.

7.2.3 Node partitioning

If we had used cell partitioning, further caution would not have been necessary. With node partitioning, however, care has to be taken to the boundaries between blocks that can lead to non-rectangular macro-blocks. Indeed, as shown in Figure (7.7), there exist two configurations that produce a broken boundary line. The only solution is to split the blocks in two parts. These configurations are quite rare in the cases we have studied.
From this set of geometric considerations, an algorithm (1) has been extracted that can be applied to any 2D block-structured grid.

7.3 Block-Structured partitioner quality and performance

7.3.1 Load balancing and edge-cuts

In this section, we test the quality of the partitioner concerning the load balancing, the number of edge-cuts, the number of blocks and the time consumed by the partitioning in comparison with those using

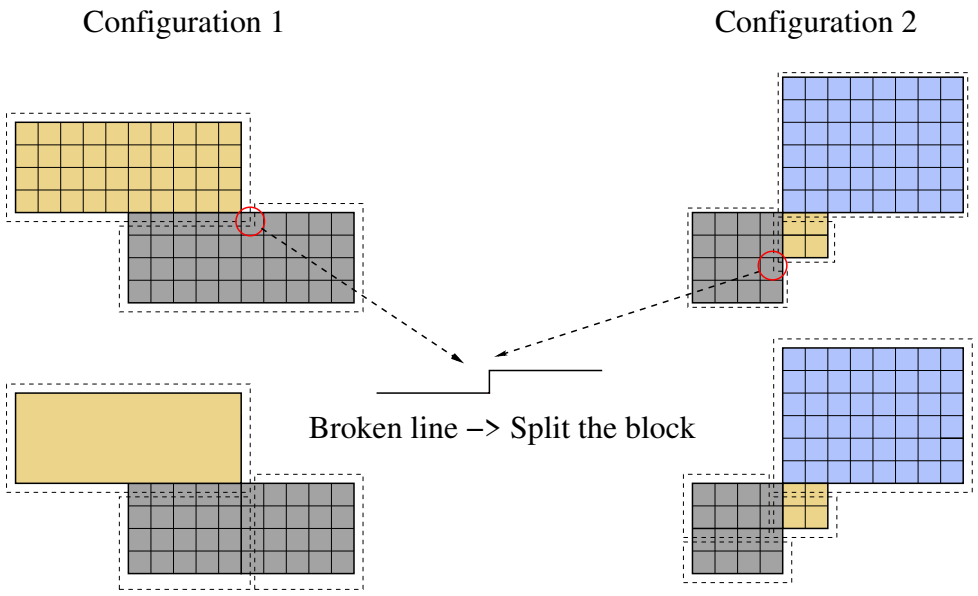

Figure 7.7: Block merging rules.

METIS, the recursive edge bisection (REB) and the greedy algorithm (GA). For the two latters, results have been obtained with elsA software [131]. Several examples were considered in [27] but we only present the double cavity geometry, composed of 3 blocks, 4 elementary blocks and 4×10^5 nodes. Figure (7.8) represents the partitions for 16 and 64 processors (one color per processor).

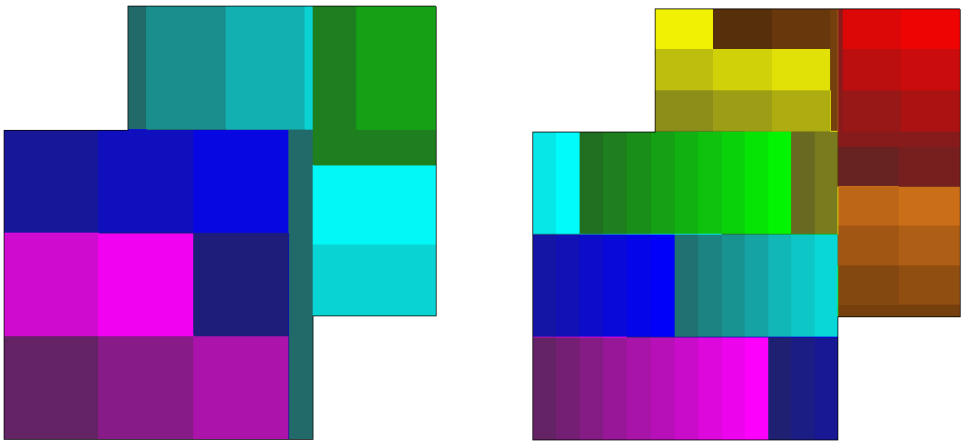

Figure 7.8: Partitioning of a double cavity mesh.

Table (7.1) compares load imbalance, edge-cut and block numbers between the different approaches.

The test cases underline very good load imbalance lower than 1% if the number of processors is not too high. It confirms that splitting macro-blocks into 3 zones is efficient, residual zones being associated to verify ideal load. Lower load imbalance cannot be reached because the precision of the partitioner is equal to the length of a mesh line (necessary to keep rectangular partitions). If the number of processors

Algorithm 1 Partitioning strategy

```
Elementary block splitting
for Each elementary block do
    Create the list of all possible rectangular macro-blocks associated to the elementary block
end for
while Macro-block partitioning not finished do
    Choose the biggest remaining macro block
    if Configuration 1 then
        Reject the macro-block from the list
    else if Configuration 2 then
        Cut the block and update macro-block list
    else
        Accept the macro-block and update macro-block list
    end if
end while
for Each macro-block do
    Construction of the main zone and residual zones
    Partitioning of the main zone
end for
return
```

increases, load imbalance increases but remains lower than 3%. Here, the partitioning effect of zone 1 is more visible: the size of a line of the mesh is relatively high in comparison with the size of the partition. The number of edge-cuts is overall very good, better than with METIS. REB method shows optimal results as regards edge-cut and block numbers but very high load imbalance (up to 47%) which is a crippling default. Moreover, this method did not provide acceptable results for the ring mesh probably because of the circular aspect of the geometry. Load imbalance produced by the GA is controlled by an epsilon parameter which has a consequence on the number of blocks generated: the lower is ε the lower is the load imbalance, but the greater is the number of blocks. Two values for ε have been used: 0.05 and 0.001. For $\varepsilon = 0.001$ load imbalance is very low, edge-cut number is acceptable but the number of blocks is more than the double of the number of processors. That leads to a high number of non-contiguous subdomains associated to a processor: it can reduce solver efficiency and it increases the memory requirement due to the multiplication of ghost cells necessary to the communications between processors [131]. For $\varepsilon = 0.05$, load imbalance is higher than our method, as well as edge-cut and block numbers. Finally for the ring example, CPU time shows that the proposed block-approach is much faster (nearly 30 times) than the other methods. This point could be even more relevant for 3D partitioning where CPU time is much longer. We can conclude that the proposed method is efficient for the studied geometries and shows a good compromise between all the partitioning requirements.

7.3.2 Scalability

The efficiency of coupling the partitioner and the HYPRE library is illustrated solving the Poisson equation obtained from one velocity correction step [130] which is very CPU time consuming in a Navier-Stokes solver. The studied problem is the double lid driven cavity flow.

The solver is a GMRES (Generalized Minimal Residual Method) associated to the geometric semi-coarsening multigrid preconditioner. The relative residual is set to 10^{-10}. The code runs on an SGI ICE

Number of processors	8	16	32	64
Load Imbalance Present (%)	0.54	0.44	1.40	2.87
Load Imbalance METIS (%)	1.54	2.28	3.17	3.28
Load Imbalance REB (%)	17.07	17.07	17.08	17.08
Load Imbalance GA 0.001 (%)	0.08	0.08	0.09	0.09
Load Imbalance GA 0.05 (%)	0.97	4.49	5	4.85
Edge-cuts Present	2829	4584	7513	11360
Edge-cuts METIS	3230	4853	7507	11176
Edge-cuts REB	2300	3800	6000	9000
Edge-cuts GA 0.001	3183	5042	7706	13259
Edge-cuts GA 0.05	3077	4636	7303	12961
Number of blocks Present	11	19	35	66
Number of blocks METIS	8	16	32	64
Number of blocks REB	8	16	32	64
Number of blocks GA 0.001	21	49	87	171
Number of blocks GA 0.05	14	22	41	94

Table 7.1: Partitioner performance for the double cavity mesh.

cluster. Two types of processors have been used: Harpertown nodes linked to a DDR Infiniband network and Nehalem nodes linked to a QDR Infiniband network.

7.3.2.1 Weak Scaling

The left part of Figure (7.9) displays for each type of processor (Harpertown and Nehalem) CPU time as a function of the number of processors, with 32500 and 65000 degrees of freedom (dof) per processor. We can see that processors Nehalem are much faster than Harpertown ones, particularly if the number of processors is low. A time ratio from 1.3 to 2.1 can be observed.

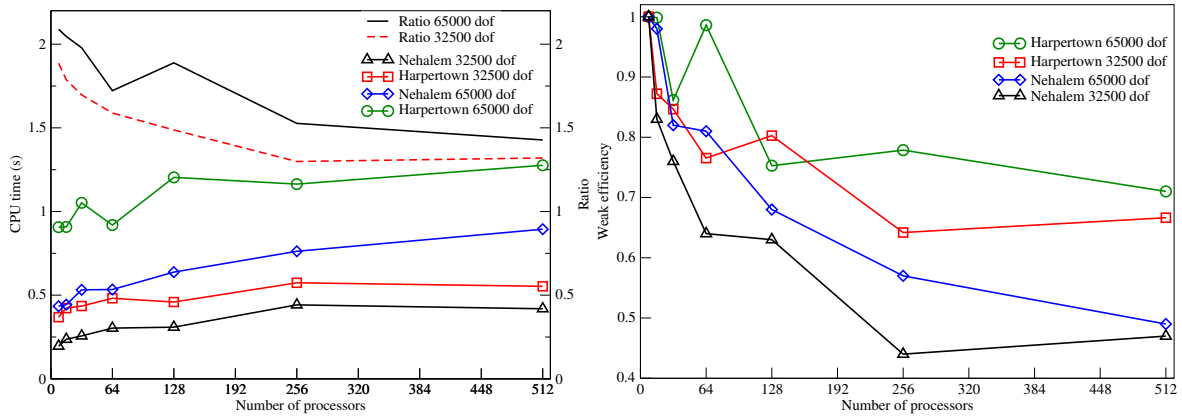

Figure 7.9: Left: CPU time versus the number of processors. Right: Weak scaling versus the number of processors.

Weak efficiency is presented in the right part of Figure (7.9). Efficiency equal to one indicates an optimal behaviour for the algorithm and the computer architecture. Indeed, CPU times remains constant, equal to the reference time, while the total size of the problem increases with the number of processors. Usually, this property is hardly verified and curves with plateaus can be observed. Values of the plateaus rise toward one with the load of each processor. This phenomenon is illustrated in Figure (7.9). Weak efficiency is better for the Harpertown cluster than the Nehalem one, besides a longer computation time.

7.3.2.2 Strong Scaling

The left part of Figure (7.10) displays for each type of processor (Harpertown and Nehalem) on a logarithmic scale, CPU time as a function of the number of processors for two fixed size problems of 1 and 16 million degrees of freedom. Again, processors Nehalem are much faster than Harpertown ones.

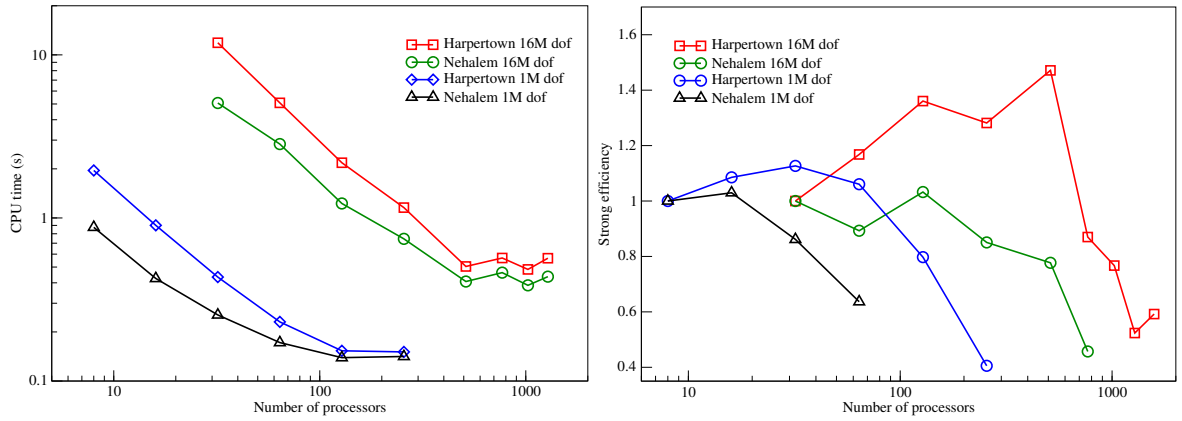

Figure 7.10: Left: CPU time versus the number of processors. Right: Strong scaling versus the number of processors.

The right part of Figure (7.10) represents the strong scaling versus the number of processors on a semi-logarithmic scale. With the Harpertown architecture and 16 million dof, a very high efficiency greater than 0.8 for up to 1024 processors can be observed (16000 dof per processor). The first part of the graph being over the expected efficiency is due to memory bandwidth saturation when the number of processors is low that leads to a long reference time in the strong efficiency formula. Using more processors leads to smaller tasks that lead to a performance increase when more and more data can be kept in cache. With 1 million dof, this effect is less visible ans scaling is very good up to 128 processors (8000 dof per processor). With the Nehalem architecture which has a much higher memory bandwidth (more than 3 times), efficiency curves have the expected behavior. Consequently, optimal efficiencies are obtained for 512 and 32 processors respectively for the 16 and 1 million dof problems. The saturation of the efficiency due to the increase of the communications between processors appears earlier with this architecture.

The next part of chapter the is devoted to the study of incompressible flows in non-rectangular geometries using the approach proposed here.

7.4 Computations of incompressible flows on non-rectangular geometries

Laminar flows in rectangular geometries, such as the lid driven cavity [73]-[240], have been extensively studied in the literature. Several numerical methods have been compared and reference solutions are available for a wide range of Reynolds numbers (leading to stationary or unsteady flows). In [27], we proposed a precise solution of flows for three non-rectangular geometries, scarcely studied so far but here we focus only on the double lid driven cavity.

Time discretization of the Navier-Stokes equations is implicit thanks to Gear's second order backward differentiation formula [124]. A pressure correction method (see Goda [130]) is used to solve the velocity-pressure coupling. Spatial discretization (second order centered scheme) is based on the finite volume method on a staggered grid of the Marker and Cells type. Solvers of the HYPRE library are used.

Flow in a double lid driven cavity has been studied in [227] and [338]. This configuration is presented in the left upper part of Figure (7.11).

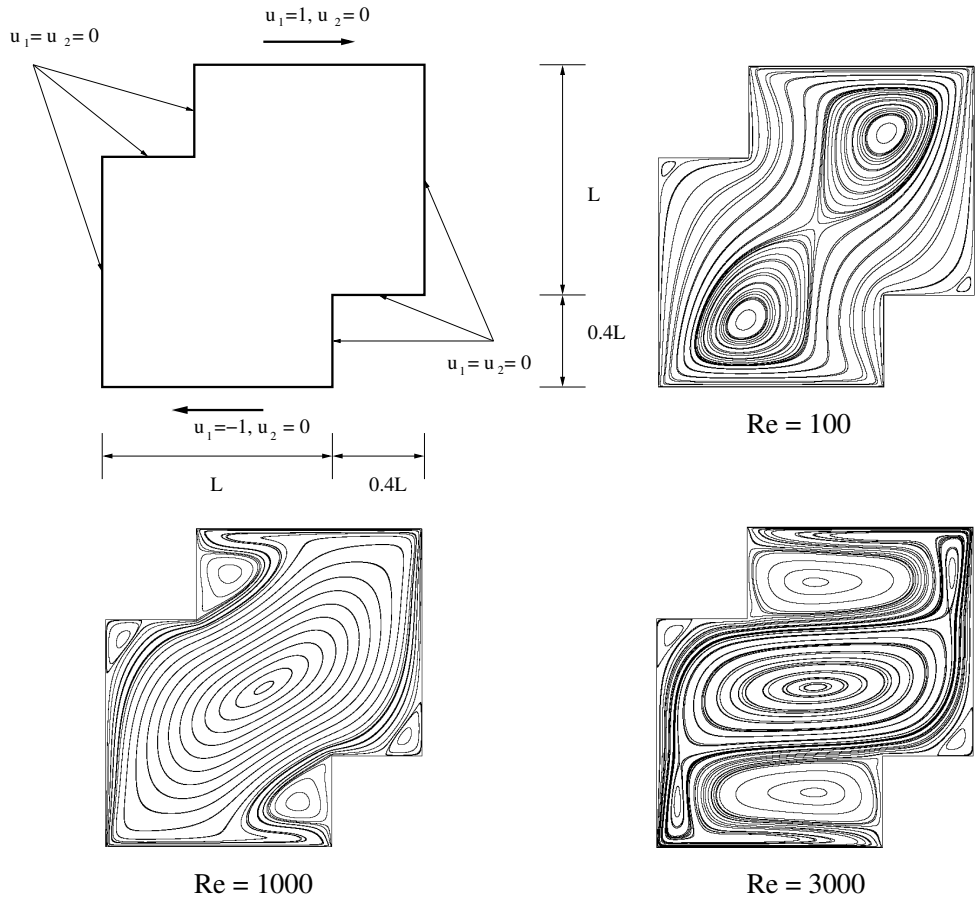

Figure 7.11: Configuration of the double lid driven cavity and streamlines for different Reynolds numbers.

The fluid is driven by the lower and upper boundaries in opposite directions. The other boundaries are walls. The Reynolds number Re is based on the cavity length L and the lid velocity. We focused on two flow ranges according to the value of the Reynolds number in relation to its critical value Re_c:

- $Re < Re_c$: the flow is stationary. We can note three different regimes represented in Figure (7.11).

On the upper right part for $Re = 100$, twin primary eddies are created between the two driving lids while secondary vortices appear in the left and right corners. In the lower left part for $Re = 1000$, the two primary vortices coalesce and two secondary vortices appear. Finally, in the lower right part for $Re = 3000$, the primary eddy becomes horizontal. The size of the two latter secondary vortices increases and two new secondary eddies appear (vertically on the upper right and lower left parts of the domain). However, it is now well-known [289] that cavity flows experience 3-dimensional global instability well below Re_c. Consequently, for $Re \geq Re_c^{3D}$ 2-dimensional studies are not physical anymore even if they can present numerical interests. Re_c^{3D} has been recently identified for the double and cross-sectional cavity flows [101]. For the former, it characterizes the transition between the two first flow regimes.

- $Re \geq Re_c$: the flow becomes 2D unsteady, from periodic to chaotic. In [240] and [73], a study was carried out to identify the transition from stable to periodic flow in the case of the 2D lid driven square cavity flow. The flow becomes unstable via a Hopf bifurcation. In [73], the first Lyapunov exponent was used to compute a critical Reynolds number Re_c close to 8000. In [240], thanks to a different approach (unsteady simulations with small time step), the first Hopf bifurcation occurs for $Re_c = 7402$. Several subcritical and supercritical flow regimes were identified.

Here we focus on the study of the steady flow ($Re = 1000$) but in [27], unsteady simulations were performed. The lower left part of Figure (7.11) displays the streamlines. As described above, a primary vortex and four secondary eddies appear. With very fine meshes, ternary vortices appear between the secondary ones and the corner of the domain (see right part of Figure (7.12)). These vortices were not shown in previous studies [338] and [227]. Figure (7.12) represents two zooms in which we define the points $P_i\,(x_i, y_i)$ of detachment and reattachment of the flow. The results found in the literature are given on the intensities and positions of the vortices. In the present study, the results were obtained with convergence criteria on stationarity below 10^{-12} between two consecutive iterations. Four increasingly fine grids with 6.25×10^4, 2.5×10^5, 10^6 and 4×10^6 nodes have been used.

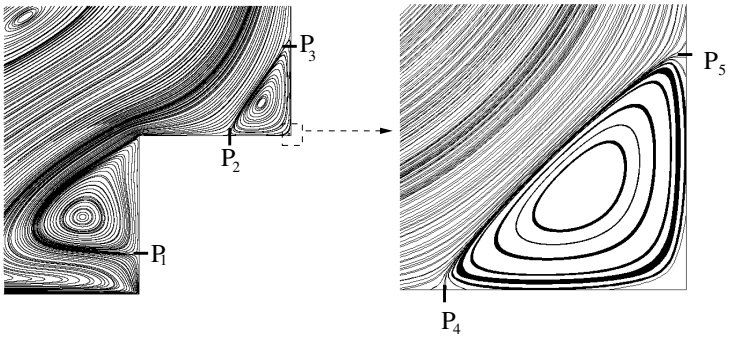

Figure 7.12: Streamlines for the double lid driven cavity for $Re = 1000$.

Velocity profiles In Figure (7.13), the velocity profiles at $x = 0.7$ and $y = 0.7$ present good accordance with those obtained by Zhou et *al* [338].

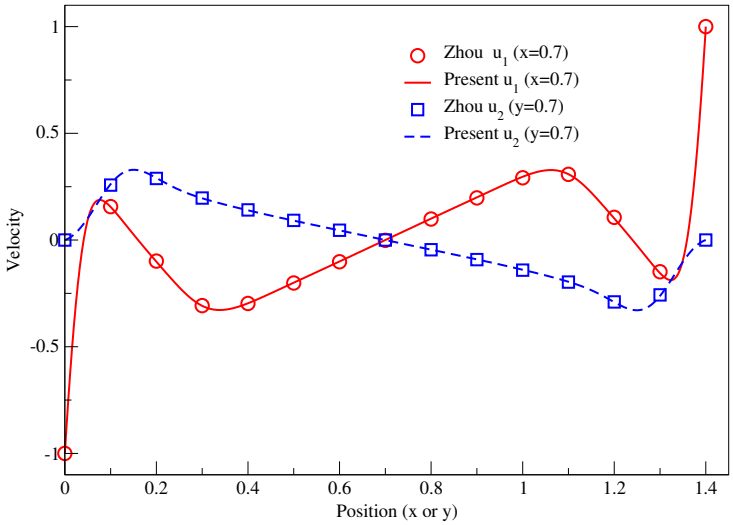

Figure 7.13: Velocity profiles at $x = 0.7$ and $y = 0.7$.

Positions and intensities of the vortices Tables (7.2) and (7.3) represent the positions and intensities of the primary and secondary vortices as a function of the mesh size for $Re = 1000$. Positions and intensities of the ternary vortex are shown in Table (7.4). For the sake of conciseness, we only focus on the positions and the intensities of one ternary and two secondary vortices. The others can be obtained symmetrically in relation to the center of the cavity. We observed symmetrical values to up to four or five significant digits. Table (7.5) displays the positions of the detachment and reattachment points $P_i\,(i = 1,5)$ defined in Figure (7.12). In [338] and [227], the authors use coarser grids that could explain the difference between their values and ours for the primary vortices.

Reference	Main Vortex (x,y)	Vorticity
Zhou [338]	(0.70000, 0.70000)	-1.41562
Nithiarasu [227]	(0.68950, 0.69690)	-1.52363
Present (Mesh 1)	(0.70099, 0.70070)	-1.49753
Present (Mesh 2)	(0.69996, 0.69996)	-1.49974
Present (Mesh 3)	(0.70000, 0.70000)	-1.49858
Present (Mesh 4)	(0.69999, 0.69999)	-1.49838

Table 7.2: Positions (x,y) and intensities of the main vortex.

7.5 Conclusion

In this chapter, we proposed a method for partitioning 2D block-structured meshes. The goal was to compute flow simulations on non-rectangular geometries. Our geometrical partitioner was coupled with the massively parallel solver and preconditioner HYPRE library. Several examples of partitioning are presented to check, both the efficiency and the performance of our strategy in comparison with other partitioners. Finally, we computed flow on non-rectangular geometries with very fine grids to propose reference solutions.

Reference	Lower secondary vortex (x,y)	Vorticity
Zhou [338]	(0.72560, 0.20000)	2.38559
Nithiarasu [227]	(0.85230, 0.20150)	2.60588
Present (Mesh 1)	(0.84952, 0.19744)	2.60184
Present (Mesh 2)	(0.85055, 0.19637)	2.59861
Present (Mesh 3)	(0.85112, 0.19587)	2.59770
Present (Mesh 4)	(0.85139, 0.19563)	2.59745
Reference	Right secondary vortex (x,y)	Vorticity
Zhou [338]	(1.32500, 0.48440)	0.53846
Nithiarasu [227]	(1.32210, 0.48360)	0.65005
Present (Mesh 1)	(1.32226, 0.48356)	0.63099
Present (Mesh 2)	(1.32243, 0.48353)	0.62956
Present (Mesh 3)	(1.32249, 0.48349)	0.62971
Present (Mesh 4)	(1.32253, 0.48346)	0.62996

Table 7.3: Positions (x,y) and intensities of the secondary vortices.

Reference	(x,y)	Vorticity
Mesh 1	——	——-
Mesh 2	(1.39579, 0.40420)	-0.002911
Mesh 3	(1.39531, 0.40468)	-0.004380
Mesh 4	(1.39522, 0.40478)	-0.004718

Table 7.4: Positions (x,y) and intensities of the right ternary vortex.

Reference	$P_1(x_1,y_1)$	$P_2(x_2,y_2)$	$P_3(x_3,y_3)$
Mesh 1	(1, 0.09999)	(1.23999, 0.4)	(1, 0.63999)
Mesh 2	(1, 0.09999)	(1.23748, 0.4)	(1, 0.64499)
Mesh 3	(1, 0.09874)	(1.23624, 0.4)	(1, 0.64874)
Mesh 4	(1, 0.09937)	(1.23563, 0.4)	(1, 0.64999)

Reference	$P_4(x_4,y_4)$	$P_5(x_5,y_5)$
Mesh 1	——	——
Mesh 2	(1.3925, 0.4)	(1, 0.4075)
Mesh 3	(1.3900, 0.4)	(1, 0.4100)
Mesh 4	(1.3887, 0.4)	(1, 0.4112)

Table 7.5: Positions (x_i,y_i) of the detachment and reattachment points $P_i\,(i=1,5)$.

Part II

Multiphase flow in porous media

Introduction

Multiphase multicomponent flow in porous media are involved in many applications related to subsurface environment and energy issues. We can mention, no exhaustively, hydrocarbon recovery in petroleum engineering, the geological sequestration of CO_2, the geological sequestration of nuclear waste, prevention of groundwater pollution and remediation or deep geothermal energy. Numerical modeling and simulation have been increasingly used for this purpose, a trend that will continue because more sophisticated physical processes involving complex mathematical and numerical issues need to be modeled.

This part contains two chapters, in which we focus on the particular case of reactive multiphase flows in porous media. For a general discussion on the physical principles of the multiphase flow in porous media, we refer e.g. to [57, 146, 244, 234], while for a description of mathematical models and computational methods for flows in porous media we refer to [85, 88], and finally for reactive transport modeling, we refer for instance to [58, 226, 254, 332] and [312] where a recent and detailed review of the applications above mentioned can be found. Reactive multiphase flow are governed by a set of highly nonlinear system of degenerate partial differential equations (PDEs) coupled to algebraic and ordinary differential equations requiring special numerical treatment. There exists a vast amount of literature on the discretization methods for such a system of PDEs (see for instance [118] for a detailed review of locally conservative discretization methods that are indispensable for the simulation of flow and transport processes in porous media). However, we can mention that Finite Volume Methods, Finite Difference Methods, Finite Element Methods or Control-Volume Finite-Element Methods have been intensively used in the numerical simulation of multiphase flow in porous media. In this chapter, we consider and focus on Finite Volume Methods. This part is organized as follows.

In Chapter 8, we start by a non exhaustive state of the art about multiphase reactive flows in porous media. We describe some applications related to reactive transport modeling. In the numerical modeling of multiphase flow, a crucial issue is the management of the possible phase appearance and disappearance. This problem needs a relevant choice in the primary variables that will be used in the computations. A considerable amount of literature is available about his topic. Another important issue is how the coupling between flow, transport and chemistry is treated. Indeed, reactive transport modeling requires to solve a set of highly nonlinear system of degenerate partial differential equations governing a compositional multiphase flow, coupled to algebraic differential equations related to equilibrium and kinetic reactions. The approaches found in the literature can be classified into two categories: the sequential and the global implicit approaches. Sequential approaches propose to decouple flow, transport and chemistry in a relevant manner while global implicit approaches solves a highly nonlinear system gathering all the equations. Both strategies are discussed. We propose a description of several reactive codes dedicated to subsurface environmental simulations and their main characteristics are highlighted. The sequel of the chapter describes briefly the simulator DuMu^X (DUNE for Multi-{Phase, Component, Scale, Physics, ...} flow and transport in porous media [3, 119]). DuMu^X is a free and open-source simulator to perform numerical simulation of complex flows in porous media. Among others, we present the numerical scheme and the numerous models available in DuMu^X.

In Chapter 9, we present our main contributions and implementations in the framework of DuMu^X in a high performance computing context. Section 9.2 deals with a scenario of gas migration in deep repository for radioactive waste. We have been involved in the European project FORGE (Fate Of Repository Gases : http://www.bgs.ac.uk/forge/) and we participated to several benchmark exercises proposed in this framework. For this, we coupled DuMu^X with an upscaling strategy to treat the strong heterogeneities present in the nuclear waste disposal. Our method allowed to reduce drastically the computational time, while producing results that were very close from the ones of the others participants. For several years, we have been interested in the numerical simulation of multiphase reactive flows. Several sequential

and fully implicit strategies have been considered. Sections 9.3 and 9.4 present respectively sequential and fully coupled fully implicit schemes that have been developed and integrated in DuMu^X. Both single phase and two-phase flow simulations were performed. We present here a part of these results and focus on the comparison between sequential and global implicit approaches in terms of accuracy and computational time. Some parallel computations are also discussed.

Chapter 8

Numerical simulation of multiphase reactive flow in porous media: a review

Contents

8.1 State of the art

8.1.1 Applications of multiphase flow in porous media

The understanding and prediction of multiphase flow in porous media is of great importance in various areas of research and industry. The field encompasses a number of diverse applications related to environment and energy issues in groundwater. We propose here a non-exhaustive list of these applications.

8.1.1.1 Hydrocarbon recovery in petroleum engineering

In petroleum engineering, the production of hydrocarbons from petroleum reservoirs require accurate numerical simulations involving multiphase compositional flow (see, e.g., [85, 109]). Primary and secondary oil recovery processes (such as water or gas injection), can be modeled with black oil simulators [88]. Concerning the ternary recovery, complex enhanced recovery techniques have emerged. Among these recovery techniques, we can mention for instance the miscible injection of gas (CO_2, natural gas, ...)[270], thermal recovery techniques (steam injection, in situ combustion [180]) or chemical flooding (polymer, foam, ...) [197]. This emergence has emphasized the need for sophisticated mathematical tools, capable of modeling intricate chemical and physical phenomena [86].

8.1.1.2 Geological sequestration of CO_2

Carbon Capture from industrial facilities and Storage (CCS) in deep saline aquifers represents a promising technology to mitigate the contribution of this gas to the acidification of the environment and to global warming. Several physical and geochemical trapping mechanisms must be combined to ensure a high containment rate [161]. These four basic mechanisms which hold the CO_2 in place are structural, residual, solubility, and mineral trappings. Gaseous CO_2 is compressed and injected in its supercritical form with ideal properties for transport (viscosity of a gas) and storage (density of a liquid). Less dense than the brine present in the aquifer, it migrates, vertically firstly and then along the top of the aquifer and finally it builds up under the cover rock. This is called structural or stratigraphic trapping. Going up, some part of the CO_2 remains in the reservoir rock in the form of small bubbles trapped in the pores: it is the residual or capillary trapping. This CO_2 trapped in the reservoir rock will dissolve slowly in water. This is the solubility trapping. Water containing dissolved CO_2 becomes heavier than the surrounding water and is going down to migrate to the bottom of the reservoir. Chemical reactions with the rock matrix transform the dissolved CO_2 into carbonate minerals. That is the mineral trapping. These mechanisms occur at different time scales (immediately after the injection in the case of solubility trapping, and up to several thousand years in the case of mineral trapping). By consequent, assessing the viability in term of risk and capacity of storage must rely on numerical simulations due to the long time scales involved. Many references can be found for the numerical approximation of such phenomena, see e. g., [32, 194, 226], and the references therein. Two mains issues concern the reactive transport in the framework of geological storage of CO_2: firstly the simulation of the different trapping mechanisms above mentioned and secondly the sustainability of the storage through the durability of well cements.
For the numerical simulation of the geological sequestration of CO_2, the studies can be classified into two categories according on whether we consider geochemical effects or not. In [252], the authors compare several codes dedicated for geologic disposal of CO_2. Even if chemical and hydro-mechanical processes are briefly discussed, most of the article focuses on the hydro-geological processes induced in CO_2 sequestration for one-dimensional geometries. Good agreements are obtained between the different codes but the authors conclude that three-dimensional computations including heterogeneities would be more relevant. In [91], several benchmarks are proposed to model compositional effects due to dissolution of CO_2 into the brine and non-isothermal effects on two- and three-dimensional heterogeneous problems. The results show that a fairly good agreement of model predictions is obtained. Three-dimensional computations are also performed in [220] where structural, solubility and residual trappings are considered while geochemical reactions are neglected. To obtain simulations of increasingly complex phenomena with higher physics fidelity, many authors consider the coupling between hydro-geological, thermal and chemical processes. These works can also classified into two categories according on whether a single (liquid) or a two-phase flow (supercritical/gas-liquid) is considered. Under certain simplifying conditions, single phase flow is considered for instance in [137] and [178]. In [137], in the framework of SHPCO2 Project [138], the gas phase is assumed to be immobile and therefore gaseous carbon dioxide is considered as a fixed species neglecting the two-phase flow effects. In [178], an initial amount of supercritical CO_2 is converted into a source term of liquid CO_2 and then the authors study the transport of the dissolved CO_2 and the precipitation/dissolution process of minerals. In [10], the authors employ a single phase reactive flow to model the leaking of CO_2-saturated brine in a fractured pathway once supercritical CO_2 is totally dissolved. CO_2 is generally injected in its supercritical form. This injection may induce important overpressure that can damage the reservoir or induce fracturing and seismic events. Moreover, the supercritical CO_2 that is less dense than the brine present in the aquifer, will migrate vertically firstly and then it will build up under the cover rock inducing a risk of leakage through faults. In [245, 297], the authors propose an alternative strategy that consists in injecting dissolved CO_2 to circumvent the above-

mentioned risks and increase the security of its geological sequestration. In [11], a study of this process and its interactions with the carbonate reservoir through geochemical reactions is proposed. Even if in [225], the authors show that modified single phase flow models can predict pressure build-up far from the injection as well as complex two-phase flow models, most of the studies deal with two-phase reactive flows. The following is a non-exhaustive list of references: [47, 113, 183, 221, 222, 260, 290], the main difference between theses references being the complexity of the geochemical system.
During its storage, liquid or supercritical CO_2 is injected through a well composed of cases of cement. Once the injection is terminated, the well is closed by a cement plug. By consequent, the integrity of the disposal and its impermeability can be strongly influenced by the chemical reactivity of cement (see for instance [48], [154] or [157] where a comparison between numerical and experimental results is given).

8.1.1.3 Geological sequestration of nuclear waste

The long-term safety of the disposal of nuclear waste is an important issue in all countries with a significant nuclear program. Repositories for the disposal of high-level and long-lived radioactive waste generally rely on a multi-barrier system to isolate the waste from the biosphere. The multi-barrier system typically comprises the natural geological barrier provided by the repository host rock and its surroundings, and an engineered barrier system. When designing nuclear waste geological repositories, a problem of possible two-phase flow of water and gas appears (for more details see, for instance, [6, 228]). Multiple recent studies have established that in such installations, important amounts of gases, mainly hydrogen, are expected to be produced, in particular due to the corrosion of metallic canisters used in the repository design. The creation and transport of a gas phase is a crucial issue concerning the capability of the engineered and natural barriers to evacuate the gas phase and avoid pressure build-up, thus preventing mechanical damage. Several studies involving two-phase compositional flow have been proposed by national and international programs to study the gas migration and its impact on the performance assessment of underground radioactive waste repositories. We can cite for instance the benchmarks Couplex-Gas [333] proposed by the French Agency for the Management of Radioactive Waste (ANDRA) and the French research group MoMaS (Mathematical Modeling and Numerical Simulation for Nuclear Waste Management) or the benchmarks proposed in the framework of the European Project FORGE: Fate Of Repository Gases (http://www.bgs.ac.uk/forge/) [13, 34, 303, 304, 305]. There is also a vast literature where, in addition to the hydrological aspects, more complex physical phenomena are taken into account. For instance in [90], the authors discuss how this complex assembly that constitutes the repository system will evolve due to thermal, hydraulic, mechanical, chemical and radiological processes. They propose a detail review of recent contributions and future challenges regarding the reactive transport modeling applied to deep repository systems. As for the geological storage of CO_2, the integrity and the sustainability of the disposal must be ensured for thousands of years. We can cite for instance [63, 214, 266, 318, 319], where the authors study the corrosion or/and the alteration of carbon steel, compacted bentonite and concrete that constitute the engineered multi-barrier system.

8.1.1.4 Prevention of groundwater pollution and remediation

Groundwater is a one of the major source of water supply in many parts of the world. It covers the needs in domestic consumption, irrigation and industrial processing. Consequently, prevention of groundwater contamination is a crucial issue in the management of the water quality. Sources of pollution can be numerous and varied and since groundwater is hidden beneath the surface, these sources are often hardly identifiable. As a consequence, modeling of multiphase flow in porous media plays a significant role to forecast the transport of the contaminant and to model some expensive remediation processes.

Many contributions deal with contaminated soils by non-aqueous-phase liquid (NAPL). For NAPL remediation, we can cite for instance [207] where remediation is performed by air sparging or [92] where a more complex three-phase non-isothermal flow (gas-water-NAPL) is considered. It can be relevant to also take into account chemical and biological processes involved in contaminant transport and remediation (see for instance [42, 58, 336]). In the event of a leak of radionuclide, the chemical interactions between the leaked radionuclide and the surrounding media must be taken into account to predict at best their migration (see for instance [268, 279, 298, 311]). Many references related to the Hanford site in the USA can be found (see for instance [190, 281]). In this case, cesium has been released into the environment accidentally due do leaking of high level waste (HLW) storage tanks and the retardation effect arising from adsorption is studied. In the remediation process, microbial bio-degradation can mitigate the dangerousness of certain contaminants. In this case, the contaminants are decomposed by action of micro-organisms. Bio-remediation of hydrocarbon-contaminated zones is studied for instance in [38] for a benzene pollution and in [204, 291] for a toluene pollution. Other potential targets of groundwater remediation are nitrate-polluted soils, particularly in rural zones as a result of agricultural activities [246, 287] or radionuclide-polluted zones (see for instance [43] for strontium remediation or [324] for uranium bioremediation).

8.1.1.5 Deep geothermal energy

Deep geothermal energy consists of extracting the heat stored inside the Earth by injecting a fluid in a fractured reservoir via an injection well. A recent overview of the worldwide applications of geothermal energy for direct utilization can be found in [195]. The fluid will circulate in the fracture network and then heat up in contact with the hot matrix rock. The fluid is then extracted by production wells and then transformed into steam through an heat exchanger to drive a turbine to produce electricity. The interactions between the fluid and the rock matrix can lead to the precipitation/dissolution of minerals and consequently have significant effects on the long-term performance of these reservoirs. Indeed, precipitation can reduce permeability and lead to complete clogging of matrix or fracture porosity while dissolution can improve the permeability. Reactive transport modeling can be essential to understand the effects of the fluid circulation on the mineralogical evolution of the reservoir and how the chemical composition of reinjection waters can be modified to improve reservoir performance by maintaining or even enhancing injectivity (see for instance [317, 320, 323]).

It is also possible to couple CO_2 storage and deep geothermal energy production. A strategy consists in replacing water by CO_2 as injection fluid [189, 251]. Numerical simulations suggest that CO_2 is superior to water in its ability to mine heat from hot fractured rock due to, in part, its relatively high mobility. Still considering a coupling between CO_2 geological storage and deep geothermal energy production, a recent strategy proposes to inject CO_2 in deep saline aquifers in dissolved form close to the emitting facilities [170, 255]. This process allows to overcome the transport issues that are inherent in massive storage. Usually, CO_2 is injected in supercritical form. As mentioned above, injection of dissolved CO_2 has several advantages in terms of storage safety. It reduces the risks of overpressure due to the injection in supercritical form, the risks of leakage by avoiding the creation of a deep gas bubble and therefore its eventual rise. Finally, it offers a potential for faster mineralization. The recovery of hot carbon-laden water and then the reinjection are performed by means of a set of injectors and producers wells, such as the heating networks.

8.1.2 Management of phase appearance and disappearance

One major issue in the numerical modeling of compositional multiphase flow concerns the management of the possible appearance/disappearance of some phases. This problem was intensively explored and the literature is vast. It is directly related to the choice of primary variables considered to solve the compositional multiphase flow. We focus here in the particular case of two-phase flow (liquid-gas) with two components in each phase where solubility of the components in the phases has to be taken into account. This particular configuration has been widely studied for nuclear waste management where a possible two-phase flow (H_2O-H_2) appears or the geological sequestration of CO_2. A standard choice for the primary variables would consist in choosing one phase pressure and one saturation but due to the possible disappearance of a phase, the saturation can no longer be used as a primary variable. A common technique consists in choosing these standard variables (pressures, saturations, mole or mass fractions) and then, primary variable switching is applied according to the present phases [93, 96, 120]: when only one phase is present, saturation is replaced by a molar fraction as primary variable. Another strategy consists in opting for a choice of persistent variables, valid whatever the composition of the flow. Several approaches exist:

- In [7, 235], the authors extend the saturation to artificial negative values, so that the system of mass conservation laws does not degenerate in the single phase region and the saturation can still be used as a primary variable.
- In [69, 70], the authors use persistent variant of the primary variables: dissolved gas mass concentration and liquid pressure that are defined both for liquid saturated and unsaturated regions.
- In [126, 158], the authors add the solubility as third primary variable to the liquid phase pressure and liquid phase saturation. Then, they use additional nonlinear complementarity constraints that describe the transition from one-phase to two-phase region, to close the system.
- In [220], the authors propose a set of primary variables that consists of gas pressure and capillary pressure. To make this set uniform for both saturated and unsaturated by gas phase regions, Henry's law is used to couple solubility and pressure whatever the composition of the flow. This idea was introduced in [155]. A similar strategy is adopted in [39, 40] where the two phase pressures are considered as primary variables, still using Henry's law to define gas pressure in zones where only liquid phase is present.
- In [182], the authors consider pressures, saturations and fugacities as primary variables. Then, they include phase transitions in the nonlinear system of equations using a set of local inequality constraints. These constraints are then directly integrated into the semi-smooth Newton method using a nonlinear complementarity function.
- In [198, 199, 200], the authors present another persistent set of primary variables that contains the total molar fraction of the light component and a mean pressure which equals the pressure of the remaining phase when one of them disappears.
- In [33], the authors also use a persistent set of primary variable set that does not depend on phase transitions. As first primary variable the authors propose to use a global pressure variable, which partially decouples the system of equations. The notion of the global pressure was introduced in [41] and [85] for immiscible incompressible two-phase flow and was then extended to compositional flow (see for instance [87]). As a second persistent variable the authors introduce the total mass density of the gas component defined in single phase and two-phase zones.

In the framework of the French research group MoMaS, several benchmarks were proposed [67]. They aimed at assessing how traditional simulators for multiphase flow in porous media are facing when attempting to simulate gas migration in deep geological repositories. Several exercises focused on simulation of the gas phase appearance/disappearance in a two-phase flow, produced by the injection of H_2 in an homogeneous porous medium initially fully saturated with pure water. In [68], the authors compare the results of several teams using different strategies to deal with the phase appearance/disappearance. Most of the results are qualitatively similar, even if some differences remain. No comparison in term of accuracy, performance (CPU time) or complexity (difficulties to solve the nonlinear system) is proposed. These test cases have also been intensively studied in other contributions (see for instance [33], [70], [198], [220] or more recently in [75]). In [201], the authors propose an advanced comparison of three strategies in terms of nonlinear solver convergence and solutions on different 1D and 3D examples involving gas appearance and liquid disappearance. These formulations are the "Natural variable formulation (NVF)" [96], the "Pressures, saturations and fugacities formulation (PSF)" [182] and the "Pressures, and fugacities formulation (PPF)" [40]. Firstly, they show that the three formulations lead to equivalent definitions of the phase transitions. They conclude that on their particular test cases, the NVF and PSF behave better than the PPF in terms of nonlinear convergence. In [125], the NVF and PSF are also compared and the NVF performs slightly better than the PSF in term of CPU time consumption. Indeed, with the PSF, the time step size decreases when the nonwetting phase disappears, leading to a higher number of time steps.

8.1.3 Sequential approach versus global implicit approach

Multiphase multicomponent reactive flows are modeled by a mass balance law for each phase, Darcy-Muskat's law, capillary pressure law, solubility laws, equations of state and closure relations. Coupling between flow and chemistry occurs through reactions rates. In the case of equilibrium reactions, these rates are unknown and are commonly eliminated through linear transformations [187, 212] and replaced by mass actions laws that are algebraic equations relating the activities of concerned species. For kinetic reactions, the rates are nonlinear functions of concentrations [181] and involve ordinary differential equations. By consequence, the problem is modeled by a system of partial differential equations (describing a multiphase compositional flow) coupled with algebraic or ordinary differential equations related to chemical reactions.

The numerical strategies for solving this system can be divided into three dominant algorithms: the global implicit (GIA), the sequential iterative (SIA) and sequential non-iterative (SNIA) approaches [282, 327]. In the GIA, one nonlinear system gathering all equations is solved at each time step. For the sequential solution approaches, flow and reactive transport (or possibly, flow, transport and chemistry) are solved sequentially at each time step. The difference between the SIA and SNIA lies on the fact that for the SIA, the procedure is present in an iterative loop. Sequential approaches are also named operator-splitting approaches. In comparison with GIA, sequential approaches can be easier to implement since existing codes and specific methods can be used for each subproblem (flow, transport, chemistry). Nonetheless, sequential approaches can introduce operator splitting errors [51, 294] and restrictions on the time step are mandatory to ensure mass conservation for instance. In [327], the authors described the GIA as "research tools for one-dimensional investigations" due to their complexity and their high computational requirements. Thanks to the advance of high-performance computing in the last decades, these restrictions are no longer relevant.

The French research group MoMaS proposed in [82] a benchmark to test numerical methods used

to deal with single phase reactive transport problems. In this framework, several sequential and implicit algorithms have been compared. In [80] and [179], the authors propose respectively a SNIA and a SIA. The other participants [37, 100, 149, 206] deal with various global implicit algorithms. More precisely, in [37], the authors propose a method where the chemical problem is eliminated locally, leading to a nonlinear system where the transport and chemistry subsystems remain separated. In [100, 108], the problem is written in the form of differential algebraic equations (DAE) allowing the use of efficient and robust DAE solvers. In [149], the authors use a reduction technique introduced in [175, 176] that aims at reducing drastically the number of coupled nonlinear differential equations. Finally in [206], a direct substitution approach (DSA) consisting in substituting the equations of chemistry directly in the equations of transport is employed. In [81], the results provided by the different teams are compared with a good agreement. The different versions of this benchmark showed that sequential approaches can be as accurate as global ones provided they are carefully implemented while global approaches are now more efficient that originally thought.

For coupled multiphase flow and reactive transport problems, most of the codes presented in [280] and [332] use a splitting approach to treat the nonlinear coupling. The global problem is split into a multiphase flow problem and a reactive transport problem. The relevant physical quantities are updated once each of these subproblems has been solved. The GIA has also been applied by few authors to couple multiphase flow and reactive transport problems [75, 113, 115, 221]. A description of several sequential and implicit codes is given in Section 8.1.4.

8.1.4 Presentation of codes for reactive transport modeling

Several codes dealing with the numerical modeling of reactive flows in porous media are described in [280, 332]. In the sequel we propose a brief and non-exhaustive description of most commonly used codes, although others exist. In their description, we focus only on some information: How are (single phase or multiphase) flow and reactive transport coupled? What is the method of discretization? What are the applications considered?

8.1.4.1 AD-GPRS

The Automatic Differentiation General Purpose Research Simulator (AD-GPRS) is a flexible and extensible multiphysics simulation platform [79, 162]. It has been extended to geochemical modeling using a fully-implicit approach. It has been applied to in-situ conversion of oil shale [112] or geological carbon sequestration [113, 115].

8.1.4.2 COORES

COORES is a code developed by IFPEN to simulate coupled multiphase flow and reactive transport processes. The first version of COORES coupled an existing 3D three phase compositional flow reservoir simulator and the geochemical module Arxim [216]. It has been widely used to simulate CO_2 geological sequestration (see for instance [137]). More recently, a new version of COORES named GEOXIM, written in C++ and based on high performance computing has been developed to treat implicitly multiphase reactive flow problems.

8.1.4.3 CORE^{2D}

An overview of the code CORE^{2D} V4 (a COde for modeling partly or fully saturated water flow, heat transport and multi-component REactive solute transport under both local chemical equilibrium and kinetic conditions) and its previous versions is given in [264]. A Sequential Partly Iterative Approach (SPIA) [263] improving the accuracy of the traditional Sequential Non-Iterative Approach (SNIA) and less CPU consuming than the general Sequential Iterative Approach (SIA) is employed. CORE^{2D}V4 and its previous versions codes have been extensively used for many applications such as long-term geochemical evolution of HLW (High Level Waste) repositories in clay [214, 325].

8.1.4.4 CrunchFlow

CrunchFlow is a multicomponent reactive flow and transport code [1]. Both global implicit approach (through a direct substitution approach (DSA)) and operator splitting approach based on SNIA are implemented in Crunchflow. Recently, CrunchFlow has been coupled with a parallel hydrologic model (ParFlow) to take benefit of high-performance computing facilities [59]. Among many applications, CrunchFlow has been used for instance for reactive contaminant transport [84] or CO_2 sequestration [46].

8.1.4.5 DARST

DARST (Delft Advanced Research Terra Simulator)[2] is a simulator using the Operator-Based Linearization (OBL) framework, which has been proposed recently for complex multiphase flow [171, 300]. A fully implicit approach using a finite volume scheme is implemented. DARST has been used for several applications including CO_2 storage in saline aquifer [164] or the prediction of heat production in geothermal reservoirs [302].

8.1.4.6 eSTOMP

eSTOMP is the parallel processing version of the Subsurface Transport Over Multiple Phases (STOMP) simulator. STOMP [308] is a suite of multifluid subsurface flow and transport simulators (see [307] for the story of the previous versions and the description of the reactive module ECKEChem). Its parallel version eSTOMP was scalable up to 131,000 processors cores. A sequential non-iterative coupling between the flow and reactive transport is performed. The code has been used, among other things, for the geological sequestration of CO_2 [223] or [224] where a coupling with geomechanics is achieved or desorption of uranium from contaminated sediments [307].

8.1.4.7 GEM-GHG

GEM-GHG [221] is a fully implicit geochemical compositional Equation-of-State (EOS) compositional simulator. An adaptive-implicit method [98] is applied to solve the nonlinear system. It consists in solving implicitly only a small number of blocks, while the remaining ones are solved explicitly, thereby reducing the size of the nonlinear system. GEM-GHG has been widely used for the numerical modeling of CO_2 storage in aquifers [221, 222, 290].

8.1.4.8 HYDROGEOCHEM

HYDROGEOCHEM [328, 329, 330], couple equations describing thermal (T), hydrology (H), mechanics (M) and chemical (C) processes (THMC). Four fully-coupled modules solving multiphase flow, thermal transport, reactive biological transport and geomechanics displacement and deformation can be com-

puted iteratively. HYDROGEOCHEM has been used for numerous applications including for instance polluted soil remediation [168] or radionuclide migration [326].

8.1.4.9 HYTEC

HYTEC [296] is a code coupling hydrodynamic flow and multi-component transport with biogeochemical processes using the geochemical module CHESS [295]. Coupling between flow and geochemical transport is achieved via a sequential iterative approach. HYTEC has been validated by several benchmark studies (for instance in the MoMaS benchmark above mentioned [81, 179]). Among the numerous applications treated by HYTEC, we can mention for instance the cement degradation [310], the performance assessment of radioactive waste disposal [102] or the geological storage of sour gases [178, 275, 276]. Recently, HYTEC has been extended to two-phase flow using an operator splitting approach [274, 275, 276].

8.1.4.10 IPARS

IPARS (Integrated Parallel and Accurate Reservoir Simulator) [306] is an environment providing some physical models for the numerical simulation of flow in oil reservoirs or aquifers. The TRCHEM (TRansport with general biogeoCHEMistry) [241] module implemented in the framework of IPARS simulates multiphase reactive transport in porous media thanks to a time splitting approach. In [242] applications to the migration of radionuclide and bioremediation of xylene are depicted while in [291], bioremediation of toluene is considered.

8.1.4.11 M++

M++ is a finite element toolbox for parallel computations based on C++ using the MPI standard for parallelization [309]. In [74, 75], the reduction technique described in [150] for reactive single phase flow was extended to the case of two-phase reactive flow and implemented in the M++ framework. Unlike the classical strategy, their general transformation method does not only eliminate unknown equilibrium reaction rates. It also potentially reduces the nonlinear coupled part of the problem, allowing the use of large time steps and avoiding the potential drawbacks of sequential approaches.

8.1.4.12 MIN3P

MIN3P [202, 205] is a general purpose multicomponent reactive transport code for variably saturated media. Flow is governed by the Richards equation while a direct substitution approach is employed to tackle reactive transport problem. MIN3P has been used to consider numerous applications involving saturated flows such as for instance the groundwater remediation [203]. To take into account more complex phenomena, some specific enhanced versions of MIN3P have been implemented. MIN3P-Bubble [38] has been developed to consider gas entrapment and release in the groundwater zone. In MIN3P-Dusty [213], some enhancements have been performed to simulate multicomponent advective and diffusive gas migration in the vadose zone. In MIN3P-THCm [55, 56], a THMC formulation has been implemented.

8.1.4.13 NUFT

NUFT (Nonisothermal Unsaturated-saturated Flow and Transport) [142] is a code for modeling multiphase, multi-component heat and mass flow and reactive transport in unsaturated and saturated porous

media. Several models of varying complexity, ranging from isothermal single phase single component flow (UCSAT module) to non-isothermal multiphase flow (USNT module) can be sequentially coupled to a geochemical multiphase transport module (TRANS module). The TRANS module combines and solves in a fully implicit manner the chemical equations (equilibrium and kinetic) and the transport equations. The numerous applications of NUFT include geological disposal of nuclear waste [128], CO_2 geologic sequestration and storage [163] or groundwater monitoring [129].

8.1.4.14 OpenGeoSys

OpenGeoSys [173] is an open-source initiative for numerical simulation of thermo-hydro-mechanical-chemical (THMC) processes in porous media. OpenGeoSys has been validated and verified through numerous benchmarks initiatives (see for instance [174]). Thanks to the IWAS-ToolBox [165], OpenGeoSys has been coupled with external geochemical simulation tools such as PHREEQC2 [313] to simulate the chemical processes in partially saturated bentonite, GEM-Selektor [177] for radium migration an retardation in [268] or BRNS [9] for organic carbon degradation in [83].

8.1.4.15 ORCHESTRA

ORCHESTRA [208] is a platform dedicated to the modeling of reactive flows in porous media. Both sequential iterative and non-iterative algorithms are available to split the flow and chemistry subproblems. ORCHESTRA has been broadly used for the management of groundwater pollution (see for instance [114] for chromium remediation or [104] for leaching of heavy metals from polluted soils). Recently, in [160] ORCHESTRA has been coupled with the parameter estimation software PEST to calculate ion-binding model parameters.

8.1.4.16 PHREEQC

PHREEQC [236, 237] is a code designed to perform a wide variety of aqueous geochemical calculations. Transport and geochemical reactions are coupled thanks to a sequential non-iterative strategy. Due to its wide range of geochemical capabilities, its open-source code and the continued support and development, PHREEQC has been coupled by many researchers with existing flow and transport codes via a sequential non-iterative approach. For instance, in the code HPx (HP1, HP2, HP3) [273], a coupling between HYDRUS [271, 272] and PHREEQC is proposed for variably saturated flow conditions. In iCP [217], a coupling between the multiphysic simulator COMSOL and PHREEQC is presented with an application to a large scale thermo-hydro-chemical (THC) problem. PHAST [238] and PHT3D [249] couple respectively the geochemical model PHREEQC and the flow and transport calculations performed by HST3D [172] and MT3DMS [337].

8.1.4.17 PFLOTRAN

PFLOTRAN [140, 188], is a massively parallel reactive flow and transport code for modeling subsurface processes. Parallelization is performed using a domain decomposition method thanks to the PETSc [50] parallel framework. Several flow modules can be sequentially coupled to a multicomponent geochemical transport module. PFLOTRAN has been used for numerous subsurface applications including for example uranium transport at the Hanford site [139] or CO_2 geological sequestration [189, 218].

8.1.4.18 PROOST

PROOST [123] is a simulator for modeling multiphase reactive transport in porous media. A sequential iterative approach is used where CHEPROO (CHEmical PRocesses Object Oriented) [54] deals with the geochemical processes. In [123], an application to the modeling of a column of porous gypsum subjected to a constant source of heat is given while in [122], evaporation of brine is considered.

8.1.4.19 RETRASO-CODEBRIGHT

RETRASO-CODEBRIGHT (RCB) is the result of the coupling between two codes: RETRASO [261] and CODE_BRIGHT [229]. RETRASO (REactive TRAnsport of SOlutes) is designed to solve reactive transport problems while CODE_BRIGHT (COupled DEformormation of BRIne Gas and Heat Transport) aims at performing coupled thermo-hydro-mechanical (THM) analysis in geological porous media. By consequence, in the coupling strategy, CODE_BRIGHT computes the flow properties (Darcy's velocity for each phase, saturation of each phase, temperature, density...) and give them to the RETRASO code for the calculation of reactive transport problem. In [260], the authors added directly the chemical equations in CodeBright to consider a fully implicit approach to deal with a scenario of geological sequestration of CO_2. The solution of the chemical problem is pre-computed by the code CHEPROO [54] for some number of reference conditions (they are shown to depend only on gas pressure), and then polynomial interpolation is used within the solution procedure, leading to a large reduction in computing time.

8.1.4.20 RT3D

RT3D [94, 95] is a code for simulating three-dimensional, multi-species, reactive transport in groundwater. It is a member of the MT3D [335] family of codes derived from MT3DMS [337]. RT3D solves only reactive transport with a prescribed velocity and is consequently coupled with the MODFLOW code [143]. RT3D has been used for many applications, particularly for bioremediation of contaminated soils (see for instance [287] and the references in [95]).

8.1.4.21 SPECY

SPECY [80] is a reactive transport code based on the non-iterative operator splitting approach (SNIA). The reactive transport equations are solved in three stages: a convection step, a dispersion step and finally a chemical equilibrium computation. Each step can be solved with a specific and relevant method. Recently in [196], the authors compared linear solvers for equilibrium geochemistry computations. Precisely, several direct solvers (LU decomposition, QR decomposition, Cholsesky decomposition...) and iterative solvers (GMRES, Gauss Seidel, Conjuate gradient, Biconjugate gradient...) are compared using a panel of chemical systems, including or excluding the formation of mineral species.

8.1.4.22 TOUGHREACT

TOUGHREACT [320, 321, 322] is a numerical simulation program for reactive flows in porous and fractured media. It was developed by adding geochemical calculations in the multiphase simulator TOUGH [250]. The reactive transport is achieved by a sequential approach that can be either iterative or not. The broad spectrum of applications of TOUGHREACT ranges from CO_2 geological sequestration [47, 320] to bentonite alteration in a nuclear waste repository [318, 319] or geothermal systems [316, 317].

8.1.4.23 Synthesis

Table 8.1 summarizes the description of the codes presented above. We focus on the supported discretization method, the coupling strategies and if there exists a parallel version of the code. To describe the coupling strategies, we consider two levels of coupling depending on whether the code deals with multiphase multicomponent flow or only saturated flow. If the code solves reactive multiphase multicomponent flow, we specify how the multiphase flow and the reactive transport problem are coupled (implicitly or sequentially). Then, if the code considers a sequential strategy, we specify what is the approach adopted to deal with the reactive transport (implicit or sequential). For codes solving only saturated flow, we specify only this latter point.

	Codes	PDE discretization[1]	Phase conservation and transport coupling [2]	Transport and reaction coupling[2]	Parallelization
Multiphase-multicomponent flow	AD-GPRS	FVM	GIA		YES
	COORES	FVM	GIA		YES
	CORE^{2D}	FEM	SEQ	SEQ	NO
	DARST	FVM	GIA		YES
	eSTOMP	IDFM	SEQ	SEQ	YES
	GEM-GHG	IDFM	GIA		YES
	HYDROGEOCHEM	FEM/MMC	SEQ	GIA	NO
	HYTEC	FVM	SEQ	SEQ	YES
	IPARS	MFEM/DGM	SEQ	SEQ	YES
	M++	FEM	GIA		YES
	MIN3P	FVM	SEQ	SEQ	YES
	NUFT	IDFM	SEQ	GIA	YES
	OpenGeoSys	FEM	SEQ	SEQ	YES
	PFLOTRAN	FVM	SEQ	GIA	YES
	PROOST	FEM/MFEM	SEQ	GIA/SEQ	NO
	RETRASO-CODEBRIGHT	FEM	GIA/SEQ	GIA/SEQ	NO
	RT3D	FDM	SEQ	SEQ	NO
	eSTOMP	IFDM	SEQ	SEQ	YES
	TOUGHREACT	FVM	SEQ	SEQ	YES
Saturated flow	CrunchFlow	FVM		GIA/SEQ	YES
	ORCHESTRA	MC		SEQ	YES
	PHREEQC	MC		SEQ	NO
	SPECY	DFEM/MHFEM		SEQ	NO

Table 8.1: Supported discretization method, coupling strategies for different reactive transport codes (adapted from [123] and [280]).

[1] FVM: Finite Volume Method, FEM: Finite Element Method, IDFM: Integrated Finited Difference Method, MMC: Modified Method of Characteristic, MFEM: Mixed Finite Element method, DGM: Discontinuous Galerkin Method, FDM: finite difference method, MC: mixing cell, DFEM: Discontinuous Finite Element Method, MHFEM: Mixed Hybrid Finite Element method.

[2] GIA: Global Implicit Approach, SEQ: Sequential Approach.

8.2 Presentation of DuMu^X

DuMu^X (DUNE for Multi-{Phase, Component, Scale, Physics, ...} flow and transport in porous media) [3] is a free and open-source simulator for flow and transport processes in porous media. It is based on DUNE (Distributed and Unified Numerics Environment) [4], a modular toolbox for solving partial differential equations with grid-based methods [52, 53]. A good overview and description of DuMu^X can be found in [119]. Nonetheless, a short description is given in the sequel.

DuMu^X includes several standard models of varying complexity, ranging from stationary isothermal single phase single-component flow to transient non-isothermal multiphase compositional flow. All models employ efficient nonlinear solvers in close combination with a sophisticated time step management. The capabilities of DUNE are heavily exploited to offer various spatial discretization schemes as well as the possibility of parallel computations.

DuMu^X is coded in C++ and employs high-level generic programming techniques. The basic principle of DuMu^X code designing is modularity. DuMu^X provides shelves of modularized objects, enabling the user to choose the appropriate parts according to the handled problem. The main shelves of this modular setup are (see Figure 8.1):

- Numerical schemes,
- Model concepts,
- Control strategies for the simulation,
- Material systems: multitude of substances (components), material laws.

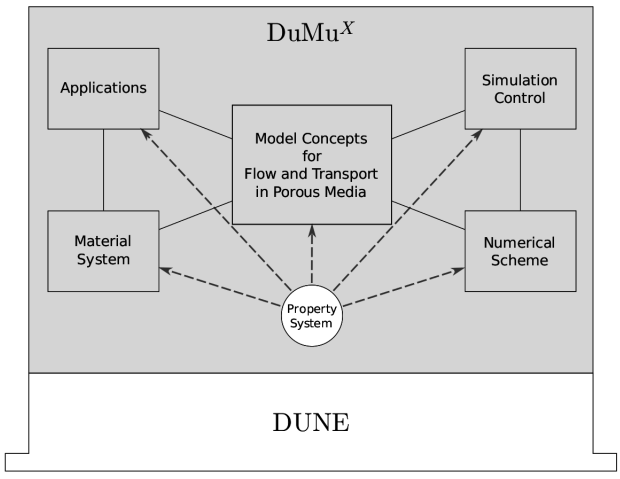

Figure 8.1: Modular design of DuMu^X (taken from [119]).

8.2.1 Numerical schemes

When using DuMu^X, we have the choice between two existing standard approaches for the solution of porous media problems: a coupled fully-implicit approach and a decoupled semi-implicit approach. The fully-implicit approach solves a large system gathering all the original coupled balance equations by an implicit method in time. For the implicit approach, two spatial discretization methods are provided: a

cell-centered finite volume method and a box method which unites the advantages of the finite-volume and finite-element methods. The decoupled approach splits the set of balance equations into one equation for the pressure and the remaining ones for mass or energy balance equations. Then, the pressure equation is solved implicitly while the transport of mass/energy is solved explicitly (as the well known IMPES strategy [88]). In comparison with a fully implicit approach, the decoupled strategy allow to use of a specific discretization methods for each equation. The standard method used in the decoupled strategy is a cell-centered finite volume method. For both the coupled fully-implicit and decoupled approaches, linearized problem obtained after the procedure of spatial and time discretization is solved by one of the linear solvers implemented in DUNE.

8.2.2 Control strategies

In DuMu^X, both the coupled fully-implicit and decoupled schemes use a unique strategy for the time-step control: the period of simulation, at first, is divided into episodes, defined as time periods where boundary conditions, source terms can be time-dependent. Then simulation time is advanced by the minimum of the time-step suggested by numerical schemes or the time span until the end of episodes. For the coupled fully-implicit schemes, the control of the time-step is based on the number of iterations required by the Newton method to achieve convergence for the last time iteration. The time-step is reduced, if the number of iterations exceeds a specified threshold, whereas it is increased if the method converges within less iterations. For the decoupled schemes, the calculation of the step size is constrained by a CFL type condition.

8.2.3 Models

DuMu^X provides several standard models of varying complexity. An overview of the available models in the version 2.12 [117] with their capabilities and characteristics is given in Table 8.2. In the names of models, "p" stands for the number of phases and "c" denotes the number of components present in each phase. Several models can be coupled with an energy balance equation and extended to non-isothermal simulations.

8.2.4 Material systems

The DuMu^X material system constitutes a framework that allows a convenient definition and usage of parameters and material laws. This framework has a modular structure and is separated into the following parts.

Components. The term component stands for constituents of the phases which can be associated with a unique chemical species or with a group of species exploiting similar physical behavior. Each component is implemented as a class with functions describing the physical properties of the component (molar mass, density, viscosity,...).

FluidSystems. A FluidSystem describes the properties of the fluid phases involved in the problem. These properties include phase densities and viscosities as well as fugacities and diffusion coefficients of components inside phases. They depend on the composition of the phases which is described in a separate object of type FluidState containing, among other things, the saturation, the pressure, the temperature or the mole fraction values.

FluidMatrixInteractions. This module collects the material laws which describe interactions of fluid phases with the porous medium (capillary pressure law and relative permeability). A collection of

	Porous Medium flow		Free Flow	Geomechanics	Multidomain
Approach	Fully Implicit	Sequential	Fully Implicit	Fully Implicit	Fully Implicit
Models	1p, 1p2c Richards 2p, 2p1c, 2p2c, 2pdfm, 2pminc 2pnc, 2pncmin co2 3p, 3p3c, 3pwateroil mpnc + non isothermal	1p 2p, 2p2c	stokes, stokesnc, stokesncni, zeroeq, zeroeqnc, zeroeqncni	el1p2c el2p elastic	2cstokes2p2c, 2cnistokes2p2cni, 2czeroeq2p2c, 2cnizeroeq2p2cn
Discretization	Box method Cell-centered FV with TPFA	Cell-centered FV with TPFA, MPFA-L, MPFA-0 (2p), MFD (2p)	Box method	Box method for flow FE for displacement	Box method
Parallelization	Yes	Yes		Yes	

Table 8.2: Available Models in DuMu^X 2.12 with some particularities and characteristics.

standard laws is provided, e.g. Van-Genuchten and Brooks and Corey models. Each material law uses a set of appropriately definable parameters (residual saturations) of type MaterialLawParams, which may depend on the location inside the domain. Each material law has a regularized version.

SpatialParameters. This part collects all parameters that may be space dependent in the computational domain (porosity, intrinsic permeability, heat capacity, heat conductivity, material law, ...).

Chapter 9

Main contributions

Contents

9.1 Introduction

This chapter aims at describing our main contributions concerning the development and the implementation of new numerical schemes in the DuMu^X framework. As mentioned in Section 8.2, DuMu^X is a free and open-source environment developed at the University of Stuttgart in which our team has developed all its codes since several years. We chose the simulator DuMu^X because it provides a sustainable environment and sophisticated tools for developers to implement some new numerical methods for the simulation of flows in porous media. Among others, it allows the users to benefit from an environment where tools for meshing, discretization and linear solvers are provided as well as usual constitutive laws for flows in porous media. Recently, the environment DuMu^X received a funding of about 680 K€ (2019-2022) from the German Research Foundation for their project "Sustainable infrastructure for the improved usability and archivability of research software on the example of the porous-media simulator DuMu^X". This recognition has reinforced our choice to continue to use this environment for our upcoming projects.
In the framework of the Euratom FP7 project FORGE: Fate Of Repository Gases, we were involved in the Work Package WP1.2 (Numerical benchmarks on Gas Migration). This Work Package aimed at comparing a number of numerical models applied to a specific problem in the context of hydrogen flow and transport in a nuclear waste repository. The processes were modeled by a two-phase (water and hydrogen) transient flow in a heterogeneous porous medium under isothermal conditions. We performed a three-dimensional numerical simulation of a module of a repository for high-level waste in a clay host

rock. Section 9.2 describes this work where we coupled an upscaling technique to manage the strong heterogeneities and a vertex-centred finite-volume method implemented in DuMu^X to yield very accurate solutions. As far as we know, concerning reactive flows, except in [65] where geological simulation of CO_2 is considered, most of the contributions in DuMu^X considering reactivity only consider kinetic reactions. For instance, in [159] and [209], a fully implicit approach is used to model evaporation and salt precipitation. In [151, 152, 153], the authors study the microbially induced calcite precipitation for preventing leakage by clogging the reservoir during geological storage of CO_2. In these contributions, the geochemistry is modeled by nonlinear souce/sink terms in the balance equations. To treat equilibrium reactions involved in our applications, in the framework of the PhD thesis of V. Vostrikov [301], we developed and integrated in DuMu^X a sequential approach to study two-phase reactive flows [29, 30]. Our scheme splits the global problem into two sub-problems. The first sub-problem computes a two-phase compositional flow where only species present in both phases are treated implicitly. Exchanges between phases are totally solved in this step and the contribution of the other species is treated explicitly. The second sub-problem calculates a reactive transport problem where flow properties (Darcy velocity for each phase, saturation of each phase, temperature, density,...) are given by the first step. In [29, 30], a SIA has been implemented for the reactive transport sub-problem. To improve the robustness of the scheme and the possible accuracy loss due to the time-splitting involved by the SIA, we switched to a GIA. More precisely, we used a direct substitution approach (DSA). Then in [15], still considering a sequential approach we have coupled this fully implicit approach for the reactive transport problem with a compositional two-phase flow. Both subproblems are now solved using a fully implicit manner. These developments have been validated by several test cases including high performance computing and considering several applications. For instance in [14], the migration of hydrogen produced by the corrosion reaction in deep geological radioactive waste repository is studied while in [15], a scenario of geological storage of CO_2 in a deep saline aquifer is treated. In this context, Section 9.3 summarizes our contributions on the numerical simulation of multiphase reactive flows using sequential approaches. More recently, in the framework of the PhD thesis of M. Id Moulay [215], we have abandoned sequential approaches to consider a fully coupled fully implicit strategy. In addition to the improvement in terms of accuracy due to the elimination of splitting errors, we expect to be able to use larger time steps during simulations. In [31], a fully implicit approach for a single phase multicomponent flow with reactive transport has been developed and validated via numerous 2D and 3D test cases including high performance computing. Then in [16], the method has been extended to consider two-phase reactive flows. An advanced comparison between sequential and fully coupled fully implicit approaches is in progress. Section 9.4 describes these recent developments.

9.2 Numerical simulations of gas migration in deep repository for radioactive waste

This section proposes a synthesis of following article [13] which can be consulted in its entirety in the Appendix:

- Ahusborde E., Amaziane B., Jurak M., 3D numerical simulation by upscaling of gas migration through engineered and geological barriers for a deep repository for radioactive waste, Geological Society, London, Special Publications, Vol 415, 123-141, 2015.

Abstract: *This paper presents the results of a benchmark study that compares a number of numerical models applied to a specific problem in the context of hydrogen flow and transport in a*

nuclear waste repository. The processes modeled are two-phase (water and hydrogen) immiscible compressible two-component transient flow in a heterogeneous porous medium under isothermal conditions. The three-dimensional (3D) model represents a module of a repository for high-level waste in a clay host rock. An upscaling technique and a vertex-centered finite-volume method are employed to yield very accurate solutions. Since the full range of results required in the benchmark is too large to be displayed in this paper, we focus on the evolution of the pressures, the saturations, the fluxes and the comparison of the numerical results with the other participants. A homemade C++ upscaling code and the parallel multiphase flow simulator DuMu^X have been adopted for this study.

Numerical simulation plays an important role in the optimization of design of a nuclear waste repository and its safety case, used as a bridge between current process knowledge and predictive assessment, on large time and space scales that experiments cannot reach. In this context, from 2009 to 2012, the Laboratory of Mathematics and its Applications of Pau (LMAP) has participated in the European project FORGE (Fate Of Repository Gases: http://www.bgs.ac.uk/forge/). The FORGE project studied key gas migration issues in repository performance assessment. We were involved in the Work Package WP1: "Treatment of gas in performance assessment" that dealt with the modeling and the numerical migration of hydrogen in a nuclear waste repository. Hydrogen is produced by the corrosion of metallic canisters used in the repository design. This Work Package brought together, in addition to the CNRS, numerous partners (ANDRA, CEA, IRSN, SCK-CEN, LEI, ENSI, NDA, Quintessa, Geofirma). Most of them are national radioactive waste management agencies. Three benchmarks at different scale were proposed (cell scale, module scale and repository scale). The processes modeled are two-phase (water and hydrogen) immiscible compressible two component transient flow in an heterogeneous porous medium under isothermal conditions. This complex flow is governed by a set of nonlinear and highly coupled partial differential equations.

Figure 9.1 represents an horizontal cross-section of the whole repository model, which is composed of 10 modules connected by the main drift going to the well that connects the repository to the surface.

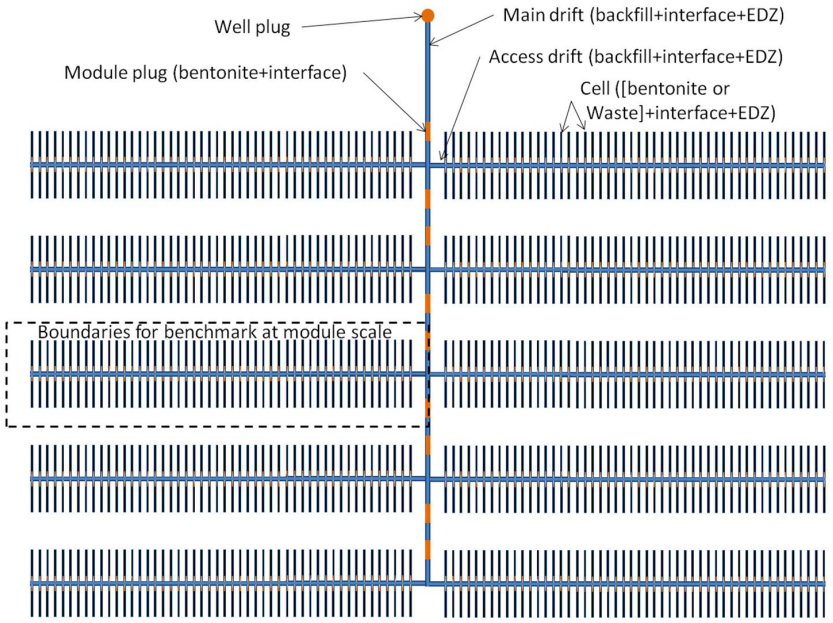

Figure 9.1: Schematic representation of a repository for high-level waste (from [304]).

Each module contains 100 waste canisters, 50 on each side of the access drift that connects them to the main drift. One of the modules is shown in Figure 9.2. Each canister in the module is separated from the access drift by a bentonite plug. The bentonite plugs are also placed in the main drift in order to separate one module from another and, finally, there is a bentonite plug in the well that separates the whole repository from the surface. All tunnels that make the repository are surrounded by a layer of the EDZ, which is a fractured medium and thus more permeable than the surrounding geological medium. The contact between the waste canister and the EDZ is not perfect, and a thin space of 1 cm exists (called the interface). It is presented in the model as a very permeable porous medium with very low capillary pressure curve (compared to other material curves).

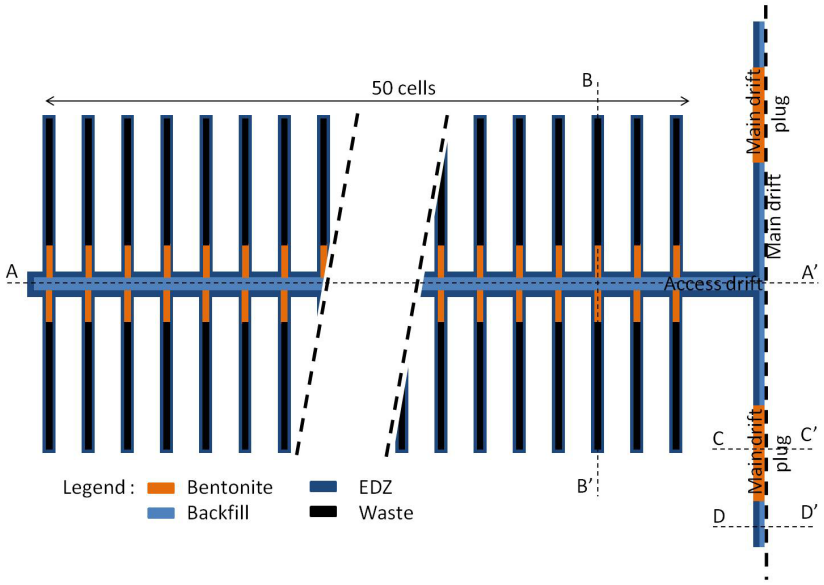

Figure 9.2: Schematic representation of the module (from [304]).

The main difficulty of the benchmark is its highly heterogeneous structure (material with very different permeabilities), and the presence of structures such as the interfaces and the EDZ, which have very small dimensions compared to the dimensions of the computational domain (thickness of the interface of 1 cm compared to the length of 700 m of the module).

A detailed 3D modeling of the FORGE module scale benchmark would require a tremendous computational effort, even when using high-performance simulator codes. Because such a detailed model can be highly CPU-time consuming, there exist various attempts that aim at the optimum compromise between the quality of the simulation and the required amount of CPU time. Upscaling refers to the techniques used to transform a fine-grid model into a more practical, coarser one. In an upscaled model, each coarse-grid block is composed of a number of fine-grid blocks, all having different physical properties. The upscaling replaces these heterogeneous properties of the porous material within the coarse-grid block with the equivalent homogeneous ones, which will be called the effective properties. To circumvent the heterogeneities and the difficulty in taking into account the thin interface surrounding the waste canisters and the bentonite plugs, we have considered a mathematical upscaling strategy. We have designed two levels of upscaling, denoted UM1 and UM2 (Upscaled Model), of increasing homogeneity in order to verify, by comparison, the capacity of the upscaled models to simulate global behaviour of the module. In UM1, the canisters and their plugs, EDZ, and the interface are substituted by an homoge-

neous block. In UM2, the homogeneous block is enlarged by the surrounding geological medium: that is, the EDZ and the interface, the canister, the plug and the surrounding geological media are substituted by one homogeneous block. The corresponding grids are shown in Figures 9.3 and 9.4.

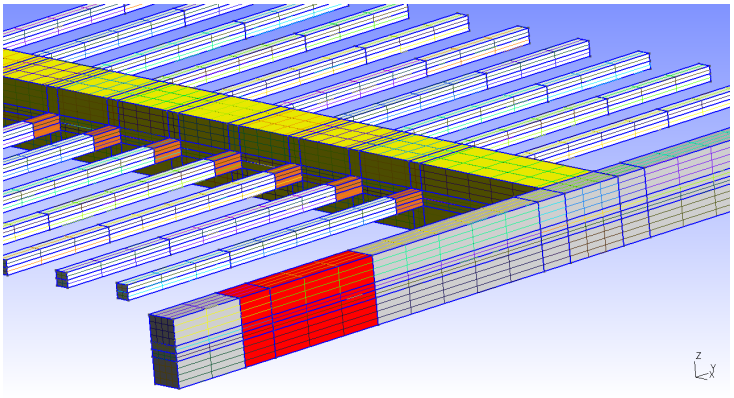

Figure 9.3: Grid of the module for UM1 (188 298 elements).

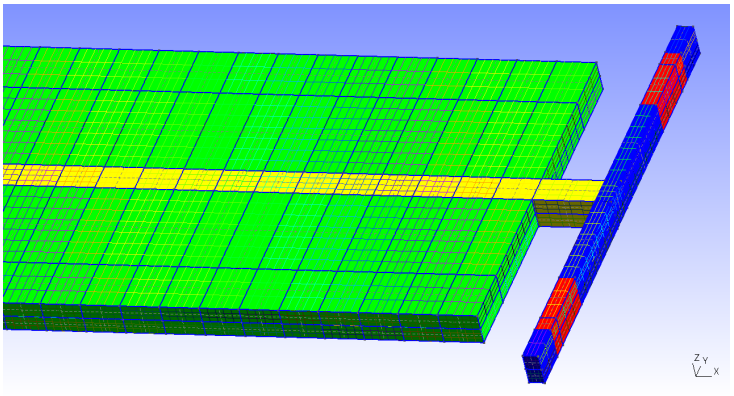

Figure 9.4: Grid of the module for UM2 (27776 elements).

A strategy of coupling between these upscaling techniques and a two-phase two-component flow has been implemented in DuMu^X. Figure 9.5 represents the pressure and the saturation at different instants. Figure 9.6 compares the gas pressure at two points C50-3 (top) and Pd-1 (bottom) between our simulations and simulations of four other participants of the benchmark: the Lithuanian Energy Institute (LEI), the Nuclear Waste Management Organization (NWMO), the Agence Nationale pour la gestion des Déchets RAdioactifs (ANDRA) and the Nuclear Decommissioning Authority (NDA).

The results are in good accordance and show the reliability of our approach. The CPU time on eight processors for the UM2 was about 4h, while the UM1 took approximately 1 month on 24 processors. Our simulations show that the maximum pressure in the module will be about 7 MPa and that, at the places where the fluxes were calculated, the convection in the gaseous phase will be the main method of hydrogen transport. The transport of hydrogen dissolved in water is about two or three orders of magnitude less significant than the transport of gaseous hydrogen. Hydrogen is transported from the cells to the access and main drifts, which represent preferential paths for the hydrogen migration. The geological medium shows only a slight desaturation of less than 2 %. The main drift bentonite blocks are almost fully resaturated after 1000 years. The above results illustrate that the proposed mathematical

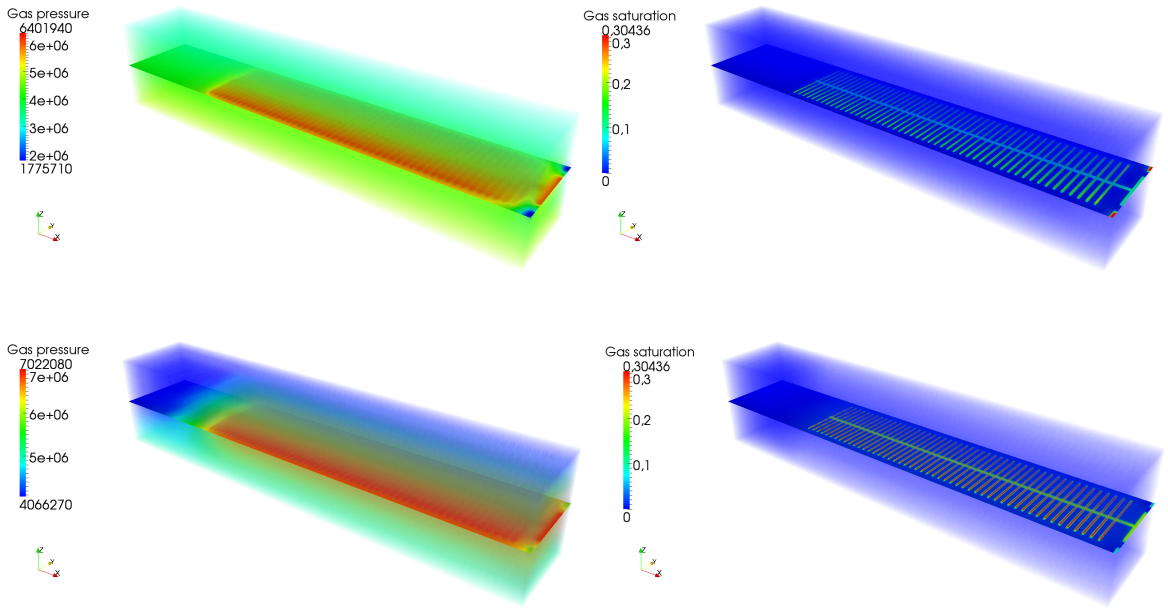

Figure 9.5: Pressure and saturation for the gas phase at t=1000 years (top) and t=10000 years (bottom) for UM1.

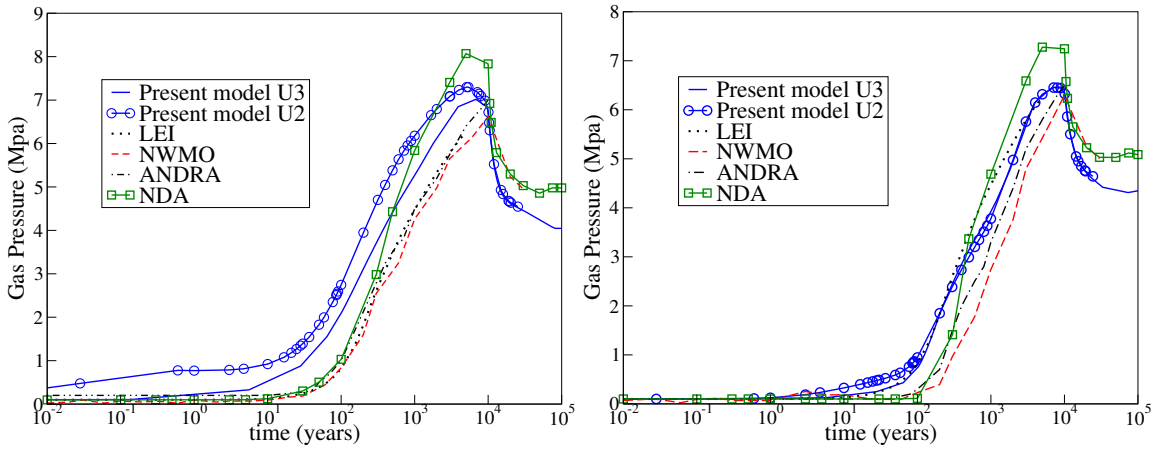

Figure 9.6: Comparison of the gas pressure. Left: P-C50-3 in the main drift. Right: P-Pd-1 in the bentonite of the access drift.

upscaling combined to a finite-volume method is capable of tackling, in a robust and accurate fashion, various physical phenomena relevant to hydrogen flow and transport in a nuclear waste repository.

9.3 Sequential algorithm for numerical simulation of two-phase reactive flows

The content of this section relies on a synthesis of article [15] and is also based on articles [14, 29, 30]. These 4 articles are listed below and can be found in the Appendix:

- Ahusborde E., Amaziane B., El Ossmani M., Improvement of numerical approximation of coupled two-phase multicomponent flow with reactive geochemical transport in porous media, Oil & Gas Science and Technology - Rev. IFP Energies nouvelles, Vol 73, 73, 2018.

Abstract: *In this paper, we consider a parallel finite volume algorithm for modeling complex processes in porous media that include multiphase flow and geochemical interactions. Coupled flow and reactive transport phenomena often occur in a wide range of subsurface systems such as hydrocarbon reservoir production, groundwater management, carbon dioxide sequestration, nuclear waste repository or geothermal energy production. This work aims to develop and implement a parallel code coupling approach for non-isothermal multiphase multicomponent flow and reactive transport simulation in the framework of the parallel open-source platform DuMu^X . Modeling such problems leads to a highly nonlinear coupled system of degenerate partial differential equations to algebraic or ordinary differential equations requiring special numerical treatment. We propose a sequential fully implicit scheme solving firstly a multiphase compositional flow problem and then a Direct Substitution Approach (DSA) is used to solve the reactive transport problem. Both subsystems are discretized by a fully implicit cell-centred finite volume scheme and then an efficient sequential coupling has been implemented in DuMu^X. We focus on the stability and robustness of the coupling process and the numerical benefits of the DSA approach. Parallelization is carried out using the DUNE parallel library package based on MPI providing high parallel efficiency and allowing simulations with several tens of millions of degrees of freedom to be carried out, ideal for large-scale field applications involving multicomponent chemistry. As we deal with complex codes, we have tested and demonstrated the correctness of the implemented software by benchmarking, including the MoMaS reactive transport benchmark, and comparison to existing simulations in the literature. The accuracy and effectiveness of the approach is demonstrated through 2D and 3D numerical simulations. Parallel scalability is investigated for 3D simulations with different grid resolutions. Numerical results for long-term fate of injected CO_2 for geological storage are presented. The numerical results have demonstrated that this approach yields physically realistic flow fields in highly heterogeneous media and showed that this approach performs significantly better than the Sequential Iterative Approach (SIA).*

- Ahusborde E., Amaziane B., El Ossmani M., Finite volume scheme for coupling two-phase flow with reactive transport in porous media, Springer Proceedings in Mathematics and Statistics, Vol 200, 407-415, 2017.

Abstract: *In this work the numerical solution of a system of coupled partial differential and differential algebraic equations describing two-phase multicomponent flow, transport and chemical reactions is considered. An implicit finite volume scheme is used to descretize a two-phase two-component flow problem, which is then sequentially coupled to a reactive transport problem solved by a direct substitution approach (DSA). More precisely, we used firstly the module 2p2c implemented in the parallel open-source simulator DuMu^X to solve a two-phase two-component flow with two dominant species without chemistry. Secondly, the reactive transport is described by*

advection dispersion equations coupled to differential algebraic equations to deal with the minor species. Again an implicit finite volume method is used to discretize this subsystem using a DSA. In this context, we have developed and integrated a reactive transport module 1pNc-react in the DuMu^X framework. Finally, numerical results for a highly complex geochemistry problem are presented to demonstrate the ability of our method to approximate solutions of two-phase flows with reactive transport in heterogeneous porous media.

- Ahusborde E., Kern M., Vostrikov V., Numerical simulation of two-phase multi-component flow with reactive transport in porous media: application to geological storage of CO_2, ESAIM: Proceedings and Surveys, Vol 49, 21-39, 2015.

Abstract: *In this work, we consider two-phase multicomponent flow in heterogeneous porous media with chemical reactions. Equations governing the system are the mass conservation law for each species, together with Darcy's law and complementary equations such as the capillary pressure law. Coupling with chemistry occurs through reactions rates. These rates can either be given nonlinear functions of concentrations in the case of kinetic chemical reactions or are unknown in the case of equilibrium chemical reactions (such as reactions in aqueous phase). In this latter case, each reaction gives rise to a mass action law, an algebraic relation that relates the activities of the implied species. The resulting system will couple partial differential equations with algebraic equations. The aim of this paper is to develop a numerical method for the simulation of this system. We consider a sequential approach that consists in splitting the initial problem into two sub-systems. The first subsystem is a two-phase two-component flow, while the second subsystem is devoted to a reactive transport problem. For the two-phase two-component flow part, we have used an already existing module of the open-source parallel multiphase flow simulator DuMu^X . To solve the reactive transport problem, we have implemented a new module in the DuMu^X framework that solves a single phase multicomponent transport problem, and we have coupled it with a locally developed code for chemical equilibrium, called ChemEqLib, through a sequential iterative approach. Then, both modules have been coupled to propose a simple, but mathematically consistent, iterative method that handles two-phase flow with reactive transport. The approach is validated on a 2D example from the literature representative of a model for the long-term fate of sequestered CO_2.*

- Ahusborde E., El Ossmani M., A sequential approach for numerical simulation of two-phase multicomponent flow with reactive transport in porous media, Mathematics and Computers in Simulation, Vol 137, 71-89, 2017.

Abstract: *We develop a new scheme for numerical solution of immiscible compressible two-phase flow in porous media with geochemistry. The problem is modeled by the mass balance law for each phase, Darcy-Muskat's law, and the capillary pressure law. Coupling with chemistry occurs through reactions rates. These rates can be either given nonlinear functions of concentrations in the case of kinetic chemical reactions or unknown for equilibrium chemical reactions. Each kinetic reaction produces an ordinary differential equation while each equilibrium reaction gives rise to a mass action law that is an algebraic relation that links the activities of concerned species. An implicit finite volume scheme is applied to solve the two-phase flow equations, which is then sequentially coupled to a method for solving the reactive transport problem. More precisely, we used firstly the module 2p2c implemented in the parallel open-source simulator DuMu^X to solve a simplified two-phase two-component flow with two dominant species without chemistry. Secondly,*

we have developed and integrated a reactive transport module in the DuMu^X framework to deal with the other species using a sequential iterative approach (SIA) where transport, equilibrium chemical reactions and kinetic chemical reactions are solved sequentially. A new module for transport and a code using the GSL library for the chemical problem have been coupled. Finally, our approach has been validated by solving several test cases. Here we will present two benchmark tests to demonstrate the ability of our method to approximate solutions of single and two-phase flows with reactive transport in heterogeneous porous media.

This section deals with the development and the implementation of numerical schemes to perform numerical simulation of two-phase multicomponent flow with reactive transport in porous media. The major difficulties related to this model are in the nonlinear degenerate structure of the equations, as well as in the strong coupling between the flow and reactive transport equations. The chemical processes involves inter-phase mass transfer as well as an host of chemical reactions, including dissolution, ion exchange, adsorption, precipitation, and oxidation/reduction.

In [14, 15, 29, 30] and in the framework of the PhD thesis of V. Vostrikov [301], we considered a sequential approach to tackle the problem consisting in a set of nonlinear partial differential equations coupled with differential algebraic equations. Instead of solving this set of equations all together, the sequential strategy splits the original problem into two sub-problems. The first sub-problem is devoted to a compositional two-phase flow where the effects of the geochemistry are treated explicitly. The second one solves a reactive transport problem. The main difference between the previous contributions is the strategy to deal with this second step, with a focus on continuous improvement. In [29, 301], the reactive transport problem was tackled by a sequential iterative approach (SIA) where transport and equilibrium chemical reactions were solved sequentially. Precisely, we developed and integrated in DuMu^X a module named 1pNc (one-phase, N-component) solving a transport problem. Then, this module was coupled iteratively with a locally developed code for chemical equilibrium, called ChemEqLib using the GSL library [5]. In [30], we abandoned the code ChemEqLib and decided to incorporate the chemistry calculation directly in DuMu^X to have an unified environment. Still considering a SIA, transport, equilibrium chemical reactions and also kinetic chemical reactions (that were not taken into account in the previous work) were solved sequentially. For this, we have developed and integrated a reactive transport module named 1pNc-React (one-phase, N-component reactive) still using the GSL library. To reduce the possible splitting errors and increase the robustness of our strategy, in [14, 15] the SIA was replaced by a global implicit approach to solve the reactive transport subproblem. More precisely, we considered the Direct Substitution Approach (DSA). All our implementations have been validated by numerous test cases including several applications. In [14], we studied the migration of hydrogen produced by the corrosion of the canisters in deep geological radioactive waste repository and obtained some results coinciding with those presented in [318]. In [15, 29, 30], we focused on different scenarios of injection of CO_2 in a deep saline aquifer. In the sequel of this section, we propose to present some numerical results for this application.

9.3.1 Geological sequestration of CO_2

To validate our sequential algorithm implemented in [15], we applied our simulator to a 3D coupled two-phase flow and reactive transport problem proposed in [113] for a scenario of geological sequestration of CO_2. In this work, the authors propose to use two variants of complex geochemical systems that include both equilibrium and kinetic reactions. We consider the test named "six-element model", whose reactions are displayed in Table 9.1.

Reactions	$log_{10}(K)$
$CO_{2(g)} = CO_{2(l)}$	-
$CO_{2(l)} + H_2O = H^+ + HCO_3^-$	-10.23
$CO_3^{2-} + H^+ = HCO_3^-$	-6.32
$OH^- + H^+ = H_2O$	-13.26
$Ano + 8\,H^+ = 4\,H_2O + Ca^{2+} + 2\,Al^{3+} + 2\,SiO_{2(l)}$	25.82
$Cal + H^+ = Ca^{2+} + HCO_3{}^-$	1.6
$Kao + 6\,H^+ = 5\,H_2O + 2\,Al^{3+} + 2\,SiO_{2(l)}$	6.82

Table 9.1: Chemical reactions.

It involves four equilibrium reactions (the first four reactions) and three kinetic reactions (the last three ones) of mineral dissolution/precipitation. For the first reaction, the solubility law for CO_2 is implemented according to [278]. Mineral data for the kinetic reactions are summarized in Table 9.2.

Mineral	$log_{10}(K^s)$	A^s	Init. conc.
Ano	-12.0	88	87
Cal	-8.80	88	238
Kao	-13.0	17600	88

Table 9.2: Mineral, precipitation and dissolution parameters.

A three-dimensional domain that is 15 km in both the x and y-directions and 100 m in the z-direction is considered. A well perforated in a single grid block located 25 m from the top of the aquifer injects a pure CO_2 stream at constant rate during the first 20 years. After the 20 years injection period, a total of 18.6×10^9 kg of CO_2 is injected. As initial conditions for the two-phase two-component H_2O-CO_2 flow we have used hydrostatic condition for liquid pressure P_l, initial liquid saturation $S_l = 1$ and initial CO_2 molality in liquid phase equals 3.55×10^{-3} mol.kg^{-1}. Initial conditions for the reactive transport problem, parameters for the B-dot model used as activity model and mineral data for the kinetic reactions can be found in [15]. Impermeable Neumann boundary conditions are enforced on the boundaries of the domain. Constitutive laws and physical parameters are given in Table 9.3.

Figure 9.7 displays concentrations of calcite, anorthite and kaolinite at 20 and 2000 years for a grid composed of 1.6×10^5 elements ($100 \times 100 \times 16$). Initially, their concentration were respectively 238, 87 and 88 mol.m^{-3}. We can see that calcite is dissolved near the injection of CO_2 and precipitated far from the injection while anorthite and kaolinite are respectively dissolved and precipitated everywhere.

Figure 9.8 depicts the molality of aqueous CO_2, the pH and the gas saturation at 20 and 2000 years. The pH and the molality of aqueous CO_2 are strongly correlated since CO_2 is a sour gas. After the injection, the gaseous CO_2 migrates upward and spreads laterally when reaching the top of the aquifer that is impermeable.

9.3.2 Parallel performances

Parallelization in the DuMu^X is carried out using the DUNE [52, 53] parallel library package. DUNE gives arbitrary data decomposition in a generic way and the employed assembly operator and linear solvers are designed correspondingly. Parallel computations on a hierarchical grid follow the "single program multiple data" (SPMD) programming paradigm based on a suitable decomposition of the grid entities. Tasks are divided and run simultaneously on several processors with different input. Processors execute their own program and communicate with each other using the Message Passing Interface (MPI).

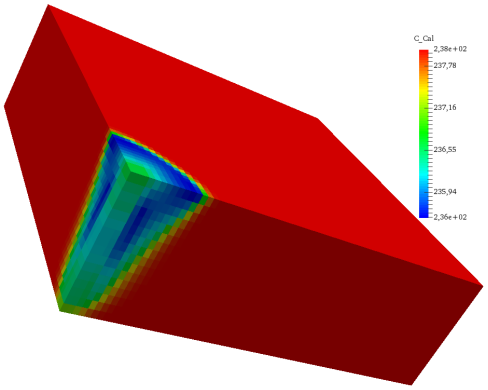

Calcite concentration at t = 20 years [mol.m^{-3}]

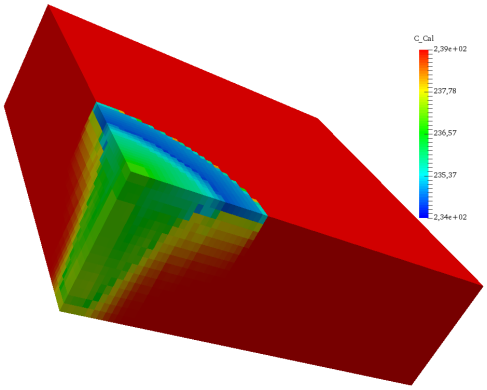

Calcite concentration at t = 2000 years [mol.m^{-3}]

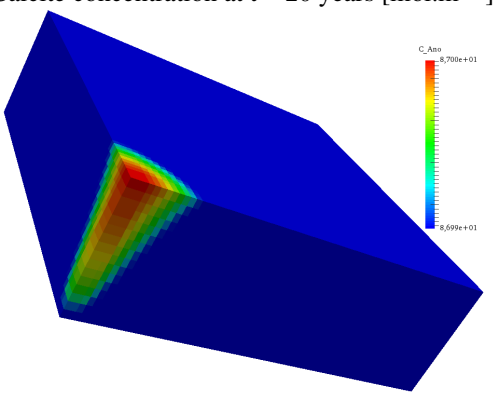

Anorthite concentration at t = 20 years [mol.m^{-3}]

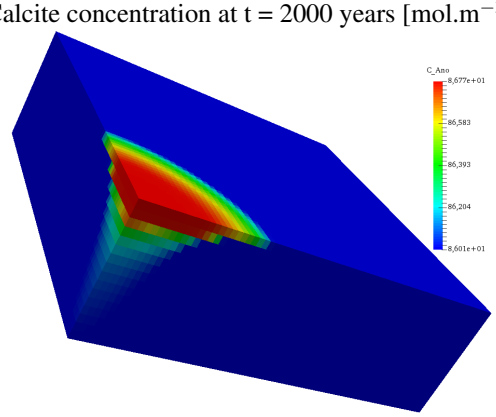

Anorthite concentration at t = 2000 years [mol.m^{-3}]

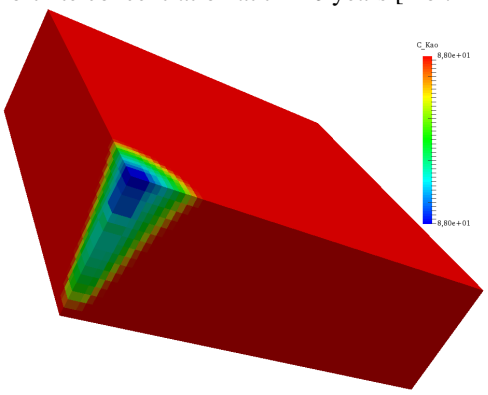

Kaolinite concentration at t = 20 years [mol.m^{-3}]

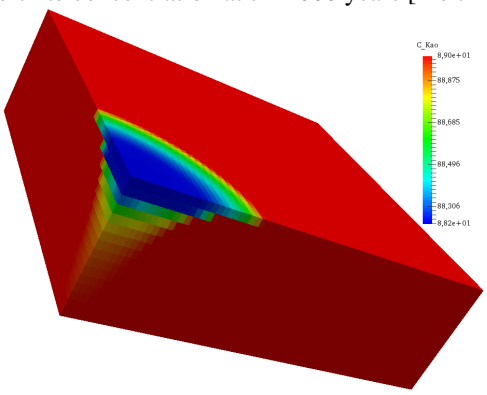

Kaolinite concentration at t = 2000 years [mol.m^{-3}]

Figure 9.7: Profiles of mineral concentrations.

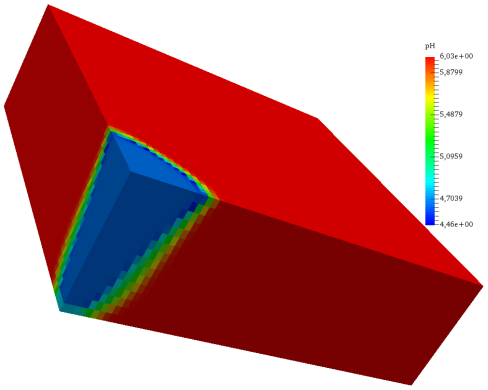

pH at t = 20 years

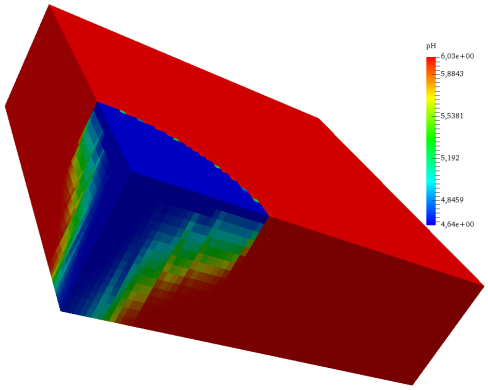

pH at t = 2000 years

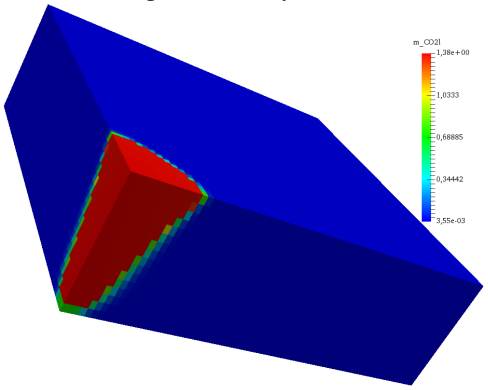

Aqueous CO_2 molality [mol.kg^{-1}] at t = 20 years

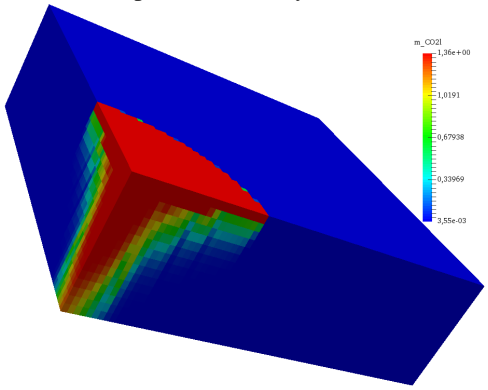

Aqueous CO_2 molality [mol.kg^{-1}] at t = 2000 years

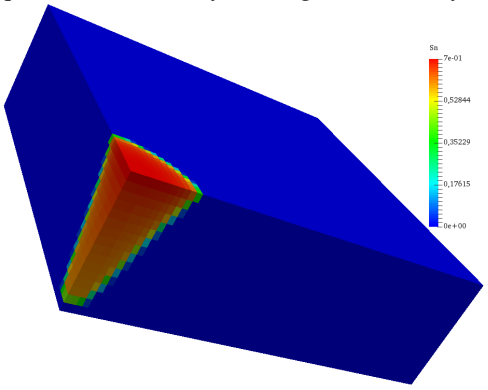

Gas saturation at t = 20 years

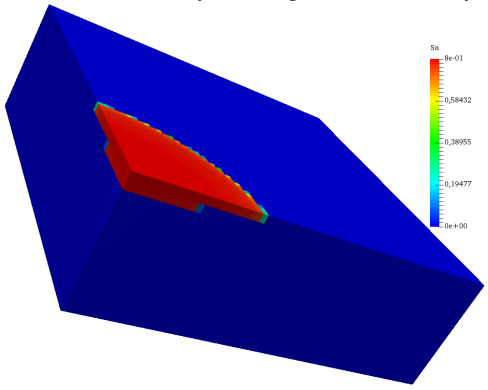

Gas saturation at t = 2000 years

Figure 9.8: Profiles of pH, aqueous CO_2 molality and gas saturation.

Constitutive law	Parameters
Capillary pressure law	$P_c = 0$ Pa
Absolute permeability	$\mathbb{K} = 10^{-13}\mathbb{I}$ [m^2]
Relative permeability	
$k_{rl} = (S_l^*)^4$	$S_l^* = \dfrac{S_l - S_{lr}}{1 - S_{lr}}$
$k_{rg} = 0.4(1 - S_l^*)^2(1 - (S_l^*)^2)$	$S_{lr} = 0.2$
Liquid diffusion tensor	
$D_l = D_m\mathbb{I}$	$D_m = 1.\ 10^{-9}$ m^2.s^{-1}
Gas diffusion tensor	Stokes-Einstein equation [315]
Porosity	$\phi = 0.18$
Temperature	$T = 50^oC$
Liquid density	Model based on [8]
Liquid viscosity	$\mu_l = 4.8\ 10^{-4}$ Pa.s^{-1}
Gas density	Model based on [277]
Gas viscosity	Model based on [116]

Table 9.3: Physical parameters for the test case of CO_2 injection.

Parallel computations up to 768 processors have been performed on several grids for the 3D version of the test. The parallel efficiency of our strategy is illustrated by solving 10 time steps. The code ran on a Bull cluster named OCCIGEN with Intel "Haswell" 12-Core E5-2690 V3 processors. In parallel computing, two types of scalability are defined. The first is the strong scaling, which represents the relation between the computation time and the number of processors for a fixed total problem size. The second is the weak scaling, for which the load per processor is fixed.

Strong scaling

Figure 9.9 a) displays on a logarithmic scale, CPU time as a function of the number of processors for three size problems of 1.6×10^5, 1.28×10^6 and 5.76×10^6 elements corresponding respectively to 1.92×10^6, 1.536×10^7 and 6.912×10^7 degrees of freedom. The dashed lines represent an ideal behavior.

Strong efficiency is given by:

$$SE(N) = \frac{\text{CPU time on } p \text{ processors } \times p}{\text{CPU time on } N \text{ processors } \times N}, \tag{9.1}$$

here p denotes the number of processors used for the reference time (not always equal to one for heavy computations). For both calculations, we took $p = 8$. It points out an optimal use of the parallel resources. Efficiency equal to one indicates that communications and synchronizations between processors are negligible. Figure 9.9 b) represents the strong scaling versus the number of processors. For this calculation, we took $p = 12$, 24 and 48 as number of processors used for the reference time. A high efficiency (greater than 0.70) is observed up to 256 processors for the computations involving 1.536×10^7 and 6.912×10^7 degrees of freedom. For the simulation with 1.92×10^6 degrees of freedom, the efficiency is good up to 72 processors. The loss of efficiency is mainly due to the increase of the communications between processors in comparison with the load of each processor. In [140, 141], the authors evaluate the parallel performance of the simulators PFLOTRAN. In [140], the authors assert that "as a general rule of thumb a minimum of 10,000 dof per core is needed to obtain good scaling performance". In [59], for the simulator ParCrunchFlow, strong scaling breaks down somewhere between 69,000 and 40,000 dof per processor. Here, a minimum of 30,000 degrees of freedom per processor seems to be required to

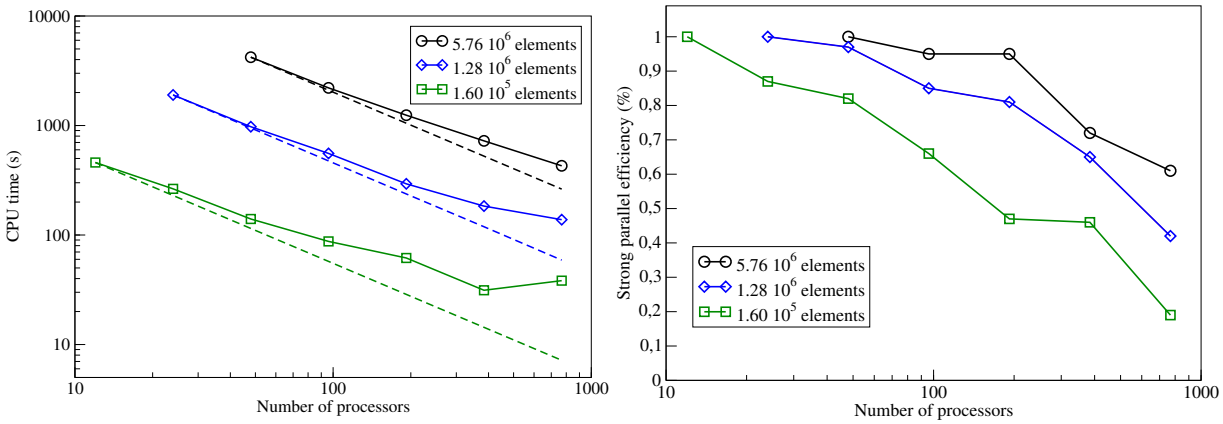

a) CPU time versus the number of processors

b) Strong parallel efficiency

Figure 9.9: CPU time and strong parallel efficiency as a function of the number of processors.

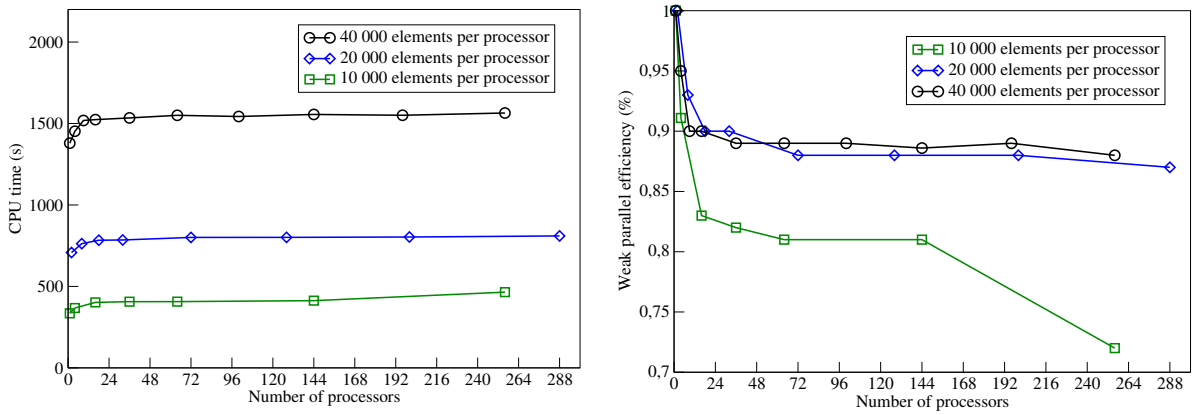

a) CPU time versus the number of processors

b) Weak parallel efficiency

Figure 9.10: CPU time and weak parallel efficiency as a function of the number of processors.

maintain a good scaling.

Weak scaling

Figure 9.10 a) displays CPU time as a function of the number of processors, with around 10000, 20000 and 40000 elements per processor.

Weak efficiency is given by:

$$WE(N) = \frac{\text{CPU time on } p \text{ processors}}{\text{CPU time on } N \text{ processors}}, \tag{9.2}$$

where p still denotes the number of processors used for the reference time. Here, $p = 1$ for the three scenarios. Weak efficiency is depicted in Figure 9.10 b). Efficiency equal to one indicates an optimal behavior for the algorithm and the computer architecture. Indeed, CPU times remains constant, equal to the reference time, while the total size of the problem increases with the number of processors. Usually, this property is hardly verified and curves with plateaus can be observed. Values of the plateaus rise toward one with the load of each processor. This phenomenon is illustrated in Figure 9.10 b)

9.3.3 Comparison between direct substitution and sequential iterative approaches

This subsection aims at comparing the DSA used in [15] with the SIA developed in [30] for solving the reactive transport subproblem for the example presented above. Both approaches adopt an adaptive time-stepping. In the DSA, the control of the time-step is based on the number of iterations required by the Newton method to achieve convergence while in the SIA, it is based on the number of iterations required in the iterative algorithm to reach the tolerance ε_{SIA}. In the sequel, tolerances for the Newton method and iterative algorithm are respectively $\varepsilon_{Newton} = 10^{-8}$ and $\varepsilon_{SIA} = 10^{-8}$.

Figure 9.11 compares the evolution of the molalities of H^+ and Ca^{2+} obtained with the DSA and the SIA close to the injection with a mesh composed of 40000 cells during the first year of injection. We can observe that the results are in good accordance and that both methods provide comparable results.

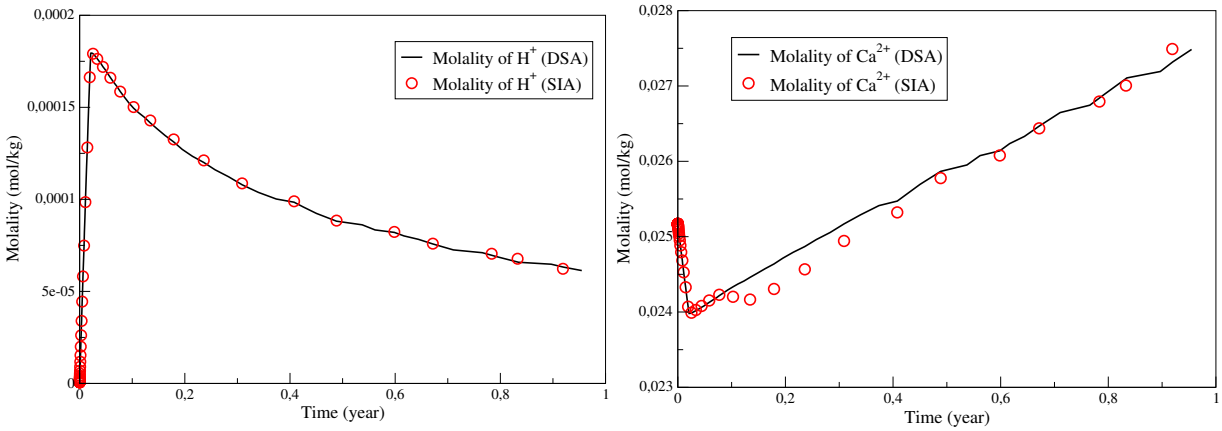

a) H^+ b) Ca^{2+}

Figure 9.11: Comparison of the molalities of H^+ and Ca^{2+} obtained with the DSA and the SIA.

Table 9.6 displays the CPU time required for the DSA and the SIA to achieve the first year of injection years on several meshes. We can see that for this example, the DSA is faster than the SIA whatever the size of the mesh. The SIA is more CPU consuming in comparison with the DSA because many iteration steps in the iterative procedure and smaller time steps are required.

Number of cells	DSA	SIA
10000	982.2	1518.8
40000	3847.5	6235.5
160000	15901.9	27235.5

Table 9.4: CPU time (s) for the DSA and the SIA.

9.4 Fully coupled fully implicit algorithms for numerical simulation of reactive flows

The content of this section relies on a synthesis of article [31] and is also based on article [16]. Both articles are listed below and can be found in the Appendix:

- Ahusborde E., El Ossmani M., Id Moulay M., A fully implicit finite volume scheme for single phase flow with reactive transport in porous media, Mathematics and Computers in Simulation, Vol 164, 3-23, 2019.

  Abstract: *Single phase flow and reactive transport modeling involve solving a highly nonlinear coupled system of partial differential equations to algebraic or ordinary differential equations requiring special numerical treatment. In this paper, we propose a fully implicit finite volume method using a direct substitution approach to improve the efficiency and the accuracy of numerical computations for such systems. The approach has been developed and implemented in the framework of the parallel open-source platform DuMu^X . The object oriented code allows solving reactive transport problems considering different coupling approaches. A number of 2D and 3D numerical tests were performed for verifying and demonstrating the capability of the coupled fully implicit approach for single phase flow and reactive transport in porous media. Numerical results for the reactive transport benchmark of MoMaS and long-term fate of injected CO_2 for geological storage including a comparison between the direct substitution approach and the sequential iterative approach are presented. Parallel scalability is investigated for simulations with different grid resolutions.*

- Ahusborde E., Amaziane B., El Ossmani M., Id Moulay M., Numerical modeling and simulation of fully coupled processes of reactive multiphase flow in porous media, Accepted for publication in Journal of Mathematical Study, 2019.

  Abstract: *In this paper, we consider a finite volume approach for modeling multiphase flow coupled to geochemistry in porous media. Reactive multiphase flows are modeled by a highly nonlinear system of degenerate partial differential equations coupled with algebraic and ordinary differential equations. We propose a fully implicit scheme using a direct substitution approach (DSA) implemented in the framework of the parallel open-source platform DuMu^X . We focus on the particular case where porosity changes due to mineral dissolution/precipitation are taken into account. This alteration of the porosity can have significant effects on the permeability and the tortuosity. The accuracy and effectiveness of the implementation of permeability/porosity and tortuosity/porosity relationships related to mineral dissolution/precipitation for single phase and two-phase flows are demonstrated through numerical simulations.*

Recently, in the framework of the PhD thesis of M. Id Moulay [215], we decided to set aside temporarily the sequential strategies presented in Section 9.3. Indeed, sequential approaches can introduce operator splitting errors and some questions about the coupling between all the physical processes have to be studied to asses if sequential approaches are relevant to solve very coupled phenomena or if implicit approaches are better suited. By consequence, we developed and implemented a parallel fully-coupled, fully implicit method to solve reactive multiphase multicomponent flow to achieve improved stability. In comparison with sequential strategies, we expect that the errors of mass conservation due to the operator splitting will be erased and that larger time steps can be used during simulations.

9.4.1 Numerical simulation of single phase reactive flows

First, we focused on the single phase case. Besides the DSA that has already been used to solve the reactive transport problem in [14, 15], several other formulations involving different choices for the primary variables were envisaged and tested. No significant change was observed and as a consequence, we maintained the choice to use a DSA. This led us to propose in [31] a fully implicit finite volume

strategy for single phase reactive flows. This fully implicit strategy has been validated by numerous test cases, notably the MoMaS benchmark [82]. Detailed results can be found in [31]. In this subsection, on the particular example of the SHPCO2 Project [137], we propose an advanced comparison between the DSA and the SIA considered in [30] in term of computational time for several grid resolutions. The three-dimensional version of the test is also calculated and parallel computations are presented with good strong and weak parallel efficiencies.

9.4.1.1 SHPCO2 test case

This test case was proposed in the framework of the SHPCO2 Project (French acronym for High Performance Simulation of CO_2 Geological Storage). Its detailed description can be found in [137]. The chemical system consists of components involved in 4 reactions displayed in Table 9.5.

No.	Reactions
(1)	$OH^- + H^+ \rightleftharpoons H_2O$
(2)	$CO_{2(g)} \rightleftharpoons CO_{2(l)}$
(3)	$HCO_3^- + H^+ \rightleftharpoons CO_{2(l)} + H_2O$
(4)	$Calcite + H^+ \rightleftharpoons Ca^{2+} + HCO_3^-$

Table 9.5: Chemical reactions for the SHPCO2 test case.

The geometry (2D and 3D) of the domain is depicted in Figure 9.12. We consider firstly the two-dimensional version of the test. It is divided into two zones: a "barrier" zone with a low permeability $K_{\text{barrier}} = 10^{-15}\ m^2$ (represented in green in Figure 9.12) and a "drain" zone (the remaining part) with higher permeability $K_{\text{drain}} = 10^{-13}\ m^2$.

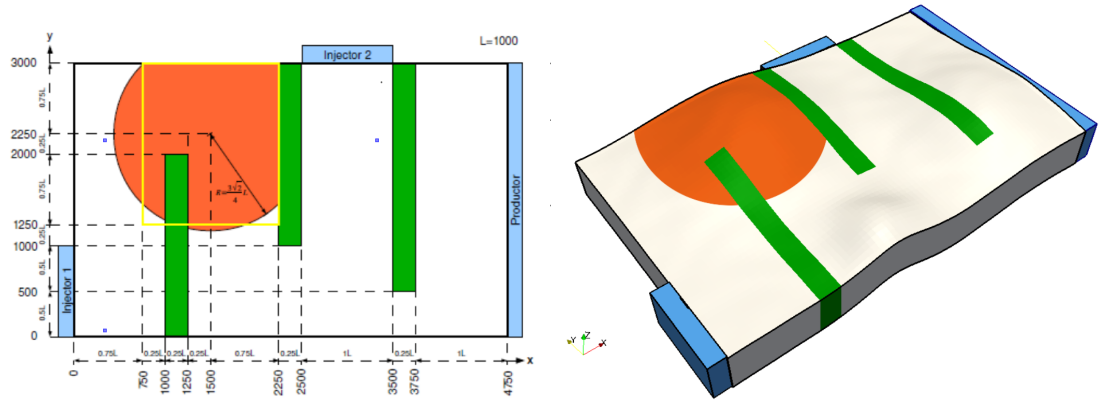

Figure 9.12: Two-dimensional (left) and three-dimensional (right) geometry of domain for the SHPCO2 test case (taken from [137]).

In this test, the gas phase is assumed to be immobile and therefore gaseous carbon dioxide $CO_{2(g)}$ is considered as a fixed species. The hypothesis of immobility of gas allows to focus on reactive transport without worrying issues of multiphase flow. Consequently, the problem is modeled by a single phase multicomponent flow with reactive transport. Initially, in the orange bubble of Figure 9.12 gaseous carbon dioxide $CO_{2(g)}$ is present while in the remaining zone, concentration of $CO_{2(g)}$ is equal to zero. For

the flow, Dirichlet boundary conditions for the pressure are enforced at the boundary surfaces Injector1, Injector2 and Productor while at the rest of the boundary of the domain, homogeneous Neumann condition are imposed. Concerning the transport, a pure advective flux on the boundary surfaces Injector1, Injector2 and Productor is imposed. On the rest of the boundary of the domain, we consider homogeneous Neumann conditions. Physical parameters and initial concentrations can be found in [30]. The period of simulation is equal to 4500 years. Several two-dimensional meshes have been used. An adaptive time step strategy is used with a maximal time step equal to 10 years.

Figure 9.13 represents the evolution of the concentration of $CO_{2(g)}$ and $CO_{2(aq)}$ at $t = 400$ years and $t = 1600$ years with a mesh composed of 233472 elements. Due to the hypothesis of the immobility of the gas phase, the position of zone with $CO_{2(g)}$ does not change with time but its size is significantly reduced. This is explained by the fact that $CO_{2(g)}$ dissolves in liquid phase and is transported by flow outside the initial gaseous zone.

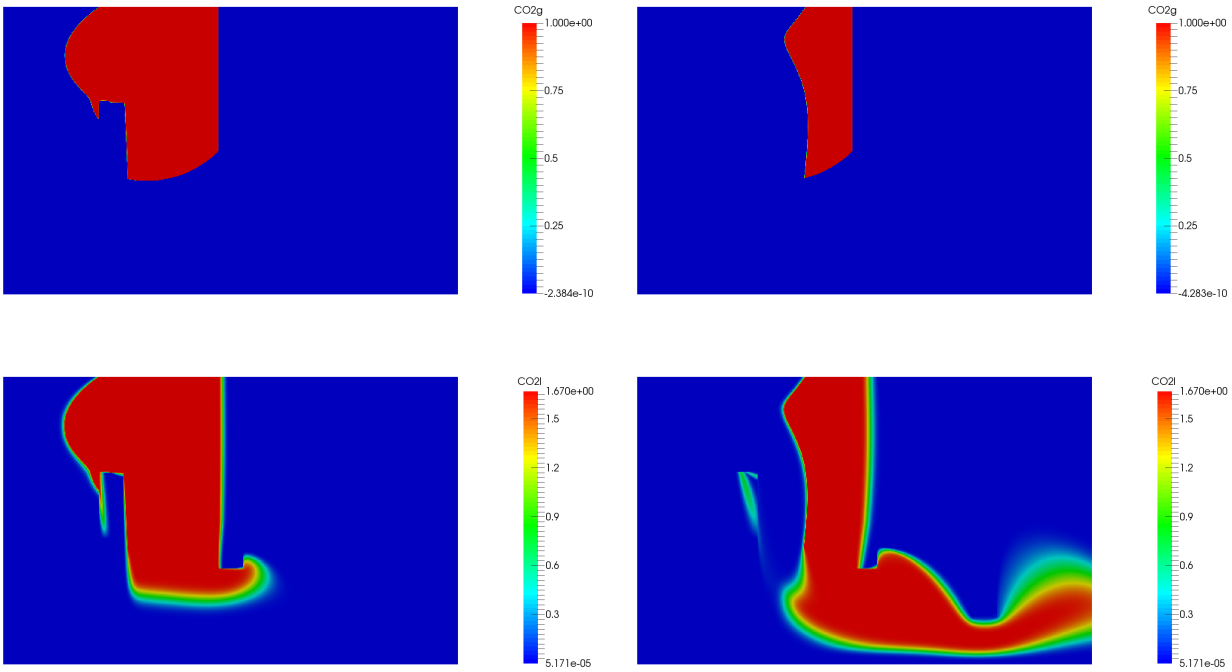

Figure 9.13: Evolution of the concentrations of $CO_{2(g)}$ (top) and $CO_{2(aq)}$ (bottom). Left: 400 years. Right: 1600 years.

9.4.1.2 Comparison between DSA and SIA

We aim at comparing DSA and SIA implemented in [30] in the same numerical environment for the example presented above. Both approaches adopt an adaptive time-stepping. In the DSA, the control of the time-step is based on the number of iterations required by the Newton method to achieve convergence while in the SIA, it is based on the number of iterations required in the iterative algorithm to reach the tolerance ε_{SIA}. In the sequel, tolerances for the Newton method and iterative algorithm are respectively $\varepsilon_{Newton} = 10^{-8}$ and $\varepsilon_{SIA} = 10^{-5}$.

Figure 9.14 compares the concentration of $CO_{2(aq)}$ obtained with DSA and SIA on the line $y = 600$ with two meshes composed of 14592 and 58368 cells at $t = 1600$ years. We can observe that the results are in great accordance.

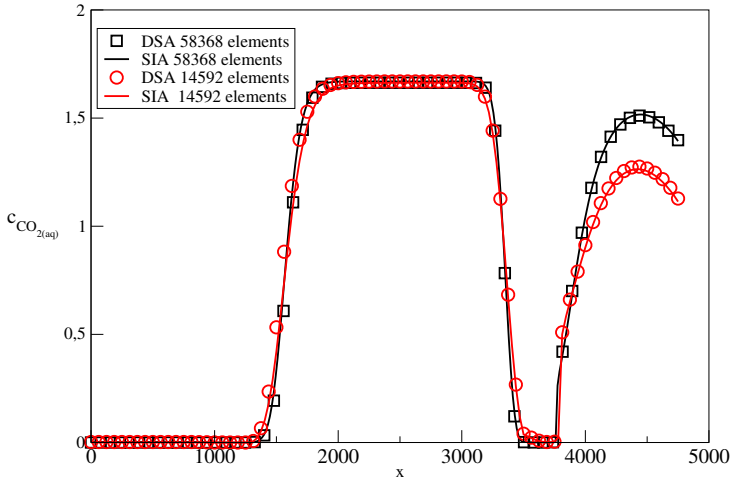

Figure 9.14: Comparison of the concentration of $CO_{2(aq)}$ obtained with DSA and SIA.

Table 9.6 displays the CPU time required and the number of time steps for the DSA and the SIA to reach 1200 years on several meshes. We can see that for this example, DSA is faster than SIA when fine meshes are used. Figure 9.15 a) represents the time steps used by the DSA and SIA during the computations for the two finest meshes. We have to specify that a maximum time step equal to 10 years was enforced for both simulations. We can remark that the implicit approach allows to use larger time steps than the sequential approach as expected. This is emphasized by Figure 9.15 b) that depicts the number of iterations required by the Newton method to achieve ε_{Newton} in the DSA and the number of iterations required in the SIA to reach the tolerance ε_{SIA}. The results are given for the mesh composed of 58368 elements. We can see that the SIA requires more iterations than the DSA and therefore, the time step can not increase as quickly as for the DSA and never reaches the maximum value equal to 10 years.

	DSA		SIA	
Cells	CPU time(s)	Number of time steps	CPU time(s)	Number of time steps
912	1118	567	741	572
3648	2272	578	2288	572
14592	8612	578	11439	575
58368	27143	579	72813	626

Table 9.6: CPU time (s) and number of time steps for DSA and SIA.

9.4.1.3 Three-dimensional simulation

In [31], we have also performed the three-dimensional version of the test, whose geometry is represented in Figure 9.12. Figure 9.16 represents several quantities after 1500 years of simulation on a mesh composed of 912000 elements. The computation has been performed with 256 processors. As for the two-dimensional case, the initial bubble of gaseous $CO_{2(g)}$ is dissolved and transported in liquid phase.

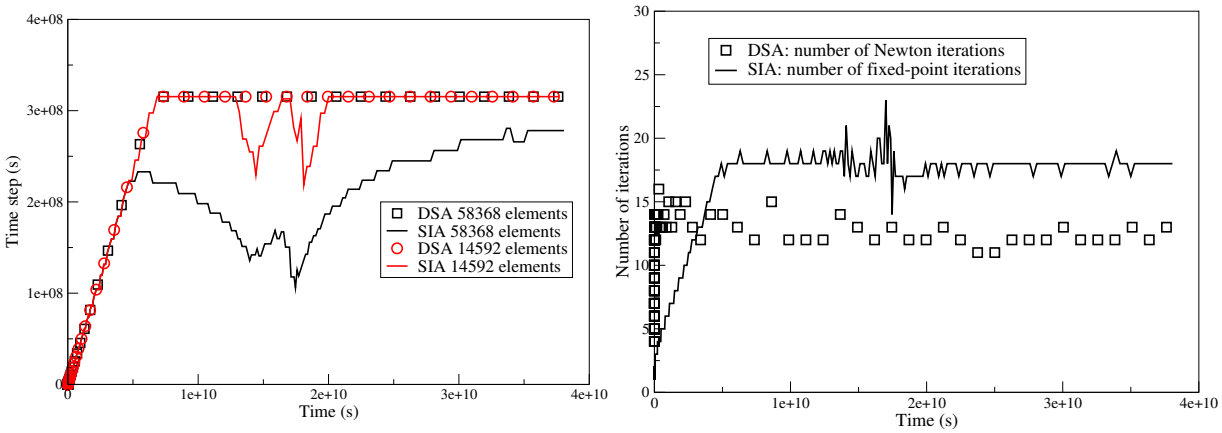

a) Time step versus time.

b) Number of iterations versus time.

Figure 9.15: Comparison between DSA ad SIA.

The concentrations of H^+ and $CO_{2(aq)}$ are very correlated since high concentrations of $CO_{2(aq)}$ acidify the medium.

9.4.1.4 Parallel performance

Parallel computations up to 512 processors have been performed on several grids for the 3D version of the test. The parallel efficiency of our strategy is illustrated by solving 100 time steps. As for the sequential strategy, the code ran on the cluster OCCIGEN and strong and weak scalabilities were evaluated.

Strong scaling

Figure 9.17 a) displays on a logarithmic scale, CPU time as a function of the number of processors for 2 size problems of 228000 and 912000 elements corresponding to approximately 1.6×10^6 and 6.4×10^6 unknowns. The dashed lines represent an ideal behaviour.

Figure 9.17 b) represents the strong scaling versus the number of processors. A high efficiency (greater than 0.85) is observed up to 256 processors for the computations involving 912000 cells. For the simulation with 228000 cells, the efficiency is good up to 64 processors. The loss of efficiency is mainly due to the increase of the communications between processors in comparison with the load of each processor.

Weak scaling

Figure 9.18 a) displays CPU time as a function of the number of processors, with 9120 and 18240 elements per processor. Efficiency equal to one indicates an optimal behavior for the algorithm and the computer architecture. Indeed, CPU times remains constant, equal to the reference time, while the total size of the problem increases with the number of processors. Usually, this property is hardly verified and curves with plateaus can be observed. This phenomenon is illustrated in Figure 9.18 b).

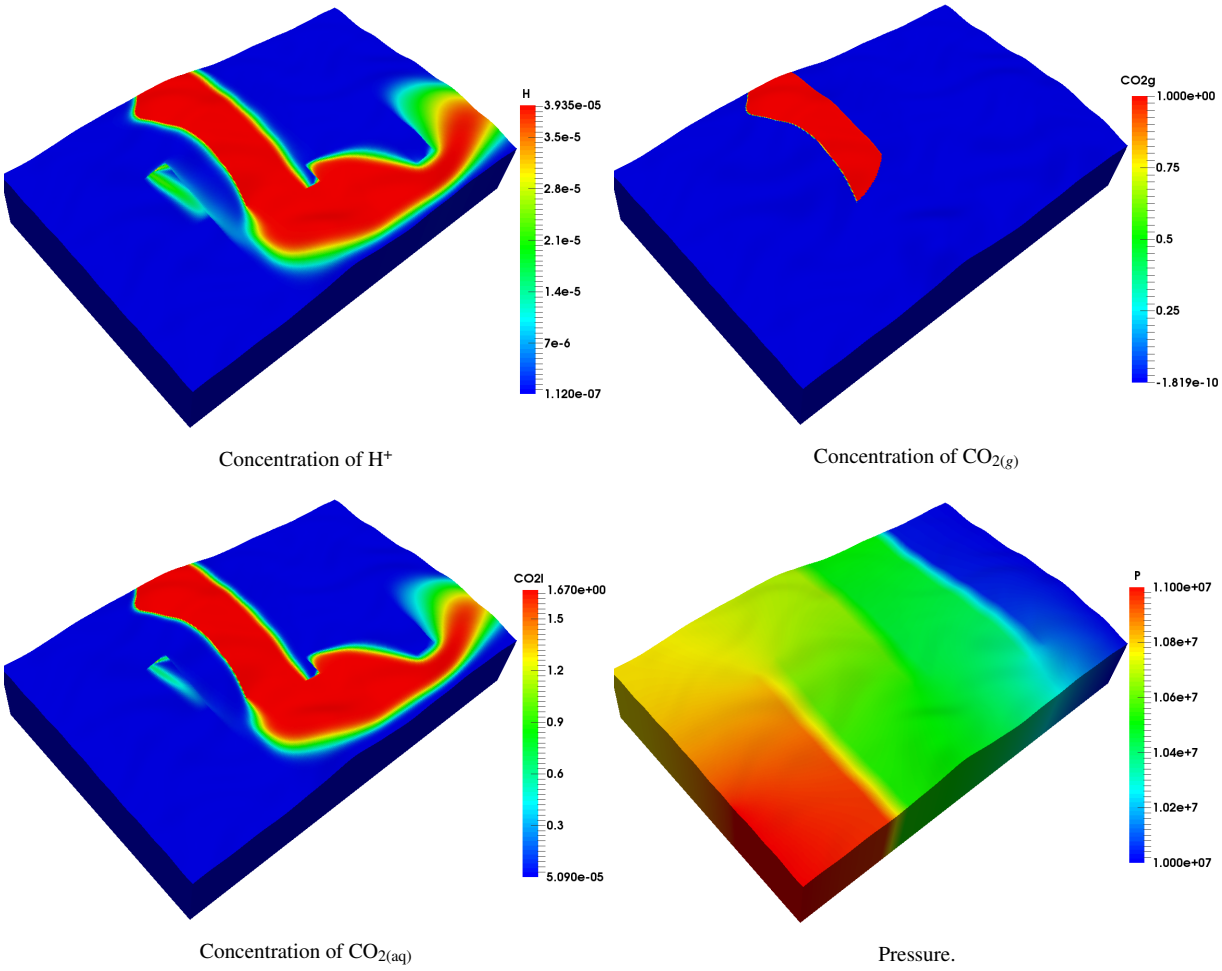

Concentration of H^+

Concentration of $CO_{2(g)}$

Concentration of $CO_{2(aq)}$

Pressure.

Figure 9.16: Profiles of concentrations and pressure at $t = 1500$ years.

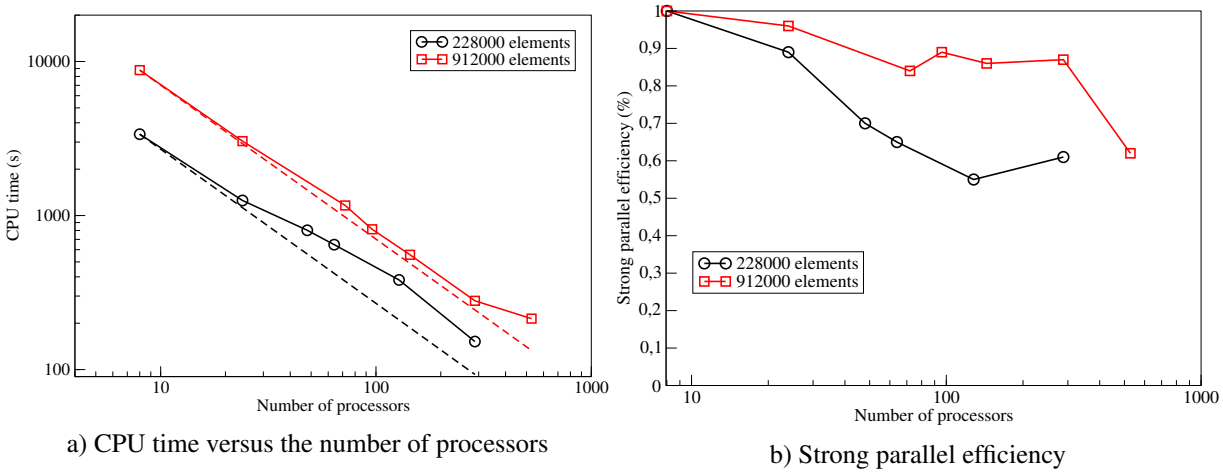

a) CPU time versus the number of processors

b) Strong parallel efficiency

Figure 9.17: CPU time and strong parallel efficiency as a function of the number of processors.

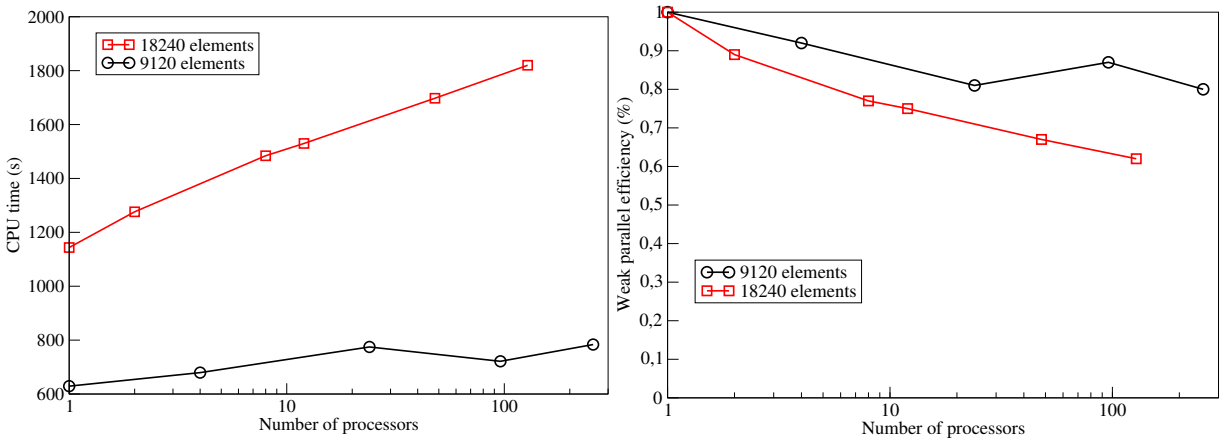

a) CPU time versus the number of processors

b) Weak parallel efficiency

Figure 9.18: CPU time and weak parallel efficiency as a function of the number of processors.

9.4.2 Numerical simulation of two-phase reactive flows

In [16], we proposed to extend the global implicit approach developed in [31] to deal with reactive two-phase flows and consequently to drop out the sequential approach considered until then. To validate our methodology, we started by considering a one-dimensional test case proposed in [267]. Despite its relatively simple geometry, this test case presents the additional difficulty to deal with porosity and permeability changes. Indeed, the simulation of permeability and tortuosity evolution due to porosity changes can be of crucial importance in the simulation of several processes. These porosity changes can occur due to the dissolution or precipitation of minerals. If the porosity is increased, new pathways can develop, facilitating solute transport while the decrease of porosity can lead to a total clogging, with a possible annihilation of any flow and/or solute transport (see also for instance [97] or [314]). The dependencies between the transport properties and porosity (Millington-Quirk's relationship for diffusivity and Kozeny-Carman's relationship) have been treated implicitly. This implicit treatment added an additional computational complexity by further increasing the strong nonlinearity of the system of equations. A numerical convergence analysis was carried out, giving numerical results in good agreement with those obtained in [267]. Numerical simulations provided validation of our implementation of permeability/porosity and tortuosity/porosity relationships related to mineral dissolution/precipitation. Then, in the framework of the PhD thesis of M. Id Moulay [215], we have pursued the validation of our fully implicit approach for reactive multiphase flows by considering a three-dimensional test case involving a more complex chemical systems. More precisely, we computed the test case proposed in [113] and presented in Subsection 9.3.1 for the sequential algorithm. An advanced comparison between the fully implicit and sequential approaches is in progress. We can already confirm that for this particular test case, both approaches provide very close results. We were also able to highlight the loss of mass for the sequential case (even if it is minimal) whereas the implicit approach is totally mass-conservative. The fully implicit approach is more CPU time consuming than the sequential one, but the difference is not significant. Even if no definitive conclusion can be drawn, we can assess that for this test case, our sequential approach can be as accurate as the fully implicit one provided it is carefully implemented. Moreover, the fully implicit approach is now more efficient that originally thought thanks to the advance of high-performance computing. We have to continue to validate our fully implicit approach by considering additional benchmarks. In this regard, we would like to point out that we encountered difficulties to find reliable and well documented benchmarks. In many articles, some data are missing. We think

that a well documented benchmark for two-phase flow with reactive transport in porous media would be very useful for the community. It is why, a contribution on this important issue is in progress. Let mention also that even if most of the presented results concern two-phase reactive flows, the platform we developed is able to treat a more complex flow by considering multiphase multicomponent reactive flows.

Finally, to make the implicit approach even more competitive, further improvements must continue to be achieved. Due to the strong coupling between multiphase flow and reactive transport inducing strong nonlinearities in the global problem, particular attention should be paid to improve the convergence of linear solvers, using for example a series of algebraic reductions (Schur complements) as in [113]. *A posteriori* estimators could be also used and implemented to achieve computational savings by stopping timely the linear and nonlinear solvers as in [299]. We could also use the PETSc (Parallel Extensible Toolkit for Scientific computing) solver library as in PFLOTRAN [140]. It could be also interesting to adapt the reduction technique proposed in [74, 75] for an integration in DuMu^X.

Chapter 10

Conclusions and Perspectives

This dissertation presents some of the results of my research activity devoted to the development and implementation of mathematical and high performance computational methods for modeling complex flows. Over the last decade, I have focused on two areas of research. In the continuity of my PhD thesis, the first one concerns CFD simulations of incompressible flows for which a wide range of issues have been raised. The second area deals with a thematic that I discovered with my recruitment at the Laboratory of Mathematics and its Applications of Pau: the numerical simulation of multiphase flow in porous media. For this topic, the numerical study of reactive flows was highlighted and several sequential and implicit strategies were implemented and compared in a high performance computing framework. The use of DuMu^X allowed to integrate all these developments in an unified and homogeneous environment and ensure their sustainability. To conclude this dissertation, I present some research directions I want to pursue in future years.

10.1 Modeling of coupled thermo-hydro-mechanical-chemical (THMC) processes in porous media

This work will be performed in collaboration with B. Amaziane (LMAP, University of Pau & Pays Adour), M. Jurak (University of Zagreb, Croatia) and M. El Ossmani (University Moulay Ismaïl, Morocco). The understanding of coupled thermal, hydraulic, mechanical and chemical (THMC) processes (illustrated in Figure 10.1) is a crucial issue for the performance assessment of geological disposal of carbon dioxide or/and radioactive waste. During the last years, we implemented several sequential and implicit strategies to couple the hydraulic and chemical processes. During the next four years (June 2019 - June 2023), we will be involved in the Horizon 2020 European Joint Program on Radioactive Waste Management (EURAD). More precisely, we participate to the Work Package untitled "Development/improvement of numerical methods & tools for modeling coupled processes (DONUT)" through the task "Numerical methods for high performance computing of coupled processes". We will develop some open access massively parallel numerical tools for coupling thermo-hydro with chemical processes (a grant for a post-doctoral position has been obtained). In parallel, we wish to go further and consider the numerical modeling of the coupling between geomechanics and fluid (gas and liquid) flow in rock formations. Our goal is to undertake some numerical simulation incorporating the coupling between gas migration and mechanical behavior, with particular emphasis placed on changes in permeability/transmissivity during mechanical loading and/or deformation. First, we will consider a sequential approach as in [56, 210, 262, 330]. However, some questions about the coupling between all the physical processes described above have to be studied to corroborate if some very coupled phenomena can be

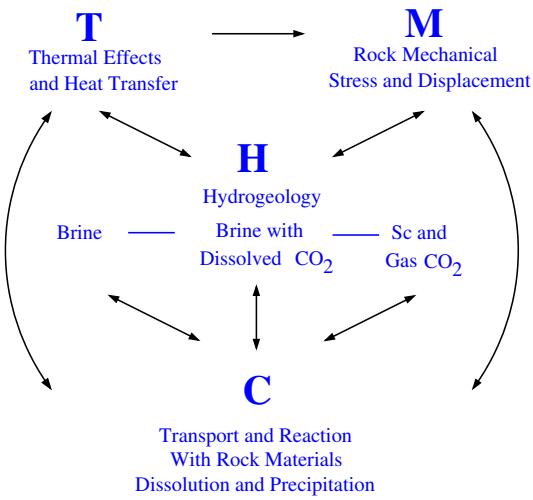

Figure 10.1: Coupled THMC processes, coupling thermal (T), hydrological (H), rock mechanical (M) and chemical (C) effects for geological storage of CO_2 (adapted from [226]).

really solved by sequential schemes or if they need to be treated as a strongly coupled entity as in [334]. We wish also consider new applications as geothermal reservoir modeling for which the understanding of coupled THMC processes is a crucial issue [233, 286]

10.2 CO_2 storage enhancement

This work will be performed in collaboration with F. Croccolo (LFCR, University of Pau & Pays Adour) and B. Amaziane (LMAP, University of Pau & Pays Adour). The CO2ES project (CO_2 Enhanced Storage) project led by F. Croccolo aims at improving the understanding of the various CO_2 trapping and transport processes involved in CO_2 geological storage. The project is mainly experimental and seeks to investigate processes to enhance CO_2 storage efficiency and safety by dissolution and by mineral trapping. However, it comprises also a numerical part in which we will be involved through our participation in the Work Package untitled "Up-scaling of CO_2 storage processes". Numerical activities are intended to scale-up the phenomena pointed out in the experimental part by using homogenization tools as well as guiding further experimental activities.

10.3 Multicomponent transport in low permeability porous media

This work will be performed in collaboration with G. Galliéro (LFCR, University of Pau & Pays Adour) and M. Azaïez (I2M, University of Bordeaux). The description of the dynamics of a multicomponent fluid confined in a nano-porous medium is an intricate task despite its wide interest for many applications (chemical engineering, geosciences). Classical approaches (such Darcy's or Stokes' formulations depending the scale) can be inappropriate in the case where the pore size is similar to that of fluid molecules since surface effects become predominant compared to volume effects. We aim at proposing a different paradigm to describe multicomponent transport in porous media based on one equation of momentum conservation per species at the pore scale as proposed in [169]. Then, we plan to use homogenization theory to move from pore scale to Darcy's scale. The coupling between these equations is achieved by a Maxwell-Stefan friction terms to ensure momentum exchange between different species

and requires the knowledge of new fluid physical properties such as partial viscosities or slip lengths by species. Up to now, these properties were difficult to obtain but using molecular dynamics simulations, it is now possible to have access to such quantities [36] which makes this new paradigm accessible. A post-doctoral fellow will be hired to work on this topic.

10.4 Reduction Order Modeling

The propose is to use Reduced Order Modeling (ROM), a new paradigm in industrial design and optimization, for the solution of the two families of problems previously described in this document. ROM provides dramatic reduction in computation times, and finds its place at the crossroads with the upcoming integration of machine learning and artificial intelligence tools in the construction and engineering sectors. This paradigm has undergone a fast development, and is progressively being applied with success to large optimization and design problems in engineering, that were deemed completely out of reach only a few years ago. I aim at collaborating with M. Azaïez and E. Prulière (I2M, University of Bordeaux) to apply and adapt these approaches to some of our applications. Two objectives can be considered:

- **Reduction in parameter space.** The processes and physical phenomena present in the manuscript depend on large number of parameters (geometrical and environmental). Reducing this number of parameters while maintaining the accuracy of the computation is of primary importance in tackling the optimization design problem.
- **Data assimilation.** The huge amount of information required to set up the conditions for the computational codes are frequently incomplete. There is a need to re-construct the fields with accurate and fast procedures.

Bibliography

[1] Crunchflow: Multicomponent reactive flow and transport software. `http://www.csteefel.com/CrunchFlowIntroduction.html`.

[2] DARTS: Delft Advanced Research Terra Simulator. `https://darts-web.github.io/darts-web/`.

[3] DuMu^X, DUNE for multi-Phase, Component, Scale, Physics, ... flow and transport in porous media. `http://www.dumux.org`.

[4] DUNE, the Distributed and Unified Numerics Environment. `http://www.dune-project.org`.

[5] GSL multidimensional root-finding. `http://www.gnu.org/software/gsl/`.

[6] Safety of geological disposal of high-level and long-lived radioactive waste in france. An International Peer Review of the " Dossier 2005 Argile" Concerning Disposal in the Callovo-Oxfordian Formation. Nuclear Energy Agency/OECD, Paris, http://www.nea.fr/html/rwm/reports/2006/nea6178-argile.pdf.

[7] A. Abadpour and M. Panfilov. Method of negative saturations for modeling two-phase compositional flow with oversaturated zones. *Transport in Porous Media*, 79:197–214, 2009.

[8] J. J. Adams and S. Bachu. Equations of state for basin geofluids: algorithm review and intercomparison for brines. *Geofluids*, 2:257–271, 2002.

[9] D.R. Aguilera, P. Jourabchi, C. Spiteri, and P. Regnier. A knowledge-based reactive transport approach for the simulation of biogeochemical dynamics in earth systems. *Geochemistry, Geophysics, Geosystems*, 6, 2005.

[10] N. Ahmad, A. Wörman, A. Bottacin-Busolin, and X. Sanchez-Vila. Reactive transport modeling of leaking CO_2-saturated brine along a fractured pathway. *International Journal of Greenhouse Gas Control*, 42:672–689, 2015.

[11] N. Ahmad, A. Wörman, X. Sanchez-Vila, J. Jarsjö, A. Bottacin-Busolin, and H. Hellevang. Injection of CO_2 saturated brine in geological reservoir: A way to enhanced storage safety. *International Journal of Greenhouse Gas Control*, 54:129–144, 2016.

[12] E. Ahusborde. *High order method for the* grad$(div(.))$ *operator and applications*. Phd thesis, University of Bordeaux 1, 2007.

[13] E. Ahusborde, B. Amaziane, and M. Jurak. 3D numerical simulation by upscaling of gas migration through engineered and geological barriers for a deep repository for radioactive waste. *Geological Society, London, Special Publications*, 415:123–141, 2015.

[14] E. Ahusborde, B. Amaziane, and M. El Ossmani. Finite volume scheme for coupling two-phase flow with reactive transport in porous media. *Springer Proceedings in Mathematics and Statistics*, 200:71–89, 2017.

[15] E. Ahusborde, B. Amaziane, and M. El Ossmani. Improvement of numerical approximation of coupled two-phase multicomponent flow with reactive geochemical transport in porous media. *Oil & Gas Science and Technology - Rev. IFP Energies nouvelles*, 73:73, 2018.

[16] E. Ahusborde, B. Amaziane, M. El Ossmani, and M. Id Moulay. Numerical modeling and simulation of fully coupled processes of reactive multiphase flow in porous media. *Accepted for publication in Journal of Mathematical Study*, 2019.

[17] E. Ahusborde, M. Azaïez, F. Ben Belgacem, and E. Palomo Del Barrio. Mercer's spectral decomposition for the characterization of thermal parameters. *Journal of Computational Physics*, 294:1–19, 2015.

[18] E. Ahusborde, M. Azaïez, F. Ben Belgacem, and C. Bernardi. Automatic simplification of darcy's equation with pressure dependent permeability. *ESAIM: Mathematical Modelling and Numerical Analysis*, 47:1797–1820, 2013.

[19] E. Ahusborde, M. Azaïez, and J.P. Caltagirone. A primal formulation for the Helmholtz decomposition. *Journal of Computational Physics*, 225:13–19, 2007.

[20] E. Ahusborde, M. Azaïez, J.P. Caltagirone, M. Gerritsma, and A. Lemoine. Discrete Hodge Helmoltz Decomposition. *Monografías Matemáticas "García de Galdeano"*, 39:1–10, 2014.

[21] E. Ahusborde, M. Azaïez, M.O. Deville, and E.H. Mund. Legendre spectral method for the -grad(div(.)) operator. *Computer Methods in Applied Mechanics and Engineering*, 196:4538–4547, 2007.

[22] E. Ahusborde, M. Azaïez, M.O. Deville, and E.H. Mund. Constructive spectral approaches for the Helmholtz decomposition of a vector field. *Applied Numerical Mathematics*, 58:955–967, 2008.

[23] E. Ahusborde, M. Azaïez, S. Glockner, and A. Poux. A contribution to the outflow boundary conditions for Navier-Stokes time-splitting methods. *Lecture Notes in Computational Science and Engineering*, 95:75–86, 2014.

[24] E. Ahusborde, M. Azaïez, and R. Gruber. Constraint oriented spectral element method. *Lecture Notes in Computational Science and Engineering*, 76:93–100, 2011.

[25] E. Ahusborde, M. Azaïez, and R. Gruber. Numerical assessment of a class of high order Stokes spectrum solver. *Journal of Mathematical Study*, 51:1–14, 2018.

[26] E. Ahusborde and S. Glockner. An implicit method for the Navier-Stokes equations on overlapping block-structured grids. *International Journal for Numerical Methods in Fluids*, 62:784–801, 2010.

[27] E. Ahusborde and S. Glockner. A 2D block-structured mesh partitioner for accurate flow simulations on non-rectangular geometries. *Computers and Fluids*, 43:2–13, 2011.

[28] E. Ahusborde, R. Gruber, M. Azaïez, and M.L. Sawley. Physics-conforming constraints-oriented numerical method. *Physical Review E*, 75:056704, 2007.

[29] E. Ahusborde, M. Kern, and V. Vostrikov. Numerical simulation of two-phase multicomponent flow with reactive transport in porous media: application to geological sequestration of CO_2. *ESAIM: Proceedings and Surveys*, 50:21–39, 2015.

[30] E. Ahusborde and M. El Ossmani. A sequential approach for numerical simulation of two-phase multicomponent flow with reactive transport in porous media. *Mathematics and Computers in Simulation*, 137:71–89, 2017.

[31] E. Ahusborde, M. El Ossmani, and M. Id Moulay. A fully implicit finite volume scheme for single phase flow with reactive transport in porous media. *Mathematics and Computers in Simulation*, 164:3–23, 2019.

[32] R. Al-Khoury and J. Bundschuh. *Computational Models for CO_2 Geo-sequestration & Compressed Air Energy Storage*. Sustainable Energy Developments, CRC Press, 2014.

[33] B. Amaziane, M. Jurak, and A. Zgaljić Keko. Modeling compositional compressible two-phase flow in porous media by the concept of the global pressure. *Computational Geosciences*, 18:297–309, 2014.

[34] B. Amaziane, M. El Ossmani, and M. Jurak. Numerical simulation of gas migration through engineered and geological barriers for a deep repository for radioactive waste. *Computing and Visualization in Science*, 15:3–20, 2013.

[35] P.R. Amestoy, I.S. Duff, and J.Y. L'Excellent. Multifrontal parallel distributed symmetric and unsymmetric solvers. *Computer Methods in Applied Mechanics and Engineering*, 184:501–520, 2000.

[36] D. Ameur and G. Galliéro. Slippage of binary fluid mixtures in a nanopore. *Microfluidics and Nanofluidics*, 15:183–189, 2013.

[37] L. Amir and m. Kern. A global method for coupling transport with chemistry in heterogeneous porous media. *Computational Geosciences*, 14:465–481, 2010.

[38] R.T. Amos and K.U. Mayer. Investigating the role of gas bubble formation and entrapment in contaminated aquifers: Reactive transport modelling. *Journal of Contaminant Hydrology*, 87:123–154, 2006.

[39] O. Angelini. *Etude de schémas numériques pour les écoulements diphasiques en milieu poreux déformable pour des maillages quelconques, Application au stockage de déchets radioactifs*. PhD Thesis, Université de Marne la Vallée, 2010.

[40] O. Angelini, C. Chavant, E. Chénier, R. Eymard, and S. Granet. Finite volume approximation of a diffusion-dissolution model and application to nuclear waste storage. *Mathematics and Computers in Simulation*, 81:2001–2017, 2011.

[41] S.N. Antontsev, A.V. Kazhikhov, and V.N. Monakhov. *Boundary Value Problems in Mechanics of Non homogeneous Fluids*. North Holland, Amsterdam, 1990.

[42] C.A.J. Appelo and D. Postma. *Geochemistry, Groundwater and Pollution, Second Edition*. Taylor & Francis, 2005.

[43] T. Arbogast, S. Bryant, C. Dawson, F. Saaf, C. Wang, and M. Wheeler. Computational methods for multiphase flow and reactive transport problems arising in subsurface contaminant remediation. *Journal of Computational and Applied Mathematics*, 74:19–32, 1996.

[44] D.N. Arnold and R.S. Falk. A uniformly accurate finite element method for the Reissner-Mindlin plate. *SIAM J. Numer. Anal.*, 26:1276–1290, 1989.

[45] K. J. Arrow, L. Hurwicz, and H. Uzawa. *Studies in linear and non-linear programming*. Stanford University Press, Stanford, 1958.

[46] A.L Atchley, R.M. Maxwell, and A.K. Navarre-Sitchler. Using streamlines to simulate stochastic reactive transport in heterogeneous aquifers: Kinetic metal release and transport in CO_2 impacted drinking water aquifers. *Advances in Water Resources*, 52:93–106, 2013.

[47] P. Audigane, I. Gaus, I. Czernichowski-Lauriol, K. Pruess, and T. Xu. Two-dimensional reactive transport modeling of CO_2 injection in a saline aquifer at the Sleipner site, North Sea. *American Journal of Science*, 307:974–1008, 2007.

[48] P. Audigane, I. Gaus, and F. Gherardi. *Modeling Reactive Transport in CO_2 Geological Storage: Applications at the Site Scale and Near-Well Effects*, page 61. In Xiao et al. [312], 2018.

[49] M. Azaïez, C. Bernardi, and M. Grundmann. Spectral methods applied to porous media equations. *East-West Journal of Numerical Mathematics*, 2:91–105, 1994.

[50] S. Balay, S. Abhyankar, M. Adams, J. Brown, P. Brune, K. Buschelman, V. Eijkhout, W. Gropp, D. Kaushik, M. Knepley, L. Curfman McInnes, K. Rupp, B. Smith, and H. Zhang. PETSc Users Manual, Revision 3.5. http://www.mcs.anl.gov/ abhyshr/downloads/petsc-manual.pdf, 2014.

[51] D.A. Barry, C.T. Miller, and P.J. Culligan-Hensley. Temporal discretisation errors in non-iterative split-operator approaches to solving chemical reaction/groundwater transport models. *Journal of Contaminant Hydrology*, 22:1–17, 1996.

[52] P. Bastian, M. Blatt, A. Dedner, C. Engwer, R. Klöfkorn, R. Kornhuber, M. Ohlberger, and O. Sander. A generic grid interface for parallel and adaptive scientific computing. II. Implementation and tests in DUNE. *Computing*, 82:121–138, 2008.

[53] P. Bastian, M. Blatt, A. Dedner, C. Engwer, R. Klöfkorn, M. Ohlberger, and O. Sander. A generic grid interface for parallel and adaptive scientific computing. i. abstract framework. *Computing*, 82:103–119, 2008.

[54] S.A. Bea, J. Carrera, C. Ayora, F. Batlle, and M.W. Saaltink. CHEPROO: A Fortran 90 object-oriented module to solve chemical processes in Earth Science models. *Computers and Geosciences*, 35:1098–1112, 2009.

[55] S.A. Bea, K.U. Mayer, and K.T.B. MacQuarrie. Modelling reactive transport in sedimentary rock environments - Phase II MIN3P-THCm code enhancements and illustrative simulations for a glaciation scenario. *Technical report: NWMO TR-2011-13*, 2011.

[56] S.A. Bea, U.K. Mayer, and K.T.B. Macquarrie. Reactive transport and thermo-hydro-mechanical coupling in deep sedimentary basins affected by glaciation cycles: Model development, verification, and illustrative example. *Geofluids*, 16:279–300, 2016.

[57] J. Bear. *Dynamics of Fluids in Porous Media*. Dover, New York, 1972.

[58] J. Bear and A.H.-D. Cheng. *Modeling Groundwater Flow and Contaminant Transport*. Springer, 2010.

[59] J.J. Beisman, R.M. Maxwell, A.K. Navarre-Sitchler, C.I. Steefel, and S. Molins. ParCrunchFlow: an efficient, parallel reactive transport simulation tool for physically and chemically heterogeneous saturated subsurface environments. *Computational Geosciences*, 19:403–422, 2015.

[60] M.J. Bergern and S.H. Bokhari. Partitioning strategy for nonuniform problems on multiprocessors. *IEEE Transactions on Computers*, 36:571–580, 1987.

[61] C. Bernardi and Y. Maday. *Spectral Methods in Handbook of Numerical Analysis*. P.G. Ciarlet and J.L. Lions, North-Holland, 1997.

[62] C. Bernardi, Y. Maday, and A.T. Patera. Domain decomposition by the mortar element method. in asymptotic and numerical methods for partial differential equations with critical parameters. Kaper HG, Garbey M (eds). NATO ASI Series C, 384, Kluwer Academic Publishers: Dordrecht,, 1993.

[63] U. Berner, D. A. Kulik, and G. Kosakowski. Geochemical impact of a low-ph cement liner on the near field of a repository for spent fuel and high-level radioactive waste. *Physics and Chemistry of the Earth*, 64:46–56, 2013.

[64] H. Bhatia, G. Norgard, V. Pascucci, and P. Bremer. The Helmholtz-Hodge Decomposition-A Survey. *IEEE Transactions on Visualization and Computer Graphics*, 19:1386–1404, 2013.

[65] A. Bielinski. *Numerical simulation of CO_2 sequestration in geological formations*. PhD Thesis, University of Stuttgart, 2006.

[66] O. Botella. On the solution of the Navier-Stokes equations using Chebyshev projection schemes with third-order accuracy in time. *Computers and Fluids*, 26:107–116, 1997.

[67] A. Bourgeat. Numerical test data base (benchmark on multiphase flow in porous media). http://math.univ-lyon1.fr/ bourgeat/MoMaS/cas_test.html, 2010.

[68] A. Bourgeat, S. Granet, and F Smaï. Compositional two-phase flow in saturated-unsaturated porous media: benchmarks for phase appearance/disappearance. *Radon Series on Computational and Applied Mathematics: Simulation of Flow in Porous Media.*, pages 81–106, 2013.

[69] A. Bourgeat, M. Jurak, and F. Smai. Two-phase, partially miscible flow and transport modeling in porous media; application to gas migration in a nuclear waste repository. *Computational Geosciences*, 13:29–42, 2009.

[70] A. Bourgeat, M. Jurak, and F. Smai. On persistent primary variables for numerical modeling of gas migration in a nuclear waste repository. *Computational Geosciences*, 17:287–305, 2013.

[71] F. Brezzi and M. Fortin. Numerical approximations of Mindlin-Reissner plates. *Math. Comp.*, 47:151–158, 1986.

[72] P.N. Brown, R.D. Falgout, and J.E. Jones. Semicoarsening multigrid on distributed memory machines. *SIAM Journal of Scientific Computing*, 21:1823–1834, 2000.

[73] C.H. Bruneau and M. Saad. The 2D lid-driven cavity problem revisited. *Computer and Fluids*, 35:326–348, 2006.

[74] F. Brunner. *Multiphase multicomponent flow in porous media with general reactions: efficient problem formulations, conservative discretizations, and convergence analysis*. PhD Thesis, University of Erlangen-Nürnberg, 2015.

[75] F. Brunner and P. Knabner. A global implicit solver for miscible reactive multiphase multicomponent flow in porous media. *Computational Geosciences*, 23:127–148, 2019.

[76] X.C. Cai, M. Dryja, and M. Sarkis. Overlapping nonmatching grid mortar element methods for elliptic problems. *SIAM Journal on Numerical Analysis*, 36:581–606, 1999.

[77] J.P. Caltagirone and J. Breil. Sur une méthode de projection vectorielle pour la résolution des équations de Navier-Stokes. *C.R. Acad. Sci. Paris*, 327:1179–1184, 1999.

[78] C. Canuto, Y. Hussaini, A. Quarteroni, and T.A. Zang. *Spectral Methods in Fluid Dynamics*. Springer Series in Computational Physics. Springer, Berlin, 1998.

[79] H. Cao. *Development of techniques for general purpose simulators*. PhD Thesis, Stanford University, 2002.

[80] J. Carrayrou. Looking for some reference solutions for the reactive transport benchmark of MoMaS with SPECY. *Computational Geosciences*, 14:393–403, 2010.

[81] J. Carrayrou, J. Hoffmann, P. Knabner, S. Kräutle, C. de Dieuleveult, J. Erhel, J. Van der Lee, V. Lagneau, K.U. Mayer, and K.T.B MacQuarrie. Comparison of numerical methods for simulating strongly nonlinear and heterogeneous reactive transport problems-the MoMaS benchmark case. *Computational Geosciences*, 14:483–502, 2010.

[82] J. Carrayrou, M. Kern, and P. Knabner. Reactive transport benchmark of MoMaS. *Computational Geosciences*, 14:385–392, 2010.

[83] F. Centler, H. Shao, C. De Biase, C.H. Park, P. Regnier, O. Kolditz, and M. Thullner. GeoSysBRNS-a flexible multidimensional reactive transport model for simulating biogeochemical subsurface processes. *Computers and Geosciences*, 36:397–405, 2010.

[84] H.-S. Chang, W. Um, K. Rod., R.J. Serne, A. Thompson, N.Perdrial, C.I Steefel, and J. Chorover. Strontium and cesium release mechanisms during unsaturated flow through waste-weathered hanford sediments. *Environmental Science and Technology*, 45, 2011.

[85] G. Chavent and J. Jaffré. *Mathematical Models and Finite Elements for Reservoir Simulation*. Studies in Mathematics and its Applications. North Holland, 1986.

[86] Z. Chen. *Reservoir Simulation Mathematical Techniques in Oil Recovery*. SIAM, 2007.

[87] Z. Chen and R.E. Ewing. From single-phase to compositional flow: applicability of mixed finite elements. *Transport in Porous Media*, 27:225–242, 1997.

[88] Z. Chen, G. Huan, and Y. Ma. *Computational Methods for Multiphase Flows in Porous Media*. Computational Science and Engineering. SIAM, 2006.

[89] A. Chorin. Numerical solution of the navier-stokes equations. *Mathematics of Computation*, 22:745–762, 1968.

[90] F. Claret, N. Marty, and C. Tournassat. *Modeling the Long-term Stability of Multi-barrier Systems for Nuclear Waste Disposal in Geological Clay Formations*, pages 395–451. In Xiao et al. [312], 2018.

[91] H. Class, A. Ebigbo, R. Helmig, H.K. Dahle, J.M. Nordbotten, M.A. Celia, P. Audigane, M. Darcis, J. Ennis-King, Y. Fan, B. Flemisch, S.E. Gasda, M. Jin, S. Krug, D. Labregere, A. Naderi Beni, R.J. Pawar, A. Sbai, S.G. Thomas, L. Trenty, and L. Wei. A benchmark study on problems related to CO_2 storage in geologic formations : Summary and discussion of the results. *Computational Geosciences*, 13:409–434, 2009.

[92] H. Class and R. Helmig. Numerical simulation of non-isothermal multiphase multicomponent processes in porous media. 2. applications for the injection of steam and air. *Advances in Water Resources*, 25:551–564, 2002.

[93] H. Class, R. Helmig, and P. Bastian. Numerical simulation of non-isothermal multiphase multicomponent processes in porous media. 1. An efficient solution technique. *Advances in Water Resources*, 25:533–550, 2002.

[94] T.P. Clement. RT3D-A modular computer code for simulating reactive multi-species transport in 3-dimensional groundwater aquifers. PNNL-11720, Pacific Northwest National Laboratory, Richland, Washington, 1997.

[95] T.P. Clement and C.D. Johnson. *RT3D: Reactive Transport in 3-Dimensions*, pages 96–111. In Zhang et al. [332], 2012.

[96] K. H. Coats. An equation of state compositional model. *Transport in Porous Media*, 20:363–376, 1980.

[97] B. Cochepin, L. Trotignon, O. Bildstein, C.I. Steefel, V. Lagneau, and J. Van der lee. Approaches to modelling coupled flow and reaction in a 2d cementation experiment. *Advances in Water Resources*, 31:1540–1551, 2008.

[98] D.A. Collins, L.X. Nghiem, Y.K. Li, and J.E. Grabenstetter. Efficient approach to adaptive-implicit compositional simulation with an equation of state. *SPE Reservoir Engineering (Society of Petroleum Engineers)*, 7:259–264, 1992.

[99] A.K. De and A. Dalal. Numerical simulation of unconfined flow past a triangular cylinder. *International Journal for Numerical Methods in Fluids*, 52:801–821, 2006.

[100] C. de Dieuleveult and J. Erhel. A global approach to reactive transport: Application to the MoMas benchmark. *Computational Geosciences*, 14:451–464, 2010.

[101] J. de Vicente, D. Rodríguez, V. Theofilis, and E. Valero. Stability analysis in spanwise-periodic double-sided lid-driven cavity flows with complex cross-sectional profiles. *Computers and Fluids*, 43:143–153, 2011.

[102] M. Debure, L. De Windt, P. Frugier, and S. Gin. HLW glass dissolution in the presence of magnesium carbonate: Diffusion cell experiment and coupled modeling of diffusion and geochemical interactions. *Journal of Nuclear Materials*, 443:507–521, 2013.

[103] M. O. Deville, P.F. Fischer, and E.H. Mund. *High-Order Methods for Incompressible Fluid Flow*. Cambridge University Press, Cambridge, 2002.

[104] J.J. Dijkstra, J.C.L. Meeussen, and R.N.J. Comans. Leaching of heavy metals from contaminated soils: An experimental and modeling study. *Environmental Science and Technology*, 38:4390–4395, 2004.

[105] J. Dongarra, I Foster, G. Fox, W. Gropp, K. Kennedy, L. Torczon, and A. White. *Sourcebook of parallel computing*. Morgan Kaufmann Publishers Inc, 2003.

[106] U. Ehrenstein and R. Peyret. A Chebyshev collocation method for the Navier-Stokes equations with application to double-diffusive convection. *International Journal for Numerical Methods in Fluids*, 9:427–452, 1989.

[107] B. Engquist. Absorbing boundary conditions for numerical simulation of waves. *Proceedings of the National Academy of Sciences*, 74:1765–1766, 1977.

[108] J. Erhel and S. Sabit. Analysis of a global reactive transport model and results for the MoMaS benchmark. *Mathematics and Computers in Simulation*, 137:286–298, 2017.

[109] R.E. Ewing. *The Mathematics of Reservoir Simulation*. Frontiers in Applied Mathematics. SIAM, 1983.

[110] R.D. Falgout. HYPRE high performance preconditioners user's manual. Center for Applied Scientific Computing, Lawrence Livermore National Laboratory, 2008.

[111] R.D. Falgout, J.E. Jones, and U.M. Yang. Conceptual Interfaces in HYPRE. *Future Generation Computer Systems, Special Issue on PDE software*, 22:239–251, 2006.

[112] Y. Fan, L.J. Durlofsky, and H.A. Tchelepi. Numerical simulation of the in-situ upgrading of oil shale. *SPE Journal*, 15:368–381, 2010.

[113] Y. Fan, L.J. Durlofsky, and H.A. Tchelepi. A fully-coupled flow-reactive-transport formulation based on element conservation, with application to CO_2 storage simulations. *Advances in Water Resources*, 42:47–61, 2012.

[114] J.G. Farmer, M.C. Graham, R.P. Thomas, C. Licona-Manzur, E. Paterson, C.D. Campbell, J.S. Geelhoed, D.G .Lumsdon, J.C.L Meeussen, M.J. Roe, A. Conner, AE. Fallick, and R.J.F. Bewley. Assessment and modelling of the environmental chemistry and potential for remediative treatment of chromium-contaminated land. *Environmental Geochemistry and Health*, 21:331–337, 1999.

[115] S.F. Farshidi, Y. Fan, L.J. Durlofsky, and H.A. Tchelepi. Chemical reaction modeling in a compositional reservoir-simulation framework. *Society of Petroleum Engineers - SPE Reservoir Simulation Symposium 2013*, 2:1417–1438, 2013.

[116] A. Fenghour, W. A. Wakeham, and V. Vesovic. The viscosity of carbon dioxide. *Journal of Physical and Chemical Reference Data*, 27:31–44, 1998.

[117] T. Fetzer, B. Becker, B. Flemisch, D. Gläser, K. Heck, T. Koch, M. Schneider, S. Scholz, and K. Weishaupt. Dumux 2.12.0. doi:10.5281/zenodo.1115500, 2017.

[118] B. Flemisch. Tackling coupled problems in porous media: Development of numerical models and an open source simulator. Habilitation Thesis, University of Stuttgart, Germany, 2013.

[119] B. Flemisch, M. Darcis, K. Erbertseder, B. Faigle, A. Lauser, K. Mosthaf, S. Muthing S., P. Nuske, A. Tatomir, M. Wolf, and R. Helmig. DuMu^X: DUNE for multi-{Phase, Component, Scale, Physics, ...} flow and transport in porous media. *Advances in Water Resources*, 34(9):1102–1112, 2011.

[120] P. A. Forsyth and R.B. Simpson. A two-phase two-component model for natural convection in a porous medium. *Transport in Porous Media*, 12:655–682, 1991.

[121] M. Fortin and R. Glowinski. *éthodes de Lagrangien Augmenté, Application à la résolution numérique de problèmes aux limites*. Collection Méthodes Mathématiques de l'Informatique, Dunod, 1982.

[122] P. Gamazo, S.A. Bea., M.W. Saaltink, J. Carrera, and C. Ayora. Modeling the interaction between evaporation and chemical composition in a natural saline system. *Journal of Hydrology*, 401:154–164, 2011.

[123] P. Gamazo, L.J. Slooten, J. Carrera, M.W. Saaltink, S. Bea, and J. Soler. PROOST: Object-oriented approach to multiphase reactive transport modeling in porous media. *Journal of Hydroinformatics*, 18:310–328, 2016.

[124] C. Gear. *Numerical Initial Value Problems in Ordinary Differential Equation*. Prentice-Hall, 1971.

[125] I. Ben Gharbia, E. Flauraud, and A. Michel. Study of compositional multi-phase flow formulations with cubic EOS. *Society of Petroleum Engineers*, 2015.

[126] I. Ben Gharbia and J. Jaffré. Gas phase appearance and disappearance as a problem with complementarity constraints. *Mathematics and Computers in Simulation*, 99:28–36, 2014.

[127] V. Girault and P. Raviart. *Finite Element Methods for Navier-Stokes Equations*. Series in Computational Mathematics. Springer-Verlag, Berlin, 1986.

[128] W.E. Glassley, J.J. Nitao, and C.W. Grant. Three-dimensional spatial variability of chemical properties around a monitored waste emplacement tunnel. *Journal of Contaminant Hydrology*, 62-63:495–507, 2003.

[129] W.E. Glassley, J.J. Nitao, C.W. Grant, J.W. Johnson, C.I. Steefel, and J.R. Kercher. The impact of climate change on vadose zone pore waters and its implication for long-term monitoring. *Computers and Geosciences*, 29:399–411, 2003.

[130] K. Goda. A multistep technique with implicit difference schemes for calculating two- or three-dimensional cavity flows. *Journal of Computational Physics*, 30:76–95, 1979.

[131] N. Gourdain, L. Gicquel, M. Montagnac, O. Vermorel O., M. Gazaix, G. Staffelbach, M. Garcia, J.F. Boussuge, and T. Poinsot. High performance parallel computing of flows in complex geometries: I. methods. *Computational Science and Discovery*, 2:015003, 2009.

[132] R. Gruber and J. Rappaz. *Finite Element Methods in Linear Ideal MHD*. Springer Series in Computational Physics, Springer-Verlag, Berlin, 1985.

[133] J. L. Guermond, P. Minev, and J. Shen. Error analysis of pressure-correction schemes for the time-dependent stokes equations with open boundary conditions. *SIAM Journal on Numerical Analysis*, 43:239–258, 2005.

[134] J. L. Guermond, P. Minev, and J. Shen. An overview of projection methods for incompressible flows. *Computer Methods in Applied Mechanics and Engineering*, 195:6001–6045, 2006.

[135] J. L. Guermond and J. Shen. Velocity-correction projection methods for incompressible flows. *SIAM Journal on Numerical Analysis*, 41:112–134, 2004.

[136] J.L. Guermond. Calculation of incompressible viscous flows by an unconditionally stable projection fem. *Journal of Computational Physics*, 132:12–33, 1997.

[137] F. Haeberlein. *Time Space Domain Decomposition Methods for Reactive Transport – Application to CO_2 Geological Storage*. PhD Thesis, Université Paris-Nord - Paris XIII, 2011.

[138] F. Haeberlein, A. Michel, and L. Halpern. A test case for multi-species reactive-transport in heterogeneous porous media applied to CO_2 geological storage. https://www.ljll.math.upmc.fr/mcparis09/Files/haeberlein_poster.pdf, 2009.

[139] G.E Hammond and P.C. Lichtner. Field-scale model for the natural attenuation of uranium at the hanford 300 area using high-performance computing. *Water Resources Research*, 46:1–31, 2010.

[140] G.E. Hammond, P.C. Lichtner, C. Lu, and R.T. Mills. *PFLOTRAN: Reactive Flow & Transport Code for Use on Laptops to Leadership-Class Supercomputers*, pages 141–59. In Zhang et al. [332], 2012.

[141] G.E. Hammond, P.C. Lichtner, and R.T. Mills. Evaluating the performance of parallel subsurface simulators: An illustrative example with PFLOTRAN. *Water Resources Research*, 150:208–228, 2014.

[142] Y. Hao, Y. Sun, and J.J. Nitao. *Overview of NUFT: A Versatile Numerical Model for Simulating Flow and Reactive Transport in Porous Media*, pages 212–239. In Zhang et al. [332], 2012.

[143] A.W. Harbaugh. MODFLOW-2005: the U.S. geological survey modular ground-water model the ground-water flow process. Techniques and Methods 6-A16, U.S. Geological Survey, Reston, Virginia, 2005.

[144] F.H. Harlow and J.E. Welch. Numerical calculation of time-dependent viscous incompressible flow of fluid with free surface. *Physics of Fluids*, 8:2182–2189, 1965.

[145] S.K. Harouna and V. Perrier. Helmholtz Hodge decomposition on $[0,1]^d$ by divergence-free and curl-free wavelets. *Lecture Notes in Computer Science*, 6920:311–329, 2012.

[146] R. Helmig. *Multiphase flow and transport processes in the subsurface: a contribution to the modeling of hydrosystems*. Springer, 1997.

[147] B. Hendrickson and R. Leland. The Chaco user's guide, version 2.0. Technical Report. Sandia National Laboratories, Albuquerque, NM, July, 1995.

[148] W.D. Henshaw and T.J. Watson. A fourth-order accurate method for the incompressible navier stokes equations on overlapping grids. *Journal of Computational Physics*, 113:13–25, 1994.

[149] J. Hoffmann, S. Kräutle, and P. Knabner. A parallel global-implicit 2-D solver for reactive transport problems in porous media based on a reduction scheme and its application to the MoMaS benchmark problem. *Computational Geosciences*, 14:421–433, 2010.

[150] J. Hoffmann, S. Kräutle, and P. Knabner. A general reduction scheme for reactive transport in porous media. *Computational Geosciences*, 16:1081–1099, 2012.

[151] J. Hommel, A.B. Cunningham, R. Helmig, A. Ebigbo, and H. Class. Numerical investigation of microbially induced calcite precipitation as a leakage mitigation technology. volume 40, pages 392–397, 2013.

[152] J. Hommel, E. Lauchnor, R. Gerlach, A.B. Cunningham, A. Ebigbo, R. Helmig, and H. Class. Investigating the influence of the initial biomass distribution and injection strategies on biofilm-mediated calcite precipitation in porous media. *Transport in Porous Media*, 114(2):557–579, 2016.

[153] J. Hommel, E. Lauchnor, A. Phillips, R. Gerlach, A.B. Cunningham, R. Helmig, A. Ebigbo, and H. Class. A revised model for microbially induced calcite precipitation: Improvements and new insights based on recent experiments. *Water Resources Research*, 51(5):3695–3715, 2015.

[154] B.M. Huet, J.H. Prevost, and G.W. Scherer. Quantitative reactive transport modeling of portland cement in CO_2-saturated water. *International Journal of Greenhouse Gas Control*, 4:561–574, 2010.

[155] O. Ippisch. *Coupled transport in natural porous media*. PhD Thesis, University of Heidelberg, 2003.

[156] C.P. Jackson. A finite-element study of the onset of vortex shedding in flow past variously shaped bodies. *Journal of Fluid Mechanics*, 182:23–45, 1987.

[157] N. Jacquemet, J. Pironon, V. Lagneau, and J. Saint-Marc. Armouring of well cement in H_2S-CO_2 saturated brine by calcite coating - experiments and numerical modelling. *Applied Geochemistry*, 27:782–795, 2012.

[158] J. Jaffré and A. Sboui. Henry's law and gas phase disappearance. *Trans. Porous Media*, 82:521–526, 2010.

[159] V.A. Jambhekar, E. Mejri, N. Schröder, R. Helmig, and M. Shokri. Kinetic approach to model reactive transport and mixed salt precipitation in a g-flow-porous-media system. *Transport in Porous Media*, 114:341–369, 2016.

[160] N. Janot, J.P. Pinheiro, W.G. Botero, J.C.L. Meeussen, and J.E. Groenenberg. PEST-ORCHESTRA, a tool for optimising advanced ion-binding model parameters: Derivation of NICA-Donnan model parameters for humic substances reactivity. *Environmental Chemistry*, 14:31–38, 2017.

[161] X. Jiang. A review of physical modelling and numerical simulation of long-term geological storage of CO_2. *Applied energy*, 88:3557–3566, 2011.

[162] Y. Jiang. *Techniques for modeling complex reservoirs and advanced wells*. PhD Thesis, Stanford University, 2007.

[163] J.W. Johnson, J.J. Nitao, and K.G. Knauss. Reactive transport modelling of CO_2 storage in saline aquifers to elucidate fundamental processes, trapping mechanisms and sequestration partitioning. *Geological Society Special Publication*, 233:107–128, 2004.

[164] K. Kala, D. Voskov, and M. Huzefa Ammiwala. Parameterization of element balance formulation in reactive compositional flow and transport. *Society of Petroleum Engineers*, pages doi:10.2118/193898–MS, 2019.

[165] T. Kalbacher, J.O. Delfs, H. Shao, W. Wang, M. Walther, L. Samaniego, C. Schneider, R. Kumar, A. Musolff, F. Centler, F. Sun, A. Hildebrandt, R. Liedl, D. Borchardt, P. Krebs, and O. Kolditz. The IWAS-ToolBox: Software coupling for an integrated water resources management. *Environmental Earth Sciences*, 65:1367–1380, 2012.

[166] G. E. Karniadakis, M. Israeli, and S. A. Orszag. High-order splitting methods for the incompressible navier-stokes equation. *Journal of Computational Physics*, 97:414–443, 1991.

[167] G. Karypis and V. Kumar. METIS: unstructured graph partitioning and sparse matrix ordering system. Technical Report, University of Minnesota, Computer Science Department, Minneapolis, 1995.

[168] D.B. Kent, J.A. Davis, L.C.D. Anderson, B.A. Rea., and T.D. Waite. Transport of chromium and selenium in the suboxic zone of a shallow aquifer: Influence of redox and adsorption reactions. *Water Resources Research*, 30, 1994.

[169] P.J.A.M. Kerkhof and M.A.M. Geboers. Analysis and extension of the theory of multicomponent fluid diffusion. *Chemical Engineering Science*, 60:3129–3167, 2005.

[170] C. Kervévan, M.-H. Beddelem, and K. OeNeil. CO2-DISSOLVED: a Novel Concept Coupling Geological Storage of Dissolved CO_2 and Geothermal Heat Recovery - Part 1: Assessment of the Integration of an Innovative Low-cost, Water- based CO_2 Capture Technology. *Energy Procedia*, 63:4508–4518, 2014.

[171] M. Khait and D. Voskov. Operator-based linearization for efficient modeling of geothermal processes. *Geothermics*, 74:7 – 18, 2018.

[172] K.L. Kipp. *Guide to the Revised Heat and Solute Transport Simulator HST3D - Version 2*. Water-Resources Investigations Report 97-4157. U.S. Geological Survey, 1997.

[173] O. Kolditz, S. Bauer, L. Bilke, N. Böttcher, J.O. Delfs, T. Fischer, U.J. Görke, T. Kalbacher, G. Kosakowski, C.I. McDermott, C.H. Park, F. Radu, K. Rink, H. Shao, H.B. Shao, F. Sun, Y.Y. Sun, A.K. Singh, J. Taron, M. Walther, W. Wang, N. Watanabe, Y. Wu, M. Xie, W. Xu, and B. Zehner. OpenGeoSys: An open-source initiative for numerical simulation of thermo-hydro-mechanical/chemical (THM/C) processes in porous media. *Environmental Earth Sciences*, 67:589–599, 2012.

[174] O. Kolditz, U.J. Görke, H. Shao, and W. Wang. Thermo-hydro-mechanical-chemical processes in fractured porous media. *Lecture Notes in Computational Science and Engineering*, 86:1–404, 2012.

[175] S. Kräutle and P. Knabner. A new numerical reduction scheme for fully coupled multicomponent transport-reaction problems in porous media. *Water Resources Research*, 41:1–17, 2005.

[176] S. Kräutle and P. Knabner. A reduction scheme for coupled multicomponent transport-reaction problems in porous media: Generalization to problems with heterogeneous equilibrium reactions. *Water Resources Research*, 43, 2007.

[177] D.A. Kulik, S.V. Dmytrieva, K.V. Chudnenko, T. Thoenen, and Th. Wagner. GEM-Selektor (GEMS-PSI) - research package for thermodynamic modeling of aquatic (geo)chemical systems by gibbs energy minimization. http://gems.web.psi.ch/, 2008.

[178] V. Lagneau, A. Pipart, and H. Catalette. Reactive transport modelling of CO_2 sequestration in deep saline aquifers. *Oil & Gas Science and Technology*, 60:231–247, 2005.

[179] V. Lagneau and J. van der Lee. HYTEC results of the MoMaS reactive transport benchmark. *Computational Geosciences*, 14:435–449, 2010.

[180] A. Lapene, L.M. Castanier, G. Debenest, M. Quintard, A.M. Kamp, and B. Corre. Effects of steam on heavy oil combustion. *SPE Reservoir Evaluation and Engineering*, 12(4):508–517, 2009.

[181] A. C. Lasaga, J. M. Soler, J. Ganor, T. E. Burch, and K. L. Nagy. Chemical weathering rate laws and global geochemical cycles. *Geochimica et Cosmochimica Acta*, 58:2361–2386, 1994.

[182] A. Lauser, C. Hager, R. Helmig, and B. Wohlmuth. A new approach for phase transitions in miscible multi-phase flow in porous media. *Advances in Water Resources*, 34:957–966, 2011.

[183] A.M.M Leal, M.J. Blunt, and T.C. LaForce. A robust and efficient numerical method for multiphase equilibrium calculations: Application to CO_2-brine-rock systems at high temperatures, pressures and salinities. *Advances in Water Resources*, 62:409–430, 2013.

[184] A. Lemoine, J.P. Caltagirone, M. Azaïez, and S. Vincent. Discrete Helmholtz-Hodge Decomposition on Polyhedral Meshes Using Compatible Discrete Operators. *Journal of Scientific Computing*, 65:34–53, 2015.

[185] E. Leriche and G. Labrosse. High-order direct Stokes solvers with or without temporal splitting: numerical investigations of their comparative properties. *SIAM Journal on Scientific Computing*, 22:1386–1410, 2000.

[186] E. Leriche and G. Labrosse. Stokes eigenmodes in a square domain and the stream function-velocity correlation. *Journal of Computational Physics*, 200:489–511, 2004.

[187] P.C. Lichtner. Continuum model for simultaneous chemical reactions and mass transport in hydrothermal systems. *Geochimica et Cosmochimica Acta*, 49:779–800, 1985.

[188] P.C. Lichtner, G.E. Hammond, C. Lu, S. Karra, G. Bisht, B. Andre, R.T. Mills, and J. Kumar. PFLOTRAN User manual: A Massively Parallel Reactive Flow and Transport Model for Describing Surface and Subsurface Processes. http://www.pflotran.org/docs/user_manual.pdf, 2015.

[189] P.C. Lichtner and S. Karra. Modeling multiscale-multiphase-multicomponent reactive flows in porous media: Application toCO_2 sequestration and enhanced geothermal energy using PFLOTRAN. *Al-Khoury, R., Bundschuh, J. (eds.) Computational Models for CO_2 Geo-sequestration & Compressed Air Energy Storage, CRC Press*, pages 81–136, 2014.

[190] P.C. Lichtner, S. Yabusaki, K. Pruess, and C.I. Steefel. Role of competitive cation exchange on chromatographic displacement of cesium in the vadose zone beneath the hanford s/sx tank farm. *Vadose Zone Journal*, 3:203–219, 2004.

[191] Z. Lilek, S. Muzaferija, M. Peric, and V. Seidl. An implicit finite-volume method using nonmatching blocks of structured grid. *Numerical Heat Transfer*, 32:385–401, 1997.

[192] P.L. Lions. On the Schwarz alternating method III: a variant for nonoverlapping subdomains. Third International Symposium on Domain Decomposition Methods for Partial Differential Equations, Philadelphia, 1990.

[193] J. Liu. Open and traction boundary conditions for the incompressible Navier-Stokes equations. *Journal of Computational Physics*, 228:7250–7267, 2009.

[194] P. Liu, T. Zhang, and S. Sun. A tutorial review of reactive transport modeling and risk assessment for geologic CO_2 sequestration. *Computers and Geosciences*, 127:1–11, 2019.

[195] J. W. Lund and T. L. Boyd. Direct utilization of geothermal energy 2015 worldwide review. *Geothermics*, 60:66–93, 2016.

[196] H. Machat and J. Carrayrou. Comparison of linear solvers for equilibrium geochemistry computations. *Computational Geosciences*, 21:131–150, 2017.

[197] A. Mandal. Chemical flood enhanced oil recovery: A review. *International Journal of Oil, Gas and Coal Technology*, 9:241–264, 2015.

[198] E. Marchand and P. Knabner. Results of the MoMaS benchmark for gas phase appearance and disappearance using generalized MHFE. *Advances in Water Resources*, 73:74–96, 2014.

[199] E. Marchand, T. Muller, and P. Knabner. Fully coupled generalised hybrid-mixed finite element approximation of two-phase two-component flow in porous media. part ii: numerical scheme and numerical results. *Computational Geosciences*, 16:691–708, 2012.

[200] E. Marchand, T. Muller, and P. Knabner. Fully coupled generalized hybrid-mixed finite element approximation of two-phase two-component flow in porous media. part i: formulation and properties of the mathematical model. *Computational Geosciences*, 17:431–442, 2013.

[201] R. Masson, L. Trenty, and Y. Zhang. Formulations of two phase liquid gas compositional Darcy flows with phase transitions. *International Journal on Finite Volumes*, 11:34, 2014.

[202] K.U. Mayer, R.T. Amos, S. Molins, and F. Gérard. *Reactive Transport Modeling in Variably Saturated Media with MIN3P: Basic Model Formulation and Model Enhancements*, pages 186–211. In Zhang et al. [332], 2012.

[203] K.U. Mayer, D.W. Blowes, and E.O. Frind. Reactive transport modeling of an in situ reactive barrier for the treatment of hexavalent chromium and trichloroethylene in groundwater. *Water Resources Research*, 37:3091–3103, 2001.

[204] K.U. Mayer, E.O. Frind, and D.W. Blowes. Multicomponent reactive transport modeling in variably saturated porous media using a generalized formulation for kinetically controlled reactions. *Water Resources Research*, 38:131–1321, 2002.

[205] K.U. Mayer, E.O. Frind, and D.W. Blowes. Multicomponent reactive transport modeling in variably saturated porous media using a generalized formulation for kinetically controlled reactions. *Water Resources Research*, 38:131–1321, 2002.

[206] K.U. Mayer and K.T.B. MacQuarrie. Solution of the MoMaS reactive transport benchmark with MIN3P-model formulation and simulation results. *Computational Geosciences*, 14:405–419, 2010.

[207] J.E. McCray and R.W. Falta. Numerical simulation of air sparging for remediation of napl contamination. *Ground Water*, 35:99–110, 1997.

[208] J.C.L. Meeussen. Orchestra: An object-oriented framework for implementing chemical equilibrium models. *Environmental Science and Technology*, 37:1175–1182, 2003.

[209] E. Mejri, R. Bouhlila, and R. Helmig. Heterogeneity effects on evaporation-induced halite and gypsum co-precipitation in porous media. *Transport in Porous Media*, pages 1–26, 2017.

[210] A. Mikelić and M.F. Wheeler. Convergence of iterative coupling for coupled flow and geomechanics. *Computational Geosciences*, 17:455–461, 2013.

[211] H.K. Moffatt. Viscous and resistive eddies near a sharp corner. *Journal of Fluid Mechanics*, 18:1–18, 1964.

[212] S. Molins, J. Carrera, C. Ayora, and M. W. Saaltink. A formulation for decoupling components in reactive transport problems. *Water Resources Research*, 40:1–13, 2004.

[213] S. Molins and K.U. Mayer. Coupling between geochemical reactions and multicomponent gas and solute transport in unsaturated media: A reactive transport modeling study. *Water Resources Research*, 43, 2007.

[214] A. Mon, J. Samper, L. Montenegro, A. Naves, and J. Fernández. Long-term non-isothermal reactive transport model of compacted bentonite, concrete and corrosion products in a HLW repository in clay. *Journal of Contaminant Hydrology*, 197:1–16, 2017.

[215] M. Id Moulay. *3D numerical simulation of reactive multiphase flow in porous media*. PhD Thesis, University of Pau & Pays de l'Adour, Defense scheduled for December 2019.

[216] J. Moutte, A. Michel, G. Battaia, T. Parra, D. Garcia, and S. Wolf. ARXIM, a library for thermodynamic modelling of reactive heterogeneous systems, with applications to the simulation of fluid - rock systems. 21st IUPAC international conference on chemical thermodynamics, Tsukuba, Japan, 2010.

[217] A. Nardi, A. Idiart, P. Trinchero, L.M. De Vries, and J. Molinero. Interface COMSOL-PHREEQC (iCP), an efficient numerical framework for the solution of coupled multiphysics and geochemistry. *Computers and Geosciences*, 69:10–21, 2014.

[218] A.K. Navarre-Sitchler, R.M. Maxwell, E.R. Siirila, G.E. Hammond, and P.C. Lichtner. Elucidating geochemical response of shallow heterogeneous aquifers to CO_2 leakage using high-performance computing: Implications for monitoring of CO_2 sequestration. *Advances in Water Resources*, 53:45–55, 2013.

[219] J.C. Nédélec. Mixed finite elements in $\mathbb{R}^3$. *Numerishe Mathematik*, 35:315–341, 1980.

[220] R. Neumann, P. Bastian, and O. Ippisch. Modeling and simulation of two-phase two-component flow with disappearing nonwetting phase. *Computational Geosciences*, 17:139–149, 2013.

[221] L. Nghiem, P. Sammon, J. Grabenstetter, and H. Ohkuma. Modeling CO_2 storage in aquifers with a fully-coupled geochemical eos compositional simulator. *SPE - DOE Improved Oil Recovery Symposium Proceedings*, 2004.

[222] L. Nghiem, V. Shrivastava, and B. Kohse. Modeling aqueous phase behavior and chemical reactions in compositional simulation. *Society of Petroleum Engineers - SPE Reservoir Simulation Symposium 2011*, 1:454–468, 2011.

[223] B.N. Nguyen, Z. Hou., D.H. Bacon, C.J. Murray, and M.D. White. Three-dimensional modeling of the reactive transport of CO_2 and its impact on geomechanical properties of reservoir rocks and seals. *International Journal of Greenhouse Gas Control*, 46:100–115, 2016.

[224] B.N. Nguyen, Z. Hou, D.H. Bacon., and M.D. White. A multiscale hydro-geochemical-mechanical approach to analyze faulted CO_2 reservoirs. *Greenhouse Gases: Science and Technology*, 7:106–127, 2017.

[225] J.-P. Nicot, S. A. Hosseini, and S. V. Solano. Are single-phase flow numerical models sufficient to estimate pressure distribution in CO_2 sequestration projects? *Energy Procedia*, 4:3919–3926, 2011.

[226] A. Niemi, J. Bear, and J. Bensabat. *Geological Storage of CO_2 in Deep Saline Formations*. Springer, 2017.

[227] P. Nithiarasu and C.B. Liu. Steady and unsteady incompressible flow in a double driven cavity using the artificial compressibility (AC)-based characteristic-based split (CBS) scheme. *International Journal for Numerical Methods in Fluids*, 63:380–397, 2005.

[228] S. Norris. Summary of gas generation and migration current state-of-the-art. *European Commission FORGE Deliverable D1.2-R. 7th Framework Project: FORGE, http://www.bgs.ac.uk/forge/docs/reports/D1.2-R.pdfApplied Geochemistry*, 2010.

[229] S. Olivella, A. Gens, J. Carrera, and E.E. Alonso. Numerical formulation for a simulator (CODE_BRIGHT) for the coupled analysis of saline media. *Engineering Computations*, 13:87–112, 1996.

[230] I. Orlanski. A simple boundary condition for unbounded hyperbolic flows. *Journal of Computational Physics*, 21:251–269, 1976.

[231] S. A. Orszag, M. Israeli, and M. O. Deville. Boundary conditions for incompressible flows. *Journal of Scientific Computing*, 1:75–111, 1986.

[232] B. Palit, A. Basu, and M.K. Mandal. Applications of the discrete Hodge Helmholtz decomposition to image and video processing. *Lecture Notes in Computer Science*, 3776:497–505, 2005.

[233] S. N. Pandey, V. Vishal, and A. Chaudhuri. Geothermal reservoir modeling in a coupled thermo-hydro-mechanical-chemical approach: A review. *Earth-Science Reviews*, 185:1157–1169, 2018.

[234] M. Panfilov. *Physicochemical Fluid Dynamics in Porous Media: Applications in Geosciences and Petroleum Engineering*. Wiley, 2018.

[235] M. Panfilov and M. Rasoulzadeh. Interfaces of phase transition and disappearance and method of negative saturation for compositional flow with diffusion and capillarity in porous media. *Transport in Porous Media*, 83:73–98, 2010.

[236] D.L. Parkhurst and C.A.J. Appelo. User's guide to PHREEQC (version 2) - a computer program for speciation, batch-reaction, one-dimensional transport and inverse geochemical calculations, water-resources investigations, report 99-4259, denver, co. *USA*, page 312, 1999.

[237] D.L. Parkhurst and C.A.J. Appelo. Description of input and examples for PHREEQC version 3-a computer program for speciation, batch-reaction, one-dimensional transport, and inverse geochemical calculations. *U.S. Geological Survey Techniques and Methods, book 6, chap. A43, 497*, page 497, 2013. available only at https://pubs.usgs.gov/tm/06/a43/.

[238] D.L. Parkhurst, K.L. Kipp, and S.R. Charlton. *PHAST Version 2-a program for simulating groundwater flow, solute transport, and multicomponent geochemical reactions*. U.S. Geological Survey Techniques and Methods, 6-A35, 2010.

[239] F. Pellegrini. SCOTCH 3.1 user's guide. Technical Report 1137-96, LaBRI, University of Bordeaux, France, 1999.

[240] Y.F. Peng, Y.H. Shiau, and R.R. Hwang. Transition in a 2-D lid driven cavity flow. *Computer and Fluids*, 32:337–352, 2003.

[241] M. Peszynska and S. Sun. Multiphase reactive transport module (TRCHEM) in IPARS. Technical Report 01-32. *ICES, The University of Texas at Austin, Austin*, 2001.

[242] M. Peszynska and S. Sun. Reactive transport model coupled to multiphase flow models. *Computational Methods in Water Resources, S. M. Hassanizadeh, R.J. Schotting, W.G. Gray, and G.F. Pinder, Eds. Elsevier*, pages 923–930, 2002.

[243] F. Petronetto, A. Paiva, M. Lage, G. Tavares, H.Lopes, and T. Lewiner. Meshless Helmholtz Hodge decomposition. *IEEE Transaction on Visualization and Computer Graphics*, 16:338–342, 2010.

[244] G. Pinder and W. Gray. *Essentials of Multiphase Flow and Transport in Porous Media*. Wiley, 2009.

[245] M. Pool, J. Carrera, V. Vilarrasa, O. Silva, and C. Ayora. Dynamics and design of systems for geological storage of dissolved CO_2. *Advances in Water Resources*, 62:533–542, 2013.

[246] N. Pous, S. Puig, M. Coma, M.D. Balaguer, and J. Colprim. Bioremediation of nitrate-polluted groundwater in a microbial fuel cell. *Journal of Chemical Technology and Biotechnology*, 88:1690–1696, 2013.

[247] A. Poux, S. Glockner, E. Ahusborde, and M. Azaïez. Open and traction boundary conditions for velocity correction scheme for Navier-Stokes equations. *Computers and Fluids*, 70:29–43, 2012.

[248] A. Poux, S. Glockner, and M. Azaïez. Improvements on open and traction boundary conditions for navier-stokes time-splitting methods. *Journal of Computational Physics*, 230:4011–4027, 2011.

[249] H. Prommer and V.E.A Post. PHT3D, a reactive multicomponent transport model for saturated porous media. *User's Manual*, 2010.

[250] K. Pruess. The TOUGH codes-a family of simulation tools for multiphase flow and transport processes in permeable media. *Vadose Zone Journal*, 3:738–746, 2004.

[251] K. Pruess. Enhanced geothermal systems (egs) using CO_2 as working fluid-a novel approach for generating renewable energy with simultaneous sequestration of carbon. *Geothermics*, 35:351–367, 2006.

[252] K. Pruess, J. García, T. Kovscek, C. Oldenburg, J. Rutqvist, C. Steefel, and T. Xu. Code intercomparison builds confidence in numerical simulation models for geologic disposal of CO_2. *Energy*, 29:1431–1444, 2004.

[253] A. Quarteroni and A. Valli. *Domain Decomposition Methods for Partial Differential Equations*. Oxford University Press, Oxford, 1999.

[254] M. Quintard and S. Whitaker. Coupled, nonlinear mass transfer and heterogeneous reaction in porous media. *Handbook of Porous Media, Second Edition*, pages 3–37, 2005.

[255] A. Randi, J. Sterpenich, D. Thiéry, C. Kervévan, J. Pironona, and C. Morlot. Experimental and Numerical Simulation of the Injection of a CO_2 Saturated Solution in a Carbonate Reservoir: Application to the CO2-DISSOLVED Concept Combining CO_2 Geological Storage and Geothermal Heat Recovery. *Energy Procedia*, 114:2942–2956, 2017.

[256] J. Rantakokko. Partitioning strategies for structured multiblock grids. *Parallel Computing*, 12:1661–1680, 2000.

[257] P.A. Raviart and J.M. Thomas. A mixed finite element method for second order elliptic problems. *Mathematical Aspects of Finite Element Method. Lecture Notes in Mathematics*, 606:292–315, 1977.

[258] C. Romé and S. Glockner. An implicit multiblock coupling for the incompressible Navier-Stokes equations. *International Journal for Numerical Methods in Fluids*, 47:1261–1267, 2005.

[259] C. Romé, S. Glockner, and J.P. Caltagirone. Resolution of the Navier-Stokes equations on block-structured meshes. *International Journal for Numerical Methods in Fluids*, 54:1239–1268, 2007.

[260] M. Saaltink, V. Vilarrasa, F. De Gaspari, O. Silva, J. Carrera, and T.S. Rötting. A method for incorporating equilibrium chemical reactions into multiphase flow models for CO_2 storage. *Advances in Water Resources*, 62:431–441, 2013.

[261] M.W. Saaltink, F. Batlle, C. Ayora, J. Carrera, and S. Olivella. RETRASO, a code for modeling reactive transport in saturated and unsaturated porous media. *Geologica Acta*, 2:235–251, 2004.

[262] J. Samper, A. Mon, L. Montenegro, J. Cuevas, M.J. Turrero, A. Naves, R. Fernández, and E. Torres. Coupled THCM model of a heating and hydration concrete-bentonite column test. *Applied Geochemistry*, 94, 2018.

[263] J. Samper, T. Xu, and C. Yang. A sequential partly iterative approach for multicomponent reactive transport with CORE2D. *Computational Geosciences*, 13:301–316, 2009.

[264] J. Samper, C. Yang, L. Zheng, L. Montenegro, Y. Xu, Z. Dai, G. Zhang, C. Lu, and S. Moreira. *CORE^{2D} V4: A code for water flow, heat and solute transport, geochemical reactions, and microbial processes*, pages 160–185. In Zhang et al. [332], 2012.

[265] S. Schaffer. A semicoarsening multigrid method for elliptic partial differential equations with highly discontinuous and anisotropic coefficients. *SIAM Journal of Scientific Computing*, 20:228–242, 1998.

[266] M. Sedighi, H.R. Thomas, S. Al Masum, P.J. Vardon, D. Nicholson, and Q. Chen. Geochemical modelling of hydrogen gas migration in an unsaturated bentonite buffer. *Geological Society Special Publication*, 415:189–201, 2015.

[267] N. Seigneur, V. Lagneau, J. Corvisier, and A. Dauzères. Recoupling flow and chemistry in variably saturated reactive transport modelling - an algorithm to accurately couple the feedback of chemistry on water consumption, variable porosity and flow. *Advances in Water Resources*, 122:355–366, 2018.

[268] H. Shao, S.V Dmytrieva, O Kolditz, D.A. Kulik, W. Pfingsten, and G. Kosakowski. Modeling reactive transport in non-ideal aqueous-solid solution system. *Applied Geochemistry*, 24:1287–1300, 2009.

[269] J. Shen. On error estimates of the projection methods for the Navier-Stokes equations: Second-order schemes. *Mathematics of Computation*, 65:1039–1066, 1996.

[270] J.J. Sheng. Enhanced oil recovery in shale reservoirs by gas injection. *Journal of Natural Gas Science and Engineering*, 22:252–259, 2015.

[271] J. Simůnek and M.Th. Van Genuchten. Modeling nonequilibrium flow and transport processes using hydrus. *Vadose Zone Journal*, 7:782–797, 2008.

[272] J. Simůnek, M.Th. Van Genuchten, and M. Sejna. Recent developments and applications of the HYDRUS computer software packages. *Vadose Zone Journal*, 15:25 pages, 2016.

[273] J. Simůnek, D. Jacques, M. Sejna, and M.Th. Van Genuchten. The HP2 program for HYDRUS (2D/3D): A coupled code for simulating two-dimensional variably-saturated water flow, heat transport, and biogeochemistry in porous media, version 1.0, pc progress, prague. *Czech Republic*, page 76, 2012.

[274] I. Sin. *Numerical simulation of compressible two-phase flow and reactive transport in porous media - Applications to the study of CO_2 storage and natural gas reservoirs*. PhD Thesis, MINES ParisTech, 2015.

[275] I. Sin, V. Lagneau, and J. Corvisier. Integrating a compressible multicomponent two-phase flow into an existing reactive transport simulator. *Advances in Water Resources*, 100:1339–1351, 2017.

[276] I. Sin, V. Lagneau, L. De Windt, and J. Corvisier. 2D simulation of natural gas reservoir by two-phase multicomponent reactive flow and transport-description of a benchmarking exercise. *Mathematics and Computers in Simulation*, 137:431–447, 2017.

[277] R. Span and W. Wagner. A new equation of state for carbon dioxide covering the fluid region from the triple-point temperature to 1100 K at pressures up to 800 MPa. *Journal of Physical and Chemical Reference Data*, 25:1–88, 1996.

[278] N. Spycher and K. Pruess. CO_2-H_2O mixtures in the geological sequestration of CO_2 . ii. partitioning in chloride brines at 12-100 ^{o}c and up to 600 bar. *Geochim. et Cosmochim. Acta*, 69:3309–3320, 2005.

[279] N.F. Spycher, E.L Sonnenthal, and J.A. Apps. Fluid flow and reactive transport around potential nuclear waste emplacement tunnels at Yucca Mountain, Nevada. *Journal of Contaminant Hydrology*, 62-63:653–673, 2003.

[280] C. I. Steefel, C. A. J. Appelo, B. Arora, D. Jacques, T. Kalbacher, O. Kolditz, V. Lagneau, P. C. Lichtner, K. U. Mayer, J. C. L. Meeussen, S. Molins, D. Moulton, H. Shao, J. Simůnek, N. Spycher, S. B. Yabusaki, and G. T. Yeh. Reactive transport codes for subsurface environmental simulation. *Computational Geosciences*, 19:445–478, 2015.

[281] C.I. Steefel, S. Carroll, P. Zhao, and S. Roberts. Cesium migration in hanford sediment: A multisite cation exchange model based on laboratory transport experiments. *Journal of Contaminant Hydrology*, 67:219–246, 2003.

[282] C.I. Steefel and K.T.B MacQuarrie. Approaches to modeling of reactive transport in porous media. *Reviews in Mineralogy*, 34:82–129, 1996.

[283] J.L. Steger and J.A. Benek. On the use of composite grid schemes in computational aerodynamics. *Computer Methods in Applied Mechanics and Engineering*, 64:301–320, 1987.

[284] H.S. Tang. Study on a grid algorithm for solution of incompressible Navier-Stokes equations. *Computer and Fluids*, 35:1372–1383, 2006.

[285] H.S. Tang, S. Casy Jones, and F. Sotiropoulos. An overset-grid method for 3D unsteady incompressible flows. *Journal of Computational Physics*, 191:567–600, 2003.

[286] J. Tao, Y. Wu, D. Elsworth, P. Li, and Y. Hao. Coupled thermo-hydro-mechanical-chemical modeling of permeability evolution in a CO_2-circulated geothermal reservoir. *Geofluids*, page Article ID 5210730, 2019.

[287] B. Tartakovsky, D. Millette, S. Del Isle, and S.R. Guiot. Ethanol-stimulated bioremediation of nitrate-contaminated ground water. *Ground Water Monitoring and Remediation*, 22:78–87, 2002.

[288] R. Témam. *Navier Stokes Equations: Theory and Numerical Analysis*. North-Holland Publishing Company, 1984.

[289] V. Theofilis. Advances in global linear instability analysis of nonparallel and three-dimensional flows. *Progress in Aerospace Sciences*, 39:249–315, 2003.

[290] S. Thibeau, L.X. Nghiem, and H. Ohkuma. A modeling study of the role of selected minerals in enhancing CO_2 mineralization during CO_2 aquifer storage. *Proceedings - SPE Annual Technical Conference and Exhibition*, 2:906–922, 2007.

[291] S.G. Thomas and M.F. Wheeler. Multiblock methods for coupled flow-transport and compositional flow through porous media - applications to the simulation of transport of reactive species and carbon sequestration. *Society of Petroleum Engineers - SPE Reservoir Simulation Symposium 2011*, 2:930–951, 2011.

[292] L. J. P. Timmermans, P.D. Minev, and F. N. Van De Voss. An approximate projection scheme for incompressible flow using spectral elements. *International Journal for Numerical Methods in Fluids*, 22:673–688, 1996.

[293] G. Usera, A. Vernet, and J.A. Ferré. A parallel block-structured finite volume method for flows in complex geometry with sliding interfaces. *Flow Turbulence Combustion*, 81:471–495, 2008.

[294] A.J. Valocchi and M. Malmstead. Accuracy of operator splitting for advection-dispersion-reaction problems. *Water Resources Research*, 28:1471–1476, 1992.

[295] J. van der Lee. Thermodynamic and mathematical concepts of CHESS. *Technical Report Mines ParisTech LHM/RD/98/39*, 1998.

[296] J. van der Lee, L. De Windt, V. Lagneau, and P. Goblet. Module-oriented modeling of reactive transport with HYTEC. *Computers and Geosciences*, 29:265–275, 2003.

[297] V. Vilarrasa, M. Pool, S. De Simone, and J. Carrera. Dissolved CO_2 injection to eliminate the risk of CO_2 leakage in geologic carbon storage. *Environmental Science and Engineering*, pages 89–96, 2019.

[298] H.S. Viswanathan, B.A. Robinson, A.J. Valocchi, and I.R. Triay. A reactive transport model of neptunium migration from the potential repository at Yucca Mountain. *Journal of Hydrology*, 209:251–280, 1998.

[299] M. Vohralík and M.-F. Wheeler. A posteriori error estimates, stopping criteria, and adaptivity for two-phase flows. *Computational Geosciences*, 17:789–812, 2013.

[300] D. Voskov. Operator-based linearization approach for modeling of multiphase multi-component flow in porous media. *Journal of Computational Physics*, 337:275 – 288, 2017.

[301] V. Vostrikov. *Numerical Simulation of two-phase multicomponent flow with reactive transport in porous media*. PhD Thesis, University of Pau & Pays de l'Adour, 2014.

[302] Y. Wang, M. Khait, D. Voskov, S. Saeid, and D. Bruhn. Benchmark test and sensitivity analysis for geothermal applications in the Netherlands. *PROCEEDINGS, 44th Workshop on Geothermal Reservoir Engineering, Stantford*, pages 1–11, 2019.

[303] J. Wendling, D. Justinavicius, M. Sentis, B. Amaziane, A. Bond, N.J. Calder, and E. Treille. Gas transport modelling at different spatial scales of a geological repository in clay host rock. *Environmental Earth Sciences*, https://doi.org/10.1007/s12665-019-8230-3, 2019.

[304] J. Wendling, L. Yu, E. Treille, M. Dymitrowska, D. Pellegrini, E. Ahusborde, M. Jurak, B. Amaziane, F. Caro, A. Genty, P. Poskas, D. Justinavicius, M. Sentis, S. Norris, A. Bond, H. Leung, and N.J. Calder. Final report on benchmark studies on repository-scale numerical simulations of gas migration, part 1: Cell scale benchmark. european commission forge deliverable d1.6-r. *Euratom 7th Framework Project: FORGE, http://bgs.ac.uk/forge/docs/reports/D1.4-R.pdf*, 2013.

[305] J. Wendling, L. Yu, E. Treille, M. Dymitrowska, D. Pellegrini, E. Ahusborde, M. Jurak, B. Amaziane, F. Caro, A. Genty, P. Poskas, D. Justinavicius, M. Sentis, S. Norris, A. Bond, H. Leung, and N.J. Calder. Final report on benchmark studies on repository-scale numerical simulations of gas migration, part 2: Module scale benchmark. european commission forge deliverable d1.6-r. *Euratom 7th Framework Project: FORGE*, 2013.

[306] M.F. Wheeler, S. Sun, and S.G. Thomas. *Modeling of Flow and Reactive Transport in IPARS*, pages 42–73. In Zhang et al. [332], 2012.

[307] M.D. White and Y. Fang. *STOMP-ECKEChem: An engineering perspective on reactive transport in geologic media*, pages 112–140. In Zhang et al. [332], 2012.

[308] M.D. White and M. Oostrom. STOMP, subsurface transport over multiple phases, version 4.0. user's guide. *Rep. PNNL-15782*, 2006.

[309] C. Wieners. A geometric data structure for parallel finite elements and the application to multigrid methods with block smoothing. *Computing and Visualization on Science*, 13:161–175, 2010.

[310] L. De Windt and P. Devillers. Modeling the degradation of portland cement pastes by biogenic organic acids. *Cement and Concrete Research*, 40:1165–1174, 2010.

[311] L. De Windt, D. Pellegrini, and J. Van Der Lee. Coupled modeling of cement/claystone interactions and radionuclide migration. *Journal of Contaminant Hydrology*, 68:165–182, 2004.

[312] Y. Xiao, F. Whitaker, T. Xu, and C. Steefel, editors. *Reactive Transport Modeling: Applications in Subsurface Energy and Environmental Problems*. John Wiley & Sons Ltd, 2018.

[313] M. Xie, S. Bauer, O. Kolditz, T. Nowak, and H. Shao. Numerical simulation of reactive processes in an experiment with partially saturated bentonite. *Journal of Contaminant Hydrology*, 83:122–147, 2006.

[314] M. Xie, K. U. Mayer, F. Claret, P. Alt-Epping, D. Jacques, C. Steefel, C. Chiaberge, and J. Simůnek. Implementation and evaluation of permeability-porosity and tortuosity-porosity relationships linked to mineral dissolution-precipitation. *Computational Geosciences*, 19:655–671, 2015.

[315] B. Xu, K. Nagashima, J.M. DeSimone, and C.S. Johnson. Diffusion of water in liquid and supercritical carbon dioxide: an nmr study. *The Journal of Physical Chemistry A*, 107:1–3, 2003.

[316] T. Xu, Y. Ontoy., P. Molling, N. Spycher, M. Parini, and K. Pruess. Reactive transport modeling of injection well scaling and acidizing at Tiwi field, Philippines. *Geothermics*, 33:477–491, 2004.

[317] T. Xu, P. Rose, S. Fayer, and K. Pruess. On modeling of chemical stimulation of an enhanced geothermal system using a high ph solution with chelating agent. *Geofluids*, 9:167–177, 2009.

[318] T. Xu, R. Senger, and S. Finsterle. Corrosion-induced gas generation in a nuclear waste repository: Reactive geochemistry and multiphase flow effects. *Applied Geochemistry*, 23:3423–3433, 2008.

[319] T. Xu, R. Senger, and S. Finsterle. Bentonite alteration due to thermal-hydro-chemical processes during the early thermal period in a nuclear waste repository. *Nuclear Technology*, 174:438–451, 2011.

[320] T. Xu, E. Sonnenthal, N. Spycher, and K. Pruess. TOUGHREACT - A simulation program for non-isothermal multiphase reactive geochemical transport in variably saturated geologic media: Applications to geothermal injectivity and CO_2 geological sequestration. *Computers and Geosciences*, 32:145–165, 2006.

[321] T. Xu, E. Sonnenthal, N. Spycher, G. Zhang, L. Zheng, and K. Pruess. *TOUGHREACT: A Simulation Program for Subsurface Reactive Chemical Transport under Non-isothermal Multiphase Flow Conditions*, pages 74–95. In Zhang et al. [332], 2012.

[322] T. Xu, N. Spycher, E. Sonnenthal, G. Zhang, L. Zheng, and K. Pruess. TOUGHREACT version 2.0: A simulator for subsurface reactive transport under non-isothermal multiphase flow conditions. *Computers and Geosciences*, 37:763–774, 2011.

[323] T. Xu, H. Tian, and J. Na. *Application of Reactive Transport Modeling to CO_2 Geological Sequestration and Chemical Stimulation of an Enhanced Geothermal Reservoir*, pages 1–59. In Xiao et al. [312], 2018.

[324] S.B. Yabusaki., S.S. Sengör, and Y. Fang. A uranium bioremediation reactive transport benchmark. *Computational Geosciences*, 19:551–567, 2015.

[325] C. Yang, J. Samper, and L. Montenegro. A coupled non-isothermal reactive transport model for long-term geochemical evolution of a HLW repository in clay. *Environmental Geology*, 53:1627–1638, 2008.

[326] G.T. Yeh, J.P. Gwo, M.D. Siegel, M.H Li., Y.L Fang, F. Zhang, W.S Luo, and S.B. Yabusaki. Innovative mathematical modeling in environmental remediation. *J. Environ. Radioact*, 2011.

[327] G.T. Yeh and V.S. Tripathi. A model for simulating transport of reactive multispecies components: Model development and demonstration. *Water Resources Research*, 27:3075–3094, 1991.

[328] G.T. Yeh, V.S. Tripathi, J.P. Gwo, H.P. Cheng, R.J. Cheng, K.M. Salvage, M.H. Li, Y.L. Fang, Y. Li, J.T. Sun, F. Zhang, and M.D. Siegel. *HYDROGEOCGEM: A coupled model of variably saturated flow, thermal transport, and reactive biogeochemical transport. Groundwater reactive transport models*. In Zhang et al. [332], 2012.

[329] G.T Yeh and C.H. Tsai. HYDROGEOCHEM 6.1 A Two-Dimensional Model of Coupled Fluid Flow, Thermal Transport, HYDROGEOCHEMical Transport, and Geomechanics through Multiple Phase Systems Version 6.1 (A Two Dimensional THMC Processes Model). *Graduate Institute of Applied Geology, National Central University, Jhongli*, 2015.

[330] G.T Yeh and C.H. Tsai. HYDROGEOCHEM 7.1 A Three-Dimensional Model of Coupled Fluid Flow, Thermal Transport, HYDROGEOCHEMical Transport, and Geomechanics through Multiple Phase Systems Version 7.1 (A Three Dimensional THMC Processes Model). *Graduate Institute of Applied Geology, National Central University, Jhongli*, 2015.

[331] A. Ytterström. A tool for partitioning structured multiblock meshes for parallel computational mechanics. *International Journal of Supercomputer Applications and High Performance Computing*, 11:336–343, 1997.

[332] F. Zhang, G.T. Yeh, and J.C. Parker, editors. *Groundwater reactive transport models*. Bentham e-books, 2012.

[333] K. Zhang, J. Croisé, and G. Mayer. Computation of the Couplex-Gaz exercise with TOUGH2-MP: hydrogen flow and transport in the pore water of a low-permeability clay rock hosting a nuclear waste repository. *Nuclear Technology*, 174:364–374, 2013.

[334] R. Zhang, X. Yin, P.H. Winterfeld, and Y.S. Wu. A fully coupled thermal-hydrological-mechanical-chemical model for CO_2 geological sequestration. *Journal of Natural Gas Science and Engineering*, 28:280–304, 2016.

[335] C. Zheng. MT3D: A Modular Three-dimensional transport model for simulation of advection, dispersion and chemical reactions of contaminants in groundwater systems. http://hydro.geo.ua.edu/mt3d/Mt3d_1990.pdf, 1990.

[336] C. Zheng and G. D. Bennett. *Applied Contaminant transport modeling*. John Wiley and Sons, New York, 2002.

[337] C. Zheng and P.P. Wang. MT3DMS: A modular three-dimensional multispecies transport model for simulation of advection, dispersion and chemical reactions of contaminants in ground water systems: documentation and user's guide. *Contract Report SERDP-99-1, U.S. Army Engineer Research and Development Center*, 1999.

[338] Y.C. Zhou, B.S.V. Patnaik, D.C. Wan, and G.W. Wei. DSC solution for flow in a staggered double lid driven cavity. *International Journal for Numerical Methods in Fluids*, 57:211–234, 2003.

[339] B.J. Zielinska and J.E. Wesfreid. On the spatial structure of global modes in wake flow. *Physics of Fluids*, 7:1418–1424, 1995.

Appendix

My work performed during the last decade has been summarized in the previous chapters. Some articles have been reviewed in details while others have been just summarized or mentioned. As a consequence, I propose in this Appendix 9 additional articles:

1. **Ahusborde E.**, Azaïez M., Gruber R., *Constraint oriented spectral element method*, Lecture Notes in Computational Science and Engineering, Vol 76, 93-100, 2011.

2. Poux A., Glockner S., **Ahusborde E.**, Azaïez M., *Open and traction boundary conditions for velocity correction scheme for Navier-Stokes equations*, Computers and Fluids, Vol 70, 29-43, 2012.

3. **Ahusborde E.**, Amaziane B., Jurak M., *3D numerical simulation by upscaling of gas migration through engineered and geological barriers for a deep repository for radioactive waste*, Geological Society, London, Special Publications, Vol 415, 123-141, 2015.

4. **Ahusborde E.**, Amaziane B., El Ossmani M., *Improvement of numerical approximation of coupled two-phase multicomponent flow with reactive geochemical transport in porous media*, Oil & Gas Science and Technology - Rev. IFP Energies nouvelles, Vol 73, 73, 2018.

5. **Ahusborde E.**, El Ossmani M., *A sequential approach for numerical simulation of two-phase multicomponent flow with reactive transport in porous media*, Mathematics and Computers in Simulation, Vol 137, 71-89, 2017.

6. **Ahusborde E.**, Amaziane B., El Ossmani M., *Finite volume scheme for coupling two-phase flow with reactive transport in porous media*, Springer Proceedings in Mathematics and Statistics, Vol 200, 407-415, 2017.

7. **Ahusborde E.**, Kern M., Vostrikov V., *Numerical simulation of two-phase multi-component flow with reactive transport in porous media: application to geological storage of* CO_2, ESAIM: Proceedings and Surveys, Vol 49, 21-39, 2015.

8. **Ahusborde E.**, El Ossmani M., Id Moulay M., *A fully implicit finite volume scheme for single phase flow with reactive transport in porous media*, Mathematics and Computers in Simulation, Vol 164, 3-23, 2019.

9. **Ahusborde E.**, Amaziane B., El Ossmani M., Id Moulay M., *Numerical modeling and simulation of fully coupled processes of reactive multiphase flow in porous media*, Accepted for publication in Journal of Mathematical Study, 2019.